UNIVERSITY OF ADELAIDE
30/5/02
LIBRARY

Amphibian Peptides: Their Structures and Bioactivity

A thesis submitted for the Degree of Doctor of Philosophy

by

Kate Louise Wegener B. Sc. (Hons.)

from the

Department of Chemistry
The University of Adelaide



December, 2001

CONTENTS

Acknowledgements vii

Statement of Originality ix

Abstract x

Part I. Isolation and Identification of Novel Amphibian Peptides 1

Chapter 1 Introduction 2

1.1 Amphibian Skin Secretions 2

1.2 Peptides from Australian Frogs 5

1.2a Neuropeptides 5

1.2b Antibiotics 6

1.2c Anticancer Agents 6

1.2d Pheromones 7

1.2e Other Functions 7

1.3 Peptide Biosynthesis 8

1.4 Methodology 10

1.4a Collection of Frog Secretions 10

1.4b HPLC Analysis 11

1.4c Mass Spectrometry 11

1.4d Q-TOF 2 Hybrid Quadrupole Time of Flight Mass Spectrometer 12

1.5 Peptide Sequencing 15

1.5a Mass Spectrometry 15

1.5b Automated Edman Sequencing 16

1.5c Enzyme Digestion 16

1.5d C-terminal End Group Determination 16

1.6 Bioactivity Testing 18

Chapter 2 Peptides from *Litoria dahlii* 19

2.1 Introduction 19

2.2 Results 22

2.2a General 22

2.2b Dahlein 1.2 24

2.2c Dahlein 4.1 27

2.2d Dahlein 5.6 31

2.2e Bioactivity Testing 36

2.3 Discussion 39

2.3a Peptides from *Litoria dahlii* 39

2.3b Structure and Bioactivity of the Dahleins 40

2.4 Experimental 46

2.4a Secretion Collection and Preparation 46
2.4b HPLC Separation of Glandular Secretion 46
2.4c Mass Spectrometry Analysis 47
2.4d Determination of the Peptide Terminal Group 47
2.4e Lys-C Digestion 47
2.4f Automated Edman Sequencing 48
2.4g Preparation of Synthetic Peptides 48
2.4h Antibacterial Testing 48
2.4i Anticancer Testing 48
2.4j Neuronal Nitric Oxide Synthase Inhibition Testing 49

Part II. Amphibian Antimicrobial Peptides – Structural and Mechanistic Studies **50**

Chapter 3 Introduction **51**
3.1 Antibacterial Peptides 51
3.2 Mechanisms of Action of Antibacterial Peptides 55
3.2a General Mechanism 55
3.2b The Barrel-Stave Model 55
3.2c The Toroidal Model 59
3.2d The Carpet Model 62
3.3 Specificity of Action 65
3.4 Structural Features of α-Helical Antibacterial Peptides 68
3.4a C-Terminal Amide Group 68
3.4b Helicity 69
3.4c Charge State 70
3.4d Hydrophobicity 71
3.4e Amphipathicity 72
3.4f Hydrophilic angle 73
3.4g Summary 74
3.5 Hinged α-Helices 75

Chapter 4 Protein Structure Determination **77**
4.1 General 77
4.2 Circular Dichroism 78
4.3 Nuclear Magnetic Resonance 82
4.3a One-dimensional Spectroscopy 84
4.3b Two-dimensional Spectroscopy 85
4.3c Correlated Spectroscopy (COSY) 85
4.3d Total Correlation Spectroscopy (TOCSY) 87
4.3e Heteronuclear Correlation Spectroscopy 88
4.3f Nuclear Overhauser Effect Spectroscopy (NOESY) 89

4.4 Sequential Assignments 91
4.4a Proton Assignments 91
4.4b Carbon Assignments 92
4.5 Secondary Structure Identification Using NMR Spectroscopy 94
4.5a Secondary Shifts 94
4.5b NOE Connectivities 96
4.5c Coupling Constants 98
4.5d Amide Exchange Measurements 100
4.5e Summary 101
4.6 Structure Calculations 102
4.6a Distance Restraints 102
4.6b Ambiguous NOEs 106
4.6c Stereo-specific Assignments 107
4.6d Dihedral Angle Restraints 108
4.6e Restrained Molecular Dynamics and Simulated Annealing 109
4.6f The Potential Energy Function 111
4.6g Quality of Structures 113
4.7 Models for a Membrane Environment 116
4.7a 2,2,2-Trifluoroethanol 117
4.7b Micelles 118

Chapter 5 Orientation Studies **120**
5.1 General 120
5.2 Solid-State NMR Spectroscopy 123
5.2a Orientation of Peptides 124
5.2b Peptide-Lipid Interactions 126
5.2c Head-groups – Phosphorus NMR 127
5.2d Acyl Chains – Deuterium NMR 129
5.2e Mechanically Aligned Bilayers 133
5.2f Magnetically Aligned Bicelles 134
5.3 Oriented Circular Dichroism 137

Chapter 6 Short Antibacterial Peptides **140**
6.1 Introduction 140
6.2 Citropin 1.1 145
6.2a Circular Dichroism Studies 145
6.2b NMR Studies – Assignments 146
6.2c Secondary Shifts 149
6.2d Amide Secondary Shifts 151
6.2e NOE Connectivities 151
6.2f Coupling Constants 152

6.2g Structure Calculations 152

6.3 Aurein 1.2 156

6.3a NMR Studies - Trifluoroethanol Titration 156

6.3b Assignments 157

6.3c Secondary Shifts 160

6.3d Amide Secondary Shifts 161

6.3e NOE Connectivities 162

6.3f Coupling Constants 163

6.3g Structure Calculations 163

6.4 Orientation Studies 167

6.4a Oriented Circular Dichroism - Unoriented Vesicles 167

6.4b Oriented Lipid Bilayers 168

6.4c Solid-state NMR - Unoriented Multilayers 171

6.4d Mechanically Oriented Multilayers 173

6.5 Discussion 181

6.6 Conclusion 185

Chapter 7 The Caerin Peptides 186

7.1 Introduction 186

7.2 Structure of Caerin 1.1 in DPC Micelles 192

7.2a NMR Studies - Assignments 192

7.2b Secondary Shifts 195

7.2c Amide Secondary Shifts 196

7.2d NOE Connectivities 197

7.2e Amide Exchange 198

7.2f Structure Calculations 199

7.3 Caerin 1.4 204

7.3a Circular Dichroism Studies 204

7.3b NMR Studies – Assignments 204

7.3c Secondary Shifts 210

7.3d Amide Secondary Shifts 211

7.3e NOE Connectivities 212

7.3f Amide Exchange 213

7.3g Structure Calculations 214

7.4 Discussion 221

7.5 Conclusion 225

Chapter 8 Experimental 226

8.1 Materials 226

8.2 CD Spectroscopy – Trifluoroethanol Titrations 226

8.3 Solution NMR Spectroscopy 226

	8.3a	Sample Preparation	226
	8.3b	NMR Spectroscopy	227
	8.3c	Structural Restraints	229
	8.3d	Structure Calculations	229
8.4	Oriented Circular Dichroism		230
	8.4a	Sample Preparation	230
	8.4b	CD Measurement	231
8.5	Solid-state NMR Spectroscopy		231
	8.5a	Sample Preparation - Unoriented Bilayers	231
	8.5b	Mechanically Oriented Bilayers	232
	8.5c	NMR Spectroscopy - Unoriented Bilayers	232
	8.5d	Mechanically Oriented Bilayers	232
	8.5e	Peptide Powders	233

Summary and Future Directions **234**

References **237**

Appendix – HSQC and HMBC Spectra **269**

Publications **275**

Acknowledgements

I would firstly like to thank my supervisor, Professor John H. Bowie, for his advice and guidance and for giving me the opportunity to work on such an interesting and wide-ranging project. I would also like to acknowledge the Australian Post-graduate Research Award that enabled me to undertake the research presented in this thesis.

Thanks also to Associate Professor John Carver, from the University of Wollongong, for his help and advice regarding NMR techniques and Dr. Robyn Lindner for her assistance with the acquisition of CD spectra. Many thanks as well to Associate Professor Frances Separovic and Tracy Lam, from the University of Melbourne, for teaching me aspects of solid-state NMR spectroscopy and Dr. Maurits de Planque for his help with oriented CD.

Special thanks must go to Dr. Grant Booker, from the Department of Molecular Biosciences, University of Adelaide, for allowing me the use of his computers and for being so generous with his time and advice – it was very much appreciated. Thanks also to Dr. Terry Mulhern, now of the University of Melbourne, for teaching me the computational aspects of peptide structure determination.

In addition, I'd like to acknowledge Associate Professor Mike J. Tyler and Ben Smith, from the Department of Environmental Biology, University of Adelaide, for providing the amphibian secretions and Associate Professor John C. Wallace, from the Department of Molecular Biosciences, University of Adelaide, for providing the automated Edman sequencing data. Thanks also to Dr. Lyndon E. Llewellyn, from the Australian Institute of Marine Science, for conducting the nNOS inhibition assays and the National Cancer Institute (Washington) for performing the anticancer tests.

Much thanks to the academic, research and technical staff at the University of Adelaide for their help and advice – particularly Dr. Brian Chia, Phil Clements and Dr. Simon Pyke for assistance with NMR spectroscopy, Dr. Paul Wabnitz and Andrew McAnoy for mass spectrometry advice and Craig Brinkworth for his help with the Q-TOF mass spectrometer and Edman sequencing. Thanks also to the members of the Bowie research group, especially Craig Brinkworth and Charm Boontheung for the comic relief they provide in the lab!

Thanks to Sam Lienert for being so generous with his lap-top computer and my brother Tim for his patient help with computer scripts and for attempting to answer millions of incidental questions – and both of them for being such accommodating house-mates. Thanks also to Becky Lienert and Adrian Harris for looking after me so well when I was in Melbourne. Special thanks as well to my 'Ph. D. buddy' Duncan Grove for the helpful chats (did I win the bet?) and for understanding and to my U.S. mate Anita Kishore for her warm friendship.

Thanks also to the Lawrie family (particularly Mrs Adams) for supporting me throughout my Ph.D., taking an interest in my work and for keeping me well-fed! Also, to all my family and friends, thank-you for putting up with me and for constantly asking 'how are the frogs going?'. Oh, and thanks for all the frogs Liesel.

I would especially like to thank my Mum and Dad for all the support they've given me throughout my life. It has been greatly appreciated and this wouldn't have been possible without it.

And finally, I'd like to thank Mark Lawrie, firstly for his technical assistance with the 3D lipid figures and computer scripts, but mostly for his extraordinary patience and the amazing support and encouragement he's given me over the last few years.

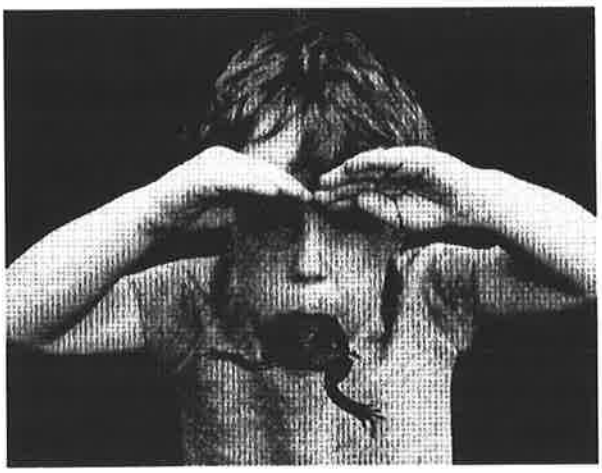

Statement of Originality

This thesis contains no material that has been accepted for the award of any other degree or diploma in any university or other tertiary institution and, to the best of my knowledge and belief, contains no material, previously published or written by another person, except where due reference has been made in the text.

I give consent for this copy of my thesis, when deposited in the University Library, to be available for loan and photocopying.



Kate Louise Wegener

21/12/2001

Date

Abstract

Amphibians secrete a cocktail of chemicals onto their skin in response to stressful stimuli, such as attack by predators. The compounds secreted include bioactive peptides, which can protect against infection, relieve pain and regulate aspects of the animal's physiology. Such peptides are potential therapeutic agents and can also be used to investigate the relationships between different amphibian species.

The skin secretion of the northern Australian frog *Litoria dahlii* has been investigated, with eleven novel peptides identified. These peptides have moderate biological activity, including antibacterial and anticancer actions, as well as the capacity to inhibit the enzyme neuronal nitric oxide synthase. The similarities between the isolated peptides and those from *L. aurea* and *L. raniformis* from southeast Australia, suggest these species are related, despite their geographical separation.

Many potent broad-spectrum antibiotics have previously been isolated from Australian amphibians. These peptides are believed to act by disrupting the bacterial cell membrane by forming transmembrane 'barrel-stave' type ion channels, lipid-incorporating toroidal pores or by assembling as a 'carpet' over the membrane surface.

The structures of several antibacterial peptides were determined using nuclear magnetic resonance spectroscopy and restrained molecular dynamics calculations. The short peptides citropin 1.1 (16 residues) and aurein 1.2 (13 residues) both form linear amphipathic α-helices, while caerin 1.1 and caerin 1.4 (both 25 residues) form amphipathic α-helical structures with flexible hinge regions around proline 15.

Oriented circular dichroism and solid-state nuclear magnetic resonance spectroscopy studies were used to investigate the orientation of citropin 1.1 and aurein 1.2 in neutral lipid bilayers. The experimental results suggest these peptides operate by the 'carpet' mechanism.

Part I. Isolation and Identification of Novel Amphibian Peptides

Chapter 1 Introduction

1.1 Amphibian Skin Secretions

The pharmacological properties of frog skin secretions have been exploited for over two thousand years [1], from their use in Chinese medicine [2] to their application as a stimulant by the Peruvian Indians [3]. The toxic nature of some secretions has been used to advantage by the Columbian Indians who apply the venom to darts used for hunting [4]. The active compounds that produce these varied effects appear to be there to protect the frog from predators. However, not all frogs produce poisonous substances, suggesting that the secretions may serve additional purposes [1].

Michael Zasloff [5] utilised *Xenopus laevis* specimens in his research and noted that these animals very rarely developed infections following surgery, despite the non-sterile procedures used and the microbially contaminated water they were returned to. This led to the postulation that skin-secretions might serve a second protective function, this time against micro-organisms.

Amphibian skin secretions have been investigated for over fifty years in an effort to identify their contents and clarify their functions [6]. The vast array of active compounds that has been identified includes biogenic amines [7], steroidal compounds, alkaloids [8] and peptides [6, 9]. The alkaloids are responsible for the toxicity of the poison-dart frogs, while particular steroid compounds account for the therapeutic effects utilised by the Chinese.

The peptide element of the secretions has a host of different functions. Hormonal effects, caused by the stimulation of various types of smooth muscle, include changes in blood pressure or stimulation of the urinary, reproductive and gastro-intestinal tracts [1]. Peptides with analgesic properties have also been detected. This group, known as the dermorphins, has activity that exceeds that of morphine by up to 300 times [10].

The amazing ability of frogs to avoid infection has also been traced to peptides. Zasloff [5] isolated two peptides with antibacterial activity from *X. laevis*, which he subsequently

named magainins. Since then, antimicrobial peptides have been identified in numerous other amphibian species [9, 11, 12]. In addition to their bactericidal properties these peptides sometimes have anticancer or antifungal activity [13-15].

Having active peptides on the skin for long periods of time may cause damage to the frog's own cells. However the frog has a mechanism for guarding against this that comes in the form of proteolytic enzymes [16]. Examination of the skin secretion after 5-10 minutes reveals new peptides whose sequences are related to potent antibacterial peptides but have had two or three residues removed from the N-terminus. Testing of these peptides shows they no longer possess antimicrobial activity.

Frog-skin secretions were recently discovered to have another function - advertising. Wabnitz *et al.* [17] found that a peptide isolated from *Litoria splendida* acted as a pheromone. When this peptide, later named splendipherin, was applied to a moist pad in a tank containing a female *L. splendida* specimen, the frog immediately moved toward the pad. It is thought that the release of splendipherin aids mating by signalling the location of the male.

Given the remarkable bioactivity of amphibian peptides, it comes as no surprise that the isolation, identification and testing of new amphibian peptides continues to this day. Already, this process has led to the development of peptides for the treatment of various medical conditions including conjunctivitis, gastrointestinal infections and even cancer [4]. Exploiting the antibacterial properties of peptides is a particularly promising avenue since it would be difficult for bacteria to acquire resistance to their destructive action on the bacterial membrane (see Section 3.2) [18]. Resistance is a major problem for the antibiotics in clinical use today [19].

Another peptide, known as caerulein, has found a range of clinical applications resulting from its potent stimulation of the gut and gall bladder [1, 20]. This peptide was first identified in the secretion of the Australian frog *L. caerulea*, but has subsequently been found in most Australian species as well as in certain South American and African frogs [12, 21].

The search for novel peptides with interesting biological functions is not the only force driving the screening of frog secretions. Identification and classification of species can also be achieved by comparing the peptides found in their secretions [22]. For example, the debate over whether the Australian frogs *L. caerulea* and *L. gilleni* are the same or different species was settled by the finding that their peptide profiles were so dissimilar that they could not have come from the same species [23]. Thus the impressive array of peptides found in the skin of amphibians has significance for the taxonomy and evolutionary study of these creatures, as well as for the discovery of interesting new compounds. Only a fraction of frog species has been examined so far, leaving a rich resource still to be mined.

1.2 Peptides from Australian Frogs

Over one hundred and thirty peptides have been identified in the dermal secretions of more than 25 species of Australian frog [24]. The majority of frogs studied have a variety of peptides within the skin glands that generally include a neuropeptide and a powerful broad-spectrum antibiotic. In addition, peptides have been found that show anticancer properties, pheromone activity and possible neurotransmitter functions [14, 17, 25].

1.2a Neuropeptides

Caerulein (1), a potent neuropeptide that has activity on smooth muscle, is found in almost all of the Australian frog species studied [24]. This peptide is modified after translation by conversion of the C-terminal group to an amide, transformation of the first residue into pyroglutamate (pE) and sulfation of the tyrosine residue. Generally, the occurrence of caerulein in dermal secretions is accompanied by a number of caerulein-like analogues, which, while as yet untested, are presumed to possess similar activity [26].

(1) Caerulein pEQDY(SO_3)TGWMDF-NH_2

Instead of caerulein, members of the genus *Uperoleia* produce the neuropeptide uperolein [27] or an analogue [28]. Uperolein (2) is a vasodilator and hypotensive peptide and unlike caerulein, it does not contain a sulfated tyrosine residue.

(2) Uperolein pEPDPNAFYGLM-NH_2

Neuropeptide activity occurs by the activation of neuronal receptors, although the actual receptor(s) responsible for caerulein's activity have not yet been identified. Recently, another group of peptides have been shown to inhibit the enzyme neuronal nitric oxide synthase (nNOS) [29] – an enzyme responsible for the production of the neurotransmitter nitric oxide. In this case, it is the ultimate effects these compounds have on the organism that are unknown.

The list of amphibian peptide nNOS inhibitors so far discovered is long and includes peptides with no clear sequence similarities. However, three general groups have been identified: i) short basic peptides, terminating with an amide group and capable of adopting amphipathic α-helical structure – these include lesueurin (3), the aureins 1 and the citropins 1, ii) frenatin 3 (4) type peptides which are also basic but terminate with carboxylic acid groups - this group also includes the caerin 2 peptides and iii) peptides with a helix-hinge-helix type structure – the caerin 1 family (e.g. 5). The majority of these peptides also show antibacterial and anticancer activity, however others, such as lesueurin and the frenatin 3 group, have shown little or no other activity.

(3) Lesueurin GLLDILKKVGKVA-NH_2

(4) Frenatin 3 GLMSVLGHAVGNVLGGLFKPKS-OH

(5) Caerin 1.8 GLFKVLGSVAKHLLPHVVPVIAEKL-NH_2

1.2b Antibiotics

The dermal secretions of almost all frog species studied have been shown to contain at least one potent, broad-spectrum antibiotic peptide. The most active of these include caerin 1.1 (6), maculatin 1.1 (7), citropin 1.1 (8) and aurein 1.2 (9). All of these peptides are believed to exert their action by interfering with the integrity of the bacterial cell membrane [30, 31]. It is still not clear exactly how this occurs and there have been many mechanisms put forward that will be elaborated on at a later stage (Section 3.2).

(6) Caerin 1.1 GLLSVLGSVAKHVLPHVVPVIAEHL-NH_2

(7) Maculatin 1.1 GLFGVLAKVAAHVVPAIAEHF-NH_2

(8) Citropin 1.1 GLFDVIKKVASVIGGL-NH_2

(9) Aurein 1.2 GLFDIIKKIAESF-NH_2

1.2c Anticancer Agents

Many amphibian peptides have also been tested for *in vitro* activity against cancer cells and, in general, the anticancer activity mirrors the antibacterial activity, suggesting a similar mode of action [14].

1.2d Pheromones

Splendipherin (10), isolated from *L. splendida*, has been shown to attract the female of the species, demonstrating its use as a pheromone [17]. Peptides from other species, with as yet unknown activities and similar sequences to splendipherin (such as aurein 5.2, 11), have been hypothesised as also having some kind of pheromone role [14]. However, the experiments needed to demonstrate this are yet to be conducted.

(10) Splendipherin GLVSSIGKALGGLLASVVKSKGQPA-OH

(11) Aurein 5.2 GLMSSIGKALGGLIVDVLKPKTPAS-OH

1.2e Other Functions

While the activity of some peptides has been identified, there are still many whose purpose in the secretion remains unknown. Included in this group are the caeridins, dynastins, rubellidins and tryptophyllins [32-34].

In the case of the tryptophyllins, those isolated from Australian frogs have shown no activity, however it has been suggested that they act as neurotransmitters. These peptides are very small, composed of only four or five residues (e.g. 12). They are related to compounds from *Phyllomedusa rohdei* that have been shown to induce sedation in pigeons [34].

(12) Tryptophyllin L2 pEFPWL-NH_2

Frogs synthesise and store their armoury of peptides at extensive metabolic cost [35]. It seems unlikely, then, that the peptides produced would have no purpose. One possibility is that the unassigned peptides are inactive bi-products of prepropeptide degradation [2] (see Section 1.3). It remains to be seen, however, whether this or some other explanation is correct.

1.3 Peptide Biosynthesis

Peptides, like all proteins, are produced by transcription of genes encoded in DNA and translation of the resulting mRNA. The peptides are initially synthesised in a prepropeptide form, consisting of a signal peptide, spacer region and the active peptide [36] (Figure 1.1). The signal peptide directs the molecule into the endoplasmic reticulum and is then removed by specific proteases to form the propeptide [37]. The molecules migrate to the Golgi complex where they are packaged and stored in secretory granules until a signal triggers their release.

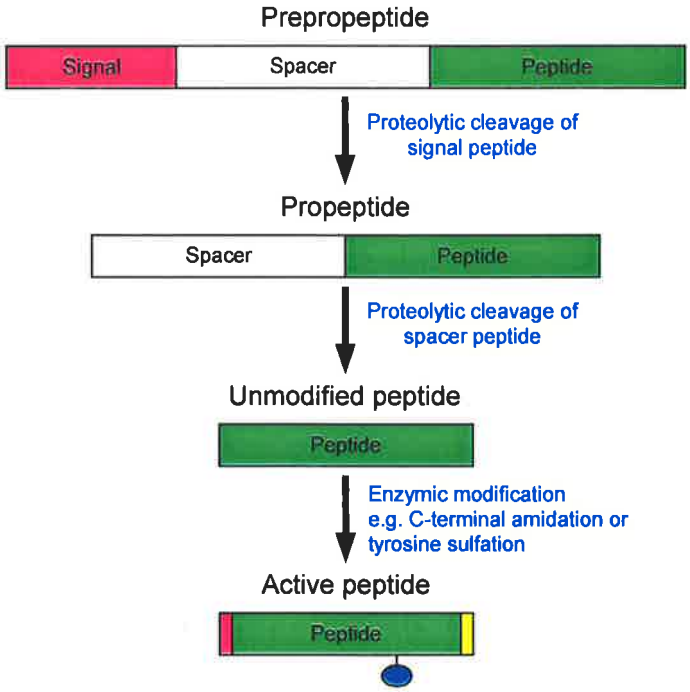

Figure 1.1 Biosynthesis of bioactive peptides. Initial translation of the mRNA produces a prepropeptide, which is processed by various enzymes to produce the active peptide.

The pro-piece, or spacer peptide, has to be cleaved to obtain the active peptide. This generally occurs at some point along the journey through the endoplasmic reticulum and Golgi complex [36]. In some cases, such as with the defensins, the molecule is stored as the inactive propeptide and the spacer segment is removed upon release of the secretion [38]. This suggests the active peptide may be cytotoxic to the host at the high concentrations present in the secretory granules.

The cleaved spacer peptide is often released with the active component. Because of this, it has been suggested that the spacer peptides may also have some as yet unrecognised activity. In fact, systems are known in which a hormone peptide is associated with an antibiotic peptide in the propeptide form. For example, the hormone xenopsin is associated with xenopsin precursor fragment (XPF), which was found to possess antibacterial activity [21].

The prepropeptide (or precursor) sequences are known for a number of peptides from *X. laevis*. Interestingly, the precursor for magainin contains many copies of the cationic active peptide sequence, each separated by acidic pro-pieces [38] (Figure 1.2). Several different precursor sequences have been detected for caerulein. Here again, numerous copies of the caerulein sequence occur, accompanied by several copies of caerulein precursor fragment (CPF), which has antibacterial activity [21] (Figure 1.2).

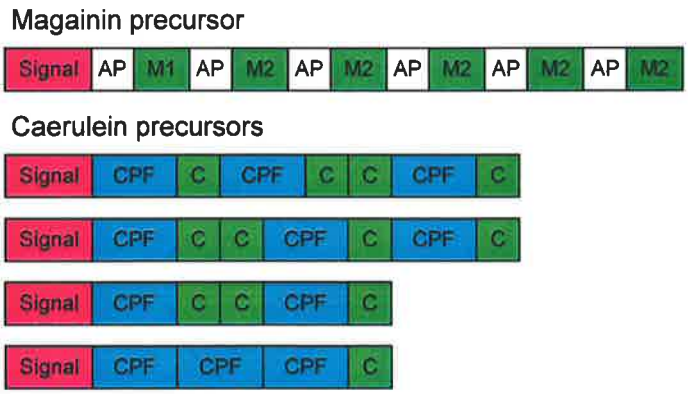

Figure 1.2 Precursor peptides for magainin (M1 and M2) and caerulein (C). The acidic propieces in the magainin precursor are designated AP, while CPF refers to the caerulein precursor fragment.

Many peptides also undergo post-translational modifications. This can include C-terminal amidation, blocking of the N-terminus by conversion of glutamic acid to pyro-glutamate, sulfation of tyrosine residues and isomerisation of L-amino acids to the D form [39]. In most cases these modifications have been found to be important for activity.

1.4 Methodology

1.4a Collection of Frog Secretions

Frog-skin secretions are released from specialized glands in the skin of the frog. Two types of gland occur here – the mucous glands, which produce a watery secretion for cooling and aiding respiration, and the granular glands, which store the active components of the secretion [40]. Both types of glands are controlled by the sympathetic nervous system, which is involved with the 'fight-or-flight' response. Secretions from the granular glands are released under conditions of stress, for example when under attack from a predator [1].

In the past, secretion collection was achieved by killing the specimen, removing the skin and extracting the peptides with an organic solvent [41]. In some cases, this has required the sacrifice of over a thousand animals for a single study [41, 42]. To continue using such invasive methods of collection would clearly be irresponsible since there is much evidence now that many frog populations are in decline, some to the brink of extinction [43, 44]. Secretions must therefore be collected using non-invasive techniques that leave the animals unharmed.

The method currently practised involves mild electrical stimulation of the frog's dorsal surface [45] (Figure 1.3). This induces the discharge of secretion from the granular glands, which can be rinsed off with water and collected. This procedure does not harm the animal and can be repeated on a monthly basis.



Figure 1.3 The surface electrical stimulation method of collecting frog skin secretion (left) and the crude aqueous secretion obtained (right).

1.4b HPLC Analysis

Once secretions have been collected, they are concentrated and subjected to high performance liquid chromatography (HPLC) to separate and purify the peptide components. This process must be undertaken as soon as possible after collection to avoid degradation of the peptides by enzymes in the secretion [16].

The chromatography is carried out using a reverse-phase column and gradient elution, where the concentration of organic solvent in the mobile phase is increased over time. Once injected onto the column, the peptides equilibrate between the mobile and stationary phases. The equilibrium is influenced by the concentration of organic solvent in the mobile phase, as well as the hydrophobicity and conformation of the peptide. Peptide elution occurs when the percentage of organic solvent is sufficient to shift the equilibrium to the mobile phase [46].

1.4c Mass Spectrometry

Mass spectrometry is a technique used to measure molecular mass. In order to do this, the mass spectrometer must be able to vaporise and ionise the sample (gas-phase ionisation), separate the component ions according to their mass-to-charge (*m/z*) ratio (analysis) and detect the resulting ions (detection) [47].

Fragmentation of the component molecular ions can occur because of excess vibrational energy imparted by the ionisation process or by collisions with inert gas molecules [48]. The fragment (or 'daughter') ions produced can give information about the structure of the original molecular ('parent') ion. In this way, peptide sequence information can be obtained from the fragmentation pattern of peptide molecular ions.

Mass spectrometry was the principal technique used in the present research to investigate peptide primary structures. This research was carried out using a Q-TOF 2 hybrid quadrupole time of flight mass spectrometer. The methods employed by the Q-TOF 2 to

carry out gas-phase ionisation, analysis and detection will be discussed in the following section.

1.4d Q-TOF 2 Hybrid Quadrupole Time of Flight Mass Spectrometer

A schematic diagram of the principal components of the Q-TOF 2 mass spectrometer is shown in Figure 1.4.

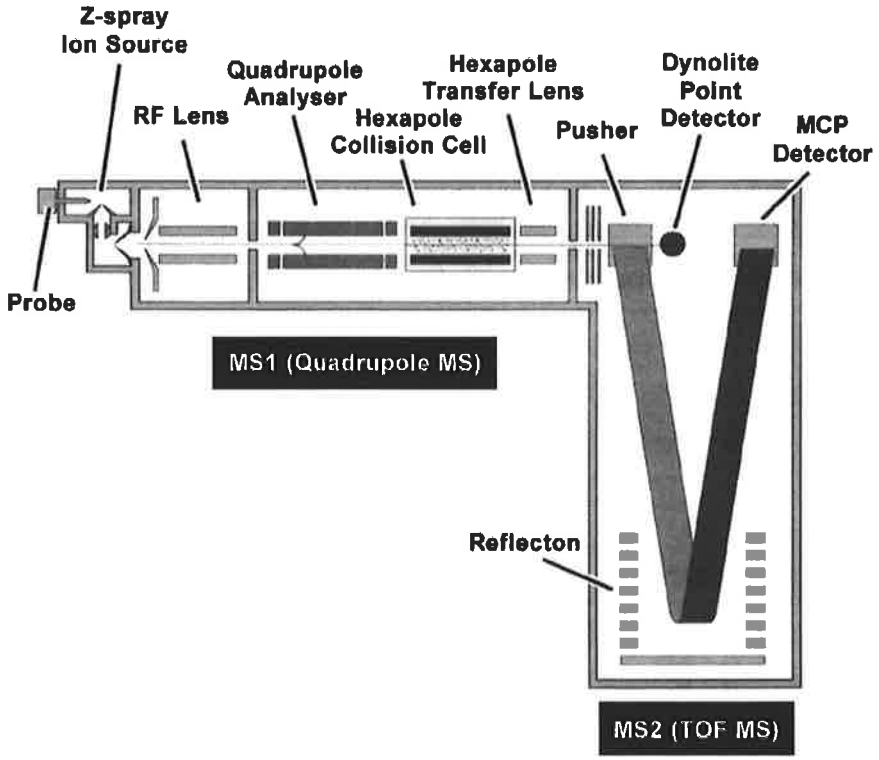

Figure 1.4 Schematic diagram of the Q-TOF 2 mass spectrometer.

Gas-phase ions are produced in the Z-spray ion source by the electrospray ionisation (ESI) technique [49]. Here, a large voltage (~3-6 kV) is applied to liquid flowing through a capillary (~1-10 $\mu L \cdot min^{-1}$). A fine spray of highly charged droplets emerges from the needle, which is evaporated by a combination of heat and dry gas. As the charged droplets decrease in size, Coulombic repulsion overcomes the cohesive forces holding the molecules together and the droplets 'explode' into smaller and smaller assemblies, until a series of free ions are obtained [50]. This process is illustrated in Figure 1.5.

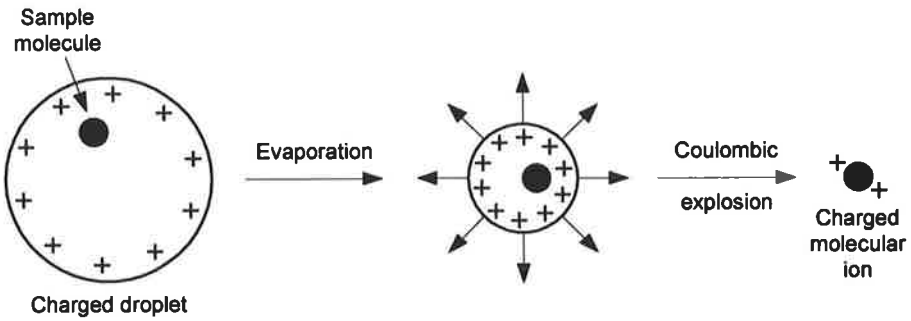

Figure 1.5 Electrospray ionisation mechanism.

This soft ionisation technique causes relatively little fragmentation and often results in the formation of multiply charged ions [51]. The latter property means that large molecules, with molecular ions outside the range of a particular mass spectrometer, can be observed if the *m/z* ratio of the multiply charged ion is decreased sufficiently. Thus ESI is a useful technique for the study of large biomolecules, such as peptides and proteins.

The charge state of the ions can be determined from the *m/z* values of the isotope peaks, since the mass difference between these peaks is inversely proportional to the charge. Thus, if there is a mass difference of 0.5 Da between the isotope peaks of a particular envelope, the ion responsible has a charge of +2.

The free ions produced by ESI are drawn through the sample cone aperture and into the ion block, before being extracted into the analyser. In the Q-TOF 2, the analyser consists of a quadrupole mass analyser and an orthogonal acceleration time of flight (TOF) mass spectrometer, separated by a hexapole collision cell (Figure 1.4).

In the TOF sector, ions are accelerated to the same kinetic energy by a positive voltage, before being pushed toward the reflectron and reflected back to the detector. Since the ions have the same kinetic energy, their velocity is inversely proportional to the square root of their mass [52]. Thus the ions can be separated according to their flight times, with ions of larger mass taking longer to reach the detector.

Ions can be selected by the quadrupole mass analyser and fragmented in the hexapole collision cell. Fragmentation results from collisions between the ions and high energy

argon atoms, in a process known as collision induced decomposition (CID). The resulting daughter ions can then be scanned by the TOF mass sector.

The Q-TOF 2 has a microchannel plate (MCP) detector that records a full spectrum every 50 μs. The spectra are summed in the memory of the time to digital converter and the resulting spectrum is transferred to the connected computer. Each spectrum on the computer will be a sum of 20000 individually detected spectra, for an acquisition rate of 1 spectrum per second.

The Q-TOF 2 records spectra with very high sensitivity (nanomolar concentrations) and a mass range to 10000 Da. These attributes are advantageous for the analysis of the small quantities of peptide isolated from amphibian secretions.

1.5 Peptide Sequencing

1.5a Mass Spectrometry

Peptide primary sequences can be elucidated using mass spectrometry. The structural information is provided by the spectrum of daughter ions produced by CID of the parent peptide ion. Advantages of the mass spectrometry (MS) method are that results are obtained very quickly and sequences can be determined from minute quantities of sample. In addition, MS can identify post-translational modifications to the primary sequence that may be difficult or impossible to detect by automated Edman degradation [53] (Section 1.5b). N-terminal pyroglutamate residues, for instance, cannot be detected by Edman sequencing.

Peptides undergo many types of characteristic fragmentation but for sequencing purposes we use only the 'B' and 'Y+2' fragmentations [53, 54]. These fragmentations occur as a result of cleavage between the carbon and nitrogen atoms of the peptide bond. For B cleavages, the positive charge remains on the N-terminal portion, thus providing information about the C-terminal end of the peptide. Conversely, for Y+2 cleavages, a proton is transferred to the C-terminal fragment leaving this portion charged and information is obtained about the N-terminal sequence [55] (Figure 1.6).

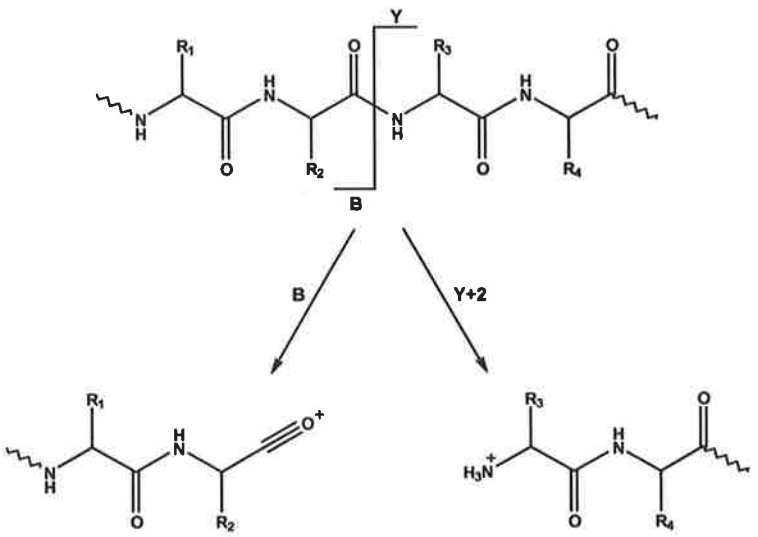

Figure 1.6 Characteristic B and Y+2 fragmentations of linear peptides in the positive mode.

The isomeric residues leucine (113 Da) and isoleucine (113 Da) and the isobaric residues lysine (128 Da) and glutamine (128 Da) are indistinguishable using this technique. Edman sequencing can be used to conclusively identify these residues. Lysine and glutamine residues can also be differentiated by enzyme digestion using Lys-C endoprotease, followed by MS.

1.5b Automated Edman Sequencing

Edman sequencing uses a standard sequence of chemical reactions to remove residues, one by one, from the N-terminal [56, 57]. The residues are subsequently identified by their retention times on HPLC. As the peptide decreases in size, there is increased likelihood that it will be washed from the solid support before sequencing is complete. In addition, post-translational modifications to the N-terminus can make the peptide impervious to the standard reactions, while other modifications will result in atypical retention times [53]. Thus Edman sequencing is not always successful but can provide complementary information to MS sequence data.

1.5c Enzyme Digestion

When CID and MS cannot determine the full sequence, endoproteases can be used to digest the peptide into smaller segments. These segments can then be sequenced to provide the missing information [57]. This technique is particularly useful for large peptides and proteins. In addition, enzyme digestion using Lys-C endoprotease can be used to differentiate between lysine and glutamine residues. This enzyme cleaves the peptide at the peptide bond following the lysine residue.

1.5d C-terminal End Group Determination

Many amphibian peptides have amide groups at the C-terminal so techniques have been developed to differentiate between C-terminal amides and acids. One way of accomplishing this is to convert the peptide to its methyl ester and measure its mass using MS. The mass difference between the ester and the parent peptide indicates the number of

amide and acid groups present. Thus, an increase of 14 Da indicates a carboxylic acid group, while an increase of 15 Da is evidence of a primary amide (Figure 1.7).

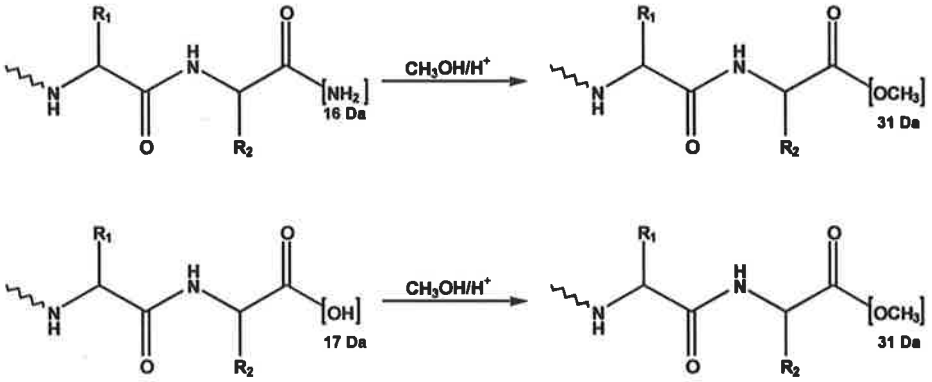

Figure 1.7 Determination of the C-terminal group by methylation.

1.6 Bioactivity Testing

Peptides isolated and sequenced from amphibian secretions are subjected to a variety of activity tests. The peptide material obtained from the frog (usually <100 μg) is generally insufficient for biological testing so the peptides must be synthesised commercially (Mimotopes, Clayton, Victoria). The synthetic peptides must be shown to be identical to the natural peptides using HPLC and MS.

Antibacterial testing is conducted by the Institute of Medical and Veterinary Science (Adelaide, South Australia). The procedure used involves adding a series of increasingly concentrated peptide solutions to bacterial cultures and determining the minimum concentration that inhibits the growth of the pathogen – the minimum inhibitory concentration (MIC, $\mu g \cdot mL^{-1}$) [58]. If no inhibition is detected at concentrations less than 100 $\mu g \cdot mL^{-1}$, the peptide is deemed to be 'inactive' against this organism.

Peptides have also been tested for anticancer activity. In the present research, this was carried out by the National Cancer Institute (Washington, DC, USA) by assessing the *in vitro* chemosensitivity of a number of human tumour cell lines to the synthetic peptide [59].

Since our discovery that certain amphibian peptides may inhibit the enzyme nNOS, a number of novel peptides, including synthetic modifications of known peptides, have been routinely tested for inhibition of this enzyme. Briefly, the assay involves measuring the nNOS catalysed conversion of [^{3}H]arginine to [^{3}H]citrulline and determining the concentration of peptide that inhibits this reaction by 50% i.e., the 50% inhibition concentration (IC_{50}). These activity tests were carried out by the Australian Institute of Marine Science (Queensland, Australia).

Chapter 2 Peptides from *Litoria dahlii*

2.1 Introduction

Litoria dahlii is a moderately large frog (49-71 mm) found in the flood plains of northern Australia (Figure 2.1) [60]. Its skin-colour is highly variable, ranging from green olive to dark slate, with irregular patches and often a pale mid-vertebral stripe [61]. Being an aquatic species, this frog spends most of its time in water, while in dry months it can often be found hiding in cracks in clay areas [62].



Figure 2.1 *Litoria dahlii.*

This species, commonly known as Dahl's Aquatic Frog, is noted for its slimy skin, which results from the release of large amounts of mucous material from its mucous glands [63]. *L. dahlii* is also known for its toxicity to large predators, such as snakes [64].

L. dahlii belongs to the *L. aurea* complex, which consists of six frog species including *L. moorei* and *L. cyclorhyncha* from southwestern Australia, and *L. flavipunctata*, *L. aurea* and *L. raniformis* from the southeast (Figure 2.2).

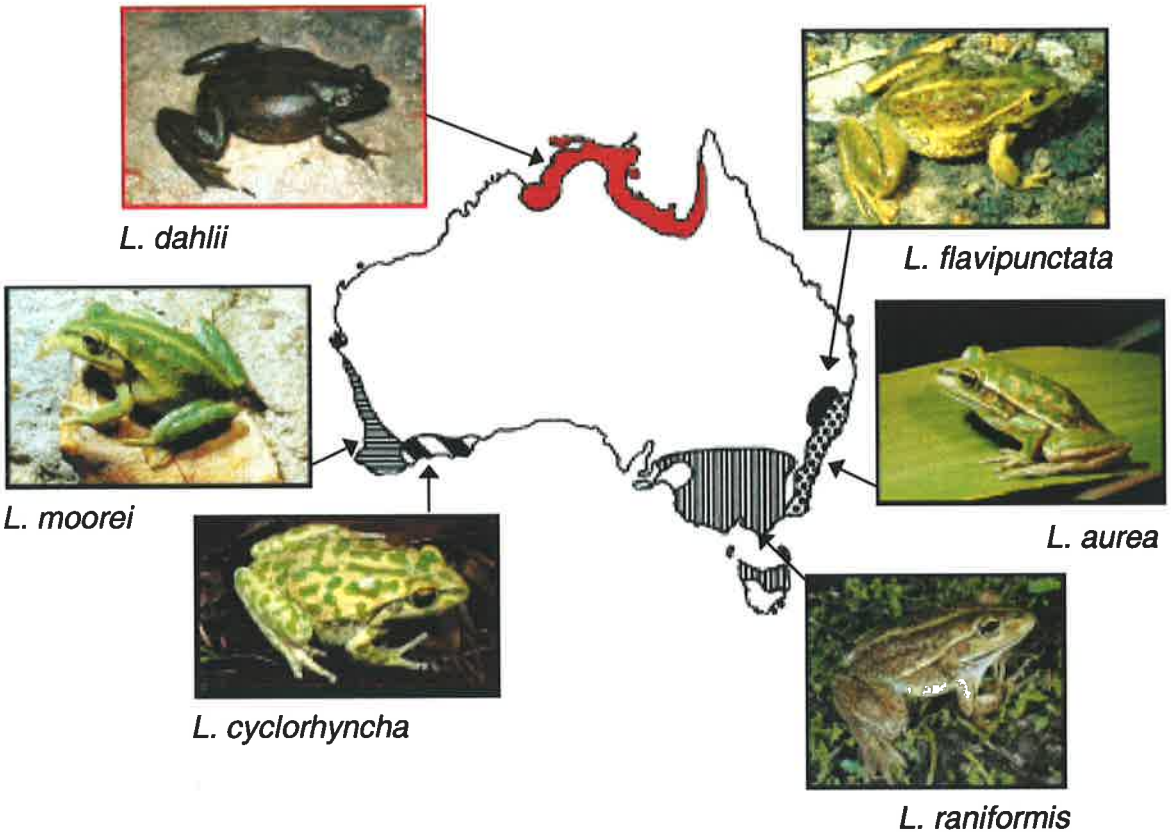

Figure 2.2 Geographical distribution of the Australian frogs *Litoria dahlii, L. moorei, L. cyclorhyncha, L. flavipunctata, L. aurea* and *L. raniformis*.

The skin secretions of *L. aurea* and *L. raniformis* have been examined recently, with five groups of novel peptides found [14]. A representative from each is shown below.

(9) Aurein 1.2 GLFDIIKIAESF-NH_2

(13) Aurein 2.2 GLLDIVKKVIGAFGSL-NH_2

(14) Aurein 3.1 GLFDIVKKIAGHIAGSI-NH_2

(15) Aurein 4.1 GLIQTIKEKLKELAGGLVTGIQS-OH

(11) Aurein 5.2 GLMSSIGKALGGLIVDVLKPKTPAS-OH

Peptides of the aurein 1, 2 and 3 groups have broad-spectrum antibacterial activity and are also active against cancer cells. Aurein 1.2 (9) is the smallest antibiotic and anticancer active peptide yet isolated from an Australian frog. NMR and CD investigations show this peptide adopts an amphipathic α-helical structure in trifluoroethanol (TFE)/water mixtures and 1,2-dimyristoylphosphatidylcholine (DMPC) vesicles (Section 6.3). Members of the

aurein 1 and 2 groups are also effective inhibitors of nNOS, with IC_{50} values in the range 1.8-34 μM.

The aureins 4 and 5 have no antibacterial or anticancer activity. Aurein 5.2 (10), however, was recently shown to inhibit nNOS with an IC_{50} of 7.8 μM (unpublished data). In addition, aurein 5.2 has some sequence similarity to the sex pheromone splendipherin from *L. splendida* [17], so it is possible that the aureins 4 and 5 have a role in chemical communication.

(10) Splendipherin GLVSSIGKALGGLLADVVKSKGQPA-OH

Species that are zoologically classified in the same complex are thought to have evolved from common ancestors [65] and, as a result, they have similar host defence peptides [12]. *L. dahlii* is classified as part of the *L. aurea* complex [61]. However, since it is geographically separated from the other members of this group by around 2000 km, there is reason to believe it may have evolved independently. This is supported by the fact that *L. dahlii* is the only member of the *L. aurea* complex that is reported to be toxic to predators [64].

The research presented in this chapter details the isolation, sequencing and bioactivity of peptides from *L. dahlii* and compares the peptides found with those from *L. aurea* and *L. raniformis*.

2.2 Results

2.2a General

A skin secretion was obtained from a single specimen of *Litoria dahlii* using the surface electrical stimulation method [45]. The peptide components of the secretion were purified using HPLC. Eleven peptides were obtained with retention times greater than 27 minutes. The elution profile for this region is shown in Figure 2.3 with the isolated peptides labelled A-K. Peptides that eluted previously included the neuropeptide caerulein (1), which was identified by its retention time and electrospray mass spectrum. This peptide is often a major component of secretions from the *Litoria* genus [12]. The remaining peptides ~~from this region~~ eluting prior to 27 minutes were not fully characterised and will not be discussed here.

(1) Caerulein pEQDY(SO_3)TGWMDF-NH_2

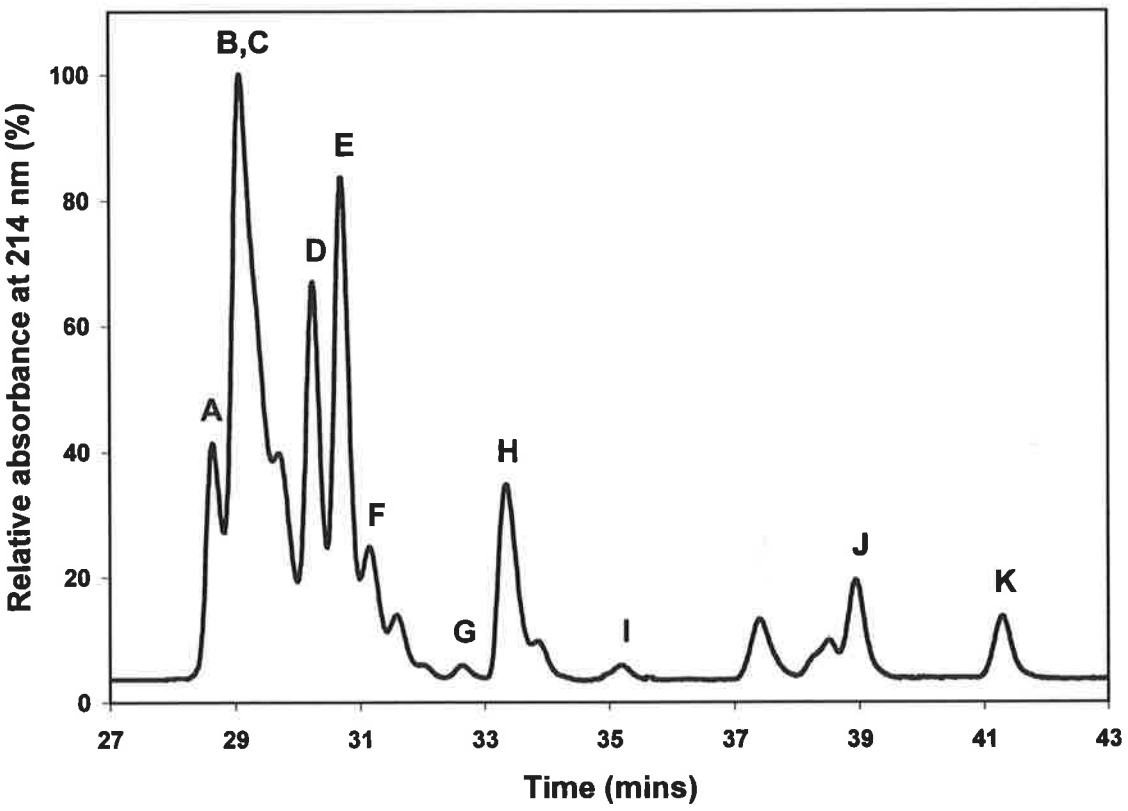

Figure 2.3 Partial chromatogram of the HPLC separation of skin secretion taken from *Litoria dahlii*. The gradient used was 10-70% acetonitrile/H_2O over 60 minutes, at a constant concentration of trifluoroacetic acid (0.1%). The absorbance is expressed as a percentage of the maximal absorbance.

The peptides obtained by HPLC were sequenced by mass spectrometry using the tandem MS (MS/MS) capabilities of a Q-TOF 2 mass spectrometer. Lysine and glutamine residues were assigned on the basis of the Lys-C digest and methylation experiments. The results were confirmed by automated Edman sequencing, which was also employed to distinguish between the isomeric leucine and isoleucine residues. The correct residue is always shown in the text. The accuracy of the Q-TOF 2 was such that the identity of the C-terminal group could be determined using the MS/MS spectrum alone. Methylation experiments verified these conclusions, except in the case of dahlein 4.3 where methylation experiments were unsuccessful.

The eleven isolated peptides have been named dahleins and their sequences are detailed in Table 2-1. Three groups of related peptides were identified and the structure determination of a representative from each of these groups will be described in detail in subsequent sections. The structure determinations of the remaining peptides are summarised in Tables 2-2, 2-3 and 2-4. The masses given are all nominal masses, i.e., the masses produced by summation of the integral mass of each amino acid residue.

Table 2-1 Peptides isolated from the skin secretion of *Litoria dahlii*. The table indicates the number assigned to the peptide, the sequence, nominal molecular weight (MW) and the HPLC fraction the peptide came from (Figure 2.3).

Dahlein	Sequence	MW	HPLC fraction
1.1	GLFDIIKNIVSTL-NH_2	1431	K
1.2	GLFDIIKNIFSGL-NH_2	1435	J
4.1	GLWQLIKDKIKDAATGFVTGIQS-NH_2	2487	D
4.2	GLWQFIKDKLKDAATGLVTGIQS-NH_2	2487	E
4.3	GLWQFIKDKFKDAATGLVTGIQS-NH_2	2521	A
5.1	GLLGSIGNAIGAFIANKLKP-OH	1953	I
5.2	GLLGSIGNAIGAFIANKLKPK-OH	2081	H
5.3	GLLASLGKVLGGYLAEKLKP-OH	2026	G
5.4	GLLASLGKVLGGYLAEKLKPK-OH	2154	F
5.5	GLLGSIGKVLGGYLAEKLKPK-OH	2140	B
5.6	GLLASLGKVFGGYLAEKLKPK-OH	2188	C

The numbering of the peptides in Table 2-1 follows that used for the five groups of aurein peptides isolated from *L. aurea* and *L. raniformis*, since there are similarities between the dahleins 1, 4 and 5 and the aureins 1, 4 and 5. Interestingly, no dahlein peptides were found to correspond to the aurein 2 and aurein 3 broad-spectrum antibiotics (e.g. aurein 2.2 (13) and aurein 3.1 (14) above).

2.2b Dahlein 1.2

The final two peptides to elute from the HPLC column were two related peptides of low molecular weight. This group of peptides was named the dahleins 1. Analysis of dahlein 1.2 by ESI-MS shows an intense MH^+ peak at *m/z* 1435. The CID mass spectrum (MS/MS) of this MH^+ parent ion is shown in Figure 2.4.

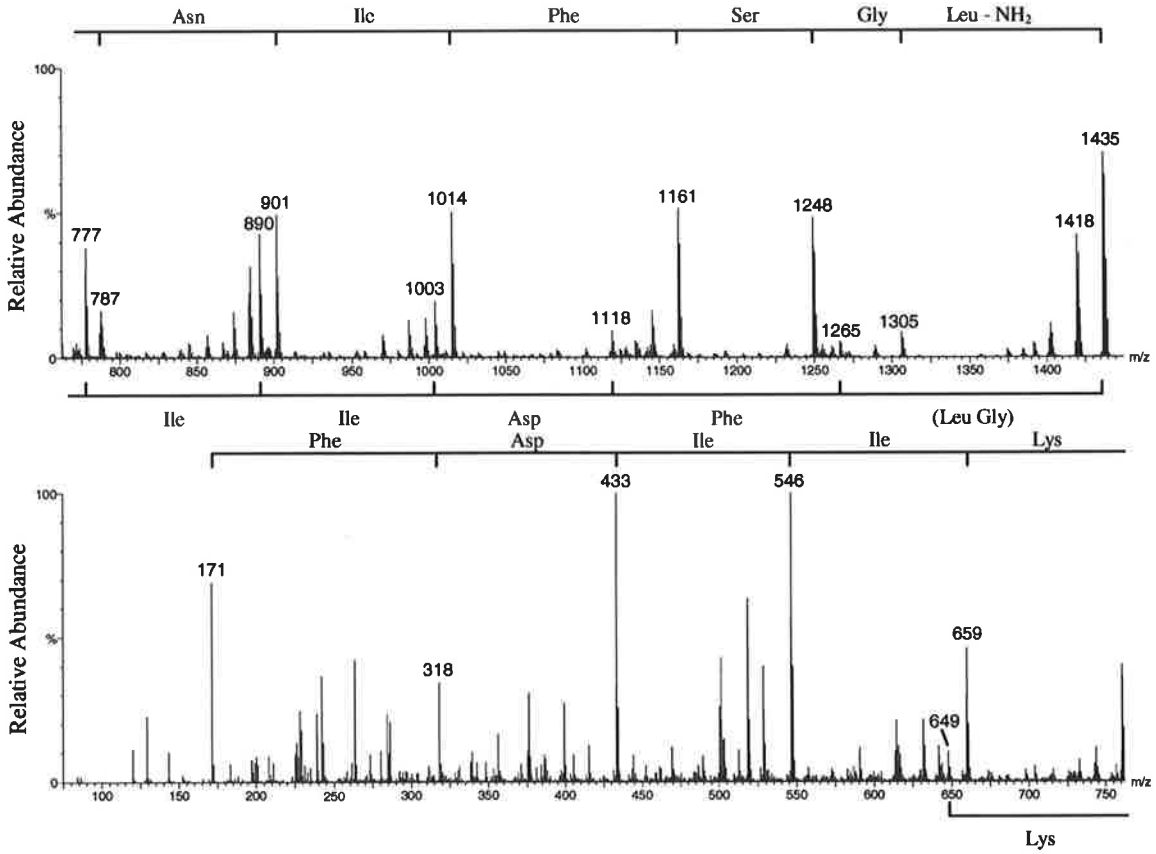

Figure 2.4 MS/MS of MH^+ 1435 of dahlein 1.2. The sequence derived from the B cleavages is shown above the spectrum, while that from the Y+2 cleavages is indicated beneath the spectrum. (See Experimental for full details).

The sequence of amino acids from the C-terminal end is given by the B cleavage ions, while the Y+2 ions indicate the N-terminal sequence. From the data in Figure 2.4 we obtain the partial sequence of (170) Phe Asp Ile Ile Lys Asn Ile Phe Ser Gly Leu–NH_2.

The C-terminal group was shown to be an amide due to the peak at *m/z* 1418 i.e., loss of 17 Da from the parent ion (loss of 18 Da indicates an acid group). The first two residues of the sequence could not be determined from this spectrum. Lys-C digestion of dahlein 1.2 gave fragments at *m/z* 805 and 649, confirming the assignment of residue 7 as lysine. Both fragments were sequenced by MS/MS data but only the sequence of *m/z* 805 was required to complete the primary structure of dahlein 1.2. Figure 2.5 shows the MS/MS spectrum for this fragment, which reveals the sequence to be Gly Leu Phe Asp Ile Ile Lys-OH.

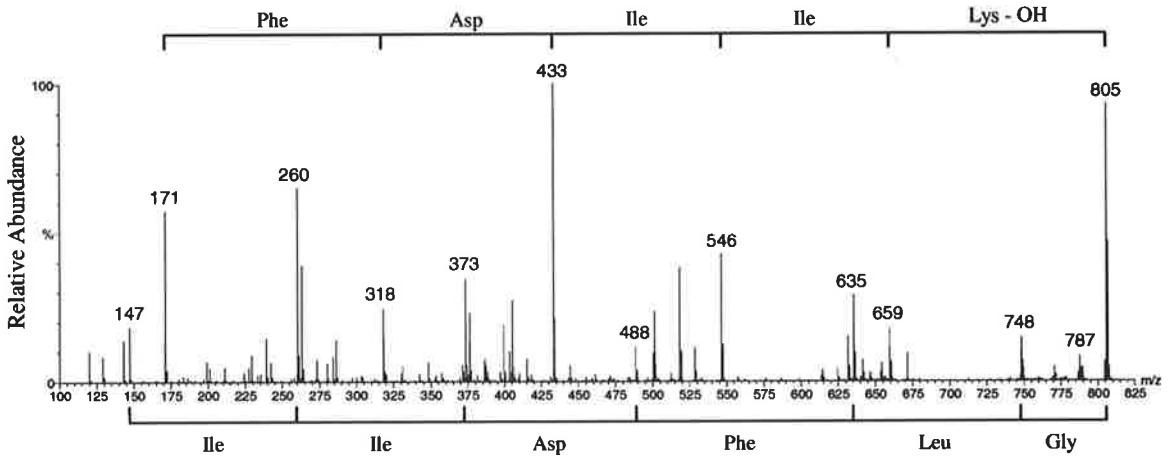

Figure 2.5 MS/MS of the Lys-C fragment MH^+ 805 of dahlein 1.2. The sequence derived from the B cleavages is shown above the spectrum, while that from the Y+2 cleavages is indicated beneath the spectrum. (See Experimental for full details).

Methylation experiments on dahlein 1.2 produced a methyl ester, MH^+ 1479. This represents a difference in mass of 44 Da, which indicates the presence of one CO_2H group and two $CONH_2$ groups. According to the sequence obtained from the MS/MS data there is one Asp residue and one Asn residue present, which account for the acid group and one of the amide groups. Thus the terminal group is an amide, confirming the conclusions from the original MS/MS spectrum.

The final sequence for dahlein 1.2 is thus Gly Leu Phe Asp Ile Ile Lys Asn Ile Phe Ser Gly Leu–NH_2. The sequence was verified by Edman sequencing, which also differentiated between the isoleucine and leucine residues. The sequencing data for this peptide and dahlein 1.1 are summarised in Table 2-2.

Table 2-2 MS data for dahlein 1 peptides isolated from *L. dahlii*.

Dahlein 1.1 [MH^+ 1431]

Methylation gives a methyl ester, MH^+ 1475 (one CO_2H and two $CONH_2$ groups).

MH^+ 1431	B ions	*m/z* 1414, 1301, 1200, 1113, 1014, 901, 787, 659, 546, 433, 318, 171 [(170) Phe Asp Ile Ile Lys Asn Ile Val Ser Thr Leu-NH_2]
	Y+2 ions	*m/z* 1114, 999, 886, 773, 645, 531, 418, 319 [(317) Asp Ile Ile Lys Asn Ile Val (318)]

Lys-C digest gives MH^+ 645 and 805

MH^+ 805	B ions	*m/z* 787, 659, 546, 433, 318, 171 [(170) Phe Asp Ile Ile Lys-OH]
	Y+2 ions	*m/z* 748, 635, 488, 260, 147 [Gly Leu Phe (228) Ile (Lys-OH)]
	Sequence	Gly Leu Phe Asp Ile Ile Lys-OH

Dahlein 1.1 sequence: Gly Leu Phe Asp Ile Ile Lys Asn Ile Val Ser Thr Leu-NH_2

Dahlein 1.2 [MH^+ 1435]

Methylation gives a methyl ester, MH^+ 1479 (one CO_2H and two $CONH_2$ groups).

MH^+ 1435	B ions	*m/z* 1418, 1305, 1248, 1161, 1014, 901, 787, 659, 546, 433, 318, 171 [(170) Phe Asp Ile Ile Lys Asn Ile Phe Ser Gly Leu-NH_2]
	Y+2 ions	*m/z* 1265, 1118, 1003, 890, 777, 649 [(170) Phe Asp Ile Ile Lys (648)]

Lys-C digest gives MH^+ 649 and 805

MH^+ 805	B ions	*m/z* 787, 659, 546, 433, 318, 171 [(170) Phe Asp Ile Ile Lys-OH]
	Y+2 ions	*m/z* 748, 635, 488, 373, 260, 147 [Gly Leu Phe Asp Ile Ile (Lys-OH)]
	Sequence	Gly Leu Phe Asp Ile Ile Lys-OH

Dahlein 1.2 sequence: Gly Leu Phe Asp Ile Ile Lys Asn Ile Phe Ser Gly Leu-NH_2

2.2c Dahlein 4.1

Dahlein 4.1 gives only a weak MH^+ ion, but a pronounced $[M+2H]^{2+}$ species is evident at *m/z* 1244. The MS/MS spectrum of the $[M+2H]^{2+}$ ion is shown below in Figure 2.6.

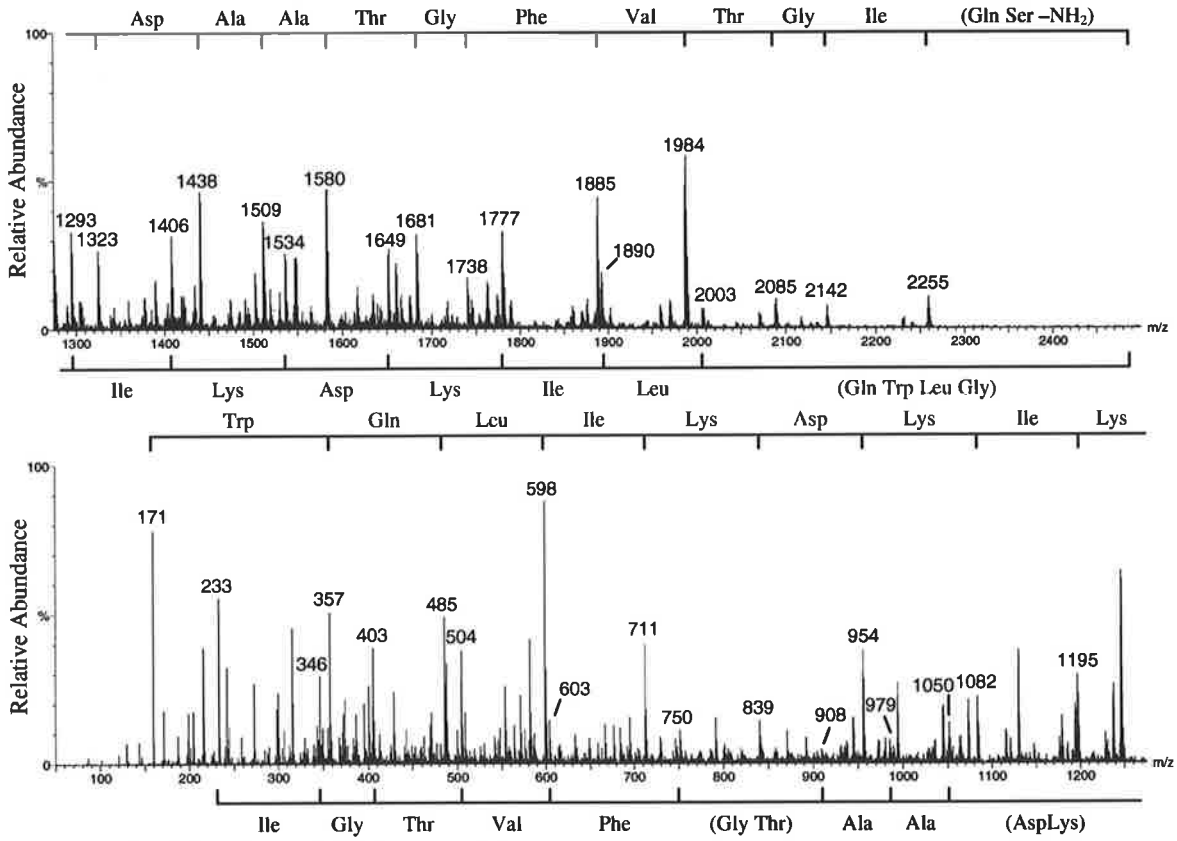

Figure 2.6 MS/MS of $[M+2H]^{2+}$ 1244 of dahlein 4.1. The sequence derived from the B cleavages is shown above the spectrum, while that from the Y+2 cleavages is indicated beneath the spectrum. (See Experimental for full details).

The data in Figure 2.6 indicate a partial amino acid sequence of (170) Trp Gln Leu Ile Lys Asp Lys Ile Lys Asp Ala Ala Thr Gly Phe Val Thr Gly Ile (232). Treatment of the peptide with Lys-C endoprotease gave four smaller peptides with MH^+ at 857, 1090, 1165 and 1406, indicating the presence of lysine residues at positions 7, 9 and 11. The collisionally induced MS/MS spectrum of the fragment with *m/z* 1165 is presented in Figure 2.7. This spectrum reveals the sequence of the final twelve residues as (Asp Ala) Ala Thr Gly Phe Val Thr Gly Ile Gln Ser–NH_2. The data from the mass spectrum of *m/z* 857 is listed in Table 2-3 and gives the first six residues of dahlein 4.1 as Gly Leu Trp Gln Leu Ile Lys–OH.

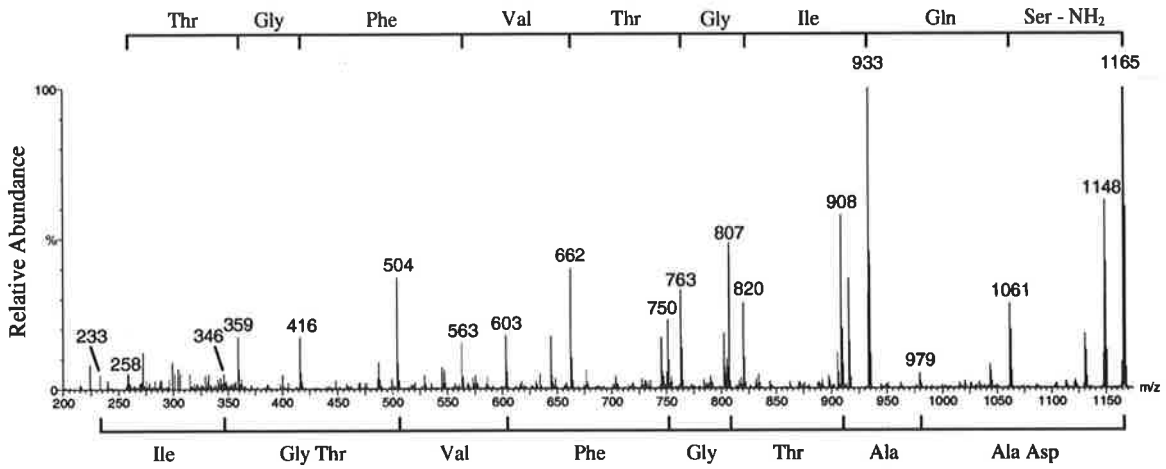

Figure 2.7 MS/MS of the Lys-C fragment MH^+ 1165 of dahlein 4.1. The sequence derived from the B cleavages is shown above the spectrum, while that from the Y+2 cleavages is indicated beneath the spectrum. (See Experimental for full details).

Methylation of dahlein 4.1 gives an ester with an $[M+2H]^{2+}$ ion at *m/z* 1280.5, indicating a mass difference of 73 Da between the ester and the parent peptide. Thus, dahlein 4.1 contains three amides and two carboxylic acid groups. Two acid and two amide-containing residues occur in the sequence so an amide group must be present at the C-terminal. This was also suggested by the $[M+2H-NH_3]^{2+}$ ion present at *m/z* 1235.5 in the MS/MS spectrum of dahlein 4.1. Combining all the MS results gives a final sequence of Gly Leu Trp Gln Leu Ile Lys Asp Lys Ile Lys Asp Ala Ala Thr Gly Phe Val Thr Gly Ile Gln Ser–NH_2, which was confirmed by Edman sequencing. The data obtained for the three dahlein 4 peptides are listed in Table 2-3.

Table 2-3 MS data for the dahlein 4 peptides isolated from *L. dahlii*.

Dahlein 4.1 [MH^+ 2487]

Methylation gives a methyl ester, $[M+2H]^{2+}$ 1280.5 (two CO_2H groups and three $CONH_2$).

$[M+2H]^{2+}$ 1244	$[M+2H\text{-}NH_3]^{2+}$ 1235.5	
	B ions	*m/z* 2255, 2142, 2085, 1984, 1885, 1738, 1681, 1580, 1509, 1438, 1323, 1195, 1082, 954, 839, 711, 598, 485, 357, 171 [(170) Trp Gln Leu Ile Lys Asp Lys Ile Lys Asp Ala Ala Thr Gly Phe Val Thr Gly Ile (232)]
	Y+2 ions	*m/z* 2003, 1890, 1777, 1649, 1534, 1406, 1293, 1050, 979, 908, 807, 750, 603, 504, 403, 346, 233 [(484) Leu Ile Lys Asp Lys Ile (243) Ala Ala Thr Gly Phe Val Thr Gly Ile (232)]

Lys-C digest gives MH^+ 857, 1090, 1165 and 1406

MH^+ 857	B ions	*m/z* 839, 711, 598, 485, 357, 171 [(170) Trp Gln Leu Ile Lys-OH]
	Y+2 ions	*m/z* 800, 687, 501, 373, 260, 147 [Gly Leu Trp Gln Leu Ile (Lys-OH)]
	Sequence	Gly Leu Trp Gln Leu Ile Lys-OH
MH^+ 1165	B ions	*m/z* 1148, 1061, 933, 820, 763, 662, 563, 416, 359, 258 [(257) Thr Gly Phe Val Thr Gly Ile Gln Ser-NH_2]
	Y+2 ions	*m/z* 979, 908, 807, 750, 603, 504, 403, 346, 233 [(Asp Ala) Ala Thr Gly Phe Val Thr Gly Ile (232)]
	Sequence	(Asp Ala) Ala Thr Gly Phe Val Thr Gly Ile Val Thr Gly Ile Gln Ser-NH_2

Dahlein 4.1 sequence:
Gly Leu Trp Gln Leu Ile Lys Asp Lys Ile Lys Asp Ala Ala Thr Gly Phe Val Thr Gly Ile Gln Ser-NH_2

Dahlein 4.2 [MH^+ 2487]

Methylation gives a methyl ester, $[M+2H]^{2+}$ 1280.5 (two CO_2H groups and three $CONH_2$).

$[M+2H]^{2+}$ 1244	$[M+2H\text{-}NH_3]^{2+}$ 1235.5	
	B ions	*m/z* 2255, 2142, 2085, 1984, 1885, 1772, 1715, 1614, 1543, 1472, 1357, 1229, 1116, 988, 873, 745, 632, 485, 357, 171 [(170) Trp Gln Phe Ile Lys Asp Lys Leu Lys Asp Ala Ala Thr Gly Leu Val Thr Gly Ile (232)]
	Y+2 ions	*m/z* 2131, 2003, 1856, 1743, 1615, 1500, 1372, 1259, 1131, 1016, 945, 874, 773, 716, 603, 504, 403, 346, 233 [(356) Gln Phe Ile Lys Asp Lys Leu Asp Ala Ala Thr Gly Leu Val Thr Gly Ile (232)]

Dahlein 4.2 [MH^+ 2487] (continued)

Lys-C digest gives MH^+ 891, 1131 and 1134

MH^+ 891	B ions	*m/z* 873, 745, 632 [(631) Ile Lys-OH]
	Y+2 ions	*m/z* 834, 721, 535, 407, 260, 147 [Gly Leu Trp Gln Phe Ile (Lys-OH)]
	Sequence	Gly Leu Trp Gln Phe Ile Lys-OH
MH^+ 1131	B ions	*m/z* 1114, 1027, 899, 786, 729, 628, 529 [(528) Val Thr Gly Ile Gln Ser-NH_2]
	Y+2 ions	*m/z* 1016, 945, 874, 773, 716, 603, 504 [Asp Ala Ala Thr Gly Phe Val (503)]
	Sequence	Asp Ala Ala Thr Gly Phe Val Thr Gly Ile Gln Ser-NH_2

Dahlein 4.2 sequence:

Gly Leu Trp Gln Phe Ile Lys Asp Lys Leu Lys Asp Ala Ala Thr Gly Leu Val Thr Gly Ile Gln Ser-NH_2

Dahlein 4.3 [MH^+ 2521]

Methylation experiments were unsuccessful for this species

$[M+2H]^{2+}$ 1261	$[M+2H-NH_3]^{2+}$ 1252.5	
	B ions	*m/z* 2176, 2119, 2018, 1919, 1806, 1749, 1648, 1577, 1506, 1391, 1263, 1116, 988, 873, 745, 632, 485, 357, 171 [(170) Trp Gln Phe Ile Lys Asp Lys Phe Lys Asp Ala Ala Thr Gly Leu Val Thr Gly (345)]
	Y+2 ions	*m/z* 2037, 1890, 1777, 1649, 1534, 1406, 1259, 1131, 1016, 945, 874. 716, 603, 504, 403, 346, 233 [(484) Phe Ile Lys Asp Lys Phe Lys Asp Ala Ala (158) Leu Val Thr Gly Ile (232)]

Lys-C digest gives MH^+ 891 and 1131

MH^+ 891	B ions	*m/z* 873, 745, 632, 485, 357, 171 [(170) Trp Gln Phe Ile Lys-OH]
	Y+2 ions	*m/z* 834, 721, 535, 407, 260, 147 [Gly Leu Trp Gln Phe Ile (Lys-OH)]
	Sequence	Gly Leu Trp Gln Phe Ile Lys-OH
MH^+ 1131	B ions	*m/z* 1114, 1027, 899, 786, 729, 628, 529, 416 [(415) Leu Val Thr Gly Ile Gln Ser-NH_2]
	Y+2 ions	*m/z* 945, 874, 773, 716, 603, 504 [(186) Ala Thr Gly Leu Val (503)]
	Sequence	(186) Ala Thr Gly Leu Val Thr Gly Ile Gln Ser-NH_2

Dahlein 4.3 sequence:

Gly Leu Trp Gln Phe Ile Lys Asp Lys Phe Lys Asp Ala Ala Thr Gly Leu Val Thr Gly Ile Gln Ser-NH_2

2.2d Dahlein 5.6

Dahlein 5.6 is a major peptide component that elutes around 29 minutes. Analysis of this compound by ESI-MS indicated a prominent $[M+2H]^{2+}$ peak at *m/z* 1094.5, as well as a minor MH^+ peak at *m/z* 2188. The MS/MS spectrum of the $[M+2H]^{2+}$ ion is shown below in Figure 2.8.

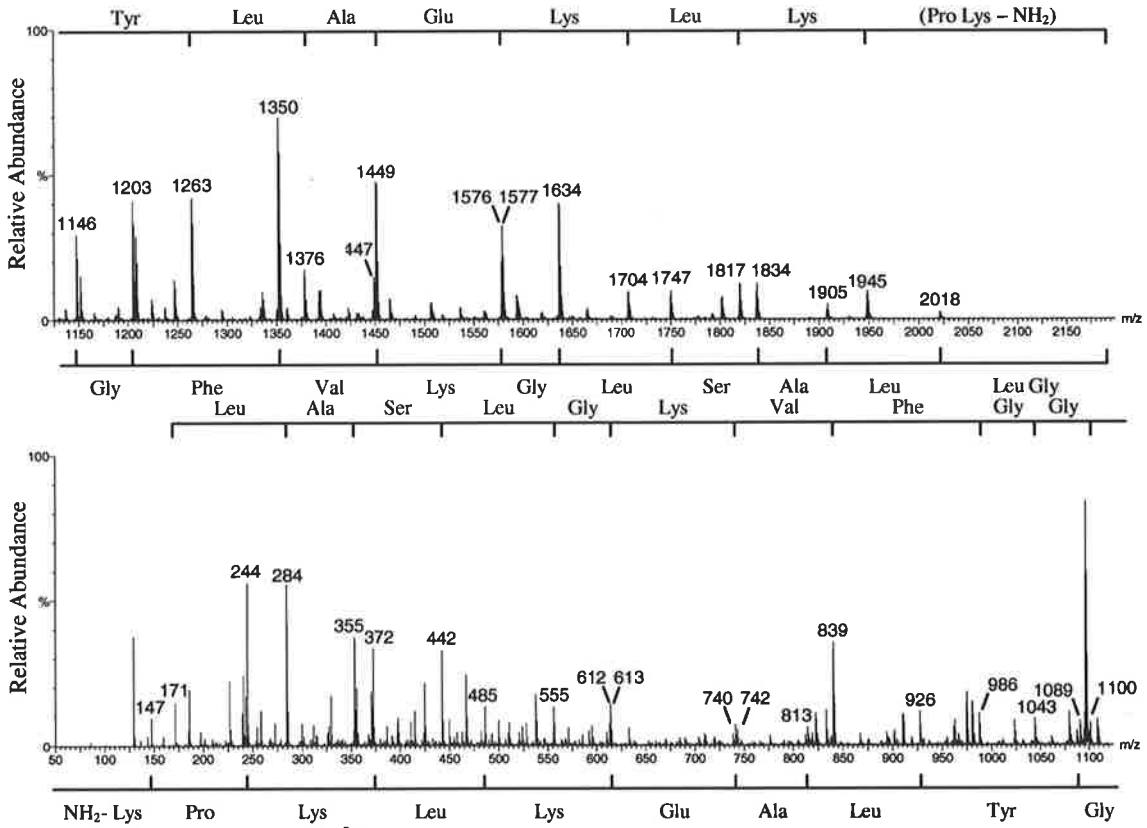

Figure 2.8 MS/MS of $[M+2H]^{2+}$ 1094.5 of dahlein 5.6. The sequence derived from the B cleavages is shown above the spectrum, while that from the Y+2 cleavages is indicated beneath the spectrum. (See Experimental for full details).

Figure 2.8 shows the partial amino acid sequence (170) Leu Ala Ser Leu Gly Lys Val Phe Gly Gly Tyr Leu Ala Glu Lys Leu Lys Pro Lys–OH for dahlein 5.6. Digestion of this peptide with Lys-C endoprotease gave three small peptides with *m/z* 485, 758 and 1449, confirming the presence of lysine residues at positions 8 and 17. The additional lysine residues at positions 19 and 21 were confirmed by Edman sequencing. The MS/MS spectrum of the fragment with MH^+ at *m/z* 758 is shown in Figure 2.9. The data give the sequence of the first eight residues as Gly Leu Leu Ala Ser Leu Gly Lys-OH.

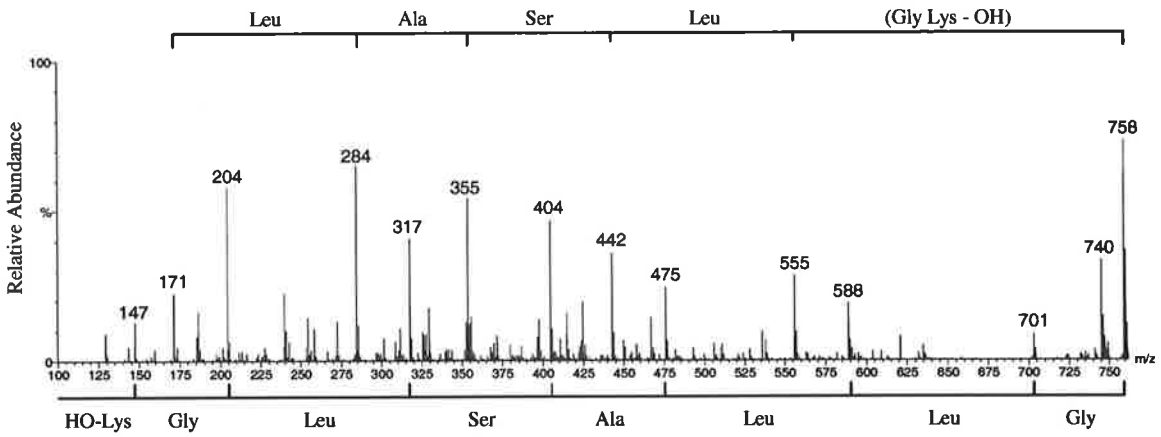

Figure 2.9 MS/MS of the Lys-C fragment MH^+ 758 of dahlein 5.6. The sequence derived from the B cleavages is shown above the spectrum, while that from the Y+2 cleavages is indicated beneath the spectrum. (See Experimental for full details).

Methylation of dahlein 5.6 produced a methyl ester, $[M+2H]^{2+}$ at *m/z* 1108.5, indicating the ester was 28 Da greater in mass than the parent peptide. Thus, dahlein 5.6 contains two acid groups and the C-terminal group must therefore be a carboxylic acid. This agrees with the assignment made from close inspection of the MS/MS spectrum of dahlein 5.6, which shows a peak at *m/z* 1085.5 due to the $[M+2H-H_2O]^{2+}$ ion. Thus we have the final sequence of Gly Leu Leu Ala Ser Leu Gly Lys Val Phe Gly Gly Tyr Leu Ala Glu Lys Leu Lys Pro Lys–OH. The MS structural data for all six dahlein 5 peptides are summarised in Table 2-4.

Dahleins 5.3-5.6 were found to contain tyrosine residues. In the more than 200 peptides characterised from Australian anurans, the only peptides shown to contain tyrosine have been the caerulein and caerulein-like neuropeptides, which are only active when the tyrosine residues are sulfated. Peptides containing sulfated tyrosine residues produce only weak MH^+ ions but have pronounced peaks in their mass spectra due to $[MH^+-SO_3]^+$ ions [26]. Thus, it is possible to miss the existence of a sulfate group using positive ion MS. Negative ion mass spectra, however, clearly indicate the presence of a sulfate group because strong peaks are observed for both the $[M-H]^-$ and $[(M-H)-SO_3]^-$ ions [26]. Negative ion spectra were recorded for dahleins 5.3-5.6 and no evidence was found for sulfation of the tyrosine residues.

Table 2-4 MS data for the dahlein 5 peptides isolated from *L. dahlii*.

Dahlein 5.1 [MH^+ 1953]

Methylation gives a methyl ester, $[M+2H]^{2+}$ 999 (one CO_2H and two $CONH_2$ groups).

$[M+2H]^{2+}$ 977	$[M+2H-H_2O]^{2+}$ 968	
	B ions	*m/z* 1935, 1838, 1710, 1597, 1469, 1355, 1284, 1171, 1024, 953, 896, 783 [(782) Ile Gly Ala Phe Ile Ala Asn Lys Leu Lys Pro-OH]
	Y+2 ions	*m/z* 1953, 1783, 1670, 1613, 1526, 1413, 1356, 1242, 1171, 1058, 1001, 930, 783, 670 [(170) Leu Gly Ser Ile Gly Asn Ala Ile Gly Ala Phe Ile (669)]

Lys-C digest gives MH^+ 357 and $[M+2H]^{2+}$ 808

	B ions	*m/z* 1469, 1355, 1284, 1171, 1024, 953, 896, 783, 712, 598, 541 [(540) Gly Asn Ala Ile Gly Ala Phe Ile Ala Asn (Lys-OH)]
	Y+2 ions	*m/z* 1445, 1332, 1275, 1188, 1075, 1018, 904, 833, 720, 663, 592, 445 [(170) Leu Gly Ser Ile Gly Asn Ala Ile Gly Ala Phe (444)]
	Sequence	(170) Leu Gly Ser Ile Gly Asn Ala Ile Gly Ala Phe Ile Ala Asn (Lys-OH)

Dahlein 5.1 sequence:
Gly Leu Leu Gly Ser Ile Gly Asn Ala Ile Gly Ala Phe Ile Ala Asn Lys Leu Lys Pro-OH

Dahlein 5.2 [MH^+ 2082]

Methylation gives a methyl ester, $[M+2H]^{2+}$ 1063 (one CO_2H and two $CONH_2$ groups).

$[M+2H]^{2+}$ 1041	$[M+2H-H_2O]^{2+}$ 1032	
	B ions	*m/z* 1935, 1838, 1710, 1469, 1355, 1284, 1171, 1024, 953, 896, 783, 712, 598, 541, 428, 341, 284, 171 [(170) Leu Gly Ser Ile Gly Asn Ala Ile Gly Ala Phe Ile Ala Asn (241) Lys Pro (Lys-OH)]
	Y+2 ions	*m/z* 1911, 1798, 1741, 1654, 1541, 1484, 1370, 1299, 1186, 1129, 1058, 911, 798, 727, 613, 485, 372, 244, 147 [(170) Leu Gly Ser Ile Gly Asn Ala Ile Gly Ala Phe Ile Ala Asn Lys Leu Lys Pro (Lys-OH)]

Lys-C digest gives MH^+ 485 and 1615

MH^+ 1615	B ions	*m/z* 1597, 1469, 1355, 1284, 1171, 1024, 953, 896, 783 [(782) Ile Gly Ala Phe Ile Ala Asn Lys-OH]
	Y+2 ions	*m/z* 1445, 1332, 1275, 1188, 1075, 1018, 904, 833, 720, 663, 592 [(170) Leu Gly Ser Ile Gly Asn Ala Ile Gly Ala (591)]
	Sequence	(170) Leu Gly Ser Ile Gly Asn Ala Ile Gly Ala Phe Ile Ala Asn Lys-OH

Dahlein 5.2 sequence:
Gly Leu Leu Gly Ser Ile Gly Asn Ala Ile Gly Ala Phe Ile Ala Asn Lys Leu Lys Pro Lys-OH

Dahlein 5.3 [MH^+ 2026]

Methylation gives a methyl ester, $[M+2H]^{2+}$ 1027.5 (two CO_2H groups).

$[M+2H]^{2+}$ 1013.5 $[M+2H-H_2O]^{2+}$ 1004.5

B ions	*m/z* 1911, 1783, 1670, 1542, 1413, 1342, 1229, 1066, 1009, 952, 839, 740, 612, 555, 442, 355, 284, 171 [(170) Leu Ala Ser Leu Gly Lys Val Leu Gly Gly Tyr Leu Ala Glu Lys Leu Lys (Pro-OH)]
Y+2 ions	*m/z* 1856, 1743, 1672, 1585, 1472, 1415, 1287, 1188, 1075, 1018, 961, 798, 685, 614, 485, 357, 244 [(170) Leu Ala Ser Leu Gly Lys Val Leu Gly Gly Tyr Leu Ala Glu Lys Leu (243)]

Lys-C digest gives MH^+ 758 and 1287

MH^+ 758

B ions	*m/z* 740, 612, 555, 442, 355, 284, 171 [(170) Leu Ala Ser Leu Gly Lys -OH]
Y+2 ions	*m/z* 701, 588, 475, 404, 317, 204, 147 [Gly Leu Leu Ala Ser Leu Gly (Lys-OH)]
Sequence	Gly Leu Leu Ala Ser Leu Gly Lys-OH

Dahlein 5.3 sequence:

Gly Leu Leu Ala Ser Leu Gly Lys Val Leu Gly Gly Tyr Leu Ala Glu Lys Leu Lys Pro-OH

Dahlein 5.4 [MH^+ 2140]

Methylation gives a methyl ester, $[M+2H]^{2+}$ 1084.5 (two CO_2H groups).

$[M+2H]^{2+}$ 1070.5 $[M+2H-H_2O]^{2+}$ 1061.5

B ions	*m/z* 1897, 1769, 1656, 1528, 1399, 1328, 1215, 1052, 995, 938, 825, 726, 598, 541, 428, 341, 284, 171 [(170) Leu Gly Ser Ile Gly Lys Val Leu Gly Gly Tyr Leu Ala Glu Lys Leu Lys (243)]
Y+2 ions	*m/z* 1857, 1800, 1713, 1600, 1543, 1415, 1316, 1203, 1146, 1089, 926, 813, 742, 613, 485, 372, 244, 147 [(283) Gly Ser Ile Gly Lys Val Leu Gly Gly Tyr Leu Ala Glu Lys Leu Lys Pro (Lys-OH)]

Lys-C digest gives MH^+ 485, 744 and 1415

MH^+ 744

B ions	*m/z* 726, 598, 541, 428, 341, 284, 171 [(170) Leu Gly Ser Ile Gly Lys-OH]
Y+2 ions	*m/z* 687, 574, 461, 404, 317, 204, 147 [Gly Leu Leu Gly Ser Ile Gly (Lys-OH)]
Sequence	Gly Leu Leu Gly Ser Ile Gly Lys-OH

Dahlein 5.4 sequence:

Gly Leu Leu Gly Ser Ile Gly Lys Val Leu Gly Gly Tyr Leu Ala Glu Lys Leu Lys Pro Lys-OH

Dahlein 5.5 [MH^+ 2154]

Methylation gives a methyl ester, $[M+2H]^{2+}$ 1091.5 (two CO_2H groups).

$[M+2H]^{2+}$ 1077.5 $[M+2H-H_2O]^{2+}$ 1068.5

B ions	*m/z* 1911, 1783, 1670, 1542, 1413, 1342, 1229, 1066, 1009, 952, 839, 740, 612, 555, 442, 355, 284, 171 [(170) Leu Ala Ser Leu Gly Lys Val Leu Gly Gly Tyr Leu Ala Glu Lys Leu Lys (243)]
Y+2 ions	*m/z* 1871, 1800, 1713, 1600, 1543, 1415, 1316, 1203, 1146, 1089, 926, 813, 742, 613, 485, 372, 244, 147 [(283) Ala Ser Leu Gly Lys Val Leu Gly Gly Tyr Leu Ala Glu Lys Leu Lys Pro (Lys-OH)]

Lys-C digest gives MH^+ 758 and 1415

MH^+ 758

B ions	*m/z* 740, 612, 555, 442, 355, 284, 171 [(170) Leu Ala Ser Leu Gly Lys-OH]
Y+2 ions	*m/z* 701, 588, 475, 404, 317, 204, 147 [Gly Leu Leu Ala Ser Leu Gly (Lys-OH)]
Sequence	Gly Leu Leu Ala Ser Leu Gly Lys-OH

Dahlein 5.5 sequence:

Gly Leu Leu Ala Ser Leu Gly Lys Val Leu Gly Gly Tyr Leu Ala Glu Lys Leu Lys Pro Lys-OH

Dahlein 5.6 [MH^+ 2188]

Methylation gives a methyl ester, $[M+2H]^{2+}$ 1108.5 (two CO_2H groups).

$[M+2H]^{2+}$ 1094.5 $[M+2H-H_2O]^{2+}$ 1085.5

B ions	*m/z* 1945, 1817, 1704, 1576, 1447, 1376, 1263, 1100, 1043, 986, 839, 740, 612, 555, 442, 355, 284, 171 [(170) Leu Ala Ser Leu Gly Lys Val Phe Gly Gly Tyr Leu Ala Glu Lys Leu Lys (243)]
Y+2 ions	*m/z* 2018, 1905, 1834, 1747, 1634, 1577, 1449, 1350, 1203, 1146, 1089, 926, 813, 742, 613, 485, 372, 244, 147 [(170) Leu Ala Ser Leu Gly Lys Val Phe Gly Gly Tyr Leu Ala Glu Lys Leu Lys Pro (Lys-OH)]

Lys-C digest gives MH^+ 485, 758 and 1449

MH^+ 758

B ions	*m/z* 740, 555, 442, 355, 284, 171 [Gly Leu Leu Ala Ser Leu (185)-OH]
Y+2 ions	*m/z* 701, 588, 475, 404, 317, 204, 147 [Gly Leu Leu Ala Ser Leu Gly (Lys-OH)]
Sequence	Gly Leu Leu Ala Ser Leu Gly Lys-OH

Dahlein 5.6 sequence:

Gly Leu Leu Ala Ser Leu Gly Lys Val Phe Gly Gly Tyr Leu Ala Glu Lys Leu Lys Pro Lys-OH

2.2e Bioactivity Testing

Selected dahlein peptides were synthesised commercially for bioactivity testing. Each synthetic peptide was shown to be identical to the natural version using mass spectrometry. Two peptides from each dahlein group were then tested for antibiotic activity. The results are given in Table 2-5, which also gives the activity of aureins 1.1, 1.2 and 5.2 for comparison. Here it can be seen that the dahleins 1 show some broad-spectrum activity against Gram-positive (G+) bacterial species, similar to that found for the aurein 1 peptides. On the other hand, the dahleins 4 and 5, like the corresponding aurein peptides, have minimal activity toward only one or two species. In contrast to *L. raniformis* and *L. aurea*, *L. dahlii* has no potent broad-spectrum antibacterial peptides.

Table 2-5 Dahlein antibiotic activities and comparison with the activity of aureins 1.1, 1.2 and 5.2. The activity is given as MIC values ($\mu g \cdot mL^{-1}$).

Peptide	Sequence
Dahlein	
1.1	GLFDIIKNIVSTL-NH_2
1.2	GLFDIIKNIFSGL-NH_2
4.1	GLWQLIKDKIKDAATGFVTGIQS-NH_2
4.2	GLWQFIKDKLKDAATGLVTGIQS-NH_2
5.1	GLLGSIGNAIGAFIANKLKP-OH
5.6	GLLASLGKVFGGYLAEKLKPK-OH
Aurein	
1.2	GLFDIIKKIAESF-NH_2
5.2	GLMSSIGKALGGLIVDVLKPKTPAS-OH

	MIC ($\mu g \cdot mL^{-1}$)[a]								
Organism	**Dahlein**						**Aurein**[b]		
	1.1	**1.2**	**4.1**	**4.2**	**5.1**	**5.6**	**1.1**	**1.2**	**5.2**
Bacillus cereus	100	100					50	100	
Escherichia coli									
Leuconostoc lactis	25	25	100	50	50	12	25	12	100
Listeria innocua							100	100	
Micrococcus luteus					100			100	
Pasteurella multocida								100	
Staphylococcus aureus	100	100						50	
Staphylococcus epidermis	100	100						50	
Streptococcus uberis	100	50				100	100	50	50

[a] Where there is no figure listed the MIC value is >100 $\mu g \cdot mL^{-1}$.
[b] Data for the aurein peptides are from Rozek *et al.* [14]

Six representative dahlein peptides have been tested for anticancer activity by the National Cancer Institute (Washington DC, USA). The preliminary assay involves *in vitro* testing against three human tumour cell-lines – MCF7 (breast), NCI-H460 (lung) and SF-268 (central nervous system) – using a single peptide concentration (1×10^{-4} M). Compounds shown to be active are passed on for second phase testing against a full panel of 55 tumour cell lines. The results of the first and second phase tests are indicated in Table 2-6, showing that five out of the six peptides were active at a concentration of 1×10^{-4} M. Second-phase testing showed that only dahleins 5.3 and 5.6 were active at lower concentrations (1×10^{-5} M). Dahlein 4.3 was found to be inactive like its aurein counterparts. In contrast, the dahleins 5 were found to be active, while the corresponding aurein peptides are inactive [14].

Table 2-6 Anticancer activity of selected dahlein peptides. Data from the NCI testing programme [66]; asterisks indicate that the peptide was found to be active in preliminary testing but did not show activity against tumours at concentrations below 1×10^{-4} M. Activities are given as LC_{50} values, the minimum molar concentrations required to kill 50% of the cancer cells; these are shown as *n* as in 1×10^{-n} M.

Peptide	Sequence	
Dahlein		
1.1	GLFDIIKNIVSTL-NH_2*	
1.2	GLFDIIKNIFSGL-NH_2*	
4.3	GLWQFIKDKFKDAATGLVTGIQS-NH_2	
5.2	GLLGSIGNAIGAFIANKLKPK-OH*	
5.3	GLLASLGKVLGGYLAEKLKP-OH	
5.6	GLLASLGKVFGGYLAEKLKPK-OH	
Cancer[a]	**5.3**	**5.6**
Leukemia	>5	5
Lung	5	5
Colon	5	5
CNS	5	5
Melanoma	5	5
Ovarian	5	5
Renal	5	5
Prostate	5	5
Breast	5	5
Total[b]	39	38

[a] The cancers listed indicate the cancer groupings not the individual cancers within a particular grouping.
[b] Total number of cancers (out of 55) that each peptide is active against within the concentration range given.

Peptides were tested for inhibition of the enzyme nNOS by the Australian Institute of Marine Science (Queensland, Australia). The results for selected dahlein 1 and 5 peptides, given in Table 2-7, show that while the dahlein 1 peptides show minor activity, the dahleins 5 are highly potent, with activity comparable to that of the most active amphibian peptides found so far [29]. At the time of writing, the testing of the dahlein 4 group of peptides had not been completed.

Table 2-7 Inhibition of nNOS by dahlein peptides, given as IC_{50} values (μM).

Dahlein	Sequence	IC_{50} (μM)
1.1	GLFDIIKNIVSTL-NH_2	>70
1.2	GLFDIIKNIFSGL-NH_2	>70
5.1	GLLGSIGNAIGAFIANKLKP-OH	3.2
5.2	GLLGSIGNAIGAFIANKLKPK-OH	2.6
5.3	GLLASLGKVLGGYLAEKLKP-OH	3.0
5.6	GLLASLGKVFGGYLAEKLKPK-OH	3.5

2.3 Discussion

2.3a Peptides from *Litoria dahlii*

The skin secretion of *L. dahlii* has been analysed, revealing the presence of caerulein, as well as 11 novel peptides named dahleins 1.1-5.6. Caerulein is a potent neuropeptide that acts on smooth muscle to regulate temperature, induce sedation and act as an analgesic [27]. All frogs from the *Litoria* genus that have been studied so far, with the exception of *L. rubella* and *L. electrica*, secrete this peptide [24, 25].

The sequences of the 11 new dahlein peptides were found to be similar to the aureins 1, 4 and 5 (see below), except that the dahleins 4 were amidated at the C-terminal, while the aureins 4 have C-terminal acid groups.

	Dahlein 1.1	GLFDIIKNIVSTL-NH_2
(9)	Aurein 1.2	GLFDIIKKIAESF-NH_2
	Dahlein 4.1	GLWQLIKDKIKDAATGFVTGIQS-NH_2
(15)	Aurein 4.1	GLIQTIKEKLKELAGGLVTGIQS-OH
	Dahlein 5.6	GLLASLGKVFGGYLAEKLKPK-OH
(11)	Aurein 5.2	GLMSSIGKALGGLIVDVLKPKTPAS-OH

The dahleins 1 were found to be antimicrobially active, with comparable activity to their aurein counterparts. The dahleins 4 and 5, like the corresponding aurein peptides, showed little antibacterial activity. The dahleins 5.3 and 5.6 were shown to inhibit the growth of tumour cells, while the dahleins 1 were only moderately active and dahlein 4.3 was completely inactive.

Interestingly, no potent broad-spectrum antibacterial peptides were identified in the secretion from *L. dahlii*, in marked contrast to the secretions of *L. raniformis* and *L. aurea,* which each contain six or seven such peptides, i.e., the aureins 2 and 3.

The significant similarities between the peptides of *L. dahlii* and those of *L. raniformis* and *L. aurea*, suggest these frogs have a common ancestor. However, the peptide profiles

of the latter two species are much closer and have a number of common peptides, suggesting *L. raniformis* and *L. aurea* are more closely related to each other than they are to *L. dahlii.* Thus, evolutionary divergence of the *L. dahlii* species occurred, probably because of the pressures of climate and predators.

2.3b Structure and Bioactivity of the Dahleins

The three-dimensional structure of aurein 1.2 has been determined (see Section 6.3). It adopts a short amphipathic α-helix structure in the membrane mimicking solvent TFE/H_2O. It is likely that the dahlein 1 peptides also form amphipathic α-helices in membrane-like environments. This is also suggested by the Schiffer-Edmundson projection of dahlein 1.1 (Figure 2.10 (a)), which shows that an amphipathic arrangement of the residues occurs in the α-helical form.

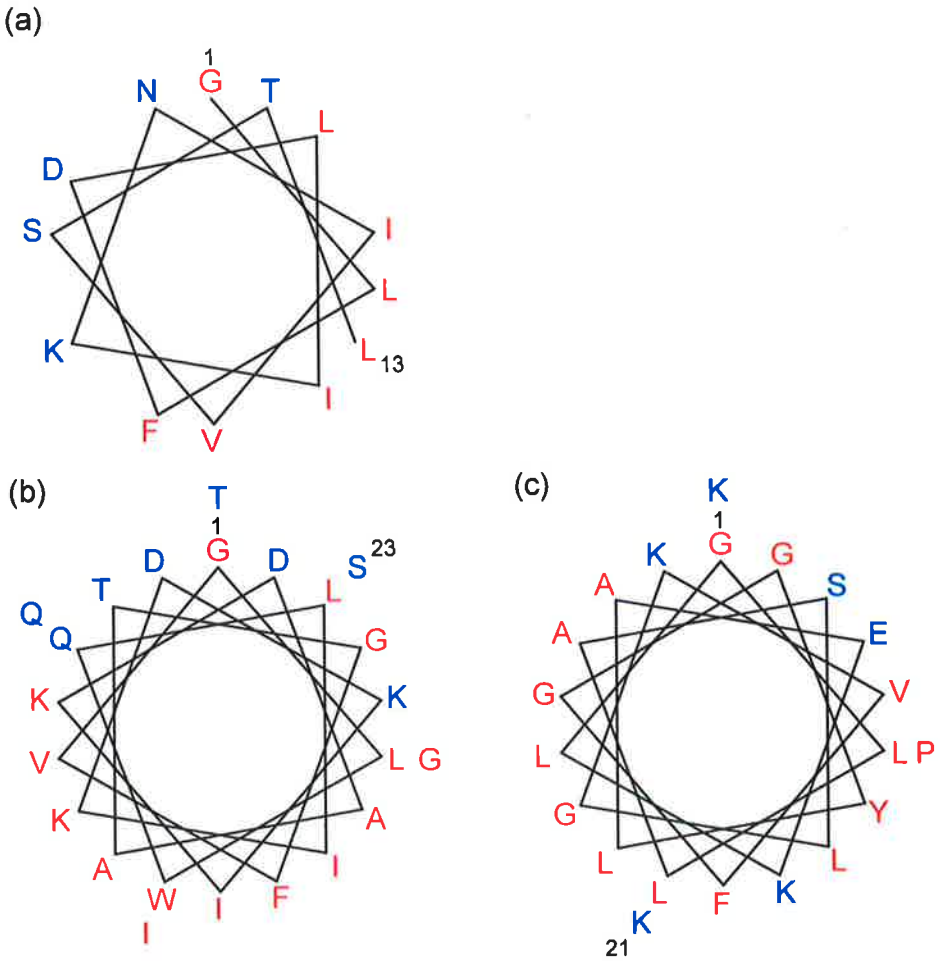

Figure 2.10 Schiffer-Edmundson wheel projections of (a) dahlein 1.1, (b) dahlein 4.1 and (c) dahlein 5.6. Hydrophilic residues are indicated in blue and hydrophobic residues in red [67].

The 'Schiffer-Edmundson' helical wheel diagram is a graphical method for visualising the degree of amphipathicity of a peptide sequence [68]. The wheel gives an end-on view of the helix looking down the long axis. Residues are placed around the wheel at intervals of 100°, corresponding to the 3.6 residues per turn for an ideal α-helix.

The Schiffer-Edmundson projection of dahlein 4.1 (Figure 2.10 (b)) also shows hydrophobic and hydrophilic zones, however the hydrophilic face is less defined because of the leucine residue at position 5. The projection for dahlein 5.6 (Figure 2.10 (c)) does not reveal any clear amphipathic distribution of residues. The disrupted amphipathicity may explain why the dahleins 4 and 5 have only weak antibacterial activity.

Schiffer-Edmundson projections assume that the peptides form linear α-helices. This may not be the case, since all of the dahleins 4 and 5 have at least two glycine residues in their sequences that could induce bends in an α-helical structure. This is particularly true for the dahleins 5.2-5.6, which have two consecutive glycine residues. Schiffer-Edmundson projections of the residues before or after the expected bends still reveal some disruption of the amphipathicity. This is illustrated in Figure 2.11 for dahlein 5.6.

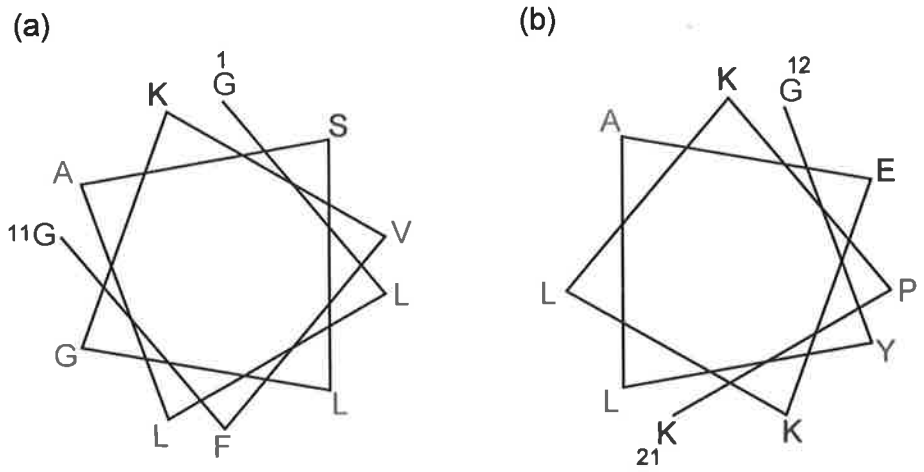

Figure 2.11 Schiffer-Edmundson wheel projections of (a) residues 1-11 and (b) residues 12-21 of dahlein 5.6. Hydrophilic residues are indicated in blue and hydrophobic residues in red [67].

The dahlein 5 peptides have been shown to inhibit nNOS at low concentrations. nNOS is one of three NOS isoforms that catalyse the formation of the signal molecule nitric oxide (NO) from L-arginine. These complex enzymes are composed of two domains – a catalytic oxygenase domain that binds heme, tetrahydrobiopterin and arginine, and an

electron-supplying reductase domain that binds flavin adenine dinucleotide (FAD), flavin mononucleotide (FMN) and nicotinamide adenine nucleotide phosphate (NADPH) [69, 70]. The region connecting the two domains binds the regulatory enzyme calmodulin (CaM), which stimulates electron transfer from the reductase to the oxygenase domains [70].

Inhibitors of NOS can act by competing with the substrate L-arginine, interfering with the binding of cofactors or binding to the enzyme itself and altering its activity [71]. Direct action of the amphibian peptides at the active site has been ruled out by studies on representative amphibian peptide inhibitors, including citropin 1.1 (5), frenatin 3 (4) and caerin 1.9 (16), which show that the inhibition is non-competitive [29].

(5) Citropin 1.1 GLFDVIKKVASVIGGL-NH_2

(4) Frenatin 3 GLMSVLGHAVGNVLGGLFKPKS-OH

(16) Caerin 1.9 GLFGVLGSIAKHVLPHVVPVIAEKL-NH_2

A more likely mechanism has been proposed, where CaM binds the amphibian peptides in preference to the nNOS calmodulin-binding site. CaM is a calcium-binding protein that regulates a large number of enzymes in addition to NOS. The sequences of the CaM binding sites vary greatly from enzyme to enzyme but they generally have some structural features in common. CaM binding sites are typically comprised of 15-20 consecutive residues that form a basic, amphipathic α-helix [72]. The dumbbell shaped CaM protein is thought to wrap around the amphipathic α-helix, in an arrangement stabilised by both hydrophobic and electrostatic interactions [73]. Figure 2.12 shows the interaction between CaM and the CaM binding domain of skeletal muscle myosin light chain kinase (SMMLCK) as revealed by NMR [74].

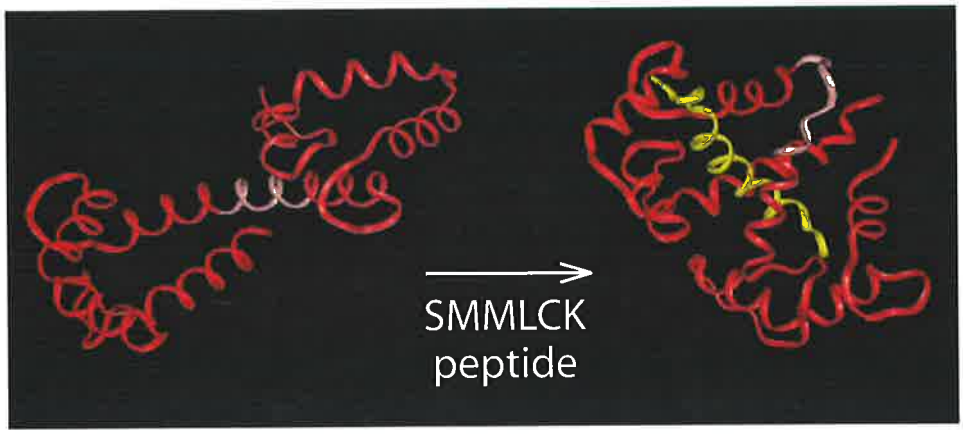

Figure 2.12 CaM (red) binds to the CaM binding domain of SMMLCK (yellow) [74].

Since the antibacterial peptides are also capable of forming basic, amphipathic α-helices, it is possible that they too may bind to CaM. In fact, the bee and wasp peptides melittin (17) and mastoparan (18), which are both haemolytic and antibacterial, have been shown to bind to CaM with dissociation constants (K_d) of 3 nM and 0.3 nM respectively [75, 76]. It is not known, however, whether these peptides inhibit NOS.

(17) Melittin GIGAVLKVLTTGLPALISWIKRKRQQ-NH_2

(18) Mastoparan INLKALAALAKKIL-NH_2

If the amphibian peptides are inhibiting NOS by binding to CaM, then other CaM regulated enzymes, such as calcineurin, should also be affected. Doyle *et al.* [29] tested selected amphibian peptides and found that these peptides did indeed inhibit calcineurin, albeit at higher IC_{50} values than were found for nNOS. Furthermore, Doyle *et al.* [29] showed that when additional CaM is added to the nNOS assay buffer, inhibition by the peptides is significantly reduced. Further studies are necessary, however, to conclusively show that the amphibian peptides are binding to CaM.

Schiffer-Edmundson wheel projections of the dahlein 5 peptides show that they are not perfectly amphipathic, but while amphipathicity does correlate with CaM binding, it need not be flawless for binding to occur [72]. For instance, the hydrophilic face of the rat cerebellar nNOS CaM-binding domain is disrupted by a number of hydrophobic residues, as judged by its wheel projection [77] (Figure 2.13).

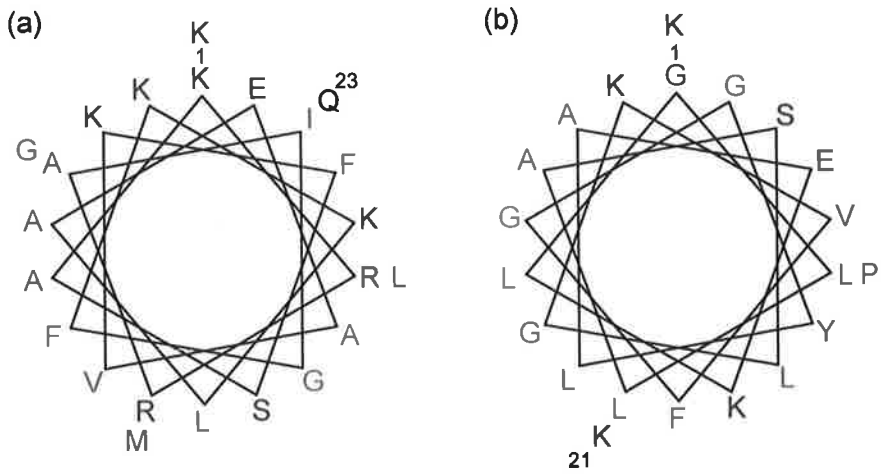

Figure 2.13 Schiffer-Edmundson wheel projections of (a) the rat cerebellar nNOS CaM-binding sequence (-KRRAIGFKKLAEAVKFSAKLMGQ-) and (b) dahlein 5.6. Hydrophilic residues are indicated in blue and hydrophobic residues in red [67].

The dahlein 1 peptides were found to be far less active against nNOS than the dahleins 5, even though the former are more amphipathic. This could be due to the fact that the dahleins 1 only contain a single positively charged residue, while the dahleins 5 contain two to four lysines.

The role of the nNOS inhibitors in the amphibian secretions is not known. The activity could simply be serendipitous, due to the similarities between the structural features required for antibiotic activity and CaM binding, except that a number of nNOS inhibitors have been identified that are not microbially active, including lesueurin (3) from *L. lesueuri* [29].

(3) Lesueurin GLLDILKKVGKVA-NH_2

These peptides must have some other role since it is unlikely the animal would produce and store inactive compounds. If the peptides are exerting their activity by binding to CaM, then they could influence the activity of a large range of enzymes causing a variety of effects. Thus, these peptides could be present to regulate some aspect of the animal's physiology, as has been suggested for other neuropeptides including caerulein [17, 24], or they could act as effective host defence agents.

The dahleins 5 could also have a role in chemical communication since they have sequence homology to splendipherin (10), the male sex pheromone of *L. splendida* [17]. Behavioural studies should be carried out in the future to determine whether or not this is the case.

	Dahlein 5.6	GLLASLGKVFGGYLAEKLKPK-OH
(10)	Splendipherin	GLVSSIGKALGGLLADVVKSKGQPA-OH

2.4 Experimental

2.4a Secretion Collection and Preparation

Glandular secretions from *L. dahlii* specimens were acquired with the assistance of Associate Professor Michael J. Tyler and Mr Ben P. Smith from the Department of Environmental Biology, University of Adelaide, where the animals were housed.

The animals, held by the back legs, were rinsed with de-ionised water to remove debris and improve electrical conduction. Electrical stimulation of the dorsal surface was accomplished using a bipolar electrode of 21G platinum, attached to a C.F. Palmer student model electrical stimulator. The electrode was rubbed gently over the glandular region, in a circular motion, applying 10 V pulses of 3 ms duration.

The resulting secretion was washed off with de-ionised water and an equal volume of HPLC grade methanol added. The resulting mixture was centrifuged and the supernatant concentrated under vacuum to approximately 4 mL.

2.4b HPLC Separation of Glandular Secretion

Secretions were separated by high performance liquid chromatography (HPLC) using the following system components: Walters Millipore Lambda Max 481 LC spectrophotometer, Walters Millipore 510 HPLC pump, Walters Millipore 501 HPLC pump, ICI DP 800 data interface and ICI DP 800 data station.

A VYDAC C18 HPLC column (5 micron, 300A, 4.6 x 250 mm) (Separations Group, Hesperia, CA, USA) was initially equilibrated with 10% acetonitrile/aqueous 0.1% trifluoroacetic acid. For each run 500 µL of secretion was injected. A linear solvent gradient, controlled by the DP 800 data station, increased the acetonitrile content to 70% over 60 minutes at a flow rate of 1 $mL \cdot min^{-1}$. The eluant was monitored by ultra-violet absorbance at 214 nm. The HPLC chromatogram was complex, such that further HPLC separation was required for a number of fractions in order to provide pure compounds. Fractions were collected, concentrated and lyophilised before subsequent analysis.

2.4c Mass Spectrometry Analysis

Electrospray mass spectra were acquired using a Micromass Q-TOF 2 hybrid orthogonal acceleration time of flight mass spectrometer with a mass range to 10000 Da. The Q-TOF 2 is fitted with an electrospray source in an orthogonal configuration with the Z-SPRAY interface. Samples were dissolved in methanol/water (1:1 v/v) and infused into the electrospray source with a flow rate of 5 $\mu L \cdot min^{-1}$. Conditions were as follows: capillary voltage 3 kV, source temperature 80°C, desolvation temperature 150°C and cone voltage 50-110 V. MS/MS data were acquired with the argon collision gas energy set to ~50 eV to give optimal fragmentation. Peptides were analysed in the positive mode.

2.4d Determination of the Peptide Terminal Group

The terminal group for each peptide was determined by methylation using 'acidified methanol'. Acidified methanol was prepared by cooling methanol (858 μL) in dry ice for 5 minutes, adding acetyl chloride (142 μL) under nitrogen and cooling again for 5 minutes. The solution was allowed to warm to room temperature over one hour, flushing with nitrogen every 15 minutes. The reagent was stored at ~ 4°C for a maximum of 5 days.

The acidified methanol (~100 μL) was added to a sample of lyophilised peptide (~5-10 μg) and the solution heated at 45°C for one to two hours. The mixture was then diluted with water and analysed by ESI mass spectrometry.

2.4e Lys-C Digestion

One microlitre of Lys-C solution (3 units dissolved in 200 μL water) was added to a solution of purified peptide (~50 μg) in aqueous ammonium hydrogen carbonate solution (0.1 M, 5 μL, pH = 8). The resulting mixture was incubated at 45°C for one to two hours, before diluting with water and analysing by ESI mass spectrometry.

2.4f Automated Edman Sequencing

Automated Edman sequencing was used to distinguish between the isomeric residues isoleucine and leucine and the isobaric residues glutamine and lysine, and to confirm the sequence as determined by mass spectrometry. This was carried out at the Department of Molecular Biosciences, University of Adelaide, using an applied Biosystem 470A sequencer equipped with a 900A data analysis module.

2.4g Preparation of Synthetic Peptides

Peptides were synthesised by Mimotopes (Clayton, Victoria) using L-amino acids via the standard N-α-Fmoc method. Full details, including protecting groups and deprotection, have been reported [78]. Synthetic peptides were shown to be identical to the natural samples by mass spectrometry.

2.4h Antibacterial Testing

Antibacterial testing was carried out by the Microbiology Department of the Institute of Medical and Veterinary Science (Adelaide, South Australia). The method used involved the measurement of inhibition zones, produced by the applied peptide, on a thin agarose plate containing the micro-organisms of interest. The procedures are standard [58].

Activities are recorded as minimum inhibitory concentration (MIC) values, which are the minimum peptide concentrations ($\mu g \cdot mL^{-1}$) needed to totally inhibit the growth of the micro-organism.

2.4i Anticancer Testing

Peptides were first tested against three human tumour cell lines – MCF7 (breast), NCI-H460 (lung) and SF-268 (central nervous system). Active peptides were passed on to a second round of testing, this time against a full panel of 55 cancer cell-lines. Assays were conducted by the National Cancer Institute (Washington D.C., USA) using a standard protocol [59, 66].

2.4j Neuronal Nitric Oxide Synthase Inhibition Testing

nNOS inhibition assays were conducted by Mr Jason R. Doyle and Dr Lyndon E. Llewellyn (Australian Institute of Marine Science, Queensland). Inhibition was measured by monitoring the conversion of [^{3}H]arginine to [^{3}H]citrulline, using standard methods [29].

Part II. Amphibian Antimicrobial Peptides – Structural and Mechanistic Studies

Chapter 3 Introduction

3.1 Antibacterial Peptides

A variety of microbially active peptides have been found in plants, insects, crustaceans, mammals and even in microbes themselves. These peptides are an important form of defence against pathogens, especially for plants and invertebrates, which do not have highly developed and adaptive immune systems [79].

Even vertebrates, with their versatile immune systems that are capable of responding to an infinite number of foreign invaders, have a need for antibacterial peptides. This is illustrated by the finding that inactivation of human β-defensin peptides in cystic fibrosis sufferers, leads to terminal respiratory infections [80].

Animals are host to an assortment of microbial species, an arrangement that seems to be mutually beneficial. Stable colonies of innocuous organisms, for instance, can prevent the invasion of more pathogenic strains [81]. However, the normal flora can become pathogenic themselves if they are able to breach the body's surface. Having a defence system capable of quickly bringing these organisms under control is of high importance.

Animals, as seemingly diverse as hippopotami and amphibians, are known to protect their skin from microbes using peptides [39]. As well as defending their skin from infection, amphibians also release antibacterial peptides into the stomach [82]. Insects, on the other hand, synthesise such peptides in the fat body (the equivalent of a mammal's liver), then circulate these throughout the haemo-lymphatic system in response to tissue damage [83].

In humans, the antibacterial defensin peptides are expressed in the epithelial cells of the airways and gastro-intestinal tract, in close proximity to potential sites of infection [30]. They are also sequestered in granules within neutrophils [84]. These cells circulate in the blood and are the first immune system cells to arrive following an inflammatory response. Thus antibacterial peptides are produced close to potential sites of infection and/or are

released into the circulation for fast distribution once the external barriers have been breached.

While this 'innate' immune system is not nearly as specific or adaptive as the acquired immune system, with its infinite repertoire of antigen-specific antibodies, it does have advantages of its own. For one thing, antibacterial peptides are less costly to synthesise and require less genetic information [35]. Their production is fast and they can be stored for immediate release [82]. They can also diffuse more rapidly than antibodies [30].

Each peptide is generally active against a wide range of bacteria. Organisms often produce a series of different peptides, each with a different spectrum of activity, to protect against an even greater number of pathogens. The mixture of peptides can also have a dramatic synergistic effect, as has been shown for the magainins and dermaseptins [85, 86]. In the case of the dermaseptins, combining the peptides can result in 100 times the activity of the individual peptides [86].

For antibacterial peptides to be useful, they must be selective for pathogenic cells. The majority of the peptides studied so far have been shown to satisfy this condition [87]. The magainins, for example, are active against bacteria at concentrations of 10-100 $\mu g \cdot mL^{-1}$ while more than 1 $mg \cdot mL^{-1}$ is necessary to lyse erythrocytes [88]. Other peptides have strong haemolytic activity as well as antibacterial action. These include melittin from bees [89], alamethicin from the fungus *Trichoderma viride* [90] and gramicidin A from the bacterium *Bacillus brevis* [91, 92].

Traditional antibiotics target specific enzymes that are essential for bacterial survival [93]. However, organisms may acquire resistance to the antibiotic, if mutations produced over successive generations change the shape of the enzyme, rendering it unrecognisable to the antibiotic. Over time, many strains of bacteria have emerged that are resistant to currently used antibiotics [19, 94]. Thus minor infections that are easily treatable today may become life threatening in the future. Clearly, new antibiotics are needed and preferably ones that have a novel mechanism of action.

Instead of inhibiting specific enzymes, most antibacterial peptides target the bacterial cell surface [88]. They are thought to destroy the integrity of the membrane, causing a swift death. Since no mutatable proteins are involved, development of resistance is more difficult. Furthermore, the speed with which the peptides kill means that there is little time for the adaptive process to occur. Hancock *et al.* [87, 94] have looked at bacteria that were exposed to peptide antibiotics over many generations and have found no measurable rates of resistance.

Antibacterial peptides can be classified into three broad groups based on their structure. The first group comprises cysteine-containing peptides that have one or more intramolecular disulphide bonds. While this group contains many sub-groups of different structural motifs, β-sheet is the main secondary structure element found [39]. The tachyplesins, from the horseshoe crab (e.g. 20), and the defensins (e.g. 21) belong to this class [38, 88].

(20) Tachyplesin I



(21) Defensin HNP-1



The second group contains peptides with a high proportion of one or more amino acids, usually proline and/or arginine [35]. These molecules have an extended helical structure and include bactenecin (22) [35], a peptide from bovine neutrophils, and PR-39 (23) from pigs [31].

(22) Bactenecin

RFRPPIRRPPIRPPFYPPFRPPIRPPIFPPIRPPFRPPLGPFP-NH_2

(23) PR-39

RRRPRPPYLPRPRPPPFFPPRLPPRIPPGFPPRFPPRFP-NH_2

The final group consists of linear α-helical peptides with no cysteine residues. The insect-derived cecropins (e.g. 24) [95] and the amphibian magainin peptides (e.g. 25) [11] belong to this group. Members of this class are often kinked due to helix-breaking residues in the sequence.

(24) Cecropin A KWKLFKKIEKVGQNIRDGIIKAGPAVAVVGQATQIAK-NH_2

(25) Magainin 1 GIGKFLHSAGKFGKAFVGEIMKS-OH

Antibacterial peptides can manifest a wide range of three-dimensional structures but there is one characteristic that seems to be universally present. They all exhibit distinct hydrophobic and hydrophilic portions [96]. Thus, an amphipathic nature seems to be important for their mechanism of action.

Presumably antibiotic peptides of the same general structure will have a similar mode of action so identifying which structural group new peptides belong to will give a good idea of how they work. The antibacterial peptides isolated from Australian tree frogs seem to fit into the linear α-helical peptide category, as they do not contain cysteine residues and no amino acids are present at unusual frequencies [12].

More direct evidence comes from the solution structures that have been determined for representative members of the caerin (e.g. 6) [97, 98], maculatin (e.g. 7) [99] and uperin (e.g. 26) [100] families, in membrane-mimicking solvents. All peptides examined so far have been shown to form amphipathic α-helices, with many having a kinked region of greater flexibility in the middle of the structure.

(6) Caerin 1.1 GLLSVLGSVAKHVLPHVVPVIAEHL-NH_2

(7) Maculatin 1.1 GLFGVLAKVAAHVVPAIAEHF-NH_2

(26) Uperin 3.6 GVIDAAKKVVNVLKNLF-NH_2

3.2 Mechanisms of Action of Antibacterial Peptides

3.2a General Mechanism

Antibacterial peptides are generally believed to operate by permeabilising the bacterial cell membrane, resulting in the uncontrolled flow of ions and small molecules across the bilayer [30, 31, 87]. This leads to dissipation of the membrane potential, uncoupling of respiration and cell lysis [101-106].

The finding that the all-D isomers of selected peptides have equivalent activity to the natural L form lends weight to the idea of a membrane target as it rules out specific chiral interactions [107]. Care should be taken, however, before extrapolating this result to all peptides as alternative cellular targets, such as DNA and RNA, have been proposed for individual peptides, including buforin II [108], nisin Z [109] and indolicidin [110].

Nevertheless, the majority of antibacterial peptides are thought to act by disrupting the integrity of the cytoplasmic membrane. The exact details of how this occurs are still unclear, despite a vast number of studies [reviewed in 30, 110]. Several models have been put forward to account for the available evidence and these will be described in the following sections.

3.2b The Barrel-Stave Model

All antibiotic peptides were initially thought to act via the 'barrel-stave' mechanism [112, 113]. In this model, the unstructured cationic peptides bind to the membrane surface, where they adopt an amphipathic α-helical form [114-116]. This form allows improved interactions between the polar residues and the lipid head-groups.

The peptides aggregate on the surface, before inserting into the bilayer to form barrel-like pores (Figure 3.1). The individual peptides, or 'staves', are arranged such that they are perpendicular to the plane of the bilayer, with their hydrophobic surfaces facing the core

of the bilayer and their hydrophilic surfaces lining the central pore. Progressive insertion of additional monomers increases the size of the channel [117].

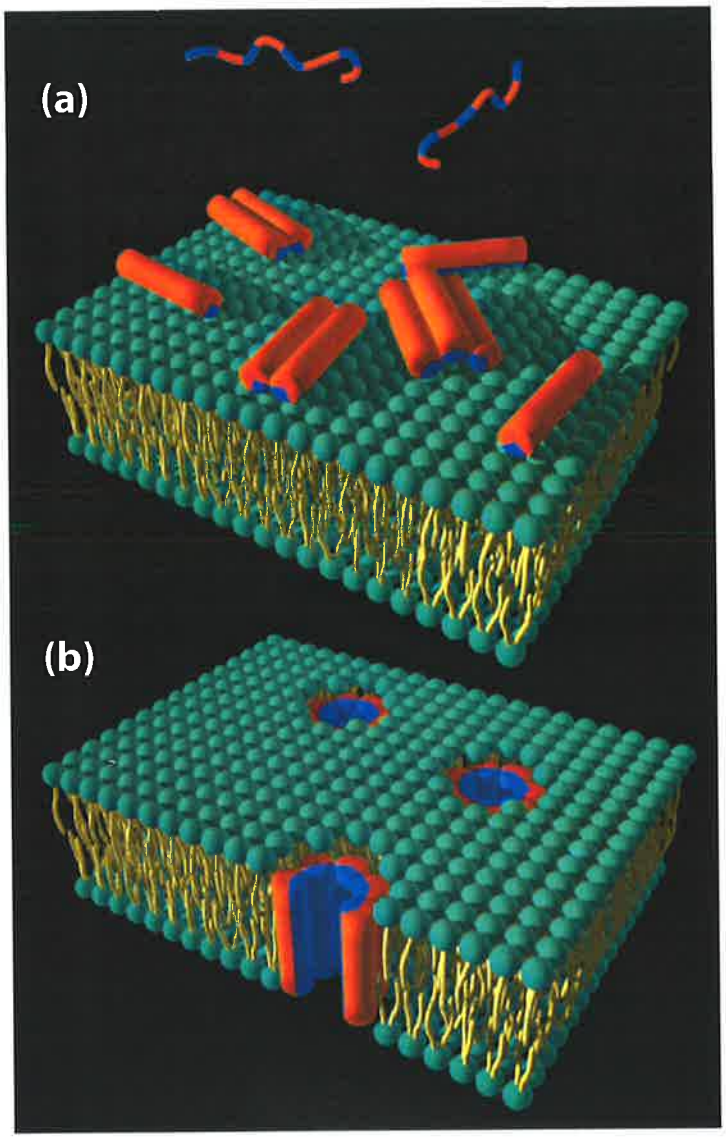

Figure 3.1 The barrel-stave mechanism: (a) the initially unstructured peptides bind to and aggregate on the membrane surface as α-helices before (b) inserting into the bilayer to form barrel-like pores. Peptides in the helical form are represented by cylinders. The hydrophilic regions of the bilayers and peptides are coloured green and blue respectively, while the hydrophobic regions are coloured yellow and red.

One of the critical points of this mechanism is the initial aggregation of peptide monomers. This step is necessary to counter the energetic cost of placing polar residues in the hydrophobic core of the bilayer during insertion [111]. Thus, evidence of aggregation, such as cooperativity of binding, implies the barrel-stave mechanism is acting [117].

Other evidence consistent with the barrel-stave mechanism includes the observation of a perpendicular orientation of the peptide monomers, induction of conductance across a model bilayer and the direct observation of channels, e.g. by neutron diffraction.

Alamethicin (27), a 20-residue antibiotic peptide isolated from the fungus *Trichoderma viride,* is generally recognised as acting via the barrel-stave mechanism [reviewed in 45]. This is supported by evidence of cooperativity in the binding isotherms of alamethicin [118] as well as the observation of reproducible multiple conductance states in lipid membranes [119-121]. The changes in conductance are consistent with monomers leaving or joining the pore structure [122].

(27) Alamethicin Acetyl-UPUAUAQUVUGLUPVUUEQ(Phol)-OH

U = α-methylalanine and Phol = phenylalaninol

A solid-state ^{15}N NMR study indicated that alamethicin adopts a transmembrane orientation at a lipid-to-peptide ratio (L/P) of 8:1 [123]. The orientation of alamethicin was also investigated by oriented circular dichroism (OCD) but was found to vary according to the particular experimental conditions used [124, 125]. Peptide concentration was found to be the most important factor determining orientation, with low concentrations favouring a surface orientation and high concentrations favouring a transmembrane orientation [122]. This suggests that at low concentrations, alamethicin is predominantly in an inactive state but as concentration increases, the active channel-forming state is increasingly favoured [126]. Similar results have been found for the magainins and cecropins [127] and melittin [124].

Neutron scattering experiments have detected alamethicin pores in model membranes [128]. Each channel consisted of eight monomers and had an internal diameter of around 18 Å. Such channels were only found when the peptides had a transmembrane orientation, as determined by OCD [128].

While it is generally agreed that alamethicin operates by the barrel-stave mechanism, there are problems with applying this model to other peptides. For instance, according to the barrel-stave model, peptides must be at least 20 residues in length to span the bilayer since

an α-helix has a length of approximately 1.5 Å per residue and the diameter of a bilayer is around 30 Å [95, 129], and yet, large numbers of short (11-16 residues) antibacterial peptides exist [e.g. 36, 60, 61].

It has been suggested that short antibacterial peptides could form end-to-end dimers to attain the length required [132, 133]. Gramicidin A (28), for example, is known to form head-to-head dimers that allow the passage of ions across lipid bilayers [92]. Gramicidin A is a special case, however, since it forms β-helices that are large enough to allow the flow of ions through the centre of the helix [92, 134].

(28) Gramicidin A Formyl-VGAlAvVvWlWlWlW-$NHCH_2CH_2OH$
(lower-case letters denote D-amino acids)

Alternatively, peptides may adopt 3_{10} helical structures, which have an average length of 2 Å per residue, compared with 1.5 Å per residue for an α-helix [132]. 3_{10} Helical structure has been observed in the peptabiol group of peptides, of which alamethicin is a member [117]. Even so, peptides would still require at least 15 residues to span a lipid bilayer.

Another problem with the barrel-stave model is that most antibacterial peptides are highly cationic along their lengths, unlike the essentially neutral alamethicin [112]. Arranging such peptides into a barrel structure would bring large numbers of positively charged residues into close proximity, resulting in considerable electrostatic repulsion. Furthermore, these pores would be expected to be anion-selective. For magainin, however, cation-selective conductance was observed [135]. Cruciani *et al.* [135] suggested that cation-selective conductance could be explained if negatively charged lipids were incorporated into the channel structure. This led to the development of the toroidal or 'worm-hole' model [136, 137].

3.2c The Toroidal Model

In the toroidal model, the surface-bound peptides undergo rotation, such that they partially sink into the membrane surface. This allows the hydrophobic residues to move into contact with the lipid acyl chains, while the hydrophilic residues maintain interactions with the polar head-groups [137].

Above a critical peptide concentration, the peptide monomers insert into the bilayer to form pore structures. Lipid molecules are interspersed between the peptides, such that the negatively charged head-groups are associated with the positive charges of the peptide side-chains, as well as the aqueous pore interior (Figure 3.2). As a consequence, the toroidal pores would be larger than those of the barrel-stave type and both lipids and peptides should be able to cross to the other side of the bilayer.

The accumulated data on the *X. laevis* peptide magainin 2 (29) suggest it conforms to the toroidal model. The results of fluorescence studies on Trp labelled magainin analogues suggest the peptides intercalate into the membrane such that they lie parallel to the surface [138]. This is consistent with solid-state ^{15}N NMR studies that also indicate a parallel orientation for magainin [139]. OCD results again indicated a parallel orientation for magainin, however at a low lipid-to-peptide (L/P) ratio (10:1) magainin was found to shift to a transmembrane orientation (i.e., perpendicular to the plane of the membrane) [140].

(29) Magainin 2 GIGKFLHSAKKFGKAFVGEIMNS-OH

Pore structures were identified by neutron scattering experiments, when magainin was incorporated into model bilayers [136]. The internal diameter of these structures ranged from 30 to 50 Å in different bilayer systems, much larger than the corresponding alamethicin pores (18 Å) [58]. It was estimated that each pore was made up of only four to seven monomers, while at least 12 monomers would be required to form a barrel-stave type pore of such diameter [122].

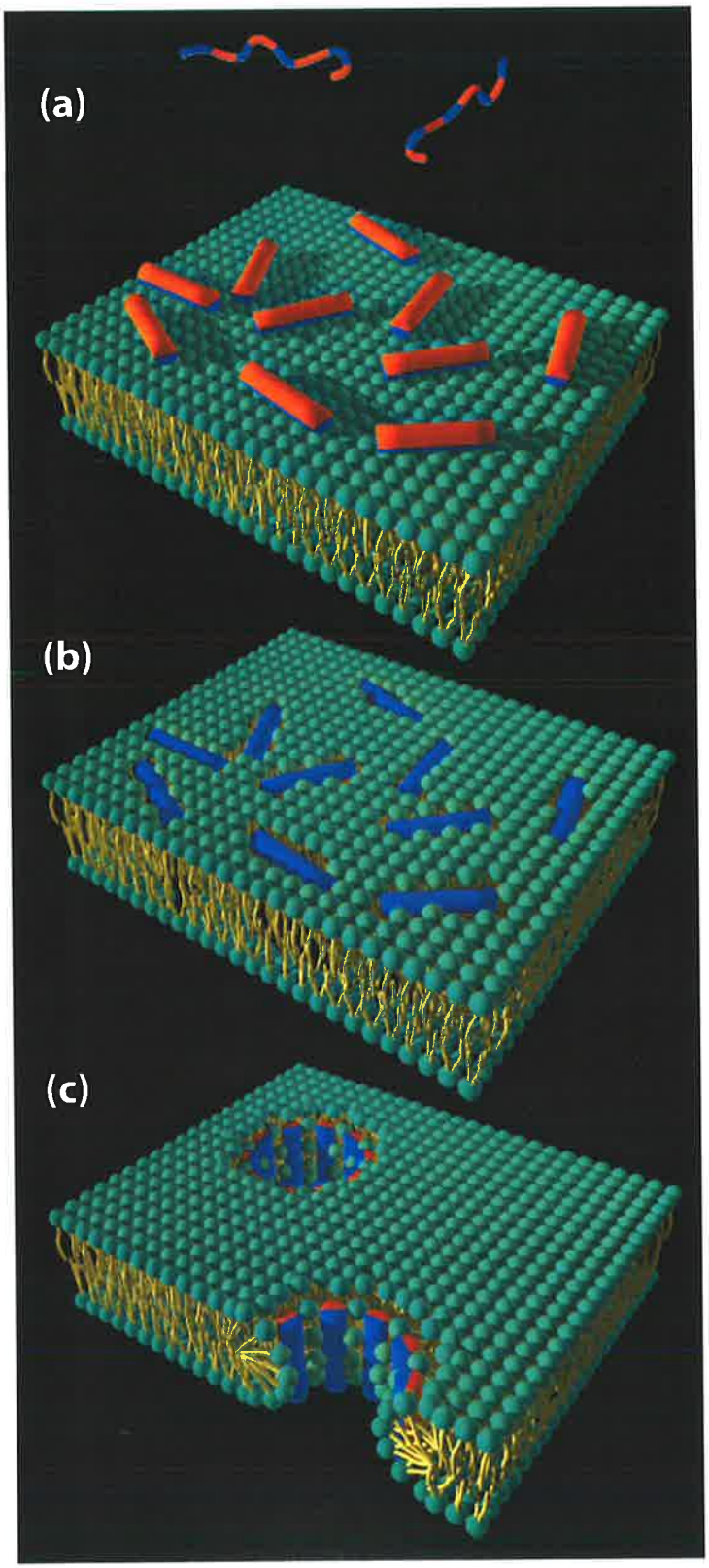

Figure 3.2 The toroidal mechanism: (a) the initially unstructured peptides bind to the membrane surface as α-helices before (b) rotating and sinking into the lipid head-group region and (c) inserting into the bilayer to form toroidal pores. Peptides in the helical form are represented by cylinders. The hydrophilic regions of the bilayers and peptides are coloured green and blue respectively, while the hydrophobic regions are coloured yellow and red.

Matsuzaki *et al.* [141, 142] were able to detect the translocation of both magainin and lipid from the outer to the inner leaflet of the membrane. The lipid translocation (or 'flip-flop') half-lives were accelerated from around 8 days in the absence of peptide to the order of minutes in the presence of magainin [142].

Accumulated data for melittin (17), a 26-residue peptide isolated from bee venom [89], is also consistent with the toroidal mechanism. OCD studies indicate that as peptide concentration increases melittin shifts from a surface to a transmembrane orientation [122]. Solid-state ^{13}C NMR results confirm that at low L/P ratios (*ca.* 15:1) melittin is oriented perpendicular to the membrane surface [143]. Neutron scattering experiments detected pore structures when melittin was transmembrane but not when it was in the surface orientation and the dimensions of the pores were comparable to those of magainin [122].

(17) Melittin GIGAVLKVLTTGLPALISWIKRKRQQ-NH_2

The toroidal model could account for the conductance activity of short antibacterial peptides, assuming the lipids are able to stabilise the ends of the pore (Figure 3.3) [144, 145]. However, the validity of this assumption has not yet been tested. It would be presumed, though, that the pores would be less stable than those formed by longer peptides. Blondelle and Houghton [146] however, found that the antibacterial activity of designed Leu/Lys analogues was optimal for peptides of 12-15 residues. Similar results were found by Castano *et al.* [147, 148] who also discovered their designed peptides were oriented parallel to the bilayer surface.

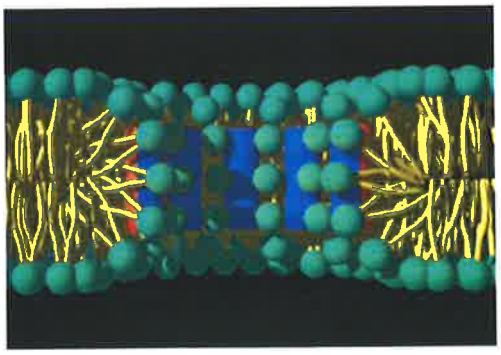

Figure 3.3 Cross-sectional view of a toroidal pore formed by short α-helical peptides. Peptides in the helical form are represented by cylinders. The hydrophilic regions of the bilayer and peptides are coloured green and blue respectively, while the hydrophobic regions are coloured yellow and red.

Further problems with the toroidal model were discovered from experiments on LAH_4 (30), a designed 26-residue peptide that contains four His residues. Solid-state ^{15}N NMR results showed that at pH 5, where the His residues were protonated, the peptide oriented parallel to the membrane surface. At pH 7.5, however, the peptide adopted a transmembrane orientation [149]. Interestingly, at pH 5 the antibacterial activity of the peptide was two orders of magnitude greater than at pH 7.5, showing that the surface oriented peptide was more active [150].

(30) LAH_4 KKALLALALHHLAHLALHLALALKKA-OH

3.2d The Carpet Model

A third model, known as the carpet mechanism, can account for the results discussed above that were inconsistent with the barrel-stave and toroidal models [15, 111]. The initial stages of this mechanism are identical to those of the toroidal mechanism – that is, the unstructured peptide binds to the lipid membrane, where it adopts an amphipathic structure before intercalating into the membrane surface. A 'carpet' is formed as additional monomers cover the surface. Once a threshold concentration is reached, permeation occurs due to strain on the bilayer curvature, formation of transient toroidal-type holes and micellisation of the membrane (Figure 3.4) [111, 151]. The formation of transient toroidal pores could account for the variable conductance activity displayed by many antibacterial peptides [122, 152].

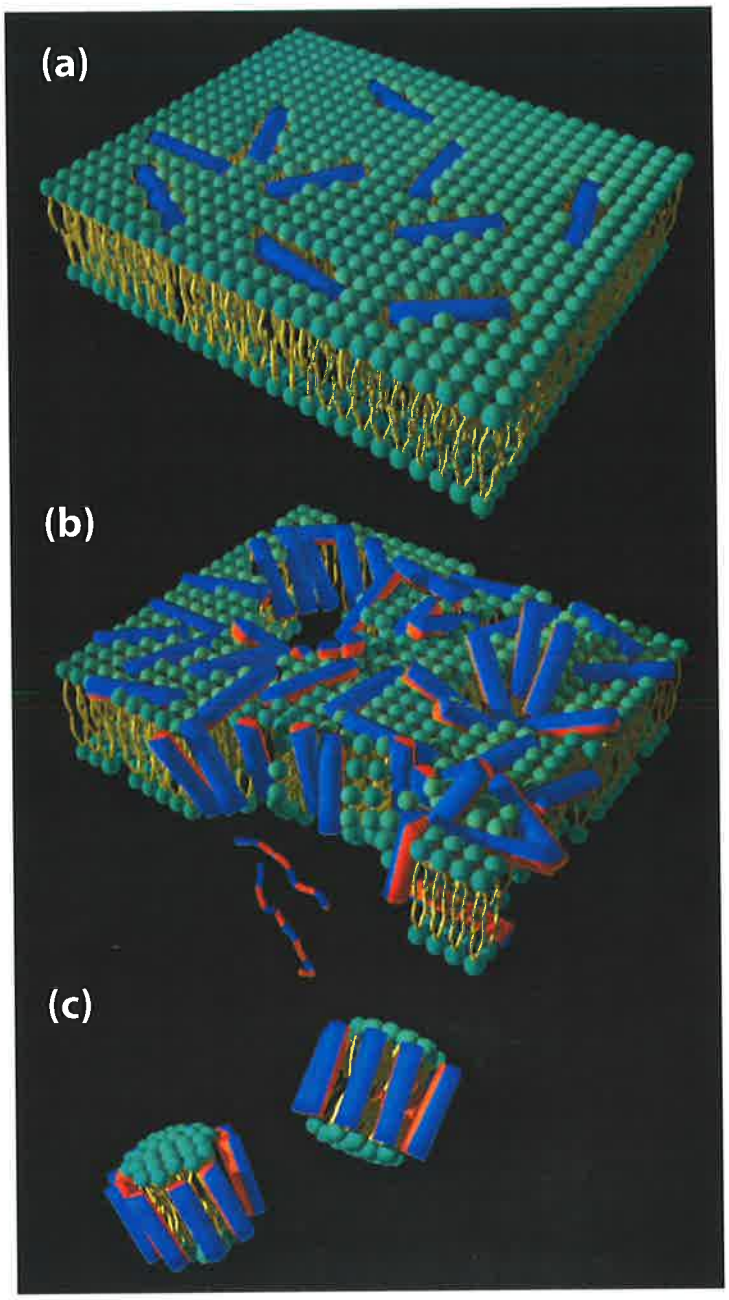

Figure 3.4 The carpet mechanism: (a) the peptides intercalate into the membrane surface; (b) once a threshold concentration is reached, the membrane disintegrates. At this stage, transmembrane pores may form allowing peptides to cross the membrane and (c) membrane segments may break off as micelles. Peptides in the helical form are represented by cylinders. The hydrophilic regions of the bilayers and peptides are coloured green and blue respectively, while the hydrophobic regions are coloured yellow and red.

It should be noted that while self-aggregation is required for the barrel-stave model, it does not necessarily occur in the carpet mechanism. Instead, the monomers are more likely to be interspersed between the lipid head-groups due to electrostatic repulsion between the cationic side-chains. Acidic lipids would help to reduce the electrostatic repulsion [152].

The binding curves for members of the cecropin family are linear, indicating they do not self-aggregate [153]. They also show a preference for binding and permeabilising acidic over zwitterionic vesicles [95]. In addition, cecropin A (24) and cecropin P1 (31) were found to orient parallel to the membrane surface [95, 154, 155] and the amount of cecropin necessary to cause vesicle permeation or bacterial cell death has been calculated as enough to form a monolayer over the entire bilayer surface [95, 156]. Thus the cecropins are thought to act by the carpet mechanism.

(24) Cecropin A KWKLFKKIEKVGQNIRDGIIKAGPAVAVVGQATQIAK-NH_2

(31) Cecropin P1 SWLSKTAKKLENSAKKRISEGIAIAIQGGPR-OH

The carpet model does not require peptides to be α-helical, provided the peptide is still hydrophobic and highly cationic [151]. This agrees with the results of Oren *et al.* [157] who designed a series of 12-residue Leu/Lys peptides, each containing four D-amino acids dispersed along the peptide. These diastereomeric peptides showed no preference for a particular secondary structure by circular dichroism (CD), yet had comparable antibiotic activity to dermaseptin S and melittin [157].

Furthermore, cyclised magainin and melittin analogues have been shown to have antibacterial activity, even though they cannot form transmembrane helices. This indicates a membrane disintegration mechanism (rather than a pore-forming mechanism) is in operation for the analogues at least [158].

Despite the similarity in the structures of antibacterial peptides, none of these models satisfies all of the evidence for all of the peptides, suggesting that a ubiquitous mechanism does not exist.

3.3 Specificity of Action

Antibacterial peptides have varying degrees of specificity. Some are active against a broad spectrum of bacterial species while others may only be active against one or two. Similarly, while some antibacterial peptides, such as magainins and cecropins, are specific for prokaryotic organisms [5, 159], others, such as melittin and gramicidin A, can kill mammalian cells as well [89, 91, 160]. Peptides that are specific for bacterial cell membranes are candidates for pharmaceutical use, as they would cause no harm to host cells.

Cell specificity is thought to be due to differences in cell architecture that can influence the access of peptides and their ability to permeabilise the cytoplasmic membrane. There are a number of marked differences between bacterial and mammalian cells that may be responsible for this, including differences in the cell surface, lipid composition and membrane potential.

The outer surfaces of bacterial cells are anionic due to the presence of lipopolysaccharides (LPS) in Gram-negative (G-) species and teichoic acids in Gram-positive (G+) organisms [161]. Bacterial cytoplasmic membranes also contain a large proportion of anionic phospholipids, including phosphatidylglycerol (PG) and cardiolipin, and at least a fraction of these are located on the outer leaflet [88, 162]. The outer leaflet of mammalian cell membranes, on the other hand, contains only neutral phospholipids [163, 164].

Many studies show that antibacterial peptides bind and permeabilise anionic lipid vesicles to a much greater extent than neutral vesicles [95, 153, 157, 165]. A correlation has also been observed between the lysis of the inner membranes of G- bacterial species and their acidic lipid content [114]. Increasing the ionic strength of the medium results in decreased binding and antibacterial activity, suggesting that the preference for acidic vesicles is electrostatic in origin [166, 167].

Matsuzaki *et al.* [168] found that magainin was unstructured in neutral phosphatidylcholine (PC) vesicles but adopted an α-helical structure when the vesicles contained the anionic lipid phosphatidylserine (PS). This corresponded to increased

permeability of the PS vesicles. Melittin, on the other hand, which is both haemolytic and antibacterial, has a far greater affinity for PC vesicles than does magainin [88].

There is also evidence for the involvement of anionic materials from the bacterial surface in antibacterial specificity. Peschel *et al.* [169], for example, showed that the teichoic acids from sensitive G+ strains were more anionic than those from resistant strains.

Polyanionic LPS molecules make up the outer surface of G- bacteria. Divalent magnesium ions form cross-links between these molecules, neutralising the charges and stabilising the membrane [170]. It has been suggested that cationic peptides can displace the magnesium ions, breaking down the cross-links and disrupting the integrity of the outer membrane. This allows the peptides to access and permeabilise the cytoplasmic membrane, resulting in cell death. Collectively, this process is known as 'self-promoted uptake' [171].

A number of antibacterial peptides have been shown to bind to LPS with high affinity, both in the pure form and in bacteria [172, 173]. These peptides can be displaced by high concentrations of magnesium but not sodium, suggesting the peptides and magnesium compete for the same binding sites [171, 174].

Magainin adopts an α-helical structure when bound to LPS/PC vesicles and is able to permeabilise these structures. Similar results are found when only the lipid A portion of the LPS is present, indicating that this is the site of peptide binding [173]. Magainin has also been shown to increase the disorder of the LPS acyl chains, depending on the charge associated with the LPS molecules, and this is consistent with the finding that resistant G- bacteria had a lower net negative charge associated with their LPS [175, 176].

Mammalian cells have a negligible membrane potential (~ –9 mV), while bacterial cells possess large inside-negative potentials (~ –70 mV) [177]. Magainin activity on both vesicles and erythrocytes was shown to increase when an inside-negative potential was generated across the membrane [85, 177]. Membrane potentials are also known to affect magainin-induced conductance [135], possibly by interacting with the helix dipole to force the peptide into a transmembrane alignment [113, 152].

Cholesterol is found in high proportions in mammalian cell membranes but is absent in those of bacteria [163] and therefore, it could also be responsible for the cell specificity of antibacterial peptides. The presence of cholesterol decreases the ability of the magainins and cecropins to permeabilise lipid vesicles [101, 165, 177]. The ability of cecropin to induce conductance events was also decreased when cholesterol was incorporated into the bilayer [178]. Furthermore, erythrocytes depleted of cholesterol were more susceptible to lysis by magainin [177]. Cholesterol is known to influence membrane fluidity [179, 180] and it has been suggested that it may interfere with peptide reorientation that may be necessary for antibacterial action [106].

Some antibacterial peptides also show activity against cancer cells [13, 14, 181]. The magainins, for example, are able to kill tumorigenic cells at concentrations that are harmless to normal cells [182]. This ability to differentiate between cancer and normal cells may be due to the significantly higher levels of PS present in the outer leaflet of cancer cells [183]. Possible differences in the membrane potentials of these cells have also been postulated to account for cancer cell specificity [182].

While many peptides are active against both G+ and G- bacterial species, some are selectively active against one or the other. Alamethicin, for instance, is active against G+ bacteria, while polymyxin B is harmful only to G- organisms [95]. To kill G- cells, peptides must overcome the LPS and the outer membrane, as well as a thin peptidoglycan layer, to get to the cytoplasmic membrane [162]. It has been suggested that peptides that self-aggregate on the cell surface are prevented from crossing the outer membrane [151]. A qualitative examination of G-/G+ specificity versus aggregation tendency, supports this proposal [95].

G+ bacteria, on the other hand, are protected by a thick multilayer of peptidoglycan [169]. Some antibacterial peptides are unable to overcome this barrier but it is not known why. However, there is evidence that the rate of permeabilisation of G+ bacteria is slower than that of G- bacteria, indicating the peptidoglycan layer is a significant obstacle [176].

3.4 Structural Features of α-Helical Antibacterial Peptides

The membrane specificity and effectiveness of α-helical antibacterial peptides ~~is~~ are also modulated by their primary and secondary structures. Some general structural properties of these peptides have been identified, including helicity, hydrophobicity, amphipathicity, hydrophilic angle and charge state. The nature of the C-terminal group has also been shown to affect activity. These characteristics and their relevance to antibacterial activity and selectivity, will be discussed below. It should be noted that no one feature is entirely responsible for antibacterial activity. Rather, it is the combination of properties that is important.

3.4a C-Terminal Amide Group

Many peptide antibiotics, including nearly all of the amphibian antimicrobials, have an amide group at the C-terminal. This is a post-translational modification that occurs by a complex enzymic route involving the donation of the amino group from a C-terminal glycine to the penultimate residue [39].

It has been noted, anecdotally, that the presence of a C-terminal amide group is a good indicator of possible bioactivity [12]. When the amide and acid forms of the same peptide are compared, the amides show consistently higher activity [165, 184]. In addition, the magainins and dermaseptins, which are not amidated naturally, show increased activity when converted to C-terminal amides [86, 185] while maculatin 1.1, which naturally occurs as an amide, loses activity when converted to the acid [99].

The naturally amidated peptide sarcotoxin has been shown to cause greater release of glucose from artificial liposomes than the carboxylic acid analogue, indicating an increased ability to permeabilise a membrane [165]. This effect also correlates with increased microbicidal activity.

One possible reason for the greater activity of the amide is the loss of a negative charge, which may improve binding to the acidic bacterial membrane [165]. A second explanation

has been proposed, which suggests that the overall dipole of the peptide helix is stabilised by removal of the negative charge at the C-terminal [186].

The helix dipole arises because of alignment of the individual peptide dipoles parallel to the helix axis. The four N-terminal amide groups and the four C-terminal carbonyl groups are non-hydrogen bonded and therefore carry partial positive and negative charges, respectively. This results in an extended dipole with the positive pole at the N-terminal and the negative pole at the C-terminal [187]. Conversion of the C-terminal carboxylic acid group to an amide reduces the negative charge at the negative pole, thus stabilizing the helix. Acylation of the N-terminal amine has also been shown to improve helical stability. Venkatachalapathi *et al.* [188] observed increased helical content in a model peptide that had both the N-terminal acylated and the C-terminal amidated. They also showed that the modified peptide had improved lipid affinity.

3.4b Helicity

The degree of helicity that a peptide adopts is determined by the amino acid sequence and it is well known that certain amino acids favour helical structure while others destabilise it [189]. The importance of helicity has been demonstrated through structure-activity-relationship (SAR) studies where individual residues are changed and the antibacterial activity tested. For example, replacing central amino-acids of cecropin with the helix-breaker proline correlated with decreased activity [95, 190], while for magainin, replacing the helix destabilising residue glycine with helix-promoting residues, such as alanine, improved the peptide's activity [159]. The relationship between helicity and activity is not clear-cut, however, as there is a whole class of α-helical peptides that require a kink, or flexible region in the helix to have activity. Replacing the hinge-forming residues, in these cases, leads to loss of activity (see Section 3.5).

The replacement of two successive residues in magainin analogues with their D-forms, has been shown to result in decreased helical content [191]. In this case, the amphipathicity, hydrophobicity and charge state of the analogues are identical to those of the original peptide, thus providing a useful means of isolating the effect of helicity on activity.

Wieprecht *et al.* [192] studied such peptides and observed a correlation between decreasing helicity and decreased binding to membranes.

It has also been shown that the efficiency of the peptides to permeabilise neutral membranes decreases with decreased helicity, while there was little change when negatively charged membranes were used [193]. Thus, while the antibacterial activity decreases somewhat when helicity decreases, haemolytic activity decreases by a greater amount since erythrocytes have neutral membranes [193]. In fact, a number of non-helical peptides retain antibacterial function but lose all haemolytic activity, provided they have a high net positive charge [130, 194].

3.4c Charge State

Antibiotic peptides are generally cationic in nature, due to the abundance of lysine or arginine residues in the sequence [94]. SAR studies have shown that replacing acidic residues with basic or hydrophobic residues leads to an increase in activity, while substituting hydrophobic or acidic residues for lysine results in a decrease or total loss of activity [12, 16, 195]. Increasing the net charge of the peptide will not improve activity, however, if the charged residues are placed randomly in the sequence [196]. Their position must be compatible with maintaining other structural properties such as amphipathicity and helicity [191].

Haemolytic activity has been found to decrease or remain unchanged when the overall positive charge is increased [191]. Thus, specificity of these peptides for prokaryotes over mammalian cells is improved with a greater positive charge [130]. This may be due to improved electrostatic interactions with the anionic bacterial cell membranes [88, 96].

While cationic peptides bind well to bacterial membranes, it has been found that positive charges inhibit the efficiency of membrane permeabilisation [191]. This may be due to a decreased ability to traverse the lipid membrane to form channels. Indeed, the charged nature of antibiotic peptides has been shown to influence their orientation in lipid bilayers [129, 149, 150]. When the peptide is highly cationic it is more likely to orient parallel to the plane of the membrane, presumably because it is energetically unfavourable to

accommodate the basic residues within the hydrophobic lipid environment [149]. The resulting decrease in permeabilising efficiency is more than offset by the improved membrane binding since antibacterial activity increases overall [191].

3.4d Hydrophobicity

The hydrophobicity of antibacterial peptides has been shown to influence antibacterial activity [191]. To be able to compare the hydrophobicity of different peptides easily, hydrophobicity scales have been developed that give hydrophobicity values for each amino acid side-chain [67]. These values were determined by measuring the affinity of the side-chains for hydrophobic phases [197]. The mean hydrophobicity, where the hydrophobicity values for the sequence are averaged over the number of residues, gives an indication of the hydrophobicity of the peptide.

Wieprecht *et al.* [198] examined the effect of hydrophobicity on activity by looking at a selection of peptides with constant helicity, amphipathicity, hydrophilic angle and charge state but with varying degrees of hydrophobicity. They found that hydrophobicity had little effect on the efficiency of membrane permeabilisation and no effect on peptide binding to negatively charged membranes. However, binding to neutral or mixed membranes increased significantly with increasing hydrophobicity. Antibiotic activity increased with hydrophobicity, due to the increase in binding, however the peptides also became haemolytic.

These results are thought to be due to the increasing importance of hydrophobic interactions, as the negative charge associated with the membrane decreases. When the membrane is comprised exclusively of acidic lipids, electrostatics determine binding and hydrophobicity has no effect, whereas hydrophobicity is the dominating factor in binding to neutral lipids [198]. Therefore, as antibacterial activity increases with hydrophobicity, so too does haemolytic activity. Haemolytic activity increases at a greater rate, however, because of the neutrality of the erythrocyte membrane [199]. Thus, selectivity for prokaryotes is reduced.

3.4e Amphipathicity

α-Helical peptide antibiotics are generally amphipathic in nature [117, 185], which means they have a hydrophobic and a hydrophilic face. These faces run parallel to the long axis of the helix. The Schiffer-Edmundson wheel projection is shown below for a model amphipathic peptide (Figure 3.5). This peptide, designed by Blondelle and Houghten [146], is composed only of leucine and lysine residues and has been shown to have moderate antibacterial activity.

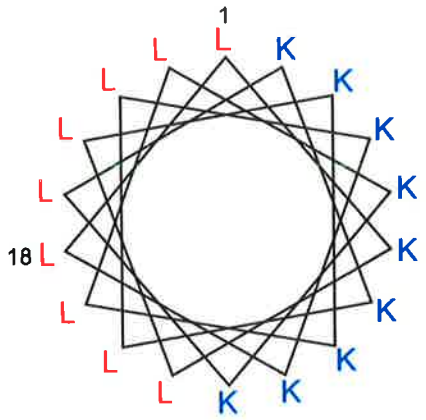

Figure 3.5 Schiffer-Edmundson wheel projection of Ac-LKLLKKLLKKLKKLLKKL-NH_2. Hydrophilic residues are indicated in blue and hydrophobic residues in red [67].

A useful quantitative measure of amphipathicity is the hydrophobic moment [200]. This quantity is the mean vector sum of the hydrophobicities of the individual residues, where the direction of the vector is the angle at which the side-chains emerge from the axis of the helix i.e., multiples of 100°. Large values of the hydrophobic moment indicate high amphipathicity and vice versa.

Model peptides, such as that shown in Figure 3.5, incorporating varying degrees of amphipathicity, have been used to demonstrate a correlation between hydrophobic moment and antimicrobial activity [146, 176]. Modifications to a melittin derivative that improved the segregation of hydrophobic and hydrophilic residues and therefore the hydrophobic moment, resulted in increased antibacterial activity [201]. However, an increase in antibacterial activity was concomitant with an increase in haemolytic activity [176, 201, 202], meaning that the specificity for bacterial membranes was reduced [203].

Pathak *et al.* [204] compared the effects of hydrophobicity, amphipathicity and helicity on antibacterial activity and found that the most important parameter was amphipathicity. Amphipathicity enables the peptide to insert into a lipid membrane, keeping the hydrophilic face in contact with the lipid head-groups and the water phase, while the hydrophobic surface stays close to the lipid acyl chains. This is reflected in the finding that membrane binding is improved by increasing peptide hydrophobic moment, while permeabilising efficiency is unaffected [203].

3.4f Hydrophilic angle

When the sequence of an amphipathic peptide is plotted on a Schiffer-Edmundson wheel, the angle subtended by the hydrophilic face can be measured. As an example, the peptide shown in Figure 3.5 has a hydrophilic angle of 180°. This angle can be varied while keeping the hydrophobic moment constant and is thought to influence the location of the peptide in the membrane [191].

Segrest *et al.* [68] classified peptides into groups according to their hydrophilic angles. Peptides with angles ≤ 100° fall into class L (for lytic), which includes the magainins and other antibacterial peptides. Known transmembrane helices (class M) were found to have hydrophilic angles of ≤ 60°. Apolipoproteins, which solubilise lipids by stabilising small discs of bilayer structure, have hydrophilic angles of ≥ 180° and are termed class A helices.

Wieprecht *et al.* [205] designed a series of peptides with different hydrophilic angles but constant hydrophobic moment and overall charge. They found that increasing the hydrophilic angle decreases the ability of the peptides to permeabilise membranes but also increases the binding of the peptide to the lipids. When combined, these factors resulted in increased antibacterial activity for peptides with a hydrophilic angle of around 140-180°. Once again, the haemolytic activity increased at the same time resulting in decreased specificity.

It is believed that when the hydrophilic angle is around 180°, the peptides are energetically better able to bind to the membrane surface but that this increased angle also disfavours

the formation of transmembrane pores (and therefore permeabilisation) because of unfavourable electrostatic interactions [191]. Transmembrane pores are favoured instead by smaller hydrophilic angles.

3.4g Summary

Table 3-1 shows a summary of the qualitative effects that helicity, hydrophobicity, amphipathicity, hydrophilic angle and charge state have on the activity of antibacterial peptides.

Table 3-1 Effect of the modification of various structural features on binding, permeabilising efficiency, antibacterial activity, haemolytic activity and specificity.

	Increasing:				
	Helicity	**H[a]**	**μ[b]**	**ϕ (°)[c,d]**	**Charge (+)**
Binding	↑	↑[g]	↑	↑	↑
Permeabilising efficiency[e]	↑[h]	≈	≈	↓	↓
Antibacterial Activity	↑	↑	↑	↑	↑
Hemolytic activity	↑	↑	↑	↑	↓
Specificity[f]	↓	↓	↓	↓	↑

[a] Mean residue hydrophobicity (H) as calculated from the consensus sequence of Eisenberg [197].
[b] Hydrophobic moment (μ) per residue [67].
[c] Hydrophilic angle (ϕ).
[d] Increasing here means from 0° to 180°.
[e] Permeabilising efficiency refers to the ability of already bound peptide to then permeabilise the membrane.
[f] The ratio of antibacterial activity to haemolytic activity.
[g] More significant for neutral lipids.
[h] For neutral lipids.

3.5 Hinged α-Helices

α-Helical peptide antibiotics can be classified into two groups. The first of these comprises the linear α-helices such as cecropin P1 from pig intestines [155] and the amphibian peptides magainin 2 [206] and PGLa [207]. The second group is made up of peptides that form helix-bend-helix structures. The bend, or hinge, is flexible and allows the two helices to move independently. Typically, the N-terminal helix of these hinged peptides is amphipathic, while the C-terminal helix is hydrophobic [87, 116, 208], although this is not always the case. Examples of hinged peptides include the amphibian peptide caerin 1.1 [97], cecropin A from insect haemolymph [116] and melittin from bee venom [209].

The hinge itself is usually a result of a proline, or one or more glycine residues, being present in this region of the sequence. Proline is an imino acid, and as such it has no amide proton unless it occurs at the N-terminal. As a result, proline residues (residue i) cannot form hydrogen bonds to the carbonyl oxygen atom of the i-4th residue. Thus, when proline residues occur within an α-helical segment, a hinge results. In the majority of peptides and proteins, the proline residue occurs on the solvent-exposed face of the helix as in this way, the unpartnered carbonyl atom can form hydrogen bonds with the solvent [210].

The bends in melittin, cecropin A, alamethicin and caerin 1.1 are all due to proline residues in the central region of their respective sequences [97, 116, 211, 212]. Less common are hinges due to glycine. As glycine has only a proton for its side-chain, it is less conformationally restricted than other residues. Thus, kinks can occur where glycines are present in the sequence and this is particularly true when multiple glycine residues are close together. For example, hybrid cecropin-melittin and cecropin-magainin peptides have flexible hinged structures due to the Gly-Ile-Gly sequence in the central portion of the peptide [132, 213]. For the cecropin-magainin peptide, replacement of this sequence with proline resulted in almost identical antibacterial activity [213]. Melittin and cecropin A also have glycine residues in close proximity to proline [214, 215], which possibly confer additional flexibility to their hinge regions.

The importance of the hinge region for function has been demonstrated repeatedly [208, 213, 216]. For instance, replacing the proline residue in maculatin 1.1 with alanine results in markedly decreased activity and it was shown that the alanine analogue forms a linear α-helical structure [99]. Oh *et al.* [213] showed that the pore-forming ability of the cecropin-magainin hybrid peptides was considerably reduced when the hinge was deleted, concomitant with decreased antibacterial activity.

Despite the acknowledged importance of the hinge in these peptides, the reason for its importance is not known. It has been suggested, though, that the additional flexibility allows insertion of the hydrophobic C-terminal helix into the bilayer, while the more amphipathic N-terminus remains parallel to the surface of the membrane [132, 217]. Thus the transition to transmembrane helix bundles is facilitated.

Chapter 4 Protein Structure Determination

4.1 General

To gain further insight into the mechanism of action of antimicrobial peptides, it would be desirable to have knowledge of their tertiary structure. The primary techniques used for determining peptide and protein structures are X-ray crystallography and nuclear magnetic resonance (NMR) spectroscopy. X-ray crystallography can be applied to any protein for which suitable crystals are available and the phase problem can be solved [218]. NMR spectroscopy, on the other hand, is limited by the size of the protein. However, advances in spectrometer technology and the development of multi-dimensional experiments, has meant that structures of proteins as large as 30 kDa are now routinely determined [219, 220].

NMR spectroscopy has a number of advantages over X-ray crystallography. For instance, X-ray structures must be determined from crystals that may be difficult to obtain, particularly for membrane proteins. Even if suitable crystals are obtained, the structure found may be different to the native structure acquired in solution because of the additional crystal-packing forces found in the solid-state. In contrast, NMR structures can be obtained in solution under near physiological conditions.

Protein structure can also be investigated using circular dichroism. This technique gives information about overall secondary structure but cannot determine which regions of the protein are structured. Nevertheless, it can provide useful complementary information. The following sections will describe the techniques of circular dichroism, NMR spectroscopy and structure calculations, as well as different types of membrane-mimicking media.

4.2 Circular Dichroism

Circular dichroism (CD) spectroscopy is a useful technique for investigating the overall secondary structure of a peptide or protein [221]. Here, the difference in absorption of left and right circularly polarised light is measured as a function of wavelength [222].

Polarised light can be described in terms of the electric field vector (E), which is perpendicular to the direction of propagation. For linearly polarised light, the magnitude of E oscillates in a plane, while for circularly polarised light, the magnitude of E is constant, while its direction rotates in a circle. Linearly polarised light can be viewed as a superposition of left (E_L) and right (E_R) circularly polarised light of equal phase and amplitude [223] (Figure 4.1).

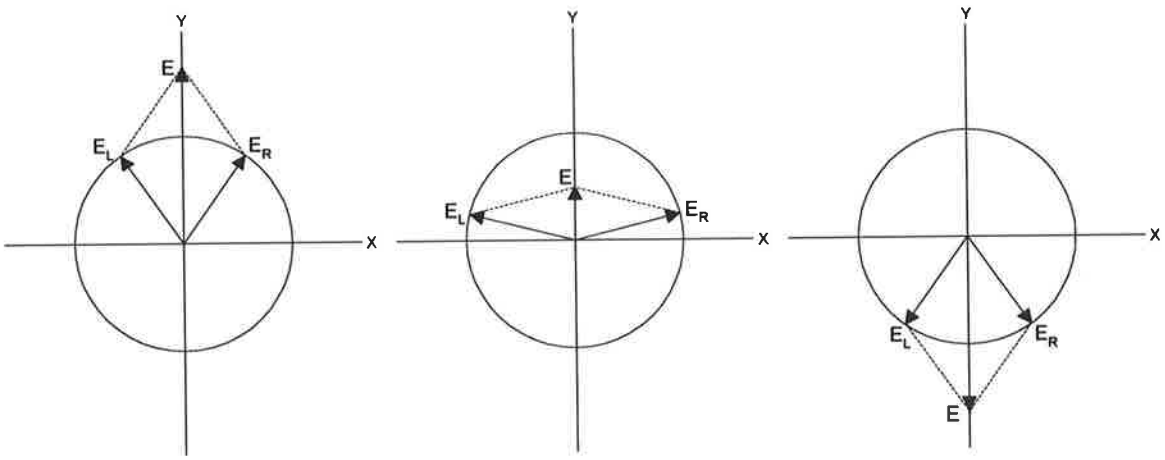

Figure 4.1 Electric field vector (E) (linearly polarised light) as the resultant of two rotating vectors E_L and E_R (circularly polarised light).

If linearly polarised light is passed through an optically active substance, one of the circularly polarised components will be absorbed to a greater extent [222]. The components of the transmitted light will therefore have unequal amplitudes that recombine as elliptically polarised light (Figure 4.2). The left and right components also pass through the optically active medium at different velocities, due to their different refractive indices [223]. This causes the axes of the ellipse to rotate through some angle, α, known as the optical rotation.

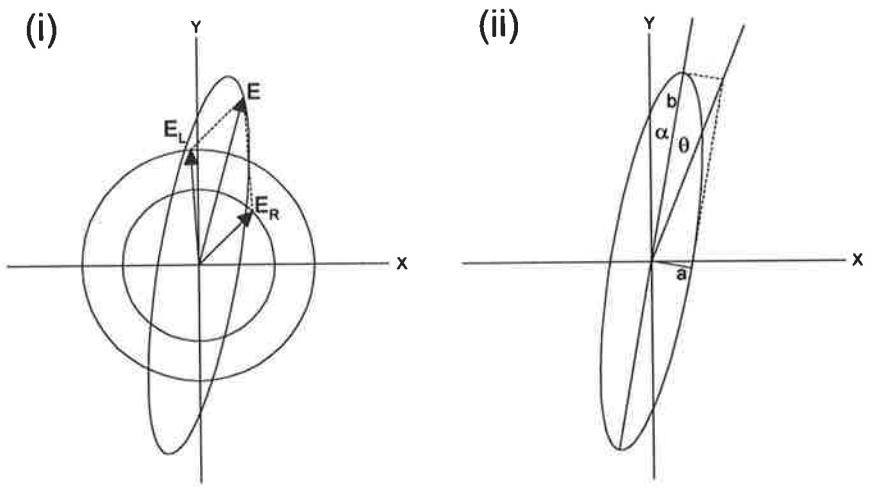

Figure 4.2 (i) E_L and E_R after passing through an optically active medium. The resultant electric field vector, E, traces out an ellipse. (ii) The ellipse is rotated through an angle (α) and the ellipticity (θ) is equivalent to the arctangent of the ratio of the minor (a) to major axes (b) of the ellipse.

The ellipticity (θ) can either be measured directly, as the arctangent of the ratio of minor to major axes of the ellipse [223], or it can be measured as the difference in absorbance of left and right circularly polarised light (A_L-A_R) [224], where

$$\theta = \frac{2.303}{4}(A_L - A_R) \times \frac{180}{\pi}$$

The units of θ are degrees. Ellipticity is usually normalised to a molar value, where the measured ellipticity is corrected for concentration and path length. For proteins and peptides, the ellipticity is also averaged over the number of residues giving the mean residue ellipticity, θ_{MRW}, in units of deg·cm^2·dmol^{-1}:

$$\theta_{MRW} = \frac{\theta \times M \times 100}{l \times c \times N_r}$$

where M is the molecular weight (g·mol^{-1}), l is the path length (cm), c is the concentration (mg·mL^{-1}), N_r is the number of residues and θ is the measured ellipticity (deg) [224].

For circular dichroism to occur, an asymmetric chromophore or, more commonly, a symmetric chromophore in an asymmetric environment, must be present in the molecule. In proteins, the chromophore that dominates the far-UV CD spectrum (180-240 nm) is the

carbonyl group of the peptide bond [225]. Other chromophores, such as aromatic side-chains or the terminal carboxylic acid group, are also present but do not significantly affect the CD spectrum in this region [225, 226].

The carbonyl group is a symmetric chromophore but is optically active because of the asymmetry of the protein molecule [223]. This asymmetry is a result of the chiral centre present in each residue (except glycine) and the overall structure of the protein. Thus, it is not surprising that CD spectroscopy is sensitive to protein secondary structure [221].

Different types of secondary structure give rise to characteristic bands in the CD spectrum. α-Helices, for example, have a large positive band around 192 nm due to the π-π* transition and reasonably strong negative bands around 208 nm and 222 nm due to the π-π* and n-π* transitions respectively [221, 226, 227]. β-Strand structures have a positive band around 195 nm (n-π*) and a negative band around 217 nm (π-π*) while random coil peptides have a negative band around 197 nm (n-π*) and a positive band around 217 nm (π-π*) [225]. Typical spectra obtained for these structural types are shown in Figure 4.3.

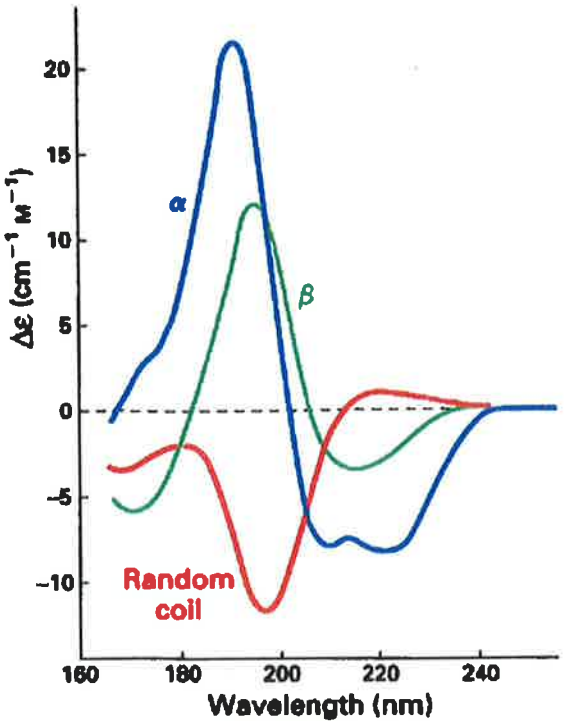

Figure 4.3 Circular dichroism spectra for α-helix, β-sheet and random-coil peptides.
Based on a figure from Johnson [221].

The CD spectrum of a protein is a combination of the spectra of the different secondary structure elements within the protein [221]. An estimate of the percentage of different structural types can be obtained by fitting the reference spectra to the protein CD spectrum [228]. α-Helices produce strong characteristic spectra so α-helical content can be measured with reasonable reliability (within 10%) [224]. In contrast, β-strand structures produce weak spectra that are dependent on chain-length and orientation so that calculations of the fraction of β-strand structure are not accurate [224].

On the other hand, CD spectroscopy is very accurate for determining changes in conformation [225]. It is therefore a useful technique for investigating protein structure as a function of pH, temperature, ligand concentration or solvent. Sonnichsen *et al.* [229], for example, investigated changes in the conformation of a synthetic actin peptide with trifluoroethanol (TFE) concentration. CD spectroscopy is also a quick and non-destructive technique that requires only very small amounts of sample.

4.3 Nuclear Magnetic Resonance

The basis of NMR spectroscopy is the quantum mechanical property of nuclear spin [220]. A nucleus is only NMR-active if the nuclear spin quantum number (I) is non-zero. Thus, some common biological nuclei such as ^{12}C and ^{16}O (I = 0) do not give NMR spectra. For the nuclei most relevant to biological NMR (^{1}H, ^{13}C, ^{15}N), I = -1/2.

In a magnetic field, a nucleus of spin I has 2I+1 possible orientations, so for I = -1/2, two possible spin states exist [48]. The nuclear spin is related to the magnetic moment and so the I = -1/2 nucleus can be thought of as a magnetic dipole that will orient either parallel or anti-parallel to an external magnetic field. These orientations have slightly different energies and nuclei can jump from one energy state to the other by absorbing or emitting electromagnetic radiation that corresponds to the energy difference [220].

The difference in populations, between the low and high energy states, is responsible for the NMR signal and because the energy difference is small, these populations are almost identical. Even at a magnetic field strength of 750 MHz, for a million ^{1}H nuclei at room temperature, only around 60 additional nuclei are in the low energy state [220]. Thus NMR spectroscopy is an inherently insensitive technique.

Nevertheless, net magnetisation results from the difference in populations of the two energy states. By irradiating the sample with suitable electromagnetic radiation, the net magnetisation can be manipulated in a multitude of useful ways, depending on the information that is required. The frequency of the applied radiation must match the energy difference between the two states and is in the radiofrequency (rf) range [48]. Typically the rf radiation is applied in pulses over a duration of the order of microseconds.

The effect of the rf pulses can be described using vector representations [230]. As Figure 4.4 shows, the rf pulses have the effect of rotating the net magnetisation through some angle, most commonly 90° or 180°. When applied to the equilibrium state, the 90° pulse equalises the populations of the two energy states, while the 180° pulse inverts the populations [220].

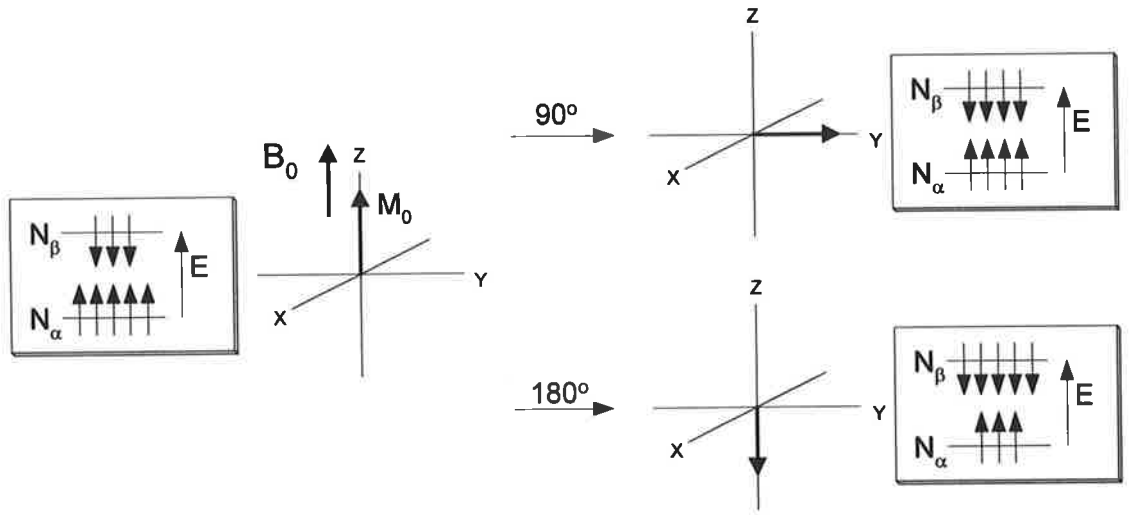

Figure 4.4 Vector diagram of the effect of applying a 90° or 180° pulse on the net magnetisation (M_0). The effect on the populations of the two energy states, N_α and N_β, is illustrated in the inset diagrams (exaggerated for clarity).

When the rf pulse ceases, the disturbed populations relax back to equilibrium, emitting rf radiation with frequency matching the energy difference between the two states. In a vector representation, this corresponds to the magnetisation precessing around B_0 (Z-axis) in the XY plane, as the net magnetisation returns to the Z-axis (Figure 4.5). Magnetisation vector diagrams are often drawn in the rotating frame, where new X- and Y-axes are defined, that rotate at the nuclear precession frequency. Thus the net magnetisation along the Y-axis is now static [230] (Figure 4.5).

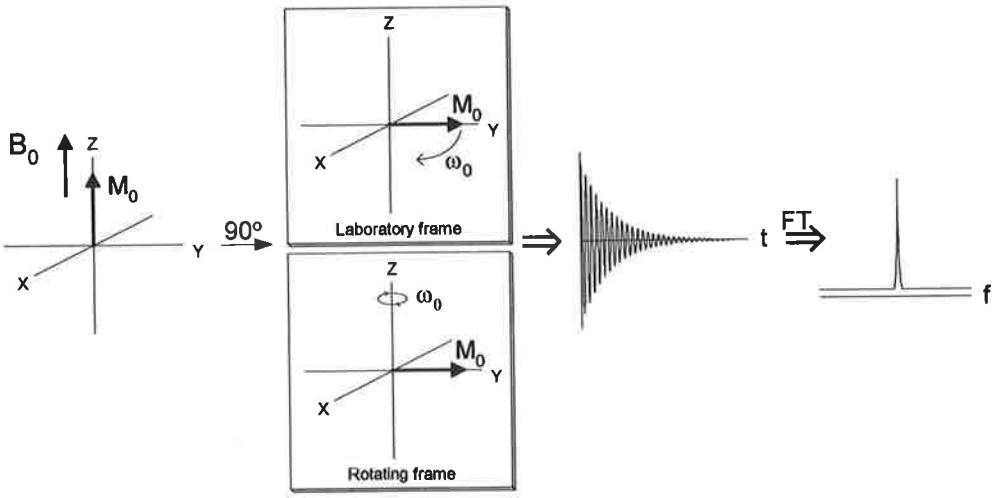

Figure 4.5 Vector diagram showing the precession of magnetisation following a 90° pulse, in both the laboratory and rotating frames. As the magnetisation returns to the Z-axis, radiofrequency is emitted as a free induction decay. Fourier transformation (FT) converts the FID from a time (t) domain function to a function in the frequency (f) domain.

The emitted rf radiation constitutes the signal, or free induction decay (FID), which decays to zero as the system returns to equilibrium [230]. The FID is the sum of the resonance frequencies for each irradiated nucleus (e.g. ^{1}H) in the sample [48]. Fourier transformation of the FID converts it from a function in the time domain to a function in the frequency domain – the NMR spectrum [231].

4.3a One-dimensional Spectroscopy

The simplest of NMR experiments is produced by applying a 90° pulse and recording the FID, which is Fourier transformed to produce the basic one-dimensional (1D) spectrum [48]. Chemically distinct nuclei can be distinguished because they resonate at different frequencies, or chemical shift values, depending on their magnetic environment [220].

Using a vector description in the rotating frame, a 90° pulse applied along the X-axis causes the net magnetisation to rotate through 90° onto the Y-axis. Magnetisation precessing at the same frequency as the rotating frame will appear static. However, the magnetisation precessing from nuclei in slightly different environments is not completely cancelled out by the rotating frame. These components precess around the Z-axis at a frequency relating to their chemical shift [231] (Figure 4.6).

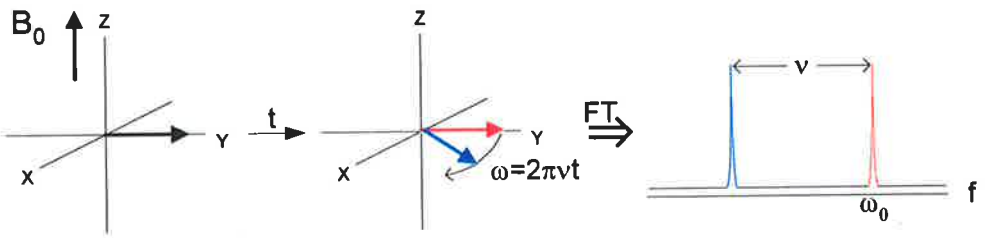

Figure 4.6 Vector diagram of a 1D NMR experiment, in the rotating frame (rotating at a frequency of ω_0), showing vectors for two resonances – one that precesses at ω_0 (red) and one that precesses at $\omega = 2\pi\nu t$ (blue). The resulting Fourier transformed (FT) spectrum is also shown.

Chemical shifts, coupling constants, signal multiplicity and integration can be obtained from 1D NMR spectra and can give information about molecular structure. However, for large molecules such as peptides and proteins, 1D ^{1}H spectra are of limited use, due to the large number of overlapped resonances.

4.3b Two-dimensional Spectroscopy

The development of two-dimensional (2D) NMR experiments meant that the resonances of small proteins (< 75 residues) could be assigned [232]. 2D experiments involve the modulation of a normal 1D spectrum as a function of some variable time interval, t_1 [230]. They utilise sequences of radiofrequency pulses, specific to each type of experiment, in order to extract different kinds of information from the sample. Some of the most useful 2D experiments in protein structure determination are discussed below.

4.3c Correlated Spectroscopy (COSY)

The pulse sequence of the simplest COSY experiment is as follows:

$$90° - t_1 - 90° - t_2$$

where t_1 is a variable time interval and t_2 is the acquisition time, during which the signal is recorded [230].

The first 90° pulse creates transverse magnetisation that is allowed to evolve during the time interval, t_1 (Figure 4.7). The Y-axis component of the evolved magnetisation is rotated through 90° by the second rf pulse. Following this pulse, magnetisation arising during t_1 is redistributed among coupled nuclei by coherence transfer [230]. The pulse sequence is repeated with incrementing values of t_1.

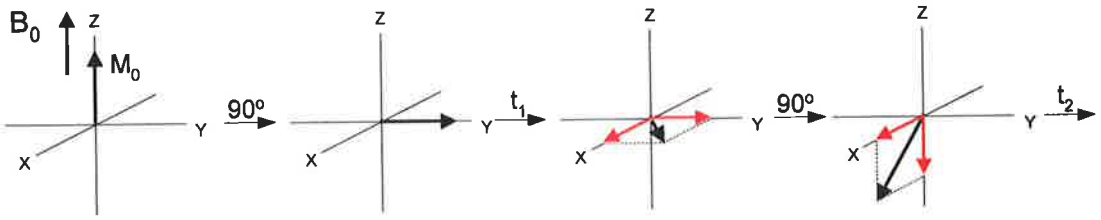

Figure 4.7 Vector diagram of the COSY experiment. Red arrows indicate X, Y and Z vector components.

After Fourier transformation of the t_1 and t_2 dimensions, a spectrum is produced that shows cross-peaks for each pair of nuclei that are coupled to each other through two or three bonds. Thus, the COSY experiment is useful for identifying spin-systems of amino-acid residues and is used in combination with the TOCSY experiment (Section 4.4a).

COSY spectra also provide a means for determining vicinal coupling constants (^3J) [233]. COSY cross-peaks occur as multiplets because of spin-spin coupling. The active coupling, between the two protons causing the peak, results in anti-phase multiplets [230] and the coupling constant, ^3J, can be measured as the separation between the peak and trough (see Section 4.5c).

There are several limitations to the use of COSY spectra, resulting from the presence of diagonal peaks [234]. These peaks, which have the same frequency in each dimension, result from magnetisation that is unaffected by the second 90° pulse [230]. The diagonal peak multiplets are in-phase and their intensity therefore increases binomially, and at a greater rate than the anti-phase cross-peak multiplets. This effect, as well as the tendency for the anti-phase components of the cross-peaks to cancel each other out, means that the diagonal peaks are enhanced relative to the information-rich cross-peaks [234]. The diagonal peaks also have dispersive line-shapes, in contrast to the absorptive line-shapes of the cross-peaks [233]. The long dispersion tails of the diagonal peaks obscure any cross-peaks in their vicinity.

A double quantum filtered COSY (DQF-COSY) experiment is often used in protein and peptide studies [230]. This version of the COSY experiment uses a double quantum filter to produce spectra with absorptive diagonal peaks and anti-phase multiplets [234]. The sensitivity (i.e., signal-to-noise ratio) of this experiment is actually reduced by a factor of

two from that of a conventional COSY. However, the effective sensitivity is greater because the cross-peak intensity is increased relative to that of the diagonal peaks [234].

4.3d Total Correlation Spectroscopy (TOCSY)

While the COSY experiment produces cross-peaks between pairs of coupled protons, the total correlation spectroscopy (TOCSY) experiment gives cross-peaks for all the protons present in the same spin system. The protons of each amino acid residue constitute a separate spin system because coupling does not occur through the peptide bond. Thus, for a cross-section going through a particular resonance, peaks will be present for all protons in the same spin system (residue) as that resonance.

The TOCSY experiment relies on cross-polarisation rather than the coherence transfer utilised by the COSY [230]. The pulse sequence of the TOCSY is shown in Figure 4.8. This variant includes an MLEV-17 decoupling scheme during the spin-lock period [230].

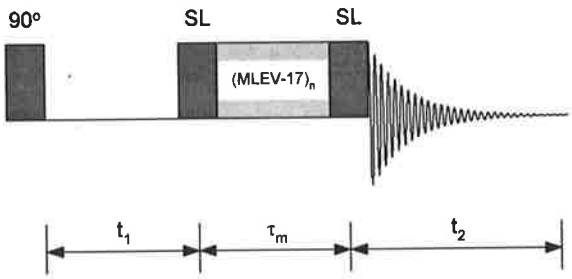

Figure 4.8 TOCSY pulse sequence, which incorporates a 90° pulse, followed by a delay (t_1), spin-locking (SL) fields, an MLEV-17 decoupling scheme applied during the mixing time (τ_m) and an acquisition period (t_2). (Based on a figure from Evans [230]).

Cross-polarisation is obtained by applying a single coherent rf field, known as a spin-locking (SL) field [235]. When the effective rf field experienced by two scalar coupled protons is identical, the two spins become temporarily equivalent and oscillatory exchange of magnetisation occurs [230]. For a simple two-spin system, complete exchange will occur with a spin-lock mixing time of 1/2J. For larger spin systems, this time dependence is more complicated [235]. Often a number of different spectra are obtained with different mixing times so as to achieve complete magnetisation exchange throughout the entire spin system [230].

The cross-peaks in a TOCSY have in-phase multiplet structure and are often stronger and easier to detect than the cross-peaks in a COSY spectrum [236]. In addition, all of the peaks in a TOCSY spectrum are absorptive in nature, including the diagonal peaks, meaning that sensitivity is enhanced relative to the conventional COSY experiment [235].

Problems with the TOCSY experiment can occur due to nuclear Overhauser effects [230] (Section 4.3f). This results in negative peaks occurring within the spectrum. At short mixing times, this is not usually a problem, but if it does occur, 'Clean' TOCSY pulse sequences are available to suppress the occurrence of the cross-relaxation peaks [236].

4.3e Heteronuclear Correlation Spectroscopy

Heteronuclear correlation spectroscopy provides information about coupling between protons (I spin) and a heteronucleus (S spin). The pulse sequence for such an experiment [230], in its simplest form, is:

I: $90° - t_1 - 90°$

S: $90° - t_2$

This experiment is analogous to the COSY but here, the coherence transfer process caused by the second pulse is coupled to a heteronucleus by applying a simultaneous pulse at the appropriate frequency [230].

A two-dimensional spectrum is produced where the I spin frequencies appear in one dimension and the S spin frequencies in the other. Diagonal peaks do not appear in the spectrum because the 90° pulse is not applied to the S spins before t_1 [230].

Multiplets will appear in the spectrum, due to proton coupling, unless delays are inserted before and after the mixing pulse [230]. This delay time is set to $1/2J_{IS}$ where, for a one-bond ^{13}C-^{1}H correlation, J_{IS} is in the vicinity of 100-200 Hz [48].

For biological NMR, the heteronuclear correlation experiments are insensitive because rare-spin (e.g. ^{13}C) magnetisation is being detected. To achieve optimum sensitivity, it is

necessary to start with proton polarisation and finish with proton detection [230]. Two experiments that do this are the heteronuclear single quantum coherence (HSQC) experiment [237] and the heteronuclear multiple-quantum coherence (HMQC) experiment [230], which both look at correlations through one-bond. For protein studies, HSQC spectra are preferred because pure absorptive line-shapes are obtained and the line-shapes are narrower than those found in an HMQC spectrum, resulting in improved resolution [230].

Heteronuclear multiple bond correlation (HMBC) is another variant of heteronuclear correlation spectroscopy, based on either the HMQC or HSQC experiments [230]. This experiment is used for looking at long-range correlations between protons and heteroatoms, through two or more bonds. Here, time delays are again inserted into the pulse sequence - equal to $1/2J_{IS}$, where J is set to around 8 Hz for ^{1}H-^{13}C long-range correlations [48]. Many two-bond and three-bond ^{13}C-^{1}H coupling constants are in the vicinity of 8 Hz and, as a result, these correlations can't be separated.

4.3f Nuclear Overhauser Effect Spectroscopy (NOESY)

The nuclear Overhauser effect (NOE) is the change in intensity of an NMR resonance when a nearby resonance is irradiated [238]. This is due to mutual dipolar relaxation between nuclei and is dependent on the internuclear distance. The NOE spectroscopy (NOESY) experiment permits the detection of all of a molecule's NOEs in a single experiment [48]. Thus, the NOESY experiment is extremely useful in studying 3D peptide structure as it provides information about the distance between pairs of protons in the molecule.

The pulse sequence of a NOESY experiment is as follows:

$$90° - t_1 - 90° - \tau_m - 90° - t_2$$

where τ_m is an interval known as the mixing time [230].

As in the COSY experiment, the first 90° pulse creates transverse magnetisation that evolves during t_1 and the second pulse rotates the Y component onto the Z-axis [230]. During the mixing period, τ_m, magnetisation exchange occurs between spins in close proximity, due to intra- or intermolecular dipolar relaxation [239]. This magnetisation transfer is due to the nuclear Overhauser effect (NOE). The third 90° pulse converts the Z magnetisation component into observable magnetisation [239].

The resulting 2D spectrum contains cross-peaks due to pairs of protons that are close together in space. The intensity of the NOESY cross-peaks drops off rapidly as the inter-proton distance increases, due to the inverse sixth-power relationship ($I \propto r^{-6}$) [230]. Thus, the maximum distance that can be detected is approximately 5 Å [48].

This intensity/distance relationship assumes that all of the protons in the molecule have the same correlation time, τ_c (correlation time is a measure of the rate of molecular tumbling). This is not the case, in practice, so distances cannot be calculated accurately. In addition, the NOEs measured are a reflection of the average inter-proton distance [238]. Methods exist, however, for estimating the maximum upper distance and some of these are described in Section 4.6a.

In practice, NOESY spectrum cross-peaks can also arise from other mechanisms such as chemical exchange, coherence transfer and spin diffusion. Chemical exchange peaks are often expected because of the known molecular structure and are not usually a problem for protein spectra. Coherence transfer gives rise to COSY type peaks but these can be suppressed by the use of phase cycling or pulsed field gradients [240].

Spin diffusion arises from cross-relaxation propagating from one nucleus to the next and can affect the cross-peak intensities [230] (also see Section 4.6a). This is more of a problem for large molecules (> 10 kDa) [241] and can be reduced by careful selection of the experimental parameters [238].

4.4 Sequential Assignments

In order to analyse data from NMR experiments, complete assignment of the protein proton resonances is required [220]. For some analyses, assignment of the alpha (αC) and carbonyl (C′) ^{13}C chemical shifts is also necessary.

4.4a Proton Assignments

One-dimensional proton experiments are not useful for assigning chemical shifts in proteins because of the high degree of signal overlap. The development of two-dimensional spectroscopy has made complete assignment of proton resonances possible [242]. This is done in two stages. Firstly, the signals for individual spin-spin coupled systems are identified. Each spin system gives the resonances for a single amino-acid residue because coupling does not occur through peptide bonds. The second stage of assignment involves allocating each spin-system to a particular position in the protein sequence.

Assignment of spin systems is achieved using COSY and TOCSY spectra. The COSY experiment shows cross-peaks for protons coupled through three bonds. Thus, amide protons (NH) can be correlated to alpha protons (αH), αH to beta protons (βH) and so on, until the entire spin system has been identified. Unfortunately, overlap frequently occurs in COSY spectra and assignment can be hindered.

TOCSY experiments correlate all of the resonances from the same spin-system, provided the appropriate mixing time is used [230]. Cross-sections of these spectra show cross-peaks from the NH to the α, β, γ, δ and ε protons (if present). TOCSY spectra have the advantage that the signal-to-noise ratio is greater than that for COSY spectra [232] (Section 4.3d) but because overlap occurs in the TOCSY spectrum as well, COSY experiments are often used to provide complementary information.

Each spin-system can be identified as a particular type of amino acid based on the number and chemical shift pattern of the correlated cross-peaks. Comparison of the cross-peak patterns with those observed for random coil residues, can aid this assignment [243].

Unless there is only one instance of a particular residue type, the position of the assigned spin-systems within the protein sequence cannot yet be identified. A method is needed for putting the spin-systems in sequential order. Wüthrich [242] analysed different types of secondary structure and found that, in all cases, short inter-proton distances are present between adjacent residues, particularly between the NH, αH and βH protons. Thus NOESY experiments, which show cross-peaks for inter-proton distances of less than 5Å, can be used to correlate the sequential spin-systems. Particularly useful signals are the NH_i to NH_{i+1} and αH_i to NH_{i+1} cross-peaks [232].

Problems with the sequential assignment can occur because of breaks in the sequential cross-peaks. This can be due to protons having almost coincident chemical shifts or αH signals being saturated by the water resonance. Using both the NH_i to NH_{i+1} and the αH_i to NH_{i+1} cross-peaks, or even the βH_i to NH_{i+1} signals, can generally overcome these hurdles. In addition, breaks in the sequential NH_i to NH_{i+1} cross-peaks occur whenever proline residues are present in the sequence since these residues do not have an amide proton. In these cases, NH_i to δH_{i+1} and δH_i to NH_{i+1} cross-peaks can be observed.

For very large proteins, problems also occur because of substantial overlap in the two-dimensional spectra. Here, three-dimensional spectra are used to increase the resolution. However, isotopic labelling of the protein with ^{15}N and ^{13}C is required in these cases, which is achieved via preparation of the recombinant protein in isotopically enriched media.

4.4b Carbon Assignments

Assignment of the αC ^{13}C resonances is made using an HSQC spectrum. In the HSQC experiment, protons are correlated to the carbon atoms via the α^1H assignments. Cross-peaks corresponding to the αHs in one dimension give the αC ^{13}C chemical shifts in the second dimension.

Carbonyl carbons are assigned from HMBC spectra. In this experiment, protons are correlated to carbons that are coupled via two or three bonds. Thus cross-peaks can be found that correlate NH_i, αH_i, βH_i, NH_{i+1} and αH_{i+1} with C'_i, as shown in Figure 4.9.

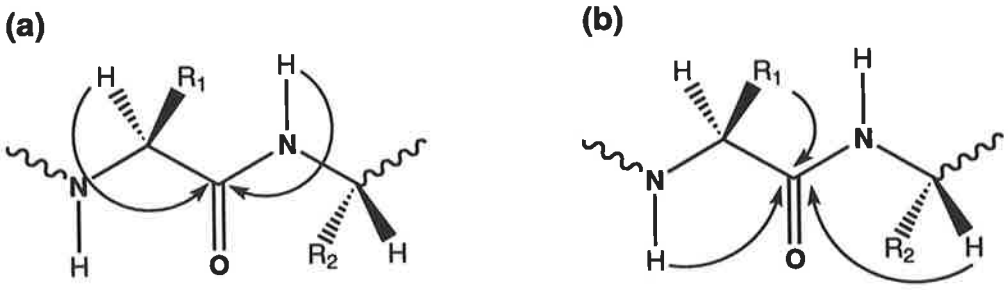

Figure 4.9 Correlations of protons to carbonyl ^{13}C atoms via (a) two bonds and (b) three bonds.

It is not possible to tell whether a cross-peak is due to coupling through two or three bonds by simple inspection. Therefore C' ^{13}C assignments must be confirmed by multiple correlations.

4.5 Secondary Structure Identification Using NMR Spectroscopy

4.5a Secondary Shifts

Chemical shift is dependent on the electronic environment of the nucleus concerned. Factors that influence the chemical shift include local fields around aromatic rings, polar and charged neighbouring groups, bond hybridisation states and local magnetic anisotropies [244]. These factors are in turn affected by conformation and molecular geometry. Thus, it is not surprising that regions of regular secondary structure have been shown to have predictable effects on chemical shift [245].

Statistical analysis of a large number of protein structures has shown that αH resonances shift upfield from random coil values by an average of 0.39 ppm, when in an α-helical structure [244]. Conversely, αH chemical shifts are moved downfield (~0.37 ppm) when the αHs are part of β-strand structure. Similar studies on αC and C′ showed that these ^{13}C resonances are shifted downfield in α-helices and upfield in β-strands [244]. Exactly why these resonances shift in the directions they do has not been satisfactorily explained as yet.

Amide proton resonances are more sensitive to temperature and pH than resonances of other backbone atoms [246]. Nevertheless, some correlation has been observed between NH shifts and secondary structure. In general, NH resonances shift upfield in helical structures and downfield in β-strands [244]. In addition, the NH protons at the N-terminal of an α-helix are generally shifted downfield relative to those at the C-terminal. This may be due to the overall helix-dipole deshielding the positive N-terminal and shielding the negative C-terminal [244].

The difference between a protein resonance and the corresponding random coil resonance is termed the secondary shift [206]. A positive Δδ means the protein resonance is downfield from the random coil chemical shift, while a negative Δδ denotes an upfield shift. Plotting Δδ values against amino acid sequence can reveal regions of the protein sequence with consistent upfield or downfield shifts, which in turn indicates that certain secondary structures are present.

Local chemical shift influences, such as nearby aromatic rings, polar or charged groups, can obscure the deviations caused by secondary structure. Pastore and Saudek [246] showed that smoothing Δδs of αH resonances over ± n residues (where n is usually set to 2 or 3) had the effect of averaging out the local effects. By plotting the smoothed Δδ values against amino-acid sequence, regions of regular secondary structure are more clearly identified. However, defining the ends of the secondary structural features is imprecise because of this averaging.

As well as α-helix and β-strand structure, chemical shifts can indicate regions of high flexibility [246]. Here, the peptide has access to a greater range of sterically allowed conformations. That is, the peptide is more random coil-like and chemical shifts will be closer to random coil values (i.e., Δδ approximately zero) [244].

The random coil values referred to above are determined empirically from many short, unstructured peptides, each containing one of the 20 common amino acids in the centre of the sequence. The other residues in the peptides are glycine or alanine, which have great conformational freedom and are therefore unlikely to adopt a fixed structure. Measurements are also taken in the presence of urea, thus denaturing any structure that may be favoured [243].

As solvent is known to have an effect on chemical shift, random coil values have also been determined in TFE, a solvent commonly used in NMR structure studies [247]. Although values have not been reported for all backbone atoms, the proton values available indicate there is little difference between shifts obtained in TFE and water [97].

Another interesting effect on NH resonances occurs for amphipathic α-helices. The NH Δδs in these structures vary with a periodicity of 3-4 residues [245, 248]. That is, the NH resonances from the hydrophobic face are generally downfield from the random coil shifts, while the NH shifts from the hydrophilic face move upfield [245]. This phenomenon is thought to be due to differences in hydrogen bond lengths along the molecule [248].

Specifically, intramolecular hydrogen bonds on the hydrophobic face are strengthened because of the hydrophobic environment provided by the side-chains. This reduces solvent access and decreases the likelihood of intermolecular hydrogen bonds forming. Hydrogen bonds on the hydrophilic face, however, are longer and less linear as the carbonyl groups from the hydrophilic residues tilt away from the helix to form additional hydrogen bonds with solvent [249].

This explanation agrees with the fact that hydrogen bonds cause deshielding of the proton involved [48]. Thus shorter hydrogen bonds would cause greater deshielding and downfield shifts and vice versa. It is also consistent with surveys of hydrogen bond lengths and angles in crystal structures of amphipathic helices [249, 250]. Macroscopically, these hydrogen bond lengths result in curvature of the helix axis, where the hydrophobic face is concave and the hydrophilic face is convex [245, 249].

4.5b NOE Connectivities

Different types of secondary structure have characteristic short inter-proton distances that are observable in NOESY spectra [242]. The standard notation for describing these distances, as developed by Wüthrich [242], is $d_{AB(i,j)}$, which is the distance between two protons A and B on residues i and j. The residue indices, i and j, are omitted for sequential distances (i.e., $d_{AB} \equiv d_{AB(i,i+1)}$).

For methylene or methyl βHs and the αHs in glycine residues, the notation refers to the shortest distance. For proline residues, which do not have amide protons, the corresponding distances are observed with the δ protons instead and, again, the notation refers to the shorter distance.

Regions of regular secondary structure can be identified from the pattern of observed NOE connectivities. α-Helices, for example, have strong sequential d_{NN}, medium $d_{\alpha N}$ and $d_{\alpha N}(i,i+3)$ and weak $d_{\alpha N}(i,i+4)$ NOEs [251]. β-Sheet structures, on the other hand, have very strong sequential $d_{\alpha N}$ cross-peaks and weak d_{NN} NOEs. They also have short inter-strand $d_{\alpha N}(i,j)$, $d_{NN}(i,j)$ and $d_{\alpha\alpha}(i,j)$ distances, which are highly diagnostic [230]. A

summary of the characteristic NOE connectivities for α-helices and β-strands, is given in Figure 4.10.

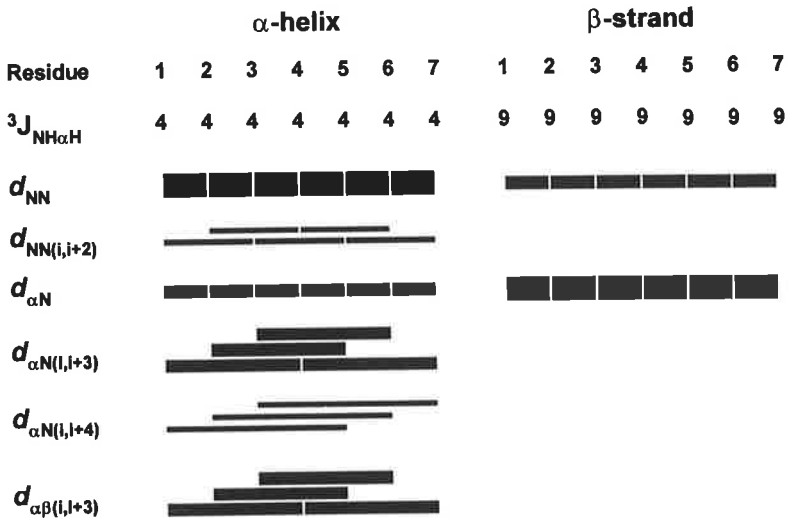

Figure 4.10 Summary of the characteristic short-range NOEs and spin-spin coupling constants, $^3J_{NH\alpha H}$, observed for ideal α-helices and β-strands. The thickness of the bars indicates the intensity of the NOEs and the $^3J_{NH\alpha H}$ values are given in Hz.

NOE connectivities can also be used to detect cis-trans isomerisation of the imide bond between proline and its preceding residue (Figure 4.11). In the cis form, the $d_{\alpha\alpha}$ and $d_{N\alpha}$ distances are closer than in the trans form. The more common trans form, however, favours short $d_{\alpha\delta}$ and $d_{N\delta}$ distances.

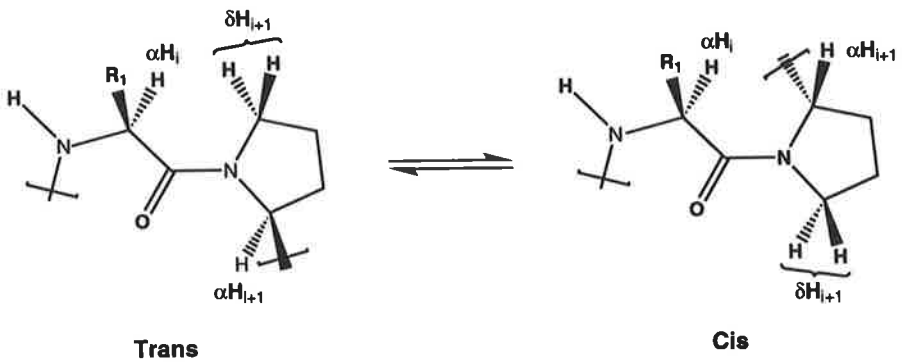

Figure 4.11 Cis-trans isomerisation of the X-Pro bond.

A full set of NOE connectivities is not always observed. Reasons for this include resonances that are too close in chemical shift to be distinguishable from the diagonal (e.g. d_{NN}) and saturation of resonances with chemical shifts close to that of water, when water

presaturation is used [232]. The latter case usually involves α protons, as these resonances often occur in this region. Thus cross-peaks such as $d_{\alpha N}$ can be lost.

4.5c Coupling Constants

Additional structural information can be obtained from vicinal spin-spin coupling constants (^{3}J), which are related to the dihedral angle by the Karplus equation [230]. This equation has the form:

$$^3J = A + B\cos\theta + C\cos^2\theta$$

where A, B and C are constants that depend upon substituent electronegativity [252]. Values for these coefficients have been empirically determined from known protein structures for different classes of protein dihedral angles [230].

The phi angle (ϕ), which is the dihedral angle defined by C'_i, N_{i+1}, αC_{i+1} and C'_{i+1}, as shown in Figure 4.12, is related to the NH-αH coupling constant ($^3J_{NH\alpha H}$) by the following specific form of the Karplus equation [253]:

$$^3J_{NH\alpha H} = 6.4\cos^2(\phi - 60°) - 1.4\cos(\phi - 60°) + 1.9$$

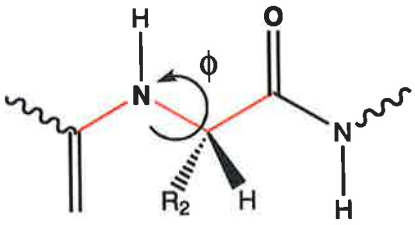

Figure 4.12 The phi (ϕ) dihedral angle. In this representation ϕ is equal to 180°.

The relationship between $^3J_{NH\alpha H}$ and ϕ is shown graphically in Figure 4.13. Here it can be seen that as many as four different values of ϕ can be attributed to a particular coupling constant. In known protein structures, however, the ϕ angles for all residues, aside from glycine, are found in the region of –30 to -180° [254]. Further, for $^3J_{NH\alpha H}$ values of less than 6 Hz, the ϕ values are clustered in the range of –50 to -90° [253].

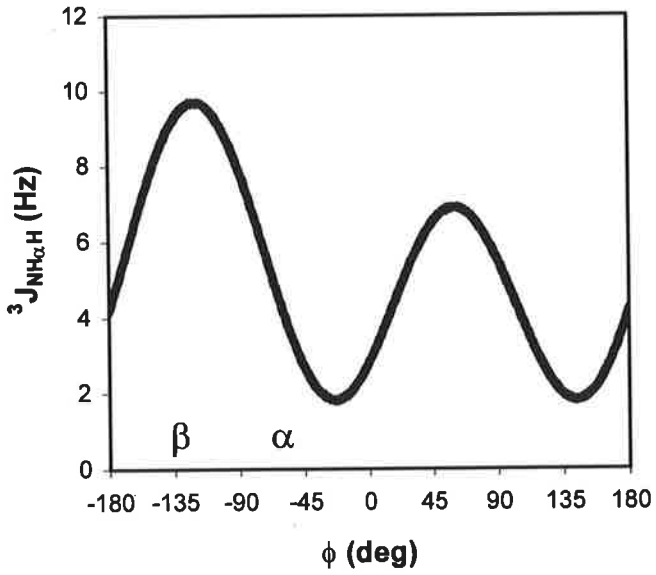

Figure 4.13 Karplus curve showing the relationship between the $^3J_{NH\alpha H}$ coupling constant (Hz) and the ϕ dihedral angle. The ϕ values for idealized α-helices (α) and β-strands (β) are also shown.

Phi is equal to -57° ($^3J_{NH\alpha H}$ = 3.9 Hz) for an ideal α-helix, -139° ($^3J_{NH\alpha H}$ = 8.9 Hz) for an antiparallel β-sheet and –119° ($^3J_{NH\alpha H}$ = 9.7 Hz) for a parallel β-sheet. However, as the secondary structural features of real proteins are frequently distorted, ϕ values vary somewhat from the ideal [254]. Consequently $^3J_{NH\alpha H}$ values vary as well.

Local motion also causes variation in dihedral angles, such that the observed vicinal coupling constant is in fact the time-average for all conformations [255]. There is minimal local motion for ϕ angles, however, which are relatively stable in highly structured regions [256]. In general, $^3J_{NH\alpha H}$ values of less than 6Hz indicate helical structure, while values greater than 8 Hz indicate β-sheet [256].

For very small peptides, $^3J_{NH\alpha H}$ values can be obtained from the amide proton region of a high resolution ^1H spectrum [100]. However, this region of the spectrum becomes highly overlapped for larger proteins, so in these cases DQF-COSY spectra are commonly used. Here the $^3J_{NH\alpha H}$ values are determined from the separation between the peak and trough of the antiphase multiplets [233].

Problems occur, however, when the value of $^3J_{NH\alpha H}$ is less than the linewidth. In these instances, the coupling constant is seriously overestimated [230]. Though increasing the

digital resolution can overcome this problem to some extent, it is limited by the large natural linewidths of proteins [251]. Methods have been developed for calculating the actual $^3J_{NH\alpha H}$ values from DQF-COSY spectra, though these too have limited reliability [257].

Despite the inaccuracies, the observation of a series of three to five small (<6 Hz) or large (>8 Hz) sequential $^3J_{NH\alpha H}$ values is a reliable indicator of the secondary structure present [242], although it is not possible to differentiate between particular helix types or between parallel and anti-parallel β-sheets.

4.5d Amide Exchange Measurements

Amide protons exchange with protons from water at varying rates, depending on a number of factors such as pH, temperature, hydrogen bonding and access to water. The mechanism by which this occurs can be either acid- or base-catalysed and the overall rate of exchange is at a minimum when the rates for each mechanism are equal [258]. This generally occurs around pH 3, although it varies according to the specific environment a proton is in [259].

The NHs in an unstructured peptide normally exchange within seconds to minutes. Even at pH 3 and at low temperature, all protons will be un-exchanged after 100 minutes [230]. When the NHs are involved in hydrogen bonding, as is the case for all types of regular secondary structure, then they can take from hours to days to even weeks to exchange [230]. Thus NH exchange rates can indicate NHs that are involved in hydrogen bonding and are therefore part of structured regions. However, the data do not reveal the acceptor atom of the hydrogen bond(s).

In β-sheets, NHs involved in inter-strand hydrogen bonds will be slow exchanging [258]. In an α-helix, hydrogen bonds are present between the carbonyl oxygen of residue i and the NH of residue i+4. The N- and C-termini are somewhat 'frayed', or less stable, because the first four NHs and the last four carbonyl oxygens cannot form hydrogen bonds within the peptide [260]. Thus the helix termini can be determined from the comparatively fast exchange rates of their NHs [242, 258]. The N-terminal NHs will exchange faster than those at the C-terminal since they are not involved in intramolecular hydrogen bonds at

all. Fast exchange will also occur around bends and regions where structural fluctuations occur [261].

NH exchange rates can also be slow in regions of the protein that are shielded from water [262]. This may be due to the 'burying' of protons in the core of a globular protein [258], because of aggregation of a number of peptide monomers [263] or because of insertion of the peptide into the hydrophobic region of a micelle [215]. For example, NH exchange rates have been used as evidence of the aggregation of melittin in solution [263].

Sometimes different rates of NH exchange are found for protons in the same α-helix. Zhou *et al.* [245] looked at the exchange rates for a monomeric, amphipathic, α-helical peptide in TFE/H_2O. They found that the rates of exchange for the hydrophobic residues were much slower than those for the hydrophilic residues. This indicated that the NHs from the hydrophobic residues were in a somewhat hydrophobic environment, excluded from water, while the NHs of the hydrophilic residues had greater access to the solvent.

NH exchange measurements are made using NMR spectroscopy, by dissolving the peptide in deuterated water and following the loss of intensity of the NH peaks over a period of time [262, 264, 265]. It is important that the NMR experiment used is quick, particularly for the initial time points, so 1D proton spectra are often used. If signal overlap is a problem, which it invariably is for larger proteins, other experiments such as TOCSY, COSY or NOESY can be used, or ^{15}N-HSQC experiments if the sample is isotopically labelled [251].

4.5e Summary

Although the chemical shifts, NOE connectivities, coupling constants and NH exchange rates are all qualitative (or at best semi-quantitative) indicators, when combined they can give a fairly accurate picture of secondary structure. The termini of each secondary structure element can be hard to define, however, and the overall tertiary structure cannot be revealed using these techniques. For a more accurate view of protein structure, NMR data must be used as input for structural calculations.

4.6 Structure Calculations

NMR spectroscopy can be used to obtain structural restraints - primarily inter-proton distance restraints from NOESY spectra - from which a protein structure can be determined with the aid of computer calculations. First, however, the NMR spectra must be assigned. This is done using a variety of experiments including COSY, TOCSY and NOESY, as outlined in Section 4.4.

NOESY cross-peaks can then be assigned and quantified to give distance restraints. Dihedral restraints can be obtained from three-bond coupling constants measured in COSY spectra. These restraints are combined with restrained molecular dynamics and simulated annealing protocols to determine the three-dimensional protein structure.

The quality of the calculated structures must then be assessed to give an indication of how well they reflect the actual protein structure. Each stage of the structure calculation process will be discussed more fully in the following sections.

4.6a Distance Restraints

NOESY cross-peak intensity initially increases with mixing time, before gradually decaying [230] (Figure 4.14). As the initial build-up rates are proportional to r^{-6}, the cross-peak intensities (I_{ij}) can be used to estimate the inter-proton distances (r_{ij}), provided that, at the mixing time used, the build-up rates approximate the initial rates [251].

Cross-peak intensity is also dependent on the correlation time (τ_c) of the molecule [255], where correlation time is a measure of the rate of molecular tumbling[†]. As correlation time increases, for example due to higher molecular weight, so does the initial rate of NOE build-up (Figure 4.14). This means that longer distances (less intense peaks) will only be observed in NOESY spectra with sufficiently long mixing times.

[†] Assuming molecular weight, M_r, is proportional to the molecular radius, r, then correlation time, τ_c, can be approximated as $\tau_c \approx M_r \times C$, where C is typically 1.3×10^{-12} [230].

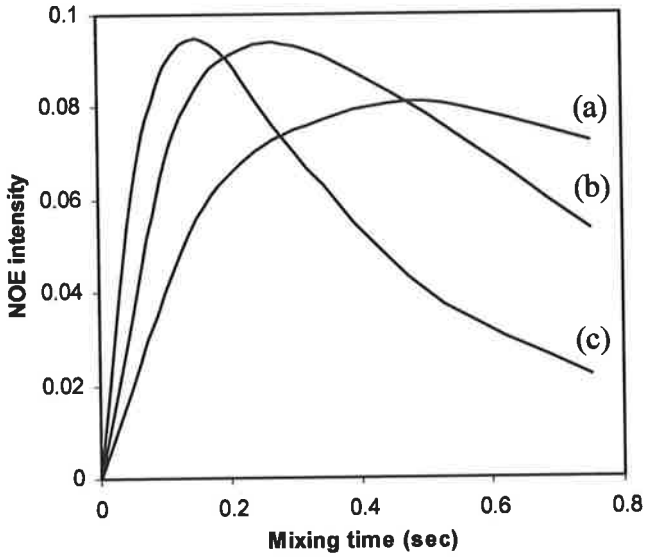

Figure 4.14 Time dependence of the intensity of the δH-εH cross-peak of Tyr68 in dihydrofolate reductase, calculated for the correlation times (a) 2 nsec, (b) 4 nsec and (c) 8 nsec (based on a figure from Barsukov and Lian [251]).

While the initial rate of cross-peak build-up increases with increasing correlation time, the onset of decay occurs sooner. Thus, as correlation time increases, the initial rate approximation only holds for shorter mixing times.

If the initial rate approximation is not met, that is, if the mixing time is too long for the molecule under consideration, then spin diffusion becomes a problem and errors will occur in the estimated distances [230]. Spin diffusion, or indirect magnetisation transfer from nucleus to nucleus, decreases the intensity of strong peaks and increases the intensity of weak peaks [218, 219]. When molecular motion is fast (short τ_c), neighbouring protons of a given proton pair have a negligible effect on the cross-peak intensity. However, for slower-moving large molecules (long τ_c), the arrangement of neighbouring protons becomes important and spin diffusion is observed [251].

Provided that the initial rate approximation is satisfied, inter-proton distances between protons i and j (r_{ij}) can be estimated by comparison with a reference distance between protons k and l (r_{kl}), for which there is a well-resolved and uniquely assigned cross-peak (I_{kl}), according to the relationship [255]:

$$r_{ij} = r_{kl} (I_{kl}/I_{ij})^{1/6}$$

This relationship assumes that the correlation time is the same for each proton in the molecule, i.e., the molecule is a rigid body, which is clearly an oversimplification. Calibrating the inter-proton distances, in this way, leads to systematic overestimates of distances that are less than the reference distance, and underestimates distances that are greater than the reference distance, because of spin diffusion [255]. These errors increase as correlation and mixing times increase [251].

The reference distance used in the above calibration procedure needs to be accurately known for the structure under study. Thus, the distance between protons with fixed relative positions, is often used – for example, the distance between non-degenerate methylene protons [251]. Methylene protons are fixed at 1.7 Å from each other. Unfortunately, their chemical shifts are usually very similar and therefore their common cross-peak is close to the diagonal. Overlap from the very intense diagonal peaks can also increase the intensity of the methylene cross-peaks, resulting in errors in the calculated distances.

Other potential reference distances include those between δ and ε aromatic protons [230], and the δ and γ protons of proline residues [97]. There are problems with these choices as well, since it is known that aromatic protons can produce highly variable NOEs, and internal motion within proline can lead to unreliable results [230]. In addition, the fixed protons are usually close together in space and spin diffusion can therefore influence intensity.

Alternatively, reference distances identified from initial secondary structure determinations (Section 4.5) can be used. For example, $d_{\alpha N}$ cross-peaks, from protons in regions identified as α-helical, can be ascribed distances of 3.5 Å [242]. This method has certain disadvantages in that it may bias the results toward a particular secondary structure type and it also assumes the secondary structure conforms to standard distances.

A related method for restraint calibration, that does not require known reference distances as such, is given by the following equations [266]:

$$r_{ij} = \left[\frac{A(I_{ij})}{I_{ij}}\right]^{1/6}$$

$$\text{where, } A(I) = \left[\frac{I - I_s}{I_w - I_s}\right]\left[A(I_w) - A(I_s)\right] + A(I_s)$$

A(I) is an intensity-dependent proportionality factor calculated using the average of the ten weakest (I_w) and ten strongest (I_s) NOEs, and the proportionality factors $A(I_w)$ and $A(I_s)$ that are derived from these values as follows [266]:

$$A(I_w) = (5.0\,\text{Å})^6\, I_w$$

$$\text{and } A(I_s) = (1.8\,\text{Å})^6\, I_s$$

The advantage of this technique is that it does not require accurately known reference distances and it uses an intensity-dependent proportionality factor that should reduce the errors due to spin diffusion. It does, however, assume that the weakest peaks correspond to a distance of 5Å, which may not be the case for certain mixing and correlation times.

Factors that can affect intensity, and therefore the calculated distances, include internal motion, alternate relaxation pathways, chemical exchange and spin diffusion. Because of these indirect effects, highly accurate distances are not obtainable in practice [230]. Thus, restraints are expressed as conservative ranges with upper and lower bounds.

The lower bound is usually determined by the sum of the van der Waal s radii and is used for all restraints, even those categorised as weak, because local motion can severely attenuate peaks [230].

There are a number of different procedures that can be used for generating the upper bound. One common method is to classify the NOEs into three categories: strong

(1.8-2.8 Å), medium (1.8-3.3 Å) and weak (1.8-5.0 Å) [267]. However, this approach results in a substantial loss of structural information [251].

Another approach to calculating the upper bounds is to add an estimate of the distance error to the calibrated distance [218]. The error is often calculated as a percentage of the distance, to allow for the errors while retaining the continuum of restraints [251, 266]. However, as the error is expected to increase at a greater than linear rate, a better approach may be to vary the error estimate with the square of the calibrated distance [218, 268].

In general, varying the tightness of the distance bounds does not have a large effect on the structures produced, as even very loose restraints drastically reduce the conformational space available to the peptide chain [218].

4.6b Ambiguous NOEs

For small molecules, assignment of NOE cross-peaks can often be done on the basis of chemical shifts alone, using 2D spectra (Section 4.4a). However, as molecular size increases, the probability of more than one proton having the same chemical shift is increased. When this occurs there will be ambiguity in assigning certain peaks. Ambiguity also occurs when methylene or isopropyl methyl resonances are degenerate.

The quality of a calculated structure depends strongly on the number of uniquely assigned peaks [251]. Thus, methods to resolve ambiguities are sought so as to improve the generated structures. One way to do this is to use 3D spectra. Separating peaks into a third dimension increases the chances of overlapped peaks becoming resolved. This method, though powerful, requires uniform labelling with ^{13}C and ^{15}N and is therefore expensive and time-consuming.

An alternative way to reduce the ambiguity is to do a preliminary calculation using only the uniquely assigned cross-peaks [255]. Distances can then be extracted for each proton pair in an ambiguous assignment, averaged over the ensemble of structures. Pairs that are very distant in the structures can be excluded, while those that are close together are

retained. Thus ambiguous restraints can be refined in an iterative process and in many cases they can become unique assignments [251].

Some assignments will remain ambiguous but this information need not be lost. Ambiguous assignments can be used in structure calculations by employing sum-averaging [269]. This method is based on the following equation:

$$r=(\Sigma_{ij}\, r_{ij}^{-6})^{-1/6}$$

where r is the distance calculated from the total NOE intensity and r_{ij} is the actual distance between pairs of protons, i and j. This equation expresses the volume of the ambiguous peak as a sum of the volumes of each peak that contributes to it. The computations restrain r_{ij} values such that this equation is satisfied.

4.6c Stereo-specific Assignments

Individual methylene protons can often be resolved, which leads to the problem of how to assign these resonances stereo-specifically, that is which resonance belongs to the pro-R proton and which to the pro-S. A similar problem exists for the methyl protons of valine and leucine residues.

Stereo-specific assignments of β-methylene protons can sometimes be made using the relative intensities of intra-residue NOEs from NH or αH to the βHs, as well as from $^3J_{\alpha H\beta H}$ coupling constants [267]. The latter method relies on the relationship between $^3J_{\alpha H\beta H}$ and the χ_1 torsion angle (where χ_1 is the dihedral angle defined by C′, αC, βC and γC). Similar methods exist for stereo-specifically assigning valine and leucine residues [251, 270]. Such assignments improve the resolution of the calculated structures [271].

It is not always possible to assign protons stereo-specifically. Pseudo-atoms are often introduced in these cases [272]. These imaginary atoms are positioned centrally between the unassigned protons and the NOE restraints from the real protons are now related to the pseudo-atom instead. Because of the displacement of the pseudo-atom, significant

corrections to the NOE restraints must also be made, resulting in a loss of information [271].

An alternative manner of dealing with these assignments is to assign them arbitrarily and use the resulting constraints in the structure calculation procedure. The protons can be allowed to 'float' between configurations by starting with a small force constant for the improper dihedrals (Section 4.6f) and gradually increasing this over the course of the calculations [267]. The final structures will have the configurations that are most consistent with the restraints [269]. Another option is to explicitly swap configurations at different points along the calculations, provided the structure obtained is lower in energy. If the structure is higher in energy, the original configuration is retained [271].

The advantage of these 'floating' chirality methods is that NOE correction factors are no longer necessary so no information is lost [271]. They provide a reliable and facile means of dealing with stereo-specificity in a calculation procedure, without having to explicitly assign these resonances [271].

4.6d Dihedral Angle Restraints

Dihedral angle restraints can be used in structure calculations to supplement the inter-proton distance information provided by NOESY spectra. As outlined in Section 4.5c, ϕ angles are related to the $^3J_{NH\alpha H}$ coupling constant by the following version of the Karplus equation, where the coefficients were determined empirically [253]:

$$^3J_{NH\alpha H} = 6.4\cos^2(\phi - 60°) - 1.4\cos(\phi - 60°) + 1.9$$

Thus, theoretically, $^3J_{NH\alpha H}$ values give specific ϕ angles. However, because coupling constants can only be obtained with limited accuracy and as local motion around the N-αC bonds results in time-averaged $^3J_{NH\alpha H}$ values, ϕ angles are restrained to a range of possibilities. For calculation purposes, the ϕ values are restrained to $-60 \pm 40°$ for $5Hz < {}^3J_{NH\alpha H} < 6Hz$, and $-60 \pm 30°$ for $^3J_{NH\alpha H} < 5Hz$. For $^3J_{NH\alpha H} > 8Hz$, ϕ values are restrained to $-120 \pm 40°$ [265].

4.6e Restrained Molecular Dynamics and Simulated Annealing

Many different approaches exist for calculating protein structures from NMR-derived restraints. Each attempts to locate the global minimum of a target energy function that incorporates the empirical restraints [273]. One approach that has been used with some success is a combination of restrained molecular dynamics and dynamical simulated annealing [261, 268, 271, 273, 274].

Molecular dynamics aims to simulate the motion of a system of particles using classical mechanics and a potential energy function that describes the forces acting on the particles [275]. Restrained molecular dynamics (RMD) is a variant on the conventional molecular dynamics used in simulations, where terms are introduced into the potential energy function to describe the experimental restraints [219].

Starting from an initial conformation, the system is allowed to evolve with time, with the positions and velocities of the particles determined for successive time-steps. The molecular trajectory is determined by solving Newton's equation of motion:

$$\mathbf{F}_i = m_i \mathbf{a}_i$$

where $\mathbf{F}_i$ is the force on atom i, m_i is the mass and $\mathbf{a}_i$ is the acceleration (bold-type indicates vector terms).

The force on atom i can be calculated from the derivative of the potential energy (V) with respect to atom position, $\mathbf{r}_i$, and since the acceleration can be expressed as the second derivative of position with respect to time, we can express the previous equation in the following form [230]:

$$\frac{dV}{dr_i} = m_i \frac{d^2 r_i}{dt_i^2}$$

Given a set of starting co-ordinates and a suitable potential energy function (or target function), and since the masses are known, this equation can be integrated over successive

time-steps, Δt, to determine the velocity and displacement of the atoms [255, 276]. The time-steps, however, must be very small to avoid large changes in the potential energy [275].

Molecular dynamics calculations require some kind of initial structure. This can be a randomised structure with physical bond lengths and angles, a completely randomised structure, an extended structure or an unrefined structure developed by some other calculation method [267]. Random velocities are then assigned to the atoms from a Maxwellian distribution for the temperature used [275].

The temperature (T) of the system is directly proportional to the kinetic energy according to the following equation:

$$\frac{1}{2}\sum_{i=1}^{N} m_i (v_i)^2 = \frac{3}{2} NkT$$

where v_i is the velocity of atom i, N is the total number of atoms in the system and k is the Boltzmann constant. Molecular dynamics efficiently minimises the energy of the system by converting excess potential energy to kinetic energy and removing it by coupling the system to a constant temperature heat bath [219].

The path to the global minimum of the potential energy function is not straightforward. There are many false minima that must be overcome. Energy minimisation procedures, for example by the steepest descent or conjugate gradient (Powell) methods, can be used for finding local minima but they are not able to overcome energy barriers [230]. These procedures are therefore highly unlikely to find the global minimum but they are useful techniques for minimising the initial and final structures calculated with RMD [219].

In RMD calculations, the kinetic energy present means some energy barriers in the target function can now be crossed [267]. However, the temperature of the system limits the available energy. Thus, RMD calculations are frequently combined with a simulated annealing (SA) protocol where the initially high temperature (*ca.* 2000 K) is gradually lowered throughout the calculations [267]. This procedure is far more successful at locating the global minimum than RMD alone [255].

The forces acting on the atoms tend to zero as the calculations proceed and the constraints become satisfied [275]. As the restraints are described as ranges, instead of discrete values, many structures may be consistent with the experimental data. Thus the calculation procedure must be repeated many times to obtain an ensemble of structures [220]. This is achieved by randomly varying the initial structure or the assigned velocities for each repetition [230].

4.6f The Potential Energy Function

The forces acting on the atoms of the system are determined by the 'force-field' or potential energy function (V). Thus the success of the RMD/SA protocol depends on the quality of the force-field used [219].

The potential energy function has both covalent and non-bonded terms, as indicated below. The terms that usually make up $V_{covalent}$ and $V_{non\text{-}bonded}$ are also indicated.

$$V_{total} = V_{covalent} + V_{non\text{-}bonded}$$

$$V_{covalent} = V_{bond} + V_{angle} + V_{improper}$$

$$V_{non\text{-}bonded} = V_{vdW} + V_{electrostatic}$$

The $V_{improper}$ term maintains the planarity of aromatic rings and the chirality of chiral centres [255].

The potential energy of the bond lengths, angles and improper dihedrals are frequently given by harmonic potentials, as shown for V_{bond} below [275]:

$$V_{bond} = \frac{1}{2}\sum_{bonds} K_b (b - b_0)^2$$

where K_b is the bond force constant, determined empirically, b is the bond length and b_0 is the ideal bond length. Deviations from the ideal values, b_0, are therefore penalised by higher energies.

The Lennard-Jones potential and the Coulomb potential describe the van der Waals (V_{vdW}) and electrostatic interactions ($V_{electrostatic}$) respectively:

$$V_{vdW} = \sum_{pairs\,(ij)} \left[\frac{A}{r_{ij}^{12}} - \frac{B}{r_{ij}^{6}} \right]$$ Lennard-Jones potential

$$V_{electrostatic} = \sum_{pairs\,(ij)} \frac{q_i q_j}{D r_{ij}}$$ Coulomb potential

where A and B are experimentally determined parameters that depend on the particular atoms involved [275] and r_{ij} refers to the distance between atoms i and j. The charges on atoms i and j are indicated by q_i and q_j and D is a dielectric function for the medium. Hydrogen bonding can be accounted for in the electrostatics term with the use of partial charges [275].

For protein structure calculations, the NMR-derived constraints must also be included in the energy function. The distance constraints can be described by a square-well potential of the form:

$$V_{NOE} = \begin{cases} K_{NOE}(r_{ij} - r_{ij}^{u})^2 & \text{if } r_{ij} > r_{ij}^{u} \\ 0 & \text{if } r_{ij}^{l} \le r_{ij} \le r_{ij}^{u} \\ K_{NOE}(r_{ij} - r_{ij}^{l})^2 & \text{if } r_{ij} < r_{ij}^{l} \end{cases}$$

where K_{NOE} is the NOE force constant, or weighting factor, and r_{ij}^{u} and r_{ij}^{l} are the upper and lower distance bounds respectively [255]. A similar potential can be devised for the dihedral angle restraints.

It is important to realise that, unlike the other potential energy terms, the NMR-restraint potentials do not correspond to any real physical force but simply provide a way to introduce the restraints into the calculations [230]. Thus, the force constants are set in a somewhat arbitrary manner. However, it is important that the values chosen are sufficiently high to ensure that the experimental restraints are the dominating factor in determining the conformation [267].

4.6g Quality of Structures

Once an ensemble of structures has been generated, it is necessary to determine their consistency, precision and accuracy. That is, how well do they satisfy the restraints imposed on them, how well are the structures defined and how closely do the calculated structures reflect the actual structure of the protein in solution.

The extent to which the calculations satisfy the NMR-derived restraints is usually expressed in terms of the number and magnitude of the restraint violations, while the precision of the structures is indicated by the root-mean-square deviation (RMSD) of the ensemble from the average structure. If the restraints are satisfied and a significant proportion of the structures have converged (generally accepted as RMSD < 2.0 Å) then it is likely that the ensemble of structures closely resembles the actual protein structure [230]. If there are large violations of the restraints and no convergence, it is likely that there are errors in the restraints [267]. This could occur because of mistakes in the assignments and means that the restraints should be reanalysed [230].

A third scenario, where the NMR restraints are satisfied but widely varying structures are produced, indicates that the information content of the restraints is insufficient for acquiring an accurate picture of the protein structure [267]. This could be due to either a lack of NOE cross-peaks or because of overly conservative distance bounds [230]. A lack of NOE cross-peaks can be the result of mobility but since other explanations are possible, such as no short inter-proton distances in the region concerned [267], mobility cannot be inferred from this alone [230].

Another method for determining the precision of the structures is to determine the angular order parameters (AOPs). These parameters provide a measure of the distribution of the dihedral angles for each residue across the ensemble of structures [277]. They are calculated from the following equation:

$$S(\alpha_i) = \frac{1}{N}\left\| \left(\sum_{j=1}^{N} \alpha_i^{\,j} \right) \right\|$$

where $S(\alpha_i)$ is the order parameter of the dihedral angle α_i of residue i, and j refers to the individual structures, from 1 to N [278].

The dihedral angle, α_i, is expressed as a 2D unit vector for AOP calculations. Thus, for a fully defined angle, with no deviation over the ensemble of structures, S is equal to one, while for a randomly distributed dihedral angle, S is equal to zero [277]. While the cut-off is somewhat arbitrary, dihedral angles are often judged to be well-defined for values of S > 0.9. This corresponds to a standard deviation of ± 24° [278].

AOPs can be calculated for any dihedral angle, however they are most often used to assess the order of the backbone angles phi (ϕ) and psi (ψ), where ϕ is defined by C'_i, N_{i+1}, αC_{i+1} and C'_{i+1} and ψ is defined by N_i, αC_i, C'_i and N_{i+1} (Figure 4.15).

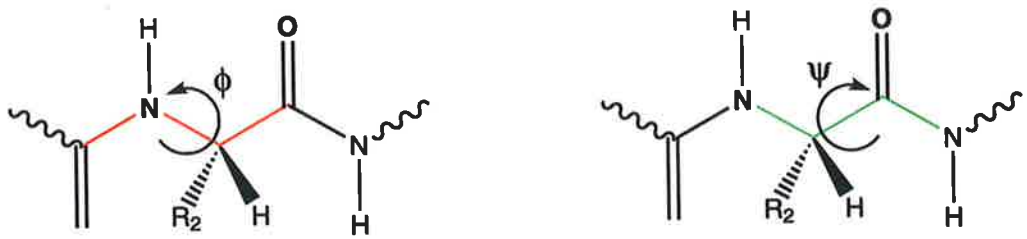

Figure 4.15 The phi (ϕ) and psi (ψ) dihedral angles. In these representations ϕ and ψ are both equal to 180°.

The calculated structures should be assessed for how well the covalent parameters, such as bond length, angles and impropers, correspond to ideal values. In addition, the ϕ and ψ angles of the well-defined residues can be evaluated to see if they are sterically allowed. This can be done using a Ramachandran plot.

Ramachandran *et al.* [279] showed that because of steric interactions, only certain combinations of ϕ and ψ angles are allowed. When the ϕ and ψ angles from known protein structures are plotted against each other they tend to fall in certain regions [280]. Note that proline and glycine residues are excluded because of their atypical ϕ/ψ distributions. The regions with the highest density of residues are collectively called the favourable region and over 80% of residues fall into this region. Other areas can be defined with progressively lower residue densities and these are known as the allowed, generous and disallowed regions. This plot, showing the different density regions, is known as a Ramachandran plot.

When placed on a Ramachandran plot, the well-defined residues from calculated structures should occur in the favourable and allowed regions if the structures are of high quality [280]. As residues from different classes of secondary structure fall into specific regions of the Ramachandran plot, these plots can also give an indication of the secondary structure.

4.7 Models for a Membrane Environment

Amphibian peptides are believed to act via destruction of bacterial cell membranes so it is their conformation in a membrane that is of interest. Attempts at NMR experiments using native membranes, or even vesicles (Figure 4.16 (b)), have shown no protein ^{1}H NMR signals because the line-widths are too broad [281-283]. This is due to the slow tumbling of these structures in solution.

It is possible to use solid-state NMR to determine protein and peptide structures in lipid bilayer systems [284, 285] (Figure 4.16 (a)), however these techniques are still in the early stages of development. They also require the isotopic labelling of the peptide or protein. A number of other model membrane systems exist, however, that can be used with both circular dichroism and NMR spectroscopy to determine structural information. These media include mixed organic solvents and micelles (Figure 4.16 (c)).

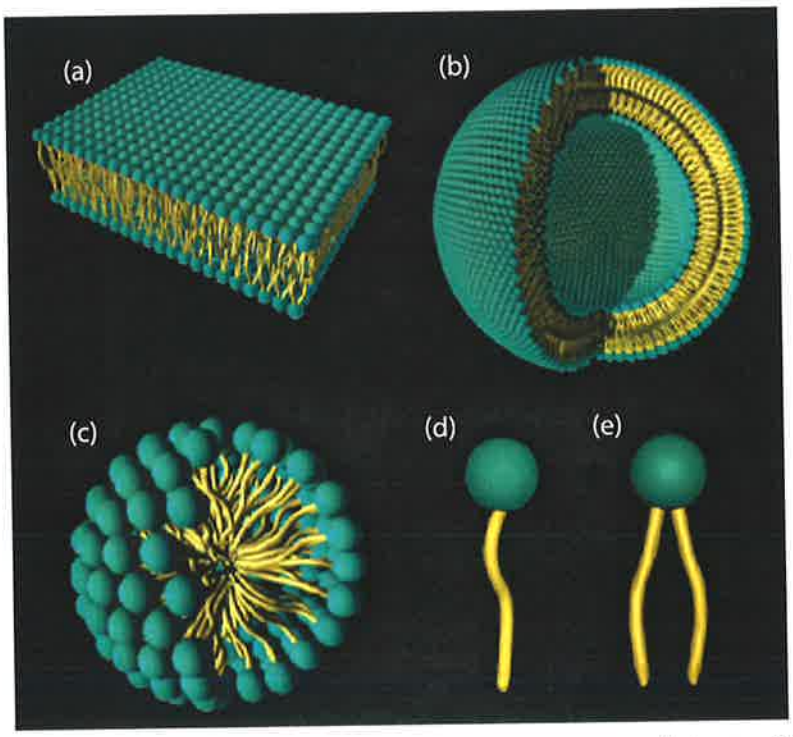

Figure 4.16 Lipid systems used to mimic natural membranes: (a) lipid bilayer, (b) vesicle and (c) micelle. Segments of the vesicle and micelle have been removed to show the internal structure. Micelles are composed of single-chain lipids (d), while bilayers and vesicles contain lipid molecules with two acyl chains (e). The polar head-groups are indicated in green and the hydrophobic acyl chains in yellow.

4.7a 2,2,2-Trifluoroethanol

The simplest and least expensive of the membrane mimicking systems are mixed organic solvents. Mixtures of alcohols and water have been shown to induce secondary structure in peptides that are similar to those observed in membrane environments [286]. Probably the most commonly used alcohol is 2,2,2-trifluoroethanol (TFE), which has a much larger structure stabilizing effect than methanol or ethanol [287].

On its own, water destabilises secondary structure because of its ability to form hydrogen bonds with the carbonyl and amide groups of the protein. The number and strength of these bonds mean that, in water, the unstructured peptide is energetically more favourable than the intramolecularly hydrogen bonded structured form. The lower polarity of alcohols, coupled with their poorer basicity, means hydrogen bonds between solvent and protein are weaker, favouring the formation of intramolecular hydrogen bonds [286, 288].

The greater stabilising effects of fluorinated alcohols, such as TFE and 3,3,3,3',3',3'-hexafluoro-2-propanol (HFIP), may be due to the formation of micelle-like clusters in aqueous solution [289]. Clustering produces microscopic regions of very low polarity where intramolecular hydrogen bonds are further strengthened. This effect is also observed for other alcohols but not to the same extent [287, 289]

TFE is widely thought of as a helix-inducing solvent, however Sonnichsen *et al.* [229] found that helical structure was only observed where there was helical propensity in the sequence. In addition, many examples of β-turn [286] and β-sheet [290, 291] structures have been observed in aqueous TFE mixtures demonstrating that TFE does not enforce helical structure but merely enhances it if the propensity exists.

Nevertheless, there is a poor correlation between native protein structures and those determined in aqueous TFE. This is thought to be due to the ability of TFE to disrupt hydrophobic interactions and thus denature tertiary structure [287, 291]. Small peptides, such as the amphibian antimicrobial peptides, do not have tertiary structure so their structures in TFE are expected to resemble their native membrane conformations.

The peptide magainin, for example, has been shown to have α-helical structure in aqueous TFE as well as in phospholipid micelles, which are believed to be a more reliable model for a membrane environment [206]. Results of solid-state NMR experiments in lipid bilayers were also consistent with α-helical structure along the length of the peptide [152]. Similarly, melittin, a 26-residue peptide from bee venom, forms helix-hinge-helix structures in aqueous methanol and dodecylphosphatidylcholine (DPC) micelles, however the average hinge angle observed varies between these studies [215, 292]. Once again, the results of solid-state studies on lipid bilayers were compatible with the solution NMR results [143].

While the reliability of TFE as a membrane mimic is still in dispute, its advantages, including low cost, simple sample preparation and the resulting well-resolved NMR spectra, make it an attractive alternative to phospholipid systems.

4.7b Micelles

Micelles are spherical aggregates of amphipathic lipid molecules that form in water when the concentration of lipids is sufficiently high (i.e., greater than the critical micelle concentration (CMC)). In these structures, the long hydrophobic tails of the lipids are directed toward the centre of the sphere, while the hydrophilic head-groups are in contact with the water (Figure 4.17 (a)).

The most commonly used lipids are zwitterionic dodecylphosphatidylcholine (DPC) and negatively charged sodium dodecylsulphate (SDS) (Figure 4.17 (c) and (d)). These lipids form stable micelles and have low CMCs (1 mM for DPC and 8 mM for SDS), low aggregation numbers and reorient rapidly in solution [293].

DPC micelles have a narrow size distribution, with micellar diameter between 40 and 55 Å [281], and about 55 DPC monomers per micelle [281, 282]. The size of peptide-bound micelles remains roughly the same, suggesting the bound peptide simply displaces a number of lipids. A ratio of one peptide molecule to every 40 lipid molecules was found for both melittin [281, 283] and glucagon [294]. These peptides were shown to be monomeric within the micelles.

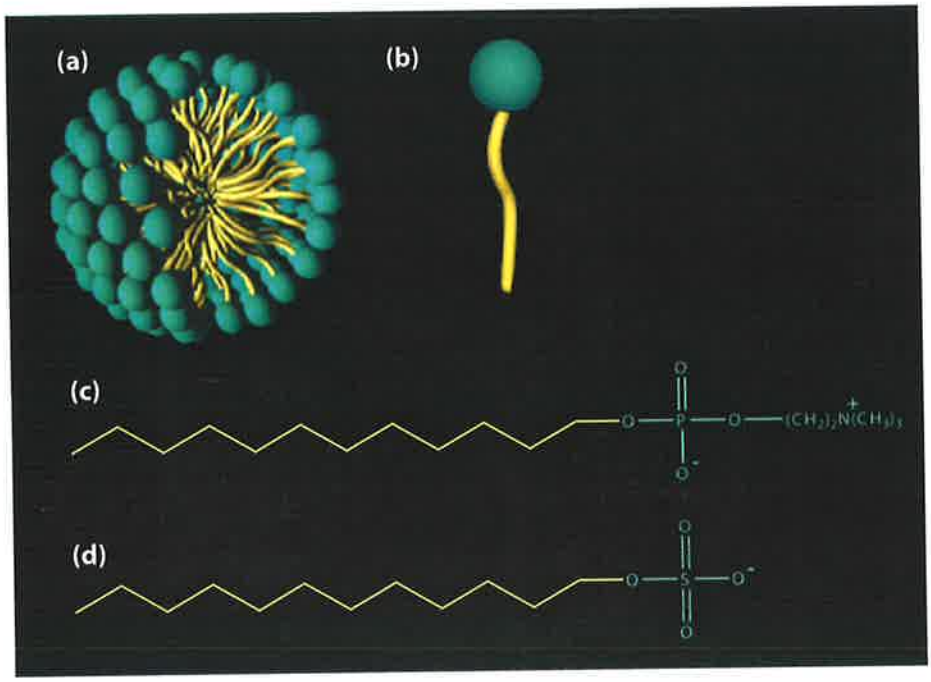

Figure 4.17 Schematic diagram of a micelle (a) composed of single-chain lipid monomers (b). A segment of the micelle has been removed to show the internal structure. The structures of the micelle forming lipids dodecylphosphatidylcholine (c) and sodium dodecylsulphate (d) are also shown. The hydrophilic head-groups are shown in green and the hydrophobic tails are shown in yellow.

Peptides are able to reorient within the micelle, as well as equilibrate between the micelle-bound form and the free form [215, 295]. In some cases, the lipid concentration needs to be well above the CMC in order to ensure the majority of peptide is in the bound state [281, 293].

Since micelles provide a similar environment to that found in a lipid bilayer - particularly in terms of the lipid/water interface - and because of their near isotropic reorientation they are suitable for use in NMR studies [293]. However, a peptide bound to a micelle will reorient many times slower than the free form, resulting in larger line-widths and decreased resolution [152]. This also results in difficulty in determining J-couplings.

Micelles are known to disrupt protein tertiary structure in a similar manner to TFE [287]. This agrees with the observation that enzymes are rarely active in micellar solutions, which may be due to the extreme surface curvature of the micelle structures [296]. Micelles have been used with success, however, to determine the structures of a range of small peptides including glucagon [294, 297], melittin [211, 215] and magainin [206].

Chapter 5 Orientation Studies

5.1 General

A number of different techniques can be used to determine the orientation of peptides in lipid bilayers. Among these are fluorescence spectroscopy, attenuated total reflection infrared spectroscopy (ATR-IR), computer simulation methods, oriented circular dichroism and solid-state NMR spectroscopy. Each technique has both advantages and disadvantages that will be outlined briefly below.

Fluorescence spectroscopy utilises the fluorescence of tryptophan or tyrosine containing peptides and specific quenchers to determine the orientation of peptides in a membrane [138, 298-300]. This is a powerful technique because of the variety of quenchers available and the option of 'labelling' the peptides with fluorescent residues at different locations [138]. However, synthesis of different labelled peptides is time-consuming and costly, and a number of experiments may have to be done on each analogue to determine the orientation of the parent peptide [299]. Furthermore, the labelled peptides may have different structures, or activity, from the native peptide and thus may have a different orientation.

Infrared spectroscopy is a technique used to study the characteristic vibrations and motions of molecular species. Orientation of molecules can be determined because the absorption of infrared radiation is dependent on the angle between the polarisation of the light and the transition moment of the vibration [301]. Sample preparation is simple and the technique is sensitive enough to obtain results with less than one microgram of peptide [302]. However, access to specialised equipment is required [303]. A large number of peptides have been studied using this technique [155, 302] but there is still debate over the accuracy of the results, given that in most cases the orientation has not been verified by another technique, under the same conditions [303].

Molecular dynamics simulations of peptide-lipid interactions are increasingly being used to probe the orientation of membrane peptides [129, 155, 304]. There are many ways to

model the system, each differing in the amount of computer time they require and the level of detail and realism they provide, so that a trade-off is necessary. While progress is being made in this area, simulations are not yet sufficiently advanced to provide a detailed view of the mechanism of action of these peptides [304]. In addition, empirical observations are necessary to verify or support the results of simulation studies.

CD can be used to study the orientation of helical peptides because an α-helix has electronic transitions that are polarised either parallel or perpendicular to the helix long axis [226, 305]. The shape of the CD spectrum of an oriented peptide/lipid sample indicates the average orientation of the helices with respect to the incident light. This approach has been used to study an array of peptides and proteins including magainin, melittin and alamethicin [124, 140, 306, 307].

Oriented circular dichroism requires only very small amounts of peptide (*ca.* 200 μg) and can be performed using a conventional CD spectrometer. Sample preparation can be tedious unless using a lipid, such as 1,2-dimyristoylphosphatidylcholine (DMPC), that forms aligned bilayers with minimal experimental effort. High absorbance of the lipid bilayers limits the amount of material that can be used and therefore, the sensitivity of the experiment.

Solid-state NMR offers yet another approach for analysing the orientation of peptides in membranes. This technique makes use of the fact that the chemical shift of a nucleus is dependent on the orientation of its chemical shift tensor, with respect to the external magnetic field [308]. Solid-state NMR is a versatile technique since a variety of nuclei can be examined in membrane samples to yield information about both the peptide and its effect on the lipid bilayer. Unfortunately, isotopic labelling is necessary to obtain much of this information.

Ambiguous results can be obtained with these techniques so a peptide's orientation is best determined using a number of different methods. At times, different techniques used to study the same peptide have produced conflicting results, however this can be explained by differences in sample preparation, bilayer hydration, lipid phase or L/P ratio. Thus, care must be taken to compare similar systems.

For the present study, the techniques of solid-state NMR and oriented circular dichroism were chosen and these will be described in further detail in the following sections.

5.2 Solid-State NMR Spectroscopy

The orientation of a peptide in a lipid bilayer can be determined using the powerful technique of solid-state NMR spectroscopy, which relies on the orientational dependence of the chemical shift. In solution the chemical shift is averaged to an isotropic value, but in the solid-state, each orientation of the nucleus results in a different chemical shift. This is known as the chemical-shift anisotropy (CSA) and is due to the electronic shielding of the nucleus from the magnetic field (B_0) [152, 308]. The shielding can be described by a tensor, which in turn can be represented graphically as an ellipsoid (Figure 5.1), where the three axes of the ellipsoid correspond to the principal tensor elements σ_{11}, σ_{22} and σ_{33} [230].

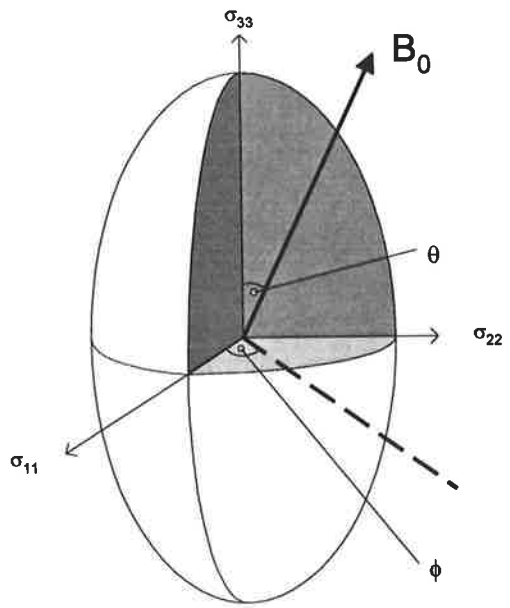

Figure 5.1 The chemical shift tensor represented by an ellipsoid is defined by the principal tensor elements σ_{11}, σ_{22} and σ_{33}. Different orientations of the tensor, relative to the external field (B_0), as defined by angles θ and ϕ, result in different chemical shift values for the nucleus. (Based on a figure from Evans [230]).

The chemical shift at a particular orientation corresponds to the length of a vector that starts at the centre and finishes at the edge of the ellipsoid, parallel to the B_0 vector [152]. In order to determine the orientation of the molecule with respect to the field, the orientation of the chemical shift tensor within the molecular frame and the values of the principal tensor elements must be known.

For a single crystal, a sharp line will be present for every unique orientation of the nucleus within the field. For a powdered sample, however, a peak will be observed for the orientation of each tiny crystal, resulting in a broad line with a distinctive shape [309]. The shape of the line is related to the principal elements of the shielding tensor (Figure 5.2) as well as the distribution, or orientations, of the micro-crystallites [230, 309]. Any motion of the nuclei that is faster than the frequency range being considered will result in some degree of averaging of the CSA [310]. In the isotropic case, the CSA is averaged to the isotropic value (δ_{iso}), which is equal to $1/3(\sigma_{11} + \sigma_{22} + \sigma_{33})$ [311].

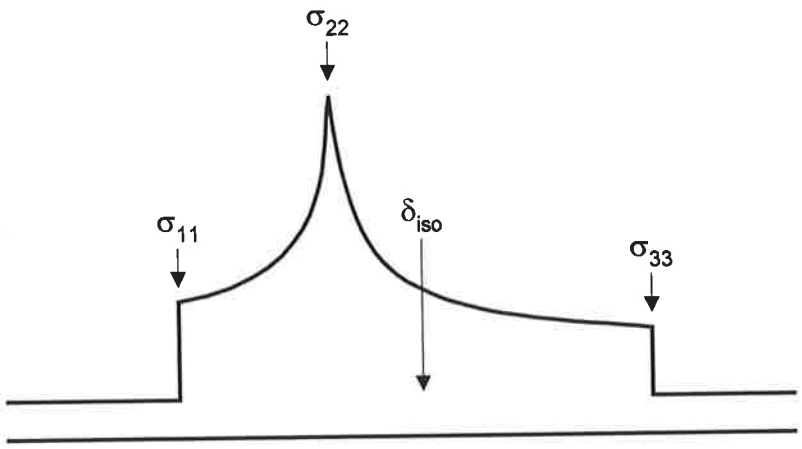

Figure 5.2 Schematic representation of a theoretical powder pattern for a nucleus with an asymmetric chemical shift anisotropy (i.e., $\sigma_{11} \neq \sigma_{22} \neq \sigma_{33}$).

Dry samples are not required for solid-state NMR. Rather, this technique can be applied to any system with anisotropic motion [310] and it is therefore appropriate for the study of lipid bilayer aggregates. The orientation of a peptide within the bilayer and the effect of the peptide on the phospholipid can be investigated, as described in the following sections.

5.2a Orientation of Peptides

In order to determine the orientation of a peptide within the applied magnetic field, the alignment of the chemical shift tensor of the nucleus of interest must be known relative to the molecular frame. Hence, the conformation of the peptide must be stable on the time-scale of the relevant NMR frequency range. Similarly, the nucleus needs to have a stable position relative to the rest of the molecule. Peptide backbone atoms fulfil the latter condition but to be useful for solid-state NMR these positions must be isotopically

labelled with either ^{15}N or ^{13}C. The orientation of the lipid bilayer must also be known. Methods for controlling this orientation will be described in later sections (Sections 5.2e and 5.2f).

The orientation and magnitude of the principal elements of the amide ^{15}N chemical shift tensor have been determined for a number of model peptides [207]. The breadth of the CSA is of the order of 150-175 ppm, with the magnitudes of the principal elements being around $\sigma_{11} = 64$ ppm, $\sigma_{22} = 77$ ppm and $\sigma_{33} = 217$ ppm [154].

The amide ^{15}N chemical shift tensor is aligned in the plane of the peptide, with σ_{33} making an angle of around 17° with the N-H bond of the amide [312, 313]. Thus the orientation of the σ_{33} element is roughly equivalent to the orientation of the amide bond and hence the long axis of the α-helix. A ^{15}N chemical shift of around 200 ppm indicates σ_{33}, and consequently the peptide, is aligned parallel to B_0. Conversely, a chemical shift of around 80 ppm indicates σ_{33} and the peptide are oriented perpendicular to the field.

The powerful technique of solid-state NMR spectroscopy has been used to study numerous peptides including antimicrobially active peptides [123, 139, 154, 207], segments of large membrane proteins [314] and model peptides [129, 149].

The broad range of the ^{15}N CSA means that there should be little ambiguity in the qualitative assignment of peptide orientation. However, this advantage is offset by the fact that ^{15}N nuclei are inherently insensitive [48, 315]. A one-dimensional ^{15}N experiment must be run with a very large number of transients such that the total running time is of the order of days (*cf.* seconds to minutes for proton spectra). Special techniques such as cross-polarisation (CP) can be used to increase the sensitivity of the ^{15}N nuclei. Here the large and rapidly acquired polarisation of the protons is transferred to nuclei of low magnetogyric ratio (γ) (in this case ^{15}N) by matching the B_1 rf fields such that $\gamma_H B_{1H} = \gamma_N B_{1N}$ [317]. CP also allows faster recycling times since the spin-lattice relaxation time (T_1) of protons is far shorter than that of ^{15}N nuclei.

Another procedure used to increase the signal-to-noise ratio is the application of a 'line-broadening' function. Sometimes called exponential multiplication, this technique involves multiplication of the FID by an exponential function during processing [231]. As implied by the name 'line-broadening function', the increase in the signal-to-noise ratio is accompanied by a broadening of the resonance lines. Thus, the line-width should be estimated before this processing is applied.

5.2b Peptide-Lipid Interactions

In addition to determining the orientation of a peptide in a bilayer, solid-state NMR can also be used to study the influence of the peptide on the bilayer phospholipids. The general structure of a phospholipid is a polar head-group connected to two hydrophobic acyl chains (Figure 5.3 (b)) and solid-state NMR can be used to look at either of these regions. The lipids form bilayers, where the acyl-chains are directed toward the middle of the bilayer and the head-groups face the water (Figure 5.3 (a)). The molecular axis that runs along the lipid length is known as the director axis [309].

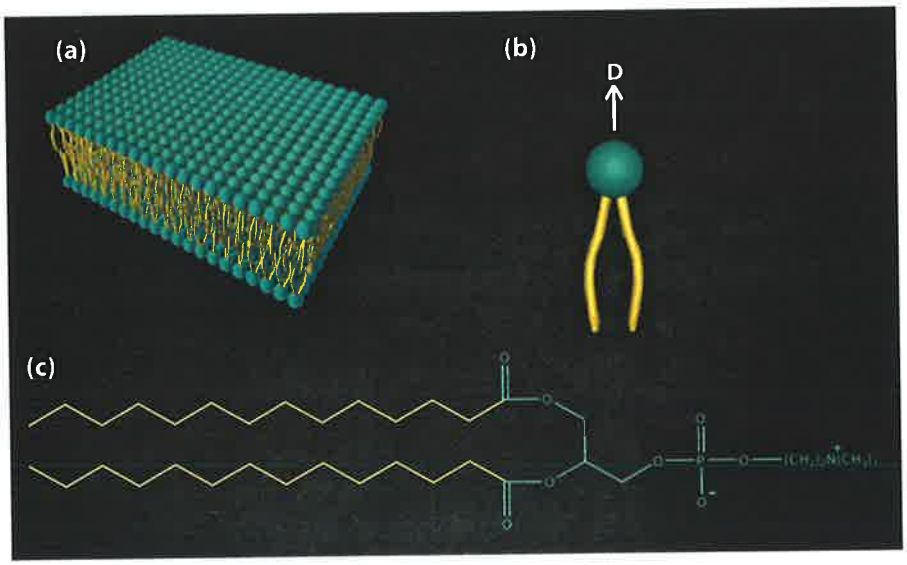

Figure 5.3 Schematic diagram of a lipid bilayer (a) composed of lipid monomers (b). The director axis (D) of the lipid monomer is indicated in (b). The structure of the bilayer-forming lipid 1,2-dimyristoylphosphatidylcholine (DMPC) is also shown (c). The hydrophilic head-groups are shown in green and the hydrophobic tails are shown in yellow.

5.2c Head-groups – Phosphorus NMR

Phospholipids each contain a phosphorus atom in their head-groups and since the magnetic isotope ^{31}P has 100% natural abundance, NMR is a convenient tool for investigating the conformation and mobility of lipid head-groups.

A ^{31}P spectrum of a dry phospholipid powder is characterised by a powder pattern similar to that shown in Figure 5.4 (a) with CSA ~ 190 ppm [318].

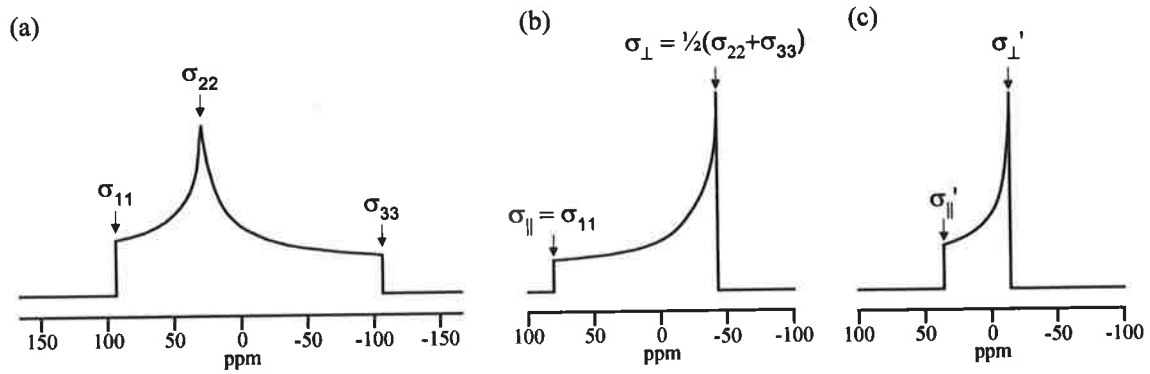

Figure 5.4 ^{31}P NMR spectra expected for phospholipids as (a) a dry powder (b) with rapid axial rotation and (c) hydrated lipid bilayers, where rapid axial rotation, as well as motion of the lipid director axes occurs. $\sigma_{\parallel}$ refers to the chemical shift when the unique axis is parallel to B_0 while $\sigma_{\perp}$ refers to the chemical shift when this axis is perpendicular to the field. (Based on a figure from Smith and Ekiel [319]).

When the phospholipids form hydrated bilayer dispersions, the phospholipids rotate rapidly about their director axes. The principal tensor elements σ_{22} and σ_{33}, which are roughly perpendicular to the director axis, are averaged to the new element $\sigma_{\perp}$, with σ_{11} now designated as $\sigma_{\parallel}$ [319]. The notation $\sigma_{\parallel}$ specifies the chemical shift when the external magnetic field is parallel to the unique axis, while $\sigma_{\perp}$ indicates the chemical shift when the unique axis is perpendicular to the external field. If this were the only motion present, then a ^{31}P spectrum similar to that shown in Figure 5.4 (b) would result. In reality, however, there is also rapid, but limited, motion of the director (σ_{11}) axis such that it moves in a cone. Now there is partial averaging of the $\sigma_{\parallel}$ and $\sigma_{\perp}$ elements and the CSA is further reduced [319]. This circumstance is illustrated in Figure 5.4 (c), which shows the effective tensor elements $\sigma_{\parallel}'$ and $\sigma_{\perp}'$. The CSA is now of the order of 50 ppm [309].

The CSA reduction is indicative of the motion around the director axis. Changes in the amplitude of this motion, for example due to a peptide inserting parallel into the surface of the lipid bilayer, will result in further alterations of the CSA. Thus, measuring the ^{31}P CSA is one way of detecting the influence of peptides on the lipid head-groups [319]. The phosphorus CSA, $\Delta\sigma$, is equal to the difference between the effective tensor elements $\sigma_{\parallel}$ and $\sigma_{\perp}$ measured at half-height of the low-frequency 'foot' of the spectrum [320], as shown below in Figure 5.5 (a).

^{31}P NMR can also be used to indicate the phase-state of the lipids. When the lipids form other phases such as inverted hexagonal phase or cubic phase, the motion and orientation of the lipids is altered, resulting in distinctive ^{31}P spectra [321] (Figure 5.5). These line-shapes can sometimes arise from more than one type of phase or head-group conformation so the phase cannot be definitively identified by ^{31}P NMR alone [322]. For example, micelles, vesicles and the cubic phase all result in a single sharp peak [321].

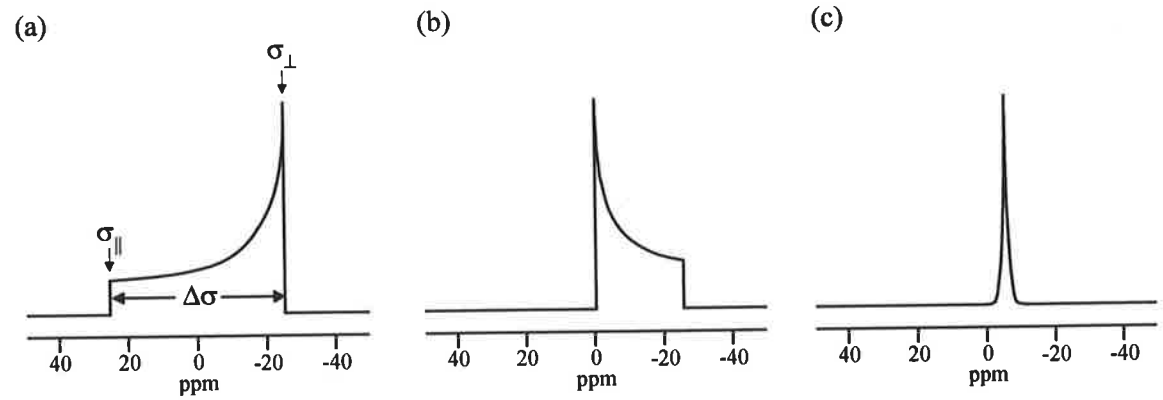

Figure 5.5 ^{31}P NMR spectra characteristic of different lipid phases – (a) bilayer (b) inverted hexagonal (H_{II}) phase and (c) isotropic phases including micelles, vesicles and cubic phases. The ^{31}P CSA ($\Delta\sigma$) is indicated for the bilayer phase.

Unless appropriate measures are taken, the line-shape of the ^{31}P spectrum will consist of contributions from both the CSA of the phosphorus nuclei and proton-phosphorus dipole-dipole interactions. To remove distortions caused by the dipole-dipole interactions, a proton decoupling field is applied during acquisition of the spectrum [323].

5.2d Acyl Chains – Deuterium NMR

^{31}P NMR provides information about the orientation and mobility of the lipid head-groups. Similarly, deuterium (^{2}H) NMR can furnish information about the orientation and mobility of the lipid acyl-chains. In this case, however, the lipids must be isotopically labelled.

Deuterium nuclei have spin (I) equal to one and therefore have a quadrupolar moment. As a result, ^{2}H NMR spectra show a pair of peaks for each type of deuterium nucleus present [310]. For a poly-crystalline sample, a doublet appears for every possible orientation of the deuterium nuclei, resulting in a characteristic spectrum known as a Pake powder pattern [230] (Figure 5.6). This is similar to the powder pattern obtained for an I = 1/2 nucleus but here two equal and opposite powder patterns overlap. The size of the quadrupolar splitting, or the frequency difference between each pair of peaks, is given by:

$$\Delta\nu = (3/4)(e^2qQ/h)(3\cos^2\theta-1)$$

where $\Delta\nu$ is the quadrupolar splitting, (e^2qQ/h) is the deuteron quadrupole coupling constant and θ describes the angle between the principal axis of the deuteron and the external magnetic field [230].

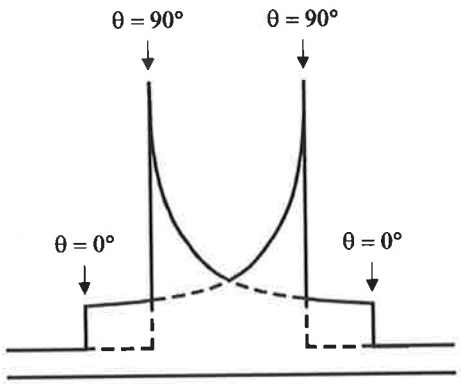

Figure 5.6 Schematic representation of the powder pattern obtained for ^{2}H, an I=1 nucleus. The solid line shows the overall pattern, while the dashed lines indicate the contributions of two equal and opposite powder patterns. Also indicated are the resonance positions for the θ = 0° and 90° orientation of the deuteron principal axis, with respect to B_0.

For an unoriented bilayer dispersion, labelled with deuterium at every carbon on the lipid acyl chains, a spectrum similar to that shown in Figure 5.7 (a) will result. This spectrum is the superposition of the Pake patterns for each type of deuteron along the acyl chains

[324]. These Pake doublets have reduced quadrupolar splitting compared with that found for a dry lipid sample because of the reorientation of the lipid molecules.

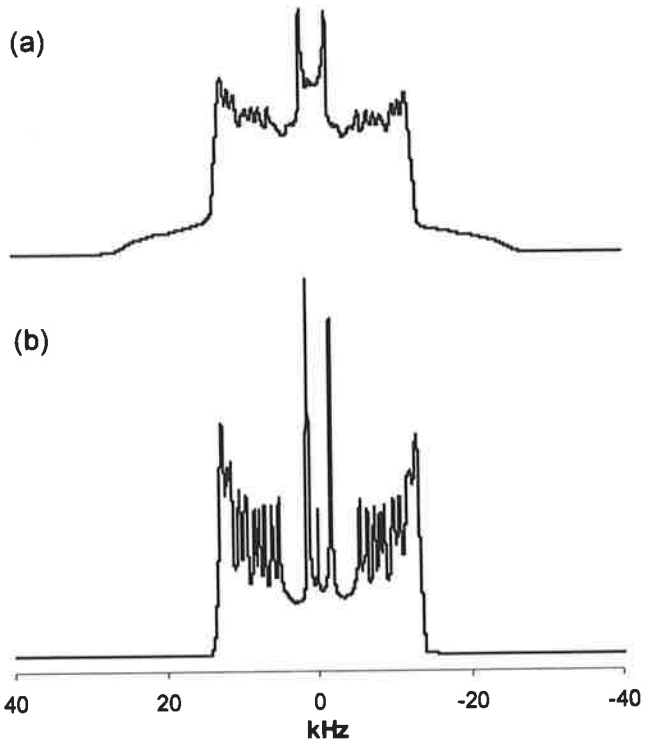

Figure 5.7 ^{2}H spectra of (a) unoriented bilayer dispersions and (b) bilayers oriented with the membrane normal 90° to the external magnetic field, B_0.

In a sample of oriented bilayers, the ^{2}H NMR spectrum produced will depend on the angle between the bilayer normal and the magnetic field. At an angle of 90° to the field, doublets will be present corresponding to the inner peaks of the Pake powder pattern for each type of ^{2}H nucleus and a spectrum similar to that shown in Figure 5.7 (b) results. At 0°, on the other hand, only the outer-most splittings of the Pake pattern will be present [325]. Oriented samples, therefore, give greatly simplified ^{2}H spectra that are easier to analyse.

Like ^{31}P NMR spectra, ^{2}H spectra can give an indication of the phase-state of the lipids because of the different quadrupolar splittings observed with different phases [321]. For example, the quadrupolar splittings of deuterated lipids in the hexagonal phase are reduced by a factor of two from those in the bilayer phase [326].

The quadrupolar splitting is dependent on the orientation of the deuterons in the magnetic field and motion of the deuterium nuclei leads to partial averaging of the splitting [327]. Thus, increased motional freedom, or decreased order of the acyl chains, will result in a reduction of the quadrupolar splitting, while restricted motion (increased order) will increase splittings. As the ends of the lipid chains are extremely mobile and disordered, the deuterons on the terminal methyl groups result in the smallest splitting present in the ^2H spectrum. As we move step-wise along the acyl chains toward the phosphocholine head-group, the methylene groups become more ordered and hence the quadrupolar splitting of the deuterons increases [325].

The mobility of the carbon-deuterium bonds can be related to an order parameter, S_{CD}, where:

$S_{CD} = <3\cos^2\theta-1>$ and

$\Delta\nu = (3/4)(e^2qQ/h)S_{CD}$ [328]

$\Delta\nu$ is the quadrupolar splitting, (e2qQ/h) is the deuteron quadrupole coupling constant and θ describes the angle between the principal axis of the deuteron and the magnetic field. The angled brackets < > indicate the time-average of the angular function. S_{CD} can be calculated from the second equation since the quadrupolar splitting can be measured from the ^2H spectrum and (e^2qQ/h) is known to be ~170 kHz for paraffin chains [328]. In order to know which carbon-deuterium bond order is being measured, however, we first need to assign the ^2H spectrum.

It is difficult to accurately assign the ^2H spectrum, firstly because of the overlap of signals and secondly because the two acyl chains are not equivalent [329]. However, there are methods for assigning these spectra if we assume that the chain order parameters, and hence the quadrupolar splittings, decrease monotonically along the chain from the segment nearest the head-groups to the free ends of the chains [324]. Such an effect was observed by Seelig and Seelig [330] using specifically deuterated phospholipids.

Peptide-lipid interactions can be investigated by comparing the order parameters of pure lipid bilayers with those in the presence of peptide. The S_{CD} order parameters can be

plotted against acyl-chain carbon position to give a visual representation of these changes. A quantitative expression of the changes can be obtained by calculating them as a percentage of the order parameters obtained from control bilayers. Such comparisons have been used to provide evidence for the insertion of proteins and peptides into bilayers. In general, peptides that insert into the bilayer, ~~perpendicular~~ parallel to the membrane normal, increase the order of the acyl chains [320, 331], while peptides inserted parallel to the bilayer surface, decrease the order of the acyl chains [332-334].

^{2}H NMR experiments are prone to certain difficulties due to the large spectral width of the signals. The spectrum is dependent on the quadrupolar splittings, which are mainly determined by the coupling constant, e^2qQ/h (~ 170 kHz for acyl chains). This results in spectra up to 250 kHz wide and it is difficult to apply a uniform rf pulse over this range because of hardware limitations.

A second problem encountered with ^{2}H NMR experiments results from the short transverse relaxation times (T_2) that occur with this nucleus [319]. Because the probes used in high-resolution NMR spectrometers have high quality (Q) factors, it takes a relatively long time for the probe to ring-down (~ several μs) [327]. As a result, the detector may pick up the remains of the rf pulse during acquisition, resulting in distortions to the signal. To reduce this, a delay is usually inserted between application of the rf pulse and acquisition of the spectrum. However, since T_2 is short, little to no signal may result [319]. An experiment, known as a solid- or quadrupole-echo, is used to circumvent this problem. The pulse sequence for this experiment is as follows:

$$90° - \tau - 90° - \tau - t_2$$

where τ represents a time delay and t_2 is the acquisition period. It is difficult to visualise what is occurring with this sequence, using a vector representation, because we are dealing with an I = 1 nucleus, with three spin states. However, there is an analogous experiment for I = 1/2 nuclei called a spin-echo experiment [230].

The pulse sequence for the spin-echo experiment is:

$90° - \tau - 180° - \tau - t_2$

During the first delay, τ, the magnetisation in the XY plane decays according to T_2 (Figure 5.8). A 180° pulse is applied followed by a second delay of time τ during which the magnetisation refocuses to reach an echo maximum [319]. The refocused signal is acquired to give the spectrum. As long as τ is longer than the ring-down time of the probe, no distortion of the signal due to ringing will remain [327].

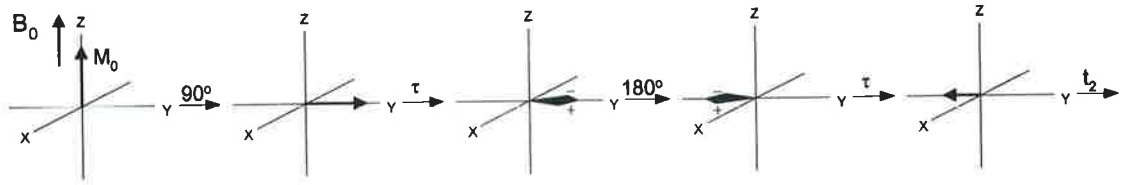

Figure 5.8 Vector representation of the spin echo experiment. Vectors travelling faster than ω_0 are labelled '+' while those travelling slower are labelled '-'. (Based on a figure from Evans [230]).

5.2e Mechanically Aligned Bilayers

To determine the orientation of peptide molecules within a bilayer, the orientation of the bilayer must be controlled. One way of doing this is to apply the lipid/peptide mixture to a number of thin glass plates, hydrating the sample and stacking the plates on top of one another [335] (Figure 5.9).

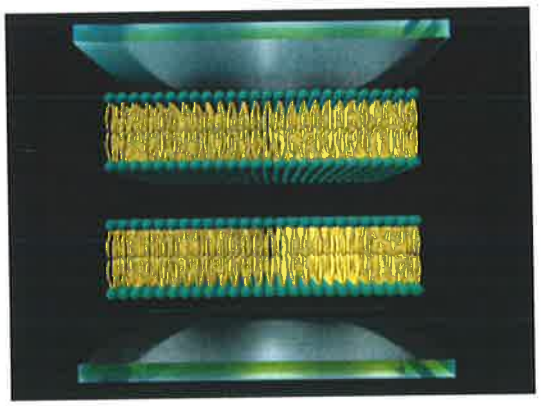

Figure 5.9 Lipid bilayers mechanically aligned between glass plates.

A high degree of alignment can be achieved using this method and the large size of the bilayers means that edge effects are minimised [284]. However, since the majority of the sample volume is glass, and the total volume is limited by the spectrometer coil size, the amount of sample that can be applied is restricted. Thus the sensitivity of the sample is reduced [325]. In addition, as only 10-30 Å separates the bilayers, the interstitial water is believed to be ordered by the bilayers, resulting in different properties to bulk water [310]. Therefore, peptides may act differently in this system than they might otherwise.

Verification of the alignment of the bilayers can be obtained from ^{31}P and ^{2}H NMR. If the bilayers are aligned with the membrane normal perpendicular to the magnetic field, the phosphorus spectrum will contain a single peak, with a chemical shift that corresponds to $\sigma_{\perp}$ (*ca.* –15 to –20 ppm) [319].

The ^{2}H NMR spectra of unoriented bilayers composed of chain-perdeuterated lipids, consist of the overlapping powder patterns from each pair of deuterons along the acyl chain, as explained in Section 5.2d (Figure 5.7 (a)). Orientation of the bilayers with the membrane normal perpendicular to the magnetic field results in resolved doublets, or splittings, for each deuteron pair (Figure 5.7 (b)).

5.2f Magnetically Aligned Bicelles

An alternative to mechanical alignment is the spontaneous alignment of molecules in a magnetic field. Placing phospholipid molecules in a magnetic field (B_0) induces a magnetic moment in the sample due to the anisotropy of the diamagnetic susceptibility tensor [310]. This magnetic moment causes alignment of the molecules within the field, provided the magnetic moment is large enough to overcome opposing forces such as the randomising effects of thermal motion [310].

It has been found that specific mixtures of long and short-chain lipids form disc shaped aggregates in solution, which orient in B_0 [310]. The discs, or 'bicelles', consist of a bilayer of long-chain lipids capped at the edges by micelle-forming short-chain lipids [336] (Figure 5.10). The most common system used at present is the combination of DMPC and 1,2-dihexanoylphosphatidylcholine (DHPC) at a ratio of around 3:1, which

form bicelles that orient with the bilayer normal perpendicular to the field [310, 325, 337, 338]. The orientation is dependent on the ratio of the two lipids, as well as the temperature [311]. At suitable ratios, smaller structures are formed that reorient rapidly and these isotropic bicelles can be used for solution NMR structure studies [296]. Thus bicelles bridge the gap between solution and solid-state NMR [311].

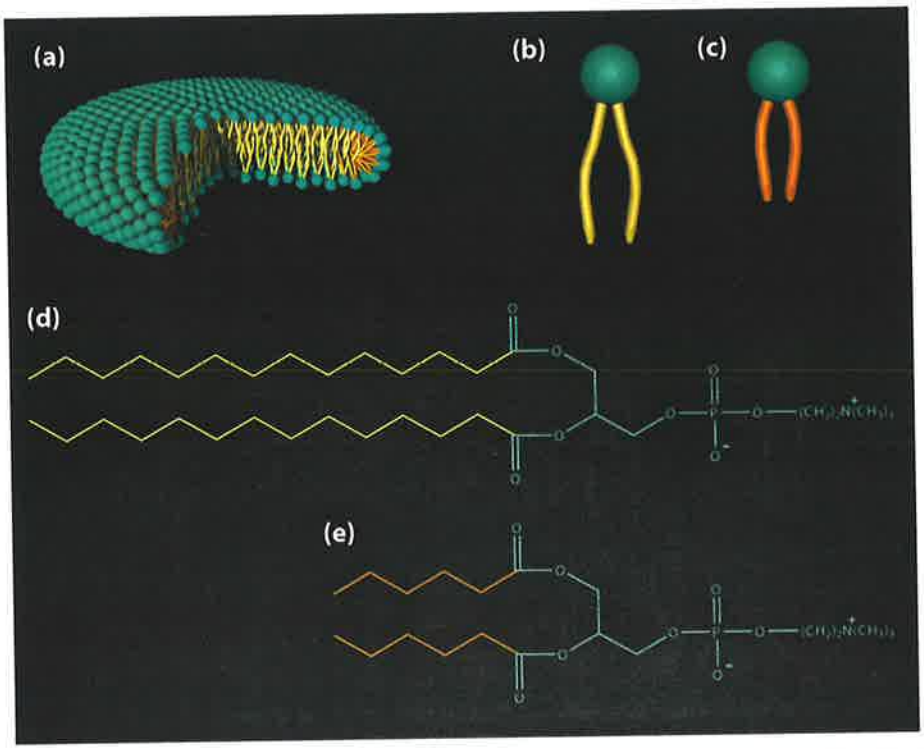

Figure 5.10 Schematic diagram of a bicelle (a) composed of (b) long- and (c) short-chain lipid monomers. A segment of the bicelle has been removed to show the internal structure. The structures of (d) the long-chain, bilayer forming lipid 1,2-dimyristoylphosphatidylcholine (DMPC) and (e) the short-chain, micelle-forming lipid 1,2-dihexanoylphosphatidylcholine (DHPC) are also shown. The hydrophobic tails of the long-chain lipids are coloured yellow, while those of the short-chain lipids are coloured orange. The hydrophilic head-groups are shown in green.

^{31}P and ^{2}H NMR can be used to monitor the level of orientation of bicelles. Oriented samples show two sharp peaks in their phosphorus spectrum at around –5 and –10 ppm, due to the DHPC and DMPC molecules respectively and thus, the peak at –10 ppm is around three times as large as that at –5 ppm [338] (Figure 5.11 (a)). ^{2}H spectra of the bicelles, when only the DMPC is deuterated, resemble those of aligned bilayers, except that the peak splitting is reduced such that the outer peaks occur at around ± 10 kHz instead of ± 15 kHz (Figure 5.11 (b)).

Addition of lanthanide ions to oriented bicelles causes the bicelles to flip, so that the bilayer normal is parallel to the field [325]. It is also possible to prepare bicelles using

acidic phospholipids such as 1,2-dimyristoyl-*n*-glycero-3-phospho-L-serine (DMPS) or 1,2-dimyristoylphosphatidylglycerol (DMPG) [337]. Thus, magnetically oriented bicelles may be a versatile alternative to mechanically aligned bilayers.

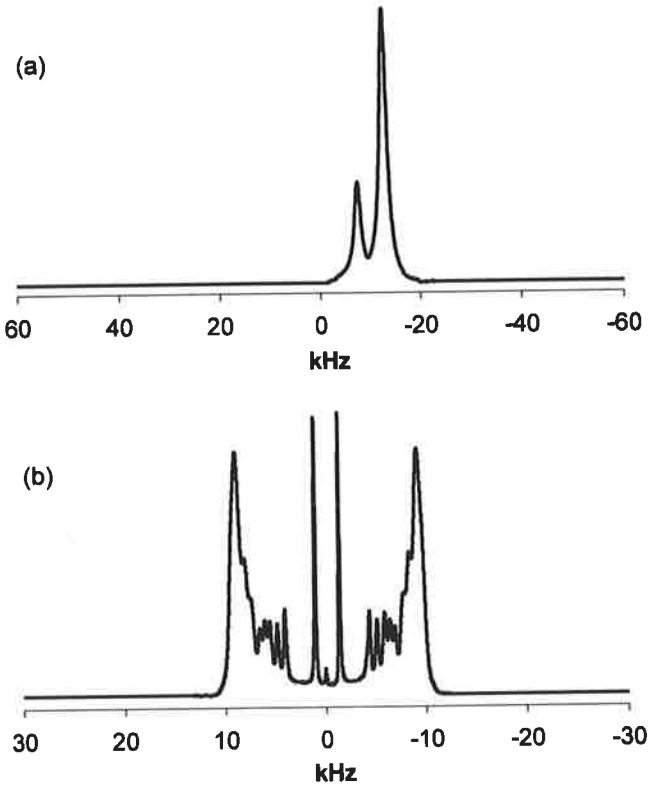

Figure 5.11 Typical (a) ^{31}P and (b) ^{2}H spectra of bicelles.

There are some problems with the use of bicelles, however. Firstly, because they are a relatively new medium, they are yet to be completely characterised [311]. Secondly, the detergent (micelle-forming lipids) present in the bicelles may cause artefactual structural perturbations of the peptide/protein under study [311]. However, the concentration of detergents in bicelles is quite low and in most cases does not seem to cause problems.

5.3 Oriented Circular Dichroism

Oriented circular dichroism (OCD) is another technique that is useful for studying the orientation of peptides in lipid bilayer environments. CD uses the difference in absorbance of left and right circularly polarised light to study molecular structure, whereas NMR spectroscopy uses the energy difference between nuclear spin states. Thus OCD provides a means of verifying NMR findings since the two techniques exploit different physical phenomena.

The theory behind CD has been described briefly in Section 4.2. Orientational information can be obtained because one of the π–π^* transition moments of the peptide backbone is polarised parallel to the helix long axis [226]. This transition results in a minimum in the CD spectrum at around 210 nm [307]. If the helices are oriented with the helix axis parallel to the incident light beam, this minimum will be absent, but if the helices are aligned with the helix axis perpendicular to the light beam, the trough at 210 nm will have maximum amplitude [305].

Reference spectra for purely parallel or purely perpendicular helices are presented in Figure 5.12 [305], which also shows the spectrum for an isotropic sample. Here it can be seen that for a parallel helix, a peak is expected at around 188 nm and a minimum around 227 nm, with a zero-degree crossover point around 210 nm. For a perpendicular arrangement of helices, a peak around 190 nm and minima around 210 nm and 220 nm occur, with a crossover point around 200 nm.

Comparison of the CD spectra of peptides in oriented bilayers with the reference spectra, enables the orientation of the peptides to be determined. This is straightforward for the ideal case, where the peptide under study orientates completely parallel or perpendicular, but if the spectra indicate an intermediate angle, more than one scenario can produce the same result since the data reveal the average conformation. For instance, all of the peptides could orient at the angle derived from the spectrum or, alternatively, a combination of parallel and perpendicular orientations could be present, such that the superposition of their spectra results in an intermediate spectrum. Therefore, there is some ambiguity in OCD results.

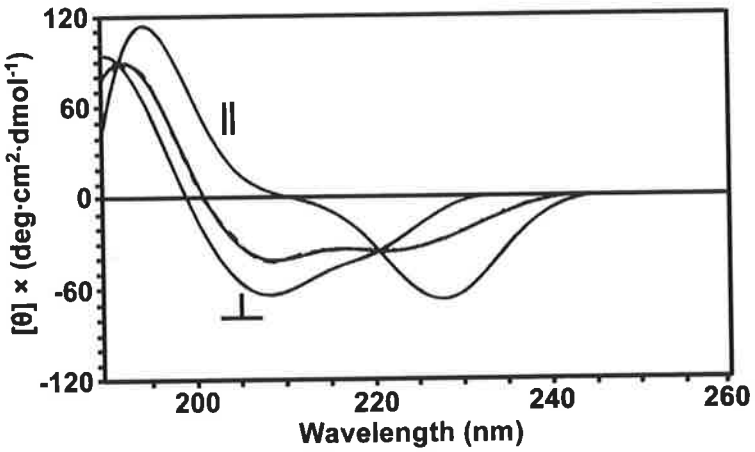

Figure 5.12 Calculated circular dichroism spectra of an α-helix oriented parallel (||) or perpendicular (⊥) to the incident light beam. The central spectrum is the summation of the parallel and perpendicular spectra, representing an isotropic distribution of α-helices. (Diagram modified from [305]).

Oriented lipid bilayer samples are required for OCD experiments. These are usually prepared from aqueous samples of peptide-DMPC mixtures. The DMPC in these solutions forms multilamellar vesicles (MLV, i.e., concentric spherical bilayers or vesicles). These solutions are sonicated to produce small unilamellar vesicles (SUV, i.e., unilamellar, or single bilayer, vesicles) that are then applied to a quartz plate. The solution is spread over the plate and dried with a stream of nitrogen gas until the majority of the water has evaporated. The DMPC is now in the form of oriented hydrated membranes [339] that can be placed in the spectrometer with the membrane normal parallel or at a specific angle to the incident light beam, and the CD spectrum recorded.

CD measures the difference between the absorption of left and right circularly polarised light, which can be small in comparison to the total absorption. In the case of lipid/peptide samples, the lipid component produces little CD signal but has high absorbance, causing difficulties for the spectrometer detectors. Thus the amount of lipid used, and hence the amount of peptide, is limited. Fortunately, the sensitivity of the CD technique is high and peptide concentrations of *ca.* 200 $\mu g \cdot mL^{-1}$ are all that is required.

Non-uniformities in the aligned DMPC samples can lead to artefacts in the CD spectrum due to linear dichroism and linear birefringence [340]. The quality of bilayer alignment can be checked by comparing the spectrum to the spectrum produced when the sample has been rotated through 180° about an axis perpendicular to the incident light [340].

CD spectra of isotropic samples must also be obtained for comparison. SUV samples are suitable for this purpose. These spectra can also confirm the binding of the peptide to the vesicles by comparison with the CD spectra of the peptides in water.

OCD studies have shown that the orientation of particular peptides can be dependent on a number of different factors, including lipid phase [124], L/P ratio [125, 140] and the hydration state of the bilayers [341]. Thus, the samples should match as close as possible the conditions used for the oriented solid-state NMR studies so that results can be compared.

Chapter 6 Short Antibacterial Peptides - Citropin 1.1 and Aurein 1.2

6.1 Introduction

A large number of novel peptides have been isolated and identified from the dermal secretion of *Litoria citropa* - a frog commonly known as the Blue Mountain's Tree Frog [342] (Figure 6.1). These peptides, subsequently named citropins, were tested for biological activity, which showed that three of the citropins had broad-spectrum antibacterial action. The citropin antibiotics were each comprised of only 16 amino acid residues, which is unusually short for antibacterial peptides, yet they show comparable activity to the longer caerin 1.1 (25 residues) and maculatin 1.1 (21 residues) peptides (Table 6-1).

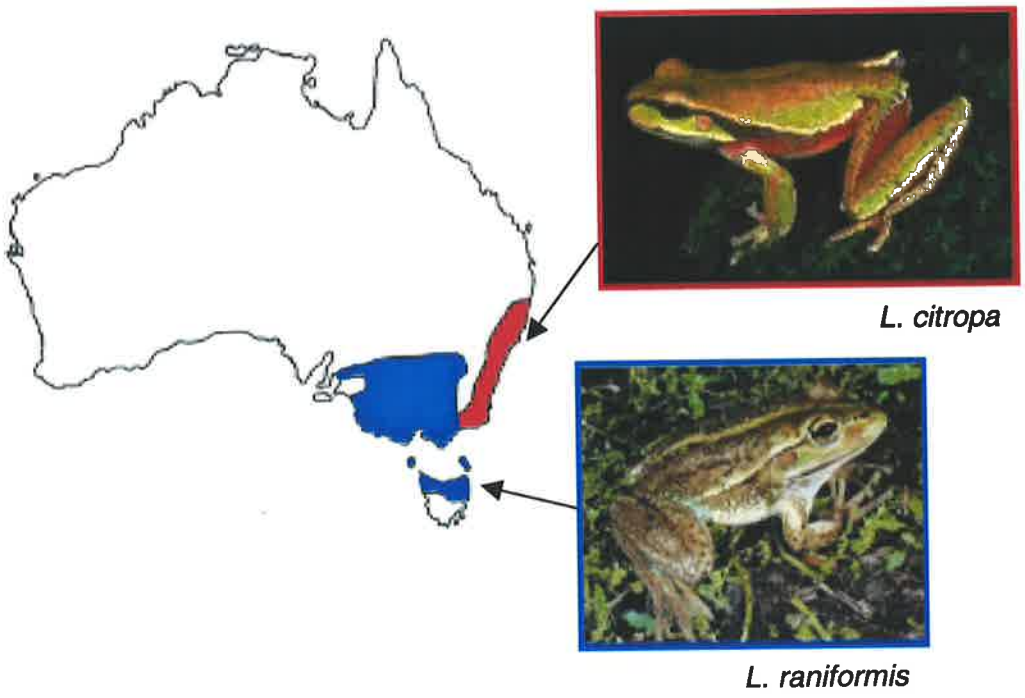

Figure 6.1 *L. citropa* and *L. raniformis* and their geographical distributions.

Recently, two even shorter antibiotic peptides were discovered in the dermal secretion of *Litoria raniformis* – the Southern Bell Frog of eastern Australia [14] (Figure 6.1). Named aurein 1.1 and aurein 1.2, these peptides contain only thirteen residues each, making them

the smallest antibiotic anuran peptides yet discovered. Their activity is modest when compared with the broad-spectrum activity of citropin 1.1 and other highly active peptides (Table 6-1) but even this level is impressive given their size.

Table 6-1 Sequences and antibacterial activities of selected natural and synthetically modified citropin and aurein peptides compared with those of caerin 1.1 (C1.1) and maculatin 1.1 (M1.1). MIC, minimum concentration of the peptide ($\mu g \cdot mL^{-1}$) necessary to inhibit the growth of the pathogen.

Peptide	Sequence
Citropin	
1.1	GLFDVIKKVASVIGGL-NH_2
1.2	GLFDIIKKVASVVGGL-NH_2
1.3	GLFDIIKKVASVIGGL-NH_2
1.1 D	Glfdvikkvasvi**G**Gl-NH_2
Aurein	
1.1	GLFDIIKKIAESI-NH_2
1.2	GLFDIIKKIAESF-NH_2
C1.1	GLLSVLGSVAKHVLPHVVPVIAEHL-NH_2
M1.1	GLFGVLAKVAAHVVPAIAEHF-NH_2

Organism	MIC ($\mu g \cdot mL^{-1}$)[a]							
	Citropin[b]				Aurein[c]		C1.1[b]	M1.1[b]
	1.1	1.2	1.3	1.1 D	1.1	1.2		
Bacillus cereus	50	25	25	25	50	100	50	25
Escherichia coli								
Leuconostoc lactis	6	3	6	3	25	12	1.5	3
Listeria innocua	25	100	25	25	100	100	25	100
Micrococcus luteus	12	12	12	25		100	12	12
Pasteurella multocida						100		25
Staphylococcus aureus	25	25	25	25		50	3	6
Staphylococcus epidermis	12	25	25	12		50	12	12
Streptococcus uberis	25	12	12	12	100	50	12	3

[a] Where there is no figure listed, the MIC value is >100 $\mu g \cdot mL^{-1}$.
[b] Data for the citropins, caerin 1.1 and maculatin 1.1 are from Wegener *et al.* [16].
[c] Data for the aurein peptides are from Rozek *et al.* [14].

The all-D isomer of citropin 1.1 was also synthesised and tested (Table 6-1). Interestingly, this analogue has essentially the same activity as the naturally occurring version, suggesting the mechanism of cell killing is via membrane disruption rather than interaction with chiral receptors.

These citropin and aurein peptides are too short to form α-helices capable of spanning a bacterial cell membrane and thus, cannot act via the barrel-stave mechanism. The width of a bacterial cell membrane is of the order of 30 Å and peptides that span a bilayer are generally 20-25 residues in length [117, 343]. Alternatively, these peptides may exert their action via the carpet-like mechanism or the toroidal mechanism (Section 3.2). As yet, the details of the activity of short antibiotic peptides are not known.

Citropin 1.1 and aurein 1.2 were chosen as model short antibiotic peptides for structural and mechanistic studies. When placed on a Schiffer-Edmundson wheel projection (Figure 6.2), the sequences of both these peptides are arranged such that the hydrophobic and hydrophilic residues are segregated. This suggests the peptides could form amphipathic α-helices with hydrophilic angles around 100°. This angle is consistent with class L peptides - a group that contains many antibacterial peptides, including magainin [68] - and translates to the high values of hydrophobic moment seen in Table 6-2.

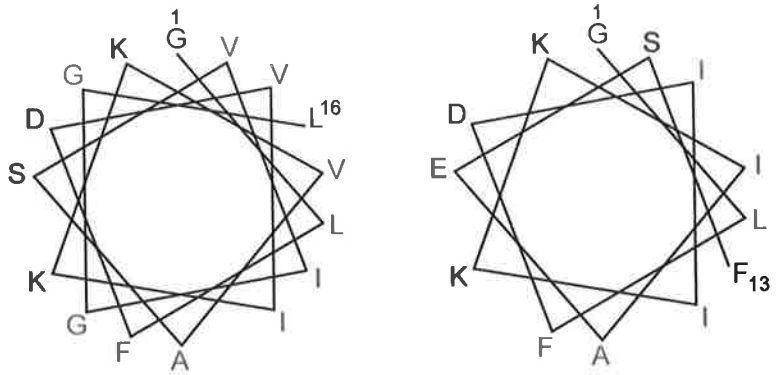

Figure 6.2 Schiffer-Edmundson wheel projection of citropin 1.1 and aurein 1.2. Hydrophilic residues are indicated in blue and hydrophobic residues in red [67].

Citropin 1.1 and aurein 1.2 are positively charged at neutral pH, which may attract these peptides to the acidic lipids of bacterial cell membranes. They are also hydrophobic, which would allow them to insert into the hydrophobic region of a bilayer. Table 6-2 summarises some of the physical characteristics of these peptides.

Table 6-2 Structural parameters of citropin 1.1 and aurein 1.2.

Peptide	Hydrophobicity[a]	Hydrophobic moment[b]	Hydrophilic angle	Charge State
Citropin 1.1	0.144	0.319	100°	+2
Aurein 1.2	0.042	0.416	140°	+1

[a] Mean residue hydrophobicity as calculated from the consensus sequence of Eisenberg [197].
[b] Hydrophobic moment (μ) per residue [67].

The structure-activity relationship (SAR) for citropin 1.1 was investigated further through the synthesis of two substitution analogues that were then tested for antibacterial activity. The sequences of these analogues and the test results are shown in Table 6-3.

Table 6-3 Sequences, antibacterial activities (MIC, $\mu g \cdot mL^{-1}$) and structural features of natural and synthetically modified analogues of citropin 1.1 (C1.1). Modified residues are indicated in red.

Peptide	Sequence		
Citropin 1.1	GLFDVIKKVASVIGGL-NH_2		
Ala4	GLFAVIKKVASVIGGL-NH_2		
Ala7	GLFDVIAKVASVIGGL-NH_2		
Organism	MIC ($\mu g \cdot mL^{-1}$)[a]		
	C1.1[b]	Ala4[c]	Ala7[c]
Bacillus cereus	50	25	100
Escherichia coli		100	
Leuconostoc lactis	6	3	25
Listeria innocua	25	25	25
Micrococcus luteus	12	12	100
Pasteurella multocida			
Staphylococcus aureus	25	25	100
Staphylococcus epidermis	12	12	100
Streptococcus uberis	25	25	100
Charge	+2	+3	+1
H[d]	0.144	0.204	0.228
μ[e]	0.319	0.261	0.266

[a] Where there is no figure listed, the MIC value is >100 $\mu g \cdot mL^{-1}$.
[b] Data for citropin 1.1 are from Wegener *et al.* [16].
[c] Unpublished data.
[d] Mean residue hydrophobicity (H) [197].
[e] Hydrophobic moment (μ) per residue [67].

The first modification, where Asp4 is replaced with alanine, results in a peptide with increased positive charge, increased hydrophobicity and reduced amphipathicity. The

activity, however, remains essentially unchanged. This suggests that the increased charge compensates for the reduced amphipathicity.

The second analogue has an alanine residue in place of Lys7. This results in a peptide with similar hydrophobicity and amphipathicity to the first analogue but with a smaller overall charge. The dramatic drop in activity of the Ala7 analogue must therefore be due to the loss of a positive charge.

These two modifications illustrate the importance of cationic nature to the activity of citropin 1.1, perhaps indicating that the rate-limiting step in its mechanism is initial binding to the cell membrane. This is supported by the results of testing these compounds against multiple cancer cell lines. Citropin 1.1 shows LC_{50} values of the order of 10^{-5} M. The Ala4 analogue, however, has an order of magnitude greater activity and the Ala7 analogue is inactive (max. conc. tested was 10^{-4} M). Thus, the activity increases with increasing positive charge, consistent with the known acidic nature of the outer leaflet of cancer cell membranes [343].

Aurein 1.2 was shown to have *in vitro* activity against 52 out of 54 tumour cell lines tested but does not lyse red blood cells at 100 $\mu g \cdot mL^{-1}$ [14]. A concentration of 1 $mg \cdot mL^{-1}$ is required to completely lyse the erythrocytes, demonstrating the selectivity aurein 1.2 has for cancer cells.

To further investigate the mechanism of action of both citropin 1.1 and aurein 1.2, their structures were determined by NMR spectroscopy and restrained molecular dynamics calculations in aqueous TFE, a membrane-mimicking solvent. Following this, the techniques of solid-state NMR spectroscopy and oriented circular dichroism were used to study the behaviour of these peptides in lipid bilayers. The results of these investigations are described in the following sections.

6.2 Citropin 1.1

6.2a Circular Dichroism Studies

CD spectra were recorded for citropin1.1 in varying amounts of TFE in water (0-50% by volume) to find the optimal solvent mixture for NMR experiments (Figure 6.3).

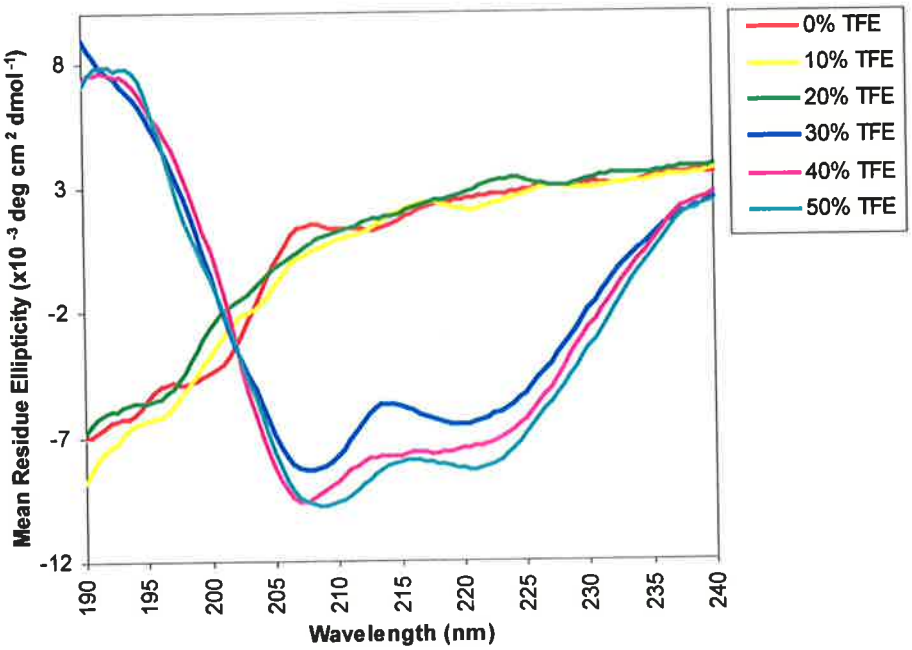

Figure 6.3 CD spectra of citropin 1.1 at the varying concentrations of TFE (by volume) indicated.

For 0-20% TFE, the spectra show a broad minimum around 200 nm that is characteristic of an unstructured peptide [344]. Increasing the amount of TFE to 30% and above results in a marked change in the spectra. These curves now have minima around 208 nm (π-π^* transition) and 222 nm (n-π^* transition) that are characteristic of a peptide with α-helical structure. These minima are at their lowest values (greatest ellipticity) at 50% TFE (by volume). Based on these results, NMR studies were undertaken using the solvent system of 50% TFE in water.

The molar ratios of TFE to water molecules at 30% and 50% TFE, are 10:90 and 20:80 respectively [97]. Thus, on a molar basis, the amount of TFE is small compared to the amount of water present. From these CD results, it seems that citropin1.1 has a high tendency to form an α-helical conformation.

6.2b NMR Studies – Assignments

The proton chemical shifts of citropin 1.1 were assigned via the sequential assignment procedure, using a combination of TOCSY, DQF-COSY and NOESY experiments, as outlined in Section 4.4a [345]. These assignments are indicated in the partial TOCSY and NOESY spectra in Figure 6.4, where cross-sections for each individual amino acid are shown. Some of the cross-sections are very close together, with those for Ser11 and Val12 being almost coincident. Ambiguous assignments were conclusively assigned from an examination of the appropriate regions of the DQF-COSY spectrum.

The amide proton chemical shifts were assigned in sequential order using the NH region of the NOESY spectrum (Figure 6.4), where the sequential d_{NN} NOE cross-peaks are found. Breaks in the sequence occurred where the chemical shifts of adjacent residues were very close. For example, the cross-peak from Gly15 (7.80 ppm) to Leu16 (7.82 ppm) occurs too close to the diagonal to be seen as a distinct peak.

The αC resonances were assigned using an HSQC experiment, specifically the $\alpha^1H/\alpha^{13}C$ region. The C′ resonances were assigned from an HMBC spectrum using the correlations between NH, αH and βH protons to the C′ ^{13}C carbons. Table 6-4 presents a summary of all the ^1H resonances, as well as the Cα and C′ ^{13}C chemical shifts.

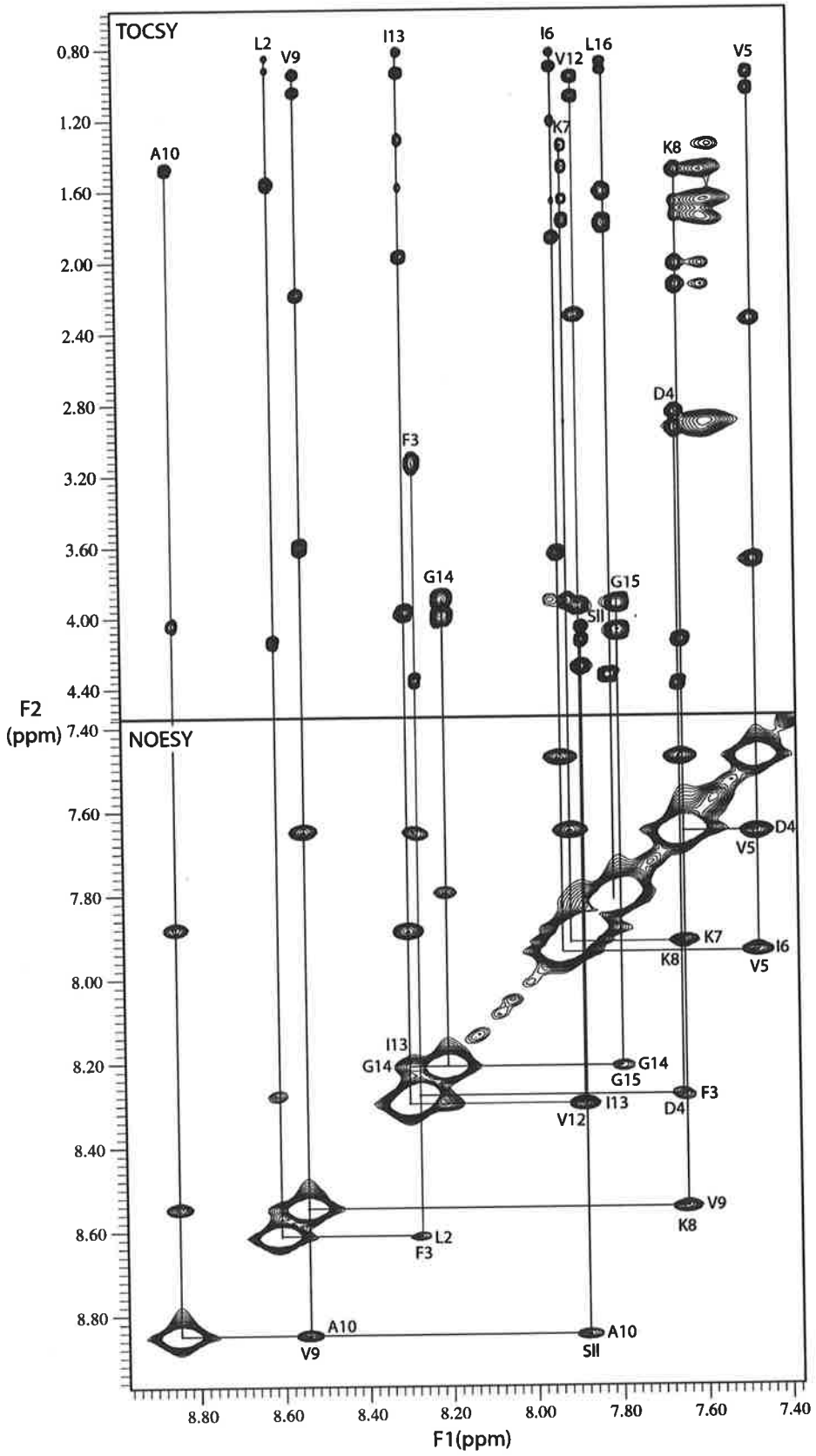

Figure 6.4 Partial NOESY (mixing time = 150 ms) and TOCSY (70 ms spin-lock time) spectra of citropin 1.1 in TFE/H_2O (1:1 by volume) at pH 2.25, 25°C. Vertical lines connect the resonances in each spin system. These are labelled with the standard single-letter abbreviation for the residue type and a number indicating the sequential position of the residue. NOEs between sequential NH protons are indicated in the NOESY spectrum.

Table 6-4 ^{1}H and ^{13}C-NMR chemical shifts for citropin 1.1 in TFE/H_2O (1:1 by volume), pH 2.25, 25°C. All ^{1}H assignments are shown whereas only αC and C′ ^{13}C resonances are indicated; n.o., not observed.

	Chemical shift (ppm)					
Residue	**NH**	**α-CH**	**β-CH**	**Others**	**α-^{13}C**	**$^{13}C'$**
Gly1	n.o.	4.03, 3.90			44.9	170.5
Leu2	8.61	4.13	1.57	γ–CH 1.57	57.0	177.2
				δ–CH_3 0.92, 0.86		
Phe3	8.28	4.35	3.13	H2,6 7.23	59.4	177.6
				H3,5 7.34		
				H4 7.29		
Asp4	7.66	4.38	2.94		55.6	176.9
Val5	7.48	3.68	2.33	γ–CH_3 1.04, 0.95	65.3	176.7
Ile6	7.94	3.64	1.86	γ–CH_2 1.67, 1.22	64.0	176.9
				γ–CH_3 0.91		
				δ–CH_3 0.83		
Lys7	7.91	3.91	1.77	γ–CH_2 1.47, 1.35	58.6	178.5
				δ–CH_2 1.66		
				ε–CH_2 2.90		
				ε-NH_3^+ 7.57		
Lys8	7.66	4.13	2.14, 2.03	γ–CH_2 1.59, 1.32	58.0	178.3
				δ–CH_2 1.75, 1.67		
				ε–CH_2 2.94, 2.86		
				ε-NH_3^+ 7.60		
Val9	8.55	3.60	2.18	γ–CH_3 1.05, 0.95	66.0	177.5
Ala10	8.84	4.04	1.48		54.2	179.9
Ser11	7.88	4.29	4.13, 4.06		60.3	175.0
Val12	7.89	3.94	2.30	γ–CH_3 1.07, 0.97	64.5	178.2
Ile13	8.30	3.97	1.97	γ–CH_2 1.59, 1.32	62.8	177.6
				γ–CH_3 0.94		
				δ–CH_3 0.83		
Gly14	8.22	3.99, 3.90			42.3	174.6
Gly15	7.80	4.08, 3.93			44.4	173.8
Leu16	7.82	4.33	1.79	γ–CH 1.61	54.3	179.6
				δ–CH_3 0.93, 0.88		
				$CONH_2$ 7.29, 6.77		

6.2c Secondary Shifts

Secondary shifts (i.e., the chemical shift difference from random coil values, Δδ), smoothed over a window of n = ±2 residues [246], were plotted against amino acid sequence for the αH, αC and C′ resonances. The random coil chemical shifts, obtained from the literature, were determined in water [242, 243] (see Section 4.5a).

Negative Δδ values indicate resonances have moved upfield from the random coil chemical shifts, while positive values indicate downfield shifts. Therefore, the plot for the αH Δδ values shows a distinct upfield shift (Figure 6.5), while those for the ^{13}C Δδ values show a distinct downfield shift (Figure 6.6), except in the vicinity of the N- and C-termini.

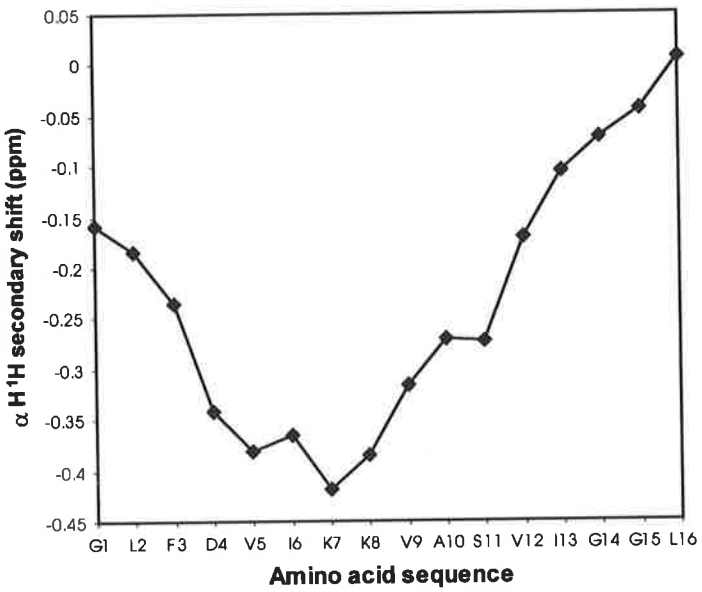

Figure 6.5 αH ^{1}H secondary shifts of citropin 1.1 in TFE/H_2O (1:1 by volume). Negative values indicate an upfield shift from the random coil value, while positive values indicate a downfield shift. Secondary shifts were smoothed over a window of n = ±2 residues [246].

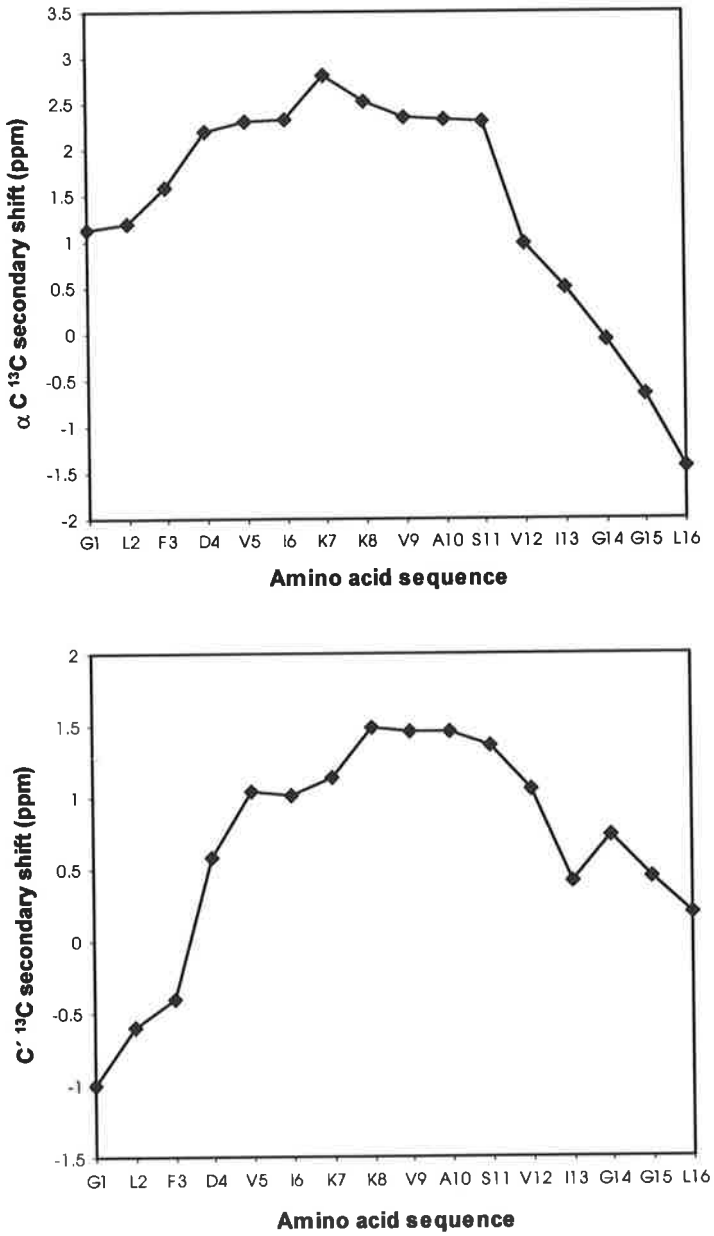

Figure 6.6 (a) αC and (b) C' ^{13}C secondary shifts of citropin 1.1 in TFE/H_2O (1:1 by volume). Positive values indicate a downfield shift from the random coil value, while negative values indicate an upfield shift. Secondary shifts were smoothed over a window of n = ±2 residues [246].

The directions of the deviations from random coil chemical shift values are consistent with the peptide having a helical structure along its length [244]. Helicity is maximal in the central region and less defined at the N- and C-termini. The lack of structure, or flexibility, at the ends of the peptide is expected as the first and last four residues of an α-helix are not as involved in the hydrogen bonding network and are therefore less likely to be in a helical structure.

6.2d Amide Secondary Shifts

Figure 6.7 reveals a periodic variation in the magnitude of the NH $\Delta\delta$ values over 3-4 residues. The NH resonances from hydrophobic residues are generally further downfield than those from the hydrophilic residues. This type of pattern is characteristic of amphipathic α-helices and is thought to be due to differences in the strength of hydrogen bonds on either face of the helix [245, 248] (Section 4.5a). The hydrogen bonds on the hydrophobic face are shorter than those on the hydrophilic face, resulting in slight curvature of the helix. The curvature of citropin 1.1 may not be significant, however, because of its short length.

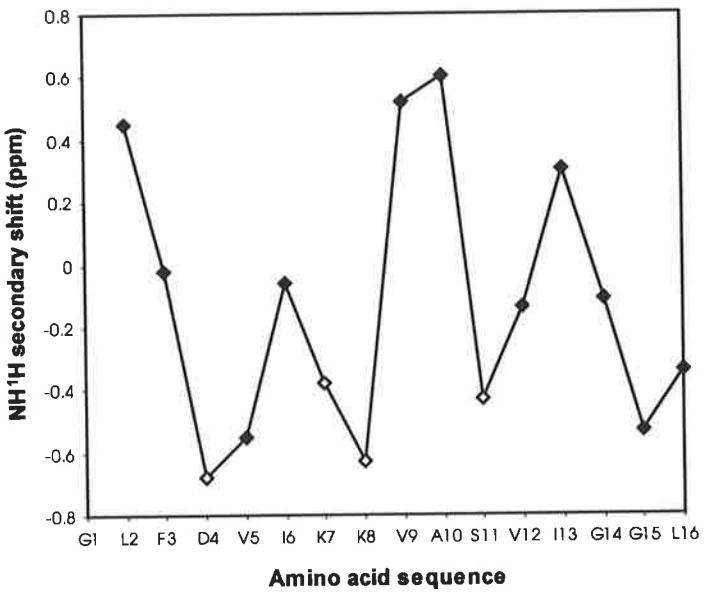

Figure 6.7 NH ^{1}H secondary shifts of citropin 1.1 in TFE/H_2O (1:1 by volume). Positive values indicate a downfield shift from the random coil value, while negative values indicate an upfield shift. The secondary shifts were left unsmoothed. Hydrophilic residues [67] are indicated by open symbols.

6.2e NOE Connectivities

A summary of the various types of NOEs found in the NOESY spectrum for citropin 1.1 is shown in Figure 6.8. Here, the series of strong d_{NN} NOEs seen already in Figure 6.4 is indicated, as well as a string of weaker $d_{NN(i,i+2)}$ NOEs that are present in the NH to NH region of the NOESY spectrum at a lower contour level. In addition, a number of

sequential $d_{\alpha N}$ NOEs occur, as well as a series of NOEs from residues three and four amino acids apart ($d_{\alpha N(i,i+3)}$, $d_{\alpha\beta(i,i+3)}$ and $d_{\alpha N(i,i+4)}$). Taken together, the observed NOEs and their intensities are consistent with citropin 1.1 having a helical structure along the majority of its sequence (see Section 4.5b). No long-range NOEs were observed, ~~inferring~~ implying the peptide is monomeric.

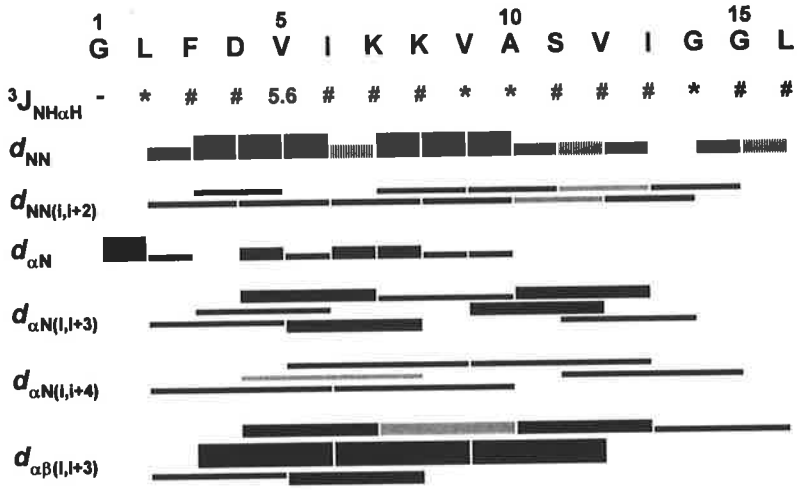

Figure 6.8 A summary of NOEs used in structure calculations for citropin 1.1 in 1:1 TFE/H_2O (by volume). The thickness of the bars indicates the relative strength of the NOEs (strong < 3.1 Å, medium 3.1-3.7 Å or weak > 3.7 Å). Grey shaded boxes represent NOEs that could not be unambiguously assigned. Striped boxes represent cross-peaks that would not be observed due to proximity to the diagonal. $^3J_{NH\alpha H}$ values are indicated where possible. Asterisks (*) indicate no coupling constant was detected, while a cross-hatch (#) indicates the coupling constant could not be reliably assigned due to overlap.

6.2f Coupling Constants

Also shown in Figure 6.8 are the $^3J_{NH\alpha H}$ values, determined from the NH region of a high-resolution 1D ^1H spectrum. Ten of the $^3J_{NH\alpha H}$ coupling constants could not be reliably determined due to overlap, while splittings were not resolved for the remaining NH signals. Only one $^3J_{NH\alpha H}$ value could be measured precisely – that of Val5. Nevertheless, its value of 5.6 Hz is consistent with α-helical structure.

6.2g Structure Calculations

After assignment of the entire NOESY spectrum (mixing time = 150 ms), the volumes of the cross-peaks were converted to distance restraints using the method of Xu *et al.* [266] (Section 4.6a). This procedure generated a total of 230 distance restraints. Of these, 133

were intra-residue restraints, 50 were sequential (i,i+1) restraints and 47 were medium range restraints (i,i+3 and i,i+4). ~~Twenty-six~~ Eighteen of the distance restraints were ambiguous. Sum-averaging was employed in the calculations to account for these. Five dihedral restraints were used.

The conclusions derived from examination of the NMR spectral data were confirmed by the structural calculations. Sixty structures were generated by RMD and dynamical SA procedures (Section 4.6e). The 20 structures of lowest potential energy were chosen for examination and the X-PLOR energies for these structures are shown in Table 6-5. The final structures had only minor deviations from idealised covalent geometry (≤ 0.05Å for bonds and ≤ 5° for angles and impropers) and there were no distance restraint violations greater than 0.34 Å.

Table 6-5 Structural statistics of citropin 1.1 following RMD/SA calculations. <SA> is the ensemble of the 20 final structures, (SA) is the mean structure obtained by best-fitting and averaging the coordinates of the backbone atoms (N, αC and C′) of the 20 final structures and $(SA)_r$ is the representative structure obtained after restrained energy minimisation of the mean structure (SA). Well-defined residues are those with angular order parameters (S) > 0.9. For citropin 1.1, residues Leu2 to Gly15 were well-defined.

XPLOR energies (kcal·mol^{-1})	**<SA>**	**$(SA)_r$**
E_{tot}	50.62 ± 2.37	46.19
E_{bond}	2.98 ± 0.18	2.66
E_{angle}	15.60 ± 1.01	13.85
$E_{improper}$	1.90 ± 0.42	1.27
E_{vdw}	6.75 ± 1.03	5.09
E_{NOE}	23.39 ± 1.48	23.32
E_{cdih}	0.01 ± 0.01	0.00
RMSD from mean geometry (Å)		
All heavy atoms	0.87 ± 0.16	-
All backbone atoms (N, αC, C′)	0.56 ± 0.16	-
Heavy atoms of well-defined residues	0.72 ± 0.13	-
Backbone atoms (N, αC, C′) of well-defined residues	0.37 ± 0.14	-

The superimposition of the 20 lowest energy structures over the backbone atoms (N, αC and C′) of the well-defined residues shows that citropin 1.1 forms a regular α-helix along its length (Figure 6.9). The greater deviation of the backbone atoms at the helix termini indicates increased flexibility in these regions. The RMSD was 0.37 Å for the backbone

atoms of the well-defined residues and 0.56 Å for the entire peptide backbone. Further statistics are listed in Table 6-5.

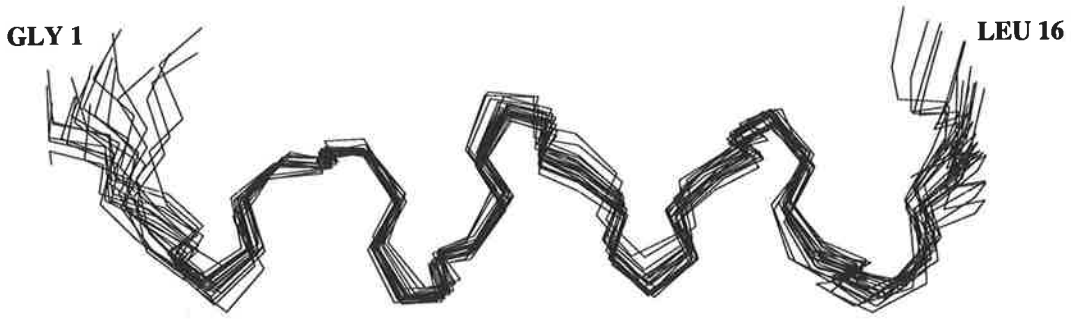

Figure 6.9 The 20 most stable calculated structures of citropin 1.1, superimposed along the backbone atoms (N, αC and C') of the well-defined residues (2-15). This picture was prepared using the program MOLMOL [346].

Analysis of the angular order parameters (S, ϕ, and ψ) of the 20 final structures indicated that, except for the N- and C- terminal residues (Gly1 and Leu16), all residues were well-defined (S > 0.9 for both their ϕ and ψ angles). A Ramachandran plot of the average ϕ and ψ angles of the well-defined residues, shows that these angles are distributed within the favoured region for α-helical structure (Figure 6.10).

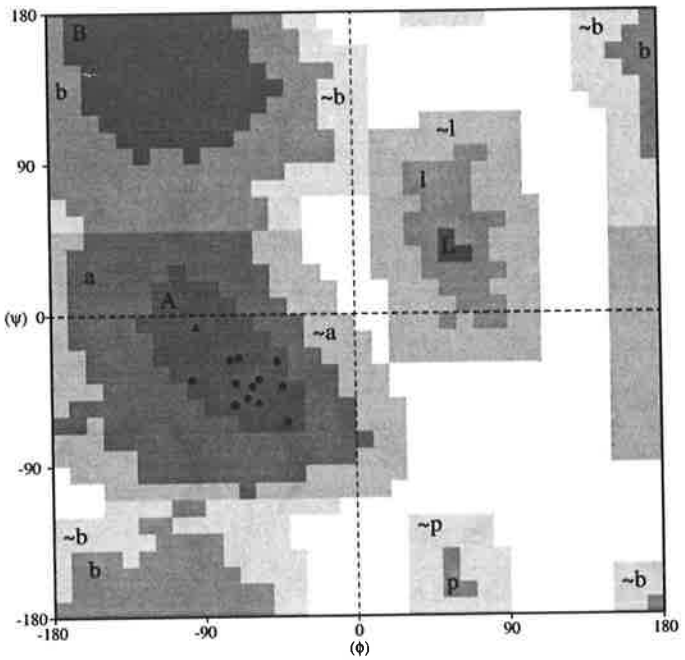

Figure 6.10 Ramachandran plot of citropin 1.1 showing that all of the residues fall in the favourable region for α-helices (A). The allowable and generous regions for α-helices are labelled as 'a' and '~a' respectively. Glycine residues are indicated by triangles, while the remaining residues are indicated by circles.

The most energetically stable of the 20 calculated structures is shown in Figure 6.11. This representation shows that citropin 1.1 forms an amphipathic α-helix, with well-defined hydrophobic and hydrophilic faces. The structured peptide was found to have a length of around 20 Å. The amphipathicity of the peptide can be seen more clearly in the axial view (Figure 6.11 (b)).

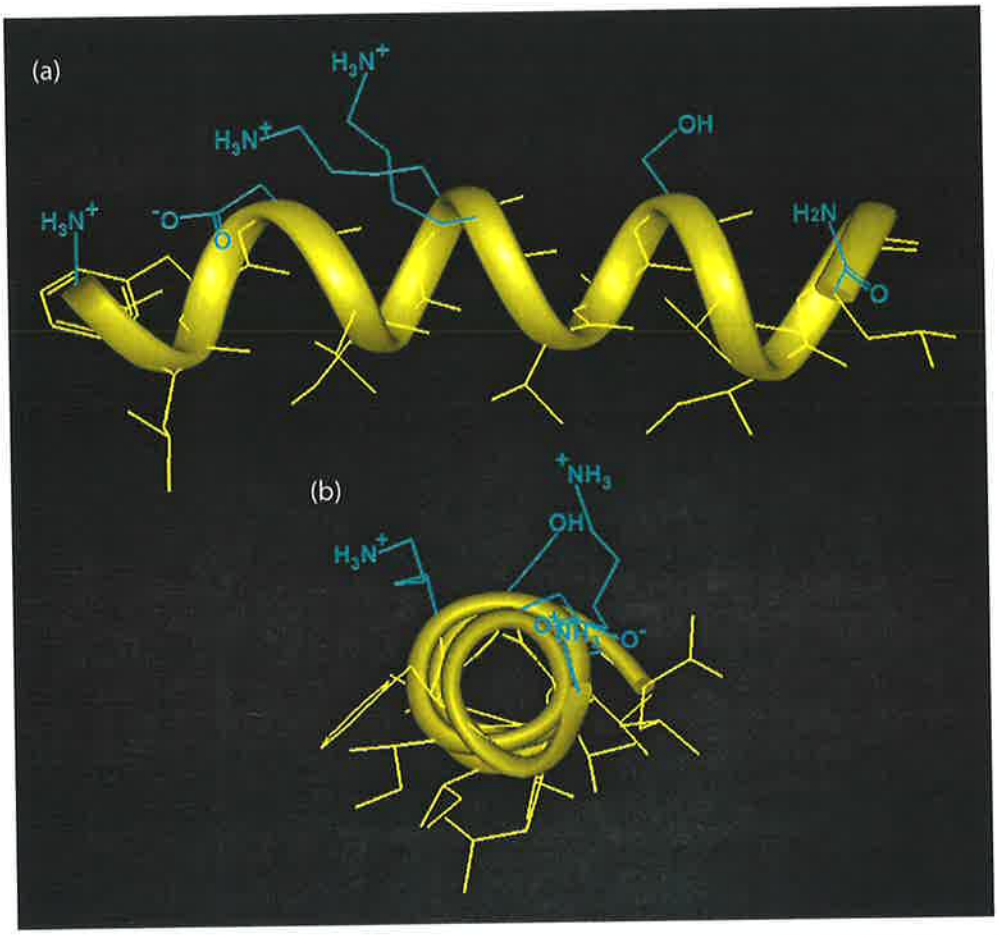

Figure 6.11 The most stable structure (lowest potential energy) of citropin 1.1 (a) shown from the side and (b) along the helix axis. The hydrophilic groups are shown in blue.

6.3 Aurein 1.2

6.3a NMR Studies - Trifluoroethanol Titration

A ^{1}H NMR TFE solvent titration was carried out on a sample of aurein 1.2 to find a solvent system suitable for structure studies. For 0-40% TFE (by volume), a doubling of resonances was observed, indicating aurein 1.2 adopts two distinct conformations in these mixtures. Presumably, this is due to an equilibrium between a random coil conformation and a structured form. At 50% TFE and above, resonance doubling was not observed, suggesting a single conformation was predominating.

In general, the chemical shifts increased with increasing amounts of TFE. This can be seen in Figure 6.12, which shows these changes for selected αH resonances. A clear plateauing of the chemical shifts is not observed, however the largest changes occurred over 20-50% TFE. A NOESY spectrum was obtained at 70% TFE/H_2O, which indicated aurein 1.2 was structured in this solvent system. Thus, this solvent was judged to be a suitable system for NMR structural studies on aurein 1.2.

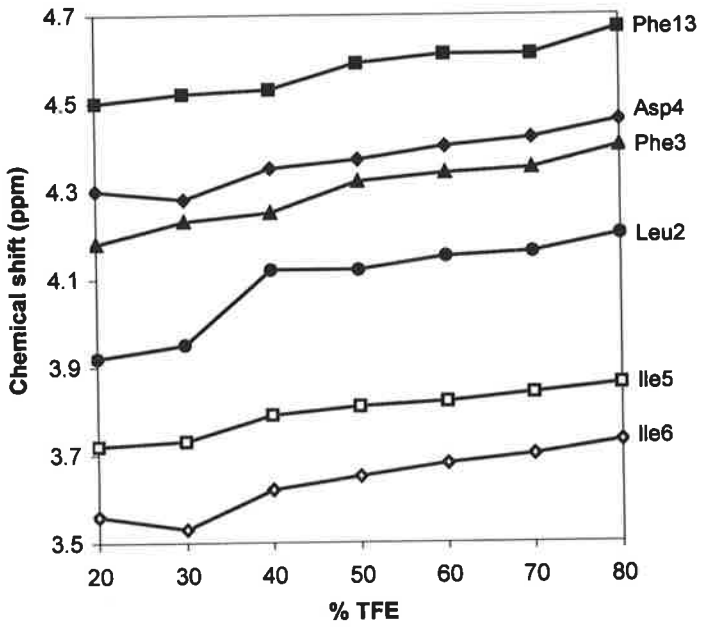

Figure 6.12 Chemical shift variation of selected aurein 1.2 αH resonances as a function of TFE concentration (by volume), at 600 MHz. In cases where resonance doubling was observed, the upfield resonance is indicated.

6.3b Assignments

The proton chemical shifts of aurein 1.2 were assigned as for citropin 1.1. These assignments are indicated in Figure 6.13, where parts of the NOESY and TOCSY spectra are shown. αC and C′ ^{13}C resonances were assigned from the HSQC and HMBC spectra, respectively. A summary of all the ^{1}H resonances and the αC and C′ ^{13}C chemical shifts is given in Table 6-6.

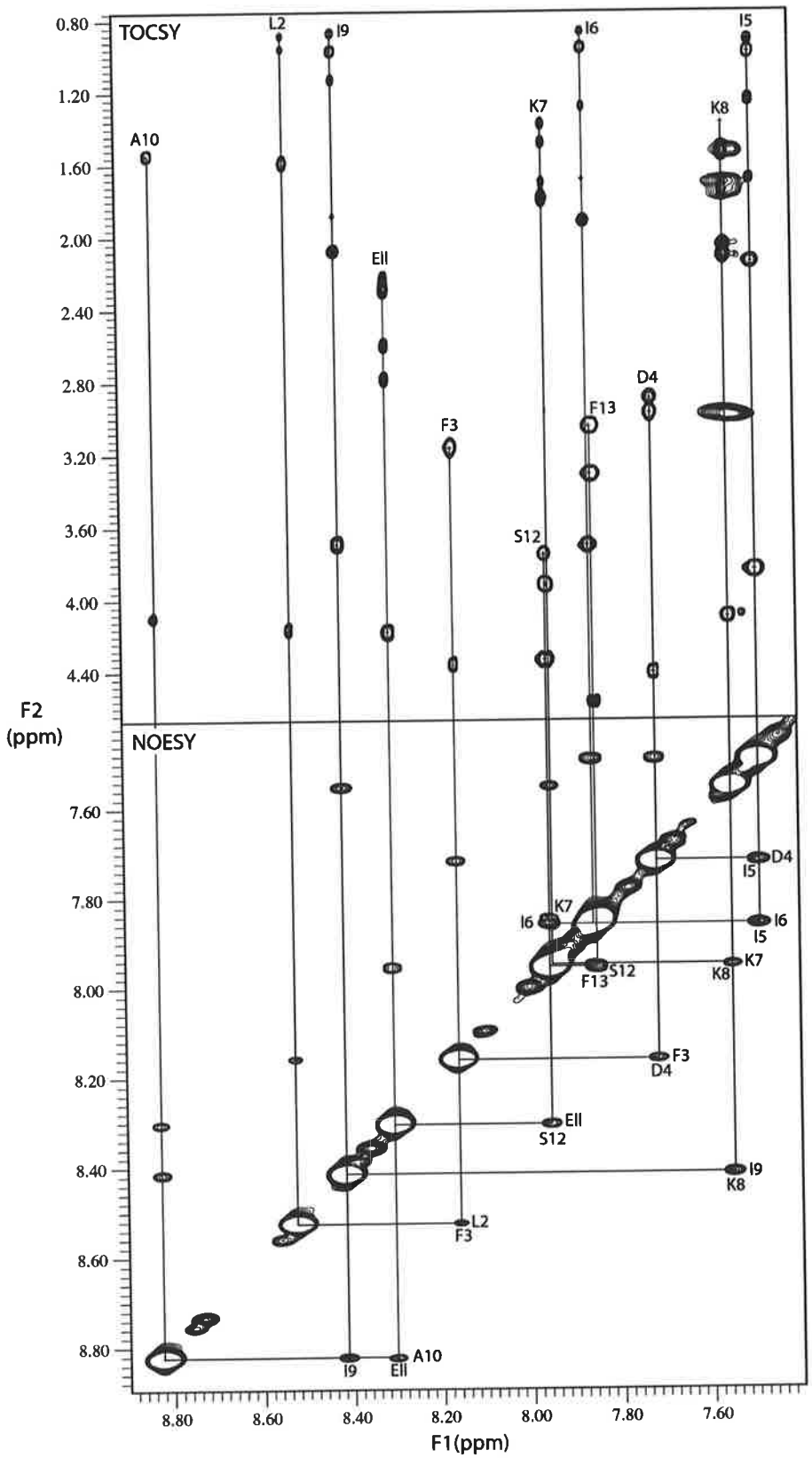

Figure 6.13 Partial NOESY (mixing time = 150 ms) and TOCSY (70 ms spin-lock time) spectra of aurein 1.2 in TFE/H_2O (70% TFE by volume) at pH 2.04, 25°C. Vertical lines connect the resonances in each spin system. These are labelled with the standard single-letter abbreviation for the residue type and a number indicating the sequential position of the residue. NOEs between sequential NH protons are indicated in the NOESY spectrum.

Table 6-6 ^{1}H and ^{13}C-NMR chemical shifts for aurein 1.2 in TFE/H_2O (70% TFE by volume), pH 2.04, 25°C. All ^{1}H assignments are shown, whereas only the αC and C′ ^{13}C resonances are indicated; n.o., not observed.

Residue	Chemical shift (ppm)					
	NH	α-CH	β-CH	Others	α-^{13}C	$^{13}C'$
Gly1	n.o.	4.04, 3.90			42.1	169.8
Leu2	8.52	4.17	1.60	γ–CH 1.60	56.9	176.6
				δ–CH_3 0.97, 0.90		
Phe3	8.16	4.36	3.17	H2,6 7.25	59.3	175.4
				H3,5 7.36		
				H4 7.31		
Asp4	7.72	4.41	2.98, 2.90		55.4	176.1
Ile5	7.49	3.84	2.15	γ–CH_2 1.69, 1.25	63.1	175.9
				γ–CH_3 0.99		
				δ–CH_3 0.92		
Ile6	7.86	3.70	1.92	γ–CH_2 1.67, 1.29	63.9	176.4
				γ–CH_3 0.96		
				δ–CH_3 0.88		
Lys7	7.95	3.92	1.80	γ–CH_2 1.49, 1.39	58.7	176.8
				δ–CH_2 1.70		
				ε–CH_2 2.97		
				ε-NH_3^+ 7.53		
Lys8	7.55	4.10	2.12, 2.06	γ–CH_2 1.54, 1.38	57.8	178.5
				δ–CH_2 1.79, 1.74		
				ε–CH_2 3.00		
				ε-NH_3^+ 7.57		
Ile9	8.41	3.70	2.09	γ–CH_2 1.89, 1.13	64.5	177.7
				γ–CH_3 0.97		
				δ–CH_3 0.88		
Ala10	8.82	4.10	1.55		54.3	179.5
Glu11	8.30	4.18	2.30, 2.23	γ–CH_3 2.78, 2.61	56.5	176.4
Ser12	7.96	4.34	3.92, 3.76		59.5	173.0
Phe13	7.85	4.63	3.31, 3.05	H2,6 7.26	57.1	177.6
				H3,5 7.38		
				H4 7.32		
				$CONH_2$ 7.28, 6.78		

6.3c Secondary Shifts

Plots of the secondary shifts (i.e., the chemical shift difference from random coil values, $\Delta\delta$) versus amino acid sequence are shown for the αH, αC and C′ resonances in Figures 6.14 and 6.15. The plot for the αH $\Delta\delta$ values shows distinct upfield shifts, while those for the ^{13}C resonances show distinct downfield shifts, except in the vicinity of the N- and C-termini. These deviations from random coil chemical shift values are consistent with the peptide having a helical structure along its length, with maximal helicity in the central region and less defined structure at the N- and C-termini [244, 347].

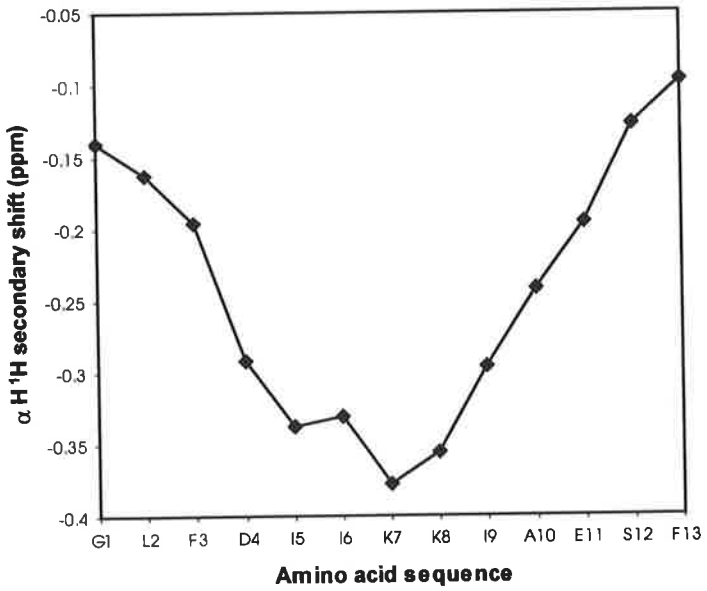

Figure 6.14 αH ^{1}H secondary shifts of aurein 1.2 in TFE/H_2O (70% TFE by volume). Negative values indicate an upfield shift from the random coil value, while positive values indicate a downfield shift. Secondary shifts were smoothed over a window of n = ±2 residues [246].

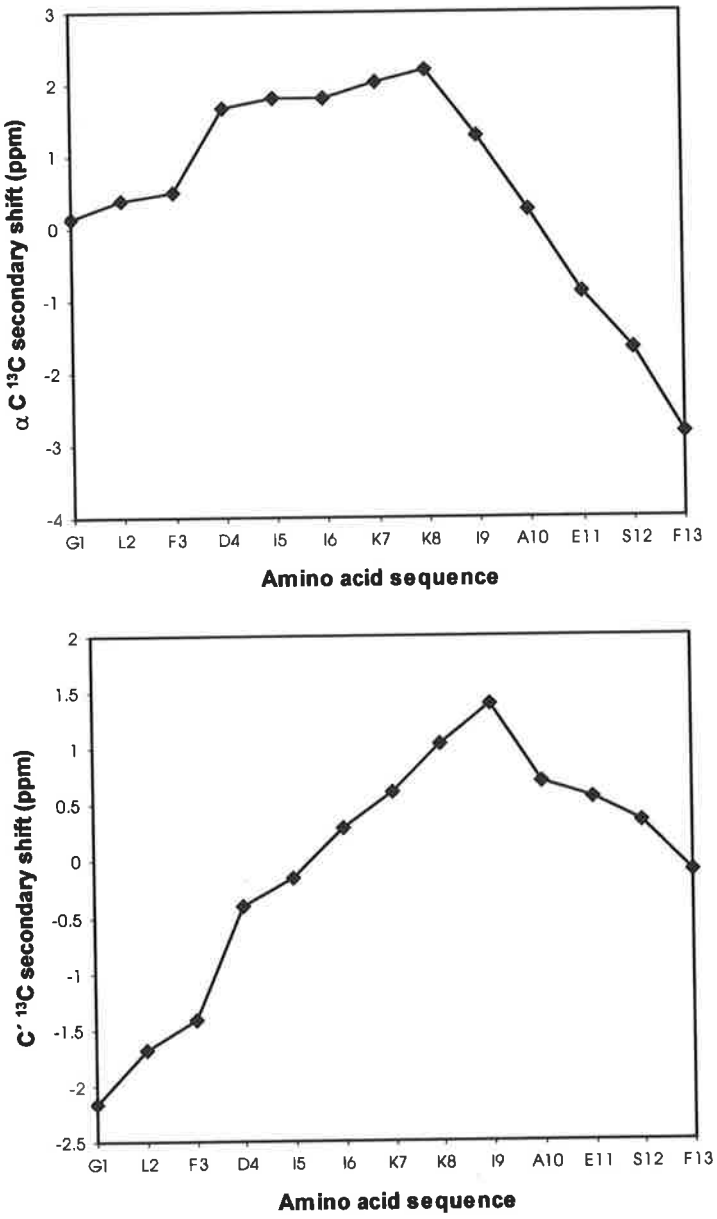

Figure 6.15 (a) αC and (b) C′ ^{13}C secondary shifts of aurein 1.2 in TFE/H_2O (70% TFE by volume). Positive values indicate a downfield shift from the random coil value, while negative values indicate an upfield shift. Secondary shifts were smoothed over a window of n = ±2 residues [246].

6.3d Amide Secondary Shifts

The NH Δδ values are plotted in Figure 6.16, showing a 3-4 residue periodic variation. The Δδ values for the hydrophobic residues are generally more positive than those of the hydrophilic residues, reflecting the different electronic environments of the two residue types and suggesting that aurein 1.2 forms an amphipathic α-helix [245, 248]. The

variation may be due to stronger hydrogen bonding on the hydrophobic face, resulting in slight curvature of the helix. For a peptide as short as aurein 1.2, however, this curvature is probably not significant.

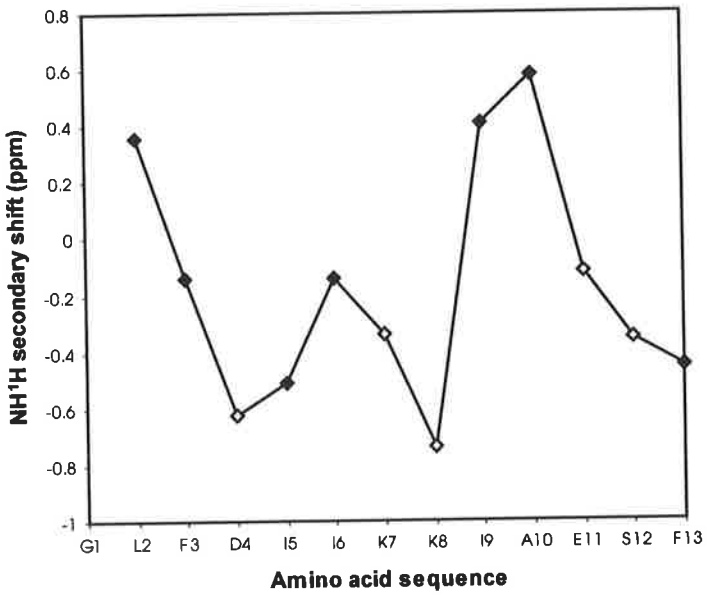

Figure 6.16 NH ^{1}H secondary shifts of aurein 1.2 in TFE/H_2O (70% TFE by volume). Positive values indicate a downfield shift from the random coil value, while negative values indicate an upfield shift. The secondary shifts were left unsmoothed. Hydrophilic residues [67] are indicated by open symbols.

6.3e NOE Connectivities

Figure 6.17 shows a summary of some of the more diagnostic NOESY cross-peaks found for aurein 1.2. A string of strong $d_{NN(i,i+1)}$ is present (see also Figure 6.13) as well as a set of weaker $d_{NN(i,i+2)}$ NOEs. Sequential $d_{\alpha N(i,i+1)}$ NOEs also occur, as well as a series of NOEs from residues three and four amino acids apart ($d_{\alpha N(i,i+3)}$, $d_{\alpha\beta(i,i+3)}$ and $d_{\alpha N(i,i+4)}$). These NOE signals and their intensities are consistent with aurein 1.2 having helical structure along the majority of its sequence. No long-range NOEs were found, suggesting that aurein 1.2 does not form dimers in this solvent system.

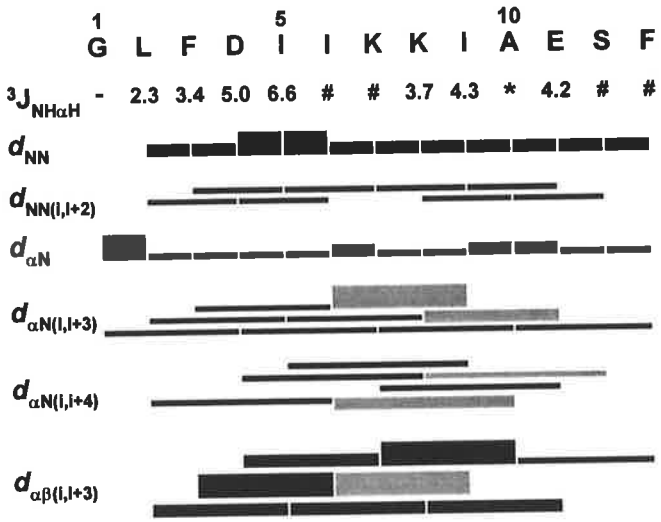

Figure 6.17 A summary of NOEs used in structure calculations for aurein 1.2 in TFE/H_2O (70% TFE by volume). The thickness of the bars indicates the relative strength of the NOEs (strong < 3.1 Å, medium 3.1-3.7 Å or weak > 3.7 Å). Grey shaded boxes represent NOEs that could not be unambiguously assigned. $^3J_{NH\alpha H}$ values are indicated where possible. Asterisks (*) show that no coupling constant was detected, while a cross-hatch (#) indicates the coupling constant could not be reliably assigned due to overlap.

6.3f Coupling Constants

Also shown in Figure 6.17 are the $^3J_{NH\alpha H}$ values obtained from the NH region of a high-resolution 1D ^1H spectrum. The splitting was not resolved for one NH signal, while four of the NH signals were overlapped, such that the coupling constants could not be reliably determined. Seven $^3J_{NH\alpha H}$ values could be measured, all but one of which were less than 6 Hz. These values are all consistent with α-helical structure.

6.3g Structure Calculations

The volumes of the NOESY cross-peaks (mixing time = 150 ms) were converted to distance restraints [266]. This procedure generated a total of 257 restraints, which included 129 intra-residue, 49 sequential (i,i+1) and 61 medium range restraints (i,i+3 and i,i+4). Eighteen of the distance restraints were ambiguous. Eight dihedral restraints were also used.

Sixty structures were generated by RMD and dynamical SA procedures (Section 4.6e). The 20 structures of lowest potential energy were chosen for examination and some statistics for these structures are shown in Table 6-7. The final structures had only minor

deviations from idealised covalent geometry (≤ 0.05Å for bonds and ≤ 5° for angles and impropers) and there were no violations of the distance restraints greater than 0.33 Å.

Table 6-7 Structural statistics of aurein 1.2 following RMD/SA calculations. <SA> is the ensemble of the 20 final structures, (SA) is the mean structure obtained by best-fitting and averaging the coordinates of the backbone atoms (N, αC, and C') of the 20 final structures, $(SA)_r$ is the representative structure obtained after restrained energy minimisation of the mean structure (SA). Well-defined residues are those with angular order parameters (S) > 0.9. For aurein 1.2, residues Leu2 to Ser12 were well-defined.

XPLOR energies (kcal·mol)	<SA>	(SA)
E_{tot}	28.57 ± 1.24	29.29
E_{bond}	2.16 ± 0.15	2.09
E_{angle}	10.24 ± 0.76	8.42
$E_{improper}$	1.95 ± 0.39	1.03
E_{vdw}	1.80 ± 0.36	2.36
E_{NOE}	12.41 ± 0.97	15.39
E_{cdih}	0.01 ± 0.01	0.00
RMSD from mean geometry (Å)		
All heavy atoms	0.82 ± 0.12	-
All backbone atoms (N, αC, C′)	0.34 ± 0.11	-
Heavy atoms of well-defined residues	0.69 ± 0.09	-
Backbone atoms (N, αC, C′) of well-defined residues	0.18 ± 0.07	-

The superimposition of the 20 lowest energy structures over the backbone atoms (N, αC and C′) of the well-defined residues shows that aurein 1.2 forms a regular α-helix along its length (Figure 6.18). The helix termini show greater variability as expected. The RMSD of the backbone atoms of the well-defined residues from the mean coordinates was 0.18 Å, while that for the backbone atoms of the entire peptide was 0.34 Å. Further statistics for these structures are given in Table 6-7.

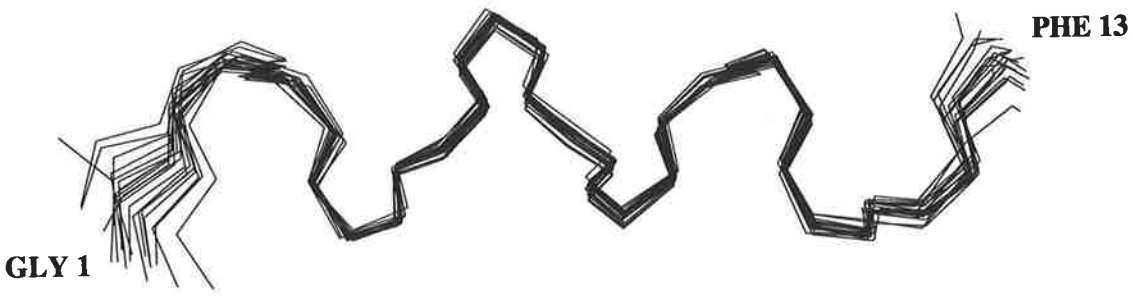

Figure 6.18 The 20 most stable calculated structures of aurein 1.2, superimposed along the backbone atoms (N, αC and C′) of the well-defined residues (2-12). This picture was prepared using the program MOLMOL [346].

Analysis of the angular order parameters (S, ϕ and ψ) for the 20 final structures showed that, with the exception of the N- and C- terminal residues (Gly1 and Phe13), all residues were well-defined (S >0.9 for both their ϕ and ψ angles).

A Ramachandran plot of the average ϕ and ψ angles for the well-defined residues shows that these angles are distributed within the favoured region for α-helical structure (Figure 6.19).

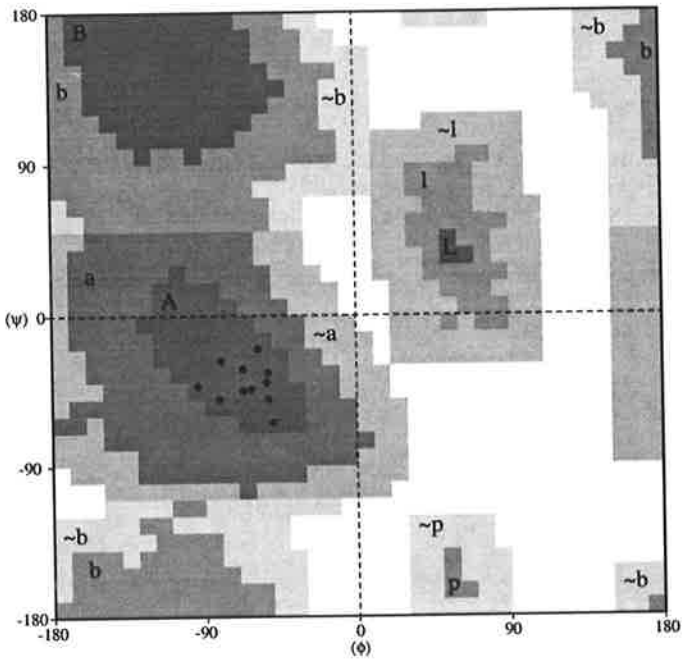

Figure 6.19 Ramachandran plot of aurein 1.2 showing that all of the residues fall in the favourable region for α-helices (A). The allowable and generous regions for α-helices are labelled as 'a' and '~a' respectively.

The most energetically stable of the 20 calculated structures is shown in Figure 6.20. This representation shows that, like citropin 1.2, aurein 1.2 forms an amphipathic α-helix, with well-defined hydrophobic and hydrophilic faces. This amphipathicity is shown more clearly in Figure 6.20 (b) - a longitudinal view through the centre of the helix. The length of α-helical aurein 1.2 was found to be around 16Å.

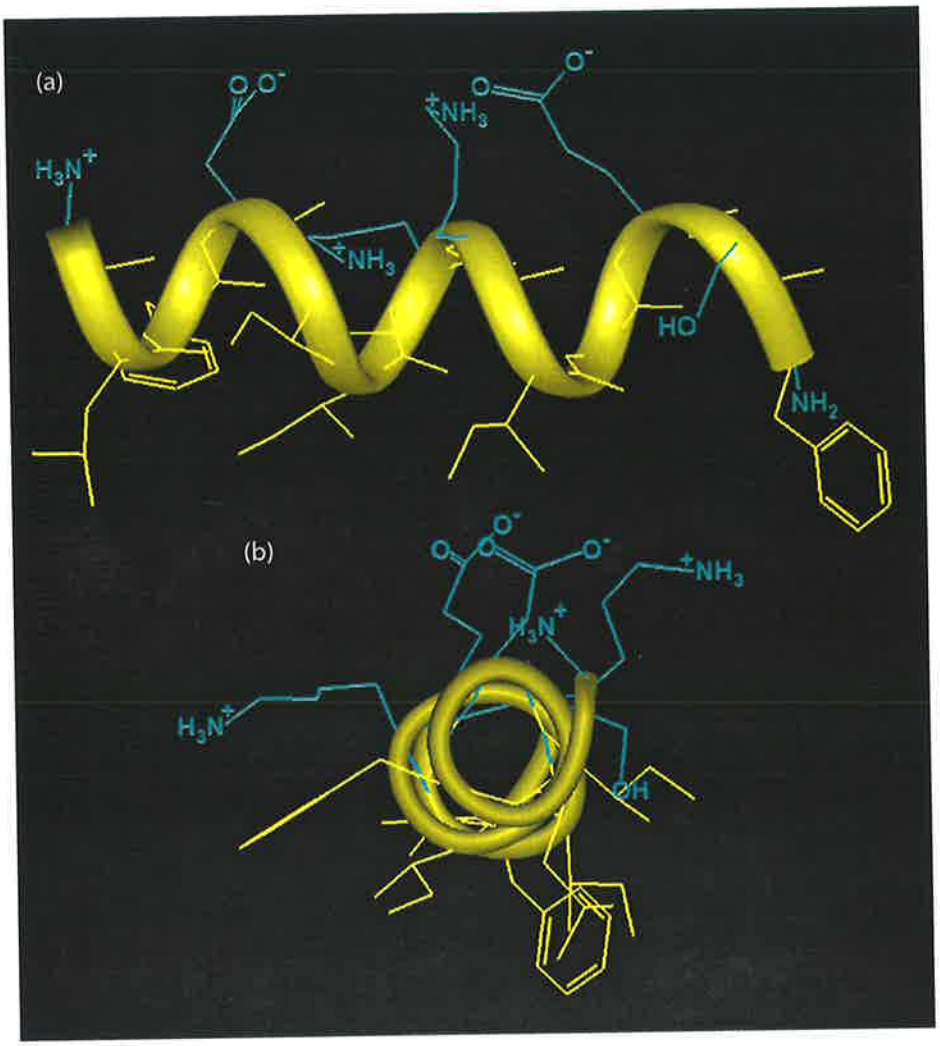

Figure 6.20 Side view (a) and axial view (b) of aurein 1.2 (energetically most stable structure). The hydrophilic groups are shown in blue.

6.4 Orientation Studies

6.4a Oriented Circular Dichroism - Unoriented Vesicles

The CD spectra for citropin 1.1 and aurein 1.2 in aqueous solution and in the presence of DMPC vesicles are shown in Figure 6.21. The spectra of the aqueous peptides are typical of those of random coil structures, while those of the vesicle samples show peaks at 190 nm and minima around 210 and 222 nm, characteristic of α-helical structure. Thus, it appears that the unstructured peptides bind to the lipid vesicles where they acquire α-helical structure.

As the L/P ratio increases (i.e., the peptide concentration decreases) the CD spectra have around the same intensity, indicating that the same proportion of peptide is bound in each case. This means that maximal binding is occurring in all samples and the vesicles are not becoming saturated at higher peptide concentrations. If saturation were occurring, the excess peptide would remain in the aqueous phase, increasing the proportion of random coil structure.

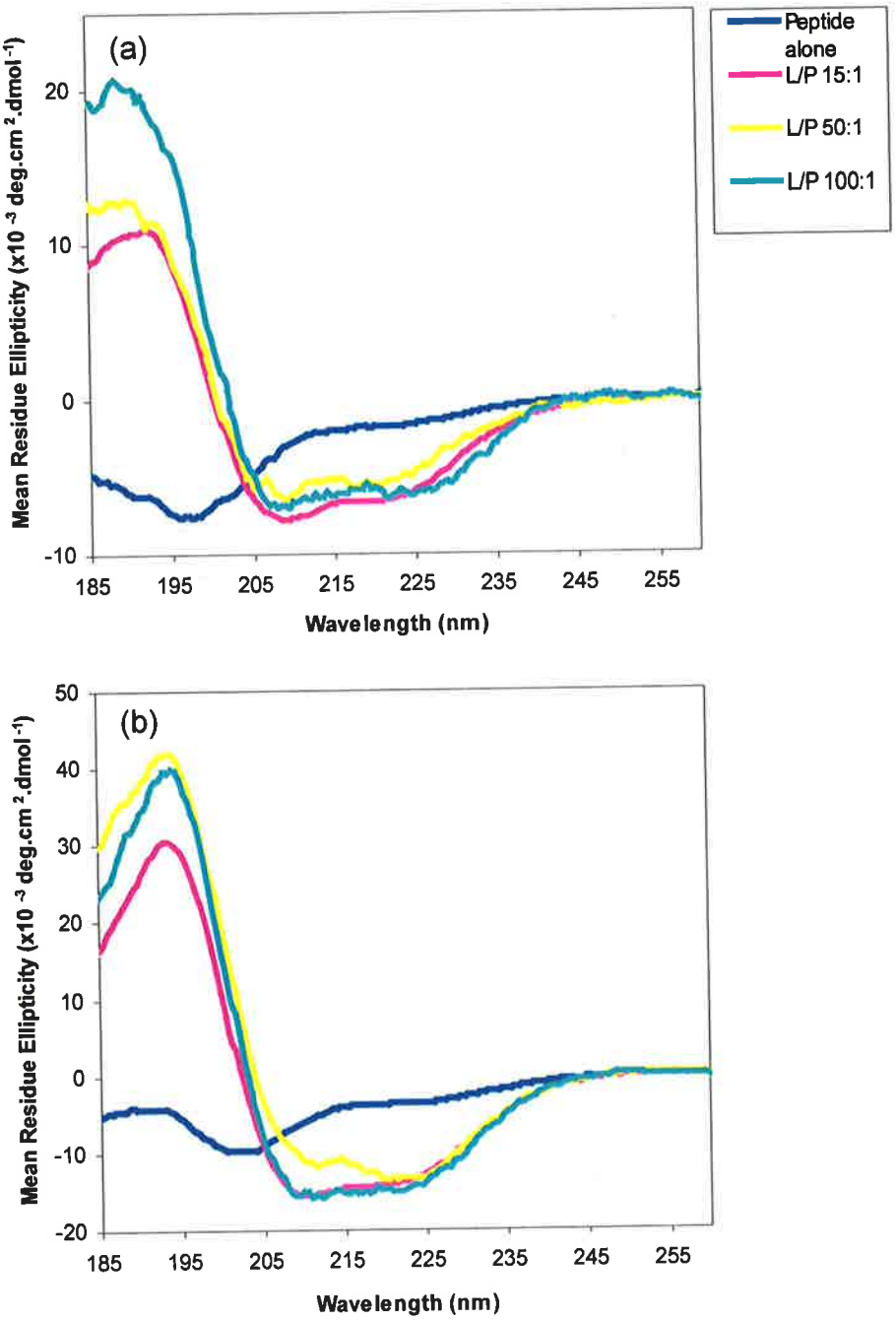

Figure 6.21 CD spectra of (a) citropin 1.1 and (b) aurein 1.2 in water, as well as in DMPC small unilamellar vesicles (SUV) at L/P ratios of 15:1, 50:1 and 100:1.

6.4b Oriented Lipid Bilayers

The CD spectra of oriented lipid bilayers were recorded at L/P ratios of 100:1, 50:1 and 15:1. Unfortunately, the spectra from samples with a L/P ratio of 100:1 were not of sufficient intensity to be reliably interpreted. The CD signal for these samples had very

low ellipticity (mdeg) such that it was comparable to the DMPC blank spectrum. The 15:1 and 50:1 samples, however, gave signals strong enough for interpretation.

To test the quality of the bilayer alignment of these samples, CD spectra of the sample and the sample rotated by 180° along its long axis were compared. These spectra are shown in Figure 6.22 for the citropin 1.1 sample (L/P 15:1). It can be seen that the two spectra have a very similar line-shape and intensity. Hence, the bilayers seem to be uniformly aligned and the spectra are not distorted by artifacts.

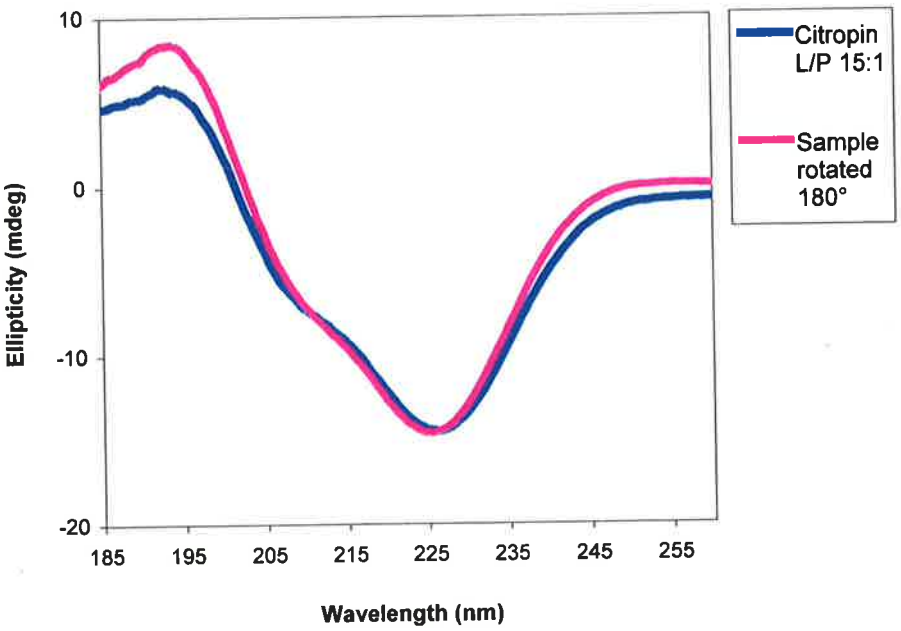

Figure 6.22 CD spectra of citropin 1.1 in oriented DMPC bilayers, at a L/P ratio of 15:1. The spectra were acquired on the same sample rotated through 180°.

The CD spectra for the oriented samples, following subtraction of the DMPC contribution, are shown in Figure 6.23. The spectra are compared with those of vesicles in excess water at a L/P ratio of 15:1. Since the exact concentration of the peptides in the oriented samples is not known, the units of the oriented spectra could not be converted from ellipticity (mdeg) to mean residue ellipticity ($deg \cdot cm^2 \cdot dmol^{-1}$). Instead, the spectra were scaled such that the intensities of their 222 nm minima were the same as those of the aqueous vesicle samples.

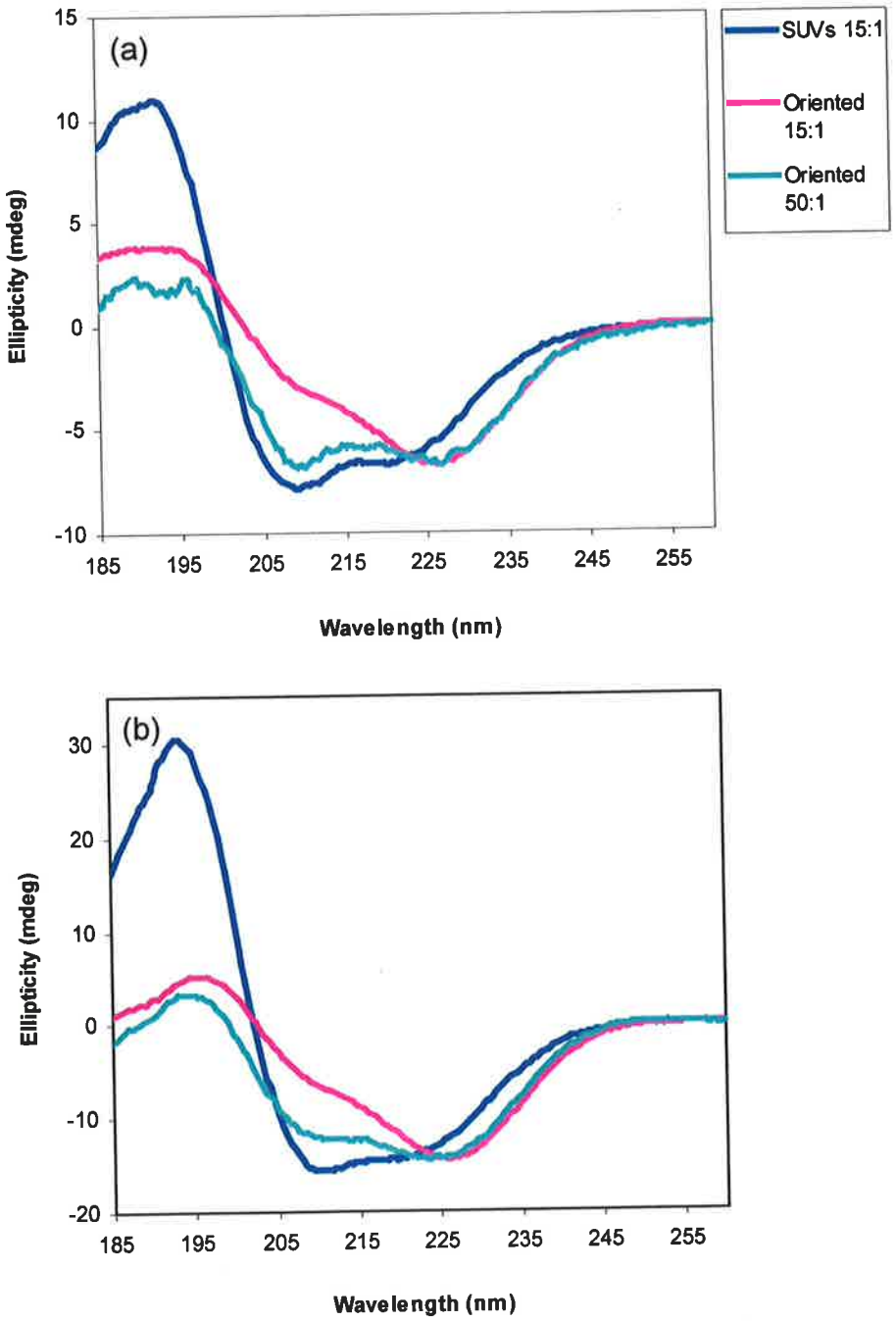

Figure 6.23 CD spectra of (a) citropin 1.1 and (b) aurein 1.2 in DMPC small unilamellar vesicles (SUV) (L/P 15:1) and oriented DMPC bilayers, at a L/P ratio of 15:1 and 50:1.

Figure 6.23 shows that, for the oriented samples of L/P 50:1, the intensity of the band around 210 nm is very similar to that of the unoriented samples. This could mean that for the higher L/P ratio, the peptides are inserting at a 45° angle, are orienting 50:50 transmembrane/surface or have no specific orientation with respect to the membrane. For the L/P 15:1 samples, however, the band at 210 nm has decreased markedly in intensity for both peptides. This indicates the peptides are more transmembrane oriented - either by

their absolute angle relative to the membrane normal, or by the percentage of helices with a transmembrane orientation.

A measure of the average angle of the peptide to the membrane normal can be obtained by comparison with reference spectra calculated for different tilt angles, as described by de Jongh *et al.* [305]. For the citropin 1.1 spectra, it was found that at a L/P ratio of 15:1, the tilt angle is approximately 30° from the membrane normal. For the 50:1 ratio, the tilt angle is found to be around 45°. Similarly, the aurein 1.2 tilt angle was found to be around 35° for the 15:1 sample and 45° for the 50:1 sample.

The average angle of 45° found for the samples with L/P 50:1 indicates that either there is no preference for a particular orientation or the peptides are all oriented at 45°. The angles of around 30-35° for the 15:1 samples mean either all of the peptides are aligned at this angle or the proportion of transmembrane oriented peptides has increased substantially. In either case, it appears that the peptides are more in line with the membrane normal when the L/P ratio is decreased from 50:1 to 15:1.

6.4c Solid-state NMR - Unoriented Multilayers

To investigate the effect of citropin 1.1 on the lipid head-groups, ^{31}P spectra were acquired on unoriented DMPC multilayers, both with and without the peptide (15:1 L/P ratio). These spectra are shown in Figure 6.24.

The shape of the spectra was consistent with that expected for uniaxially mobile phospholipids in randomly oriented lipid bilayers, indicating the integrity of the bilayer is maintained in the presence of citropin. The ^{31}P chemical shift anisotropy (CSA, $\Delta\sigma$) for the DMPC sample is -50 ppm, which is reasonable for a pure lipid multilayer sample [309, 319]. The $\Delta\sigma$ decreased to -40 ppm for the citropin/lipid sample (L/P 15:1), implying ~~inferring~~ the head-groups are more disordered in the presence of citropin 1.1. This may be due to the peptide causing an increase in the average area occupied by each phospholipid molecule, thereby giving the phosphodiester groups greater conformational freedom [319].

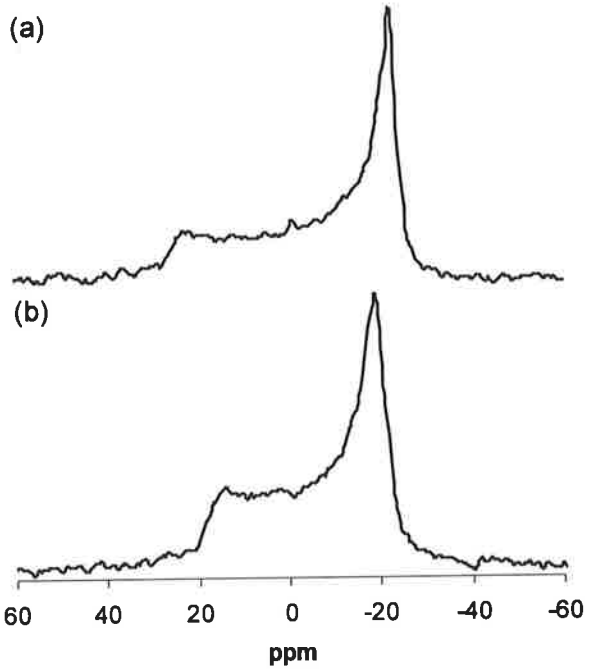

Figure 6.24 ^{31}P spectra obtained for unoriented DMPC bilayers (a) alone and (b) in the presence of citropin 1.1, at a L/P ratio of 15:1 and 26°C.

^{31}P NMR experiments were repeated on samples that had been refrigerated at ~ 4°C for several months and, interestingly, the spectrum of the citropin 1.1 sample indicated a substantial proportion of the DMPC was now in an isotropic phase (Figure 6.25). This did not occur for the control DMPC samples or for citropin 1.1 samples that had been stored in the freezer and suggests that citropin 1.1 induces non-lamellar phases over time.

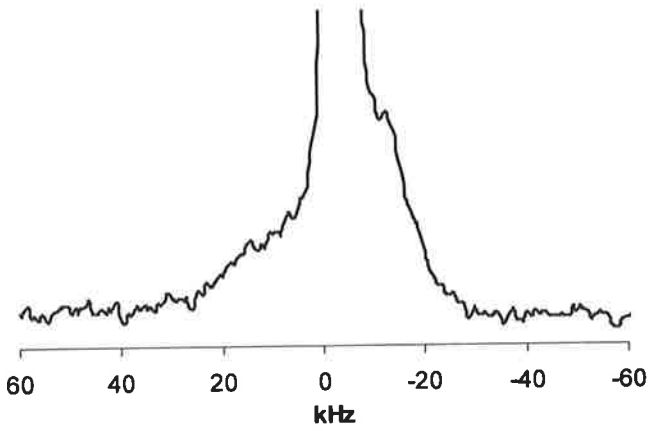

Figure 6.25 ^{31}P spectrum of citropin 1.1 in DMPC at a L/P ratio of 15:1 and 26°C, obtained after several months of refrigeration. The majority of the isotropic peak has been cut-off in order to show the underlying powder pattern.

6.4d Mechanically Oriented Multilayers

Aligned bilayer samples of DMPC (alone and in the presence of citropin or aurein (15:1 L/P ratio)) were prepared as outlined in the Experimental (Section 8.5b). To check the degree of bilayer alignment, a ^{31}P NMR spectrum was obtained for each sample. The glass plates in these samples were arranged parallel to the static magnetic field (B_0) of the NMR spectrometer (Figure 6.26 (inset)). Thus the bilayer normal will be oriented perpendicular to B_0 if the bilayers are well aligned.

The ^{31}P spectra obtained are shown in Figure 6.26. A single sharp peak can be seen in each of these spectra at similar chemical shift values (-16 to -19 ppm), consistent with bilayers arranged with the normal perpendicular to B_0 [309] [348].

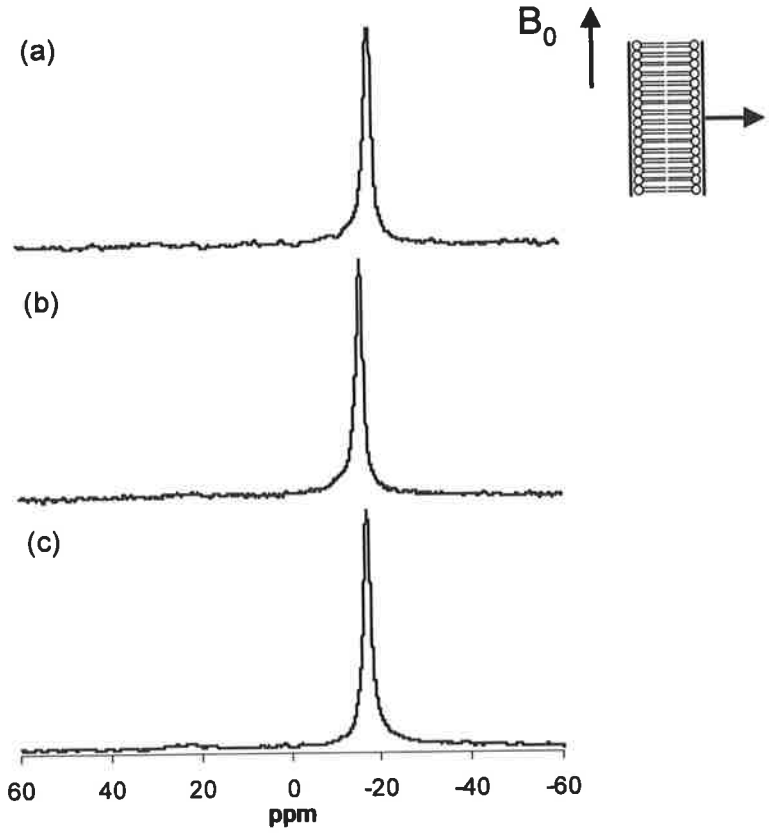

Figure 6.26 ^{31}P NMR spectra of aligned DMPC bilayers (a) alone; (b) with citropin 1.1; and (c) with aurein 1.2, at L/P ratios of 15:1 and 40°C. The orientation of the lipid bilayers is indicated in the inset diagram.

The ^{31}P NMR peaks for the peptide-containing bilayers (-17 ppm for aurein/DMPC, -16 ppm for citropin/DMPC) are slightly downfield from that of the DMPC bilayers alone

(-19 ppm), consistent with a reduction in the ^{31}P CSA for the peptide/lipid bilayers. The reduction is greater for citropin 1.1 than for aurein 1.2, suggesting citropin has a greater affect on the lipid head-groups.

The ^{2}H spectra obtained from these samples confirmed that the bilayers were well aligned (Figure 6.27). This is indicated by the well-resolved splittings, which are consistent with bilayers oriented perpendicular to B_0 (Section 5.2d).

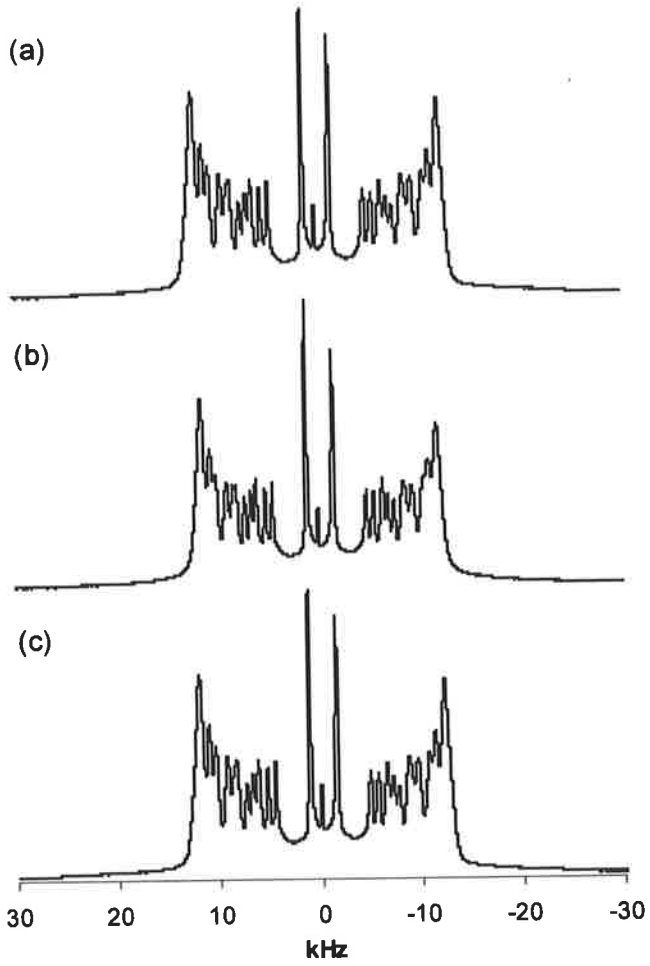

Figure 6.27 ^{2}H NMR spectra of aligned DMPC bilayers (a) alone; (b) with citropin 1.1; and (c) with aurein 1.2, at L/P ratios of 15:1, 40°C.

The sharp, intense, inner doublet seen in each spectrum is assigned to the methyl deuterons of the acyl chain termini, as these are the most disordered and their splitting is averaged to the greatest extent. The remaining splittings are assigned as follows: the first nine of the doublets are from the deuterons on carbons 13 to 5, such that the smallest splitting is assigned to carbon 13 and the largest to carbon 5 and assuming a

monotonically decreasing splitting [324]. Although the two acyl chains are not entirely equivalent [329], the assignment correlates well and the integration of each doublet is consistent with four deuterons.

The broad peaks at the outer edges of the spectra are due to the overlap of the doublets from the deuterons on carbons two to four. No attempt was made to slice this peak into three different splittings. Instead, these deuterons were assigned a single splitting value. Thus, the assignments are only approximate for some of the deuterium resonances.

The splittings from each of the doublets were measured and converted to carbon-deuterium bond order parameters [328] (Section 5.2d). A plot of the order parameters, S_{CD}, against carbon position is shown in Figure 6.28. It can be seen that the order parameters for the peptide-lipid samples have decreased, relative to those of the DMPC sample alone. In addition, the order parameters for the citropin 1.1 sample are less than those of the aurein 1.2 sample. These results indicate that the acyl chains are more disordered in the presence of the peptides - more so for citropin 1.1 than for aurein 1.2.

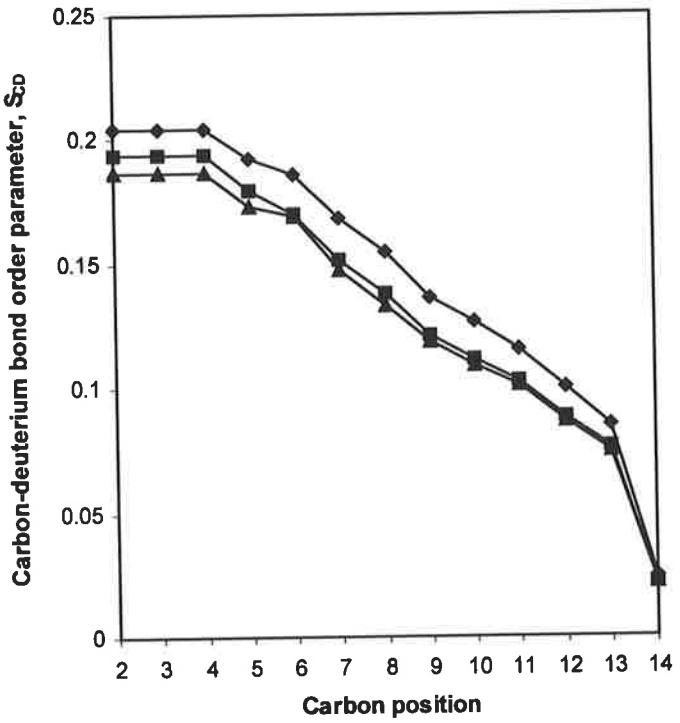

Figure 6.28 Plot of the carbon-deuterium bond order parameters (S_{CD}) against acyl chain carbon position for aligned DMPC bilayers (♦) alone and in the presence of aurein (■) or citropin (▲), 15:1 L/P ratio, 40°C. The estimated error of the bond-order parameters is ± 0.008. The plot was reproducible for a number of experiments conducted at the same or different temperatures.

These conclusions are borne out by a quantitative analysis of the splittings. Table 6-8 lists the changes in quadrupolar splitting as a percentage of the splittings obtained for the control bilayers. The decrease in order parameters for both peptide samples shows a greater change for citropin 1.1. The change in splittings for aurein 1.2 ranges from -5% to -12%, whereas that for the citropin 1.1 sample ranges from -9% to -14% (the negative sign indicates a decrease).

Table 6-8 ^{2}H quadrupolar splittings measured for DMPC bilayers both alone and in the presence of citropin 1.1 or aurein 1.2 at a 15:1 molar ratio and the percentage difference between the splittings for the peptide samples and the control DMPC multilayers.

	2H Quadrupolar Splittings (Δν) for DMPC bilayers (kHz)			% change from DMPC alone	
Carbon Position	DMPC	DMPC + Citropin 1.1	DMPC + Aurein 1.2	DMPC + Citropin 1.1	DMPC + Aurein 1.2
2	25.6	23.4	24.3	-9	-5
3	25.6	23.4	24.3	-9	-5
4	25.6	23.4	24.3	-9	-5
5	24.1	21.7	22.5	-10	-7
6	23.3	21.2	21.3	-9	-9
7	21.1	18.4	19.0	-13	-10
8	19.3	16.7	17.2	-14	-11
9	17.0	14.9	15.2	-12	-11
10	15.9	13.7	14.0	-14	-12
11	14.4	12.6	12.8	-13	-10
12	12.5	10.8	11.0	-14	-12
13	10.6	9.4	9.5	-11	-10
14	3.0	2.7	2.7	-10	-10

The change in disorder tends to be greater at the ends of the acyl chains, suggesting the peptides induce more disorder in the bilayer centre than at the hydrocarbon-water interface. However, at the chain ends the difference in splittings is of the order of 0.3 kHz (*cf.* 2.2 kHz near the head-group) and is more difficult to determine due to the inherent linewidths.

^{15}N NMR spectra were acquired for citropin 1.1 and aurein 1.2 as dry powders. These peptides both incorporated ^{15}N-alanine at position 10. Experiments were conducted under static, as well as magic angle spinning conditions, and the spectra obtained are shown in Figure 6.29. The assignments of the principal elements of the chemical shift tensor are indicated on the static spectra and these values are consistent with the isotropic chemical shifts ($\delta_{iso} = 1/3(\sigma_{11}+\sigma_{22}+\sigma_{33})$).

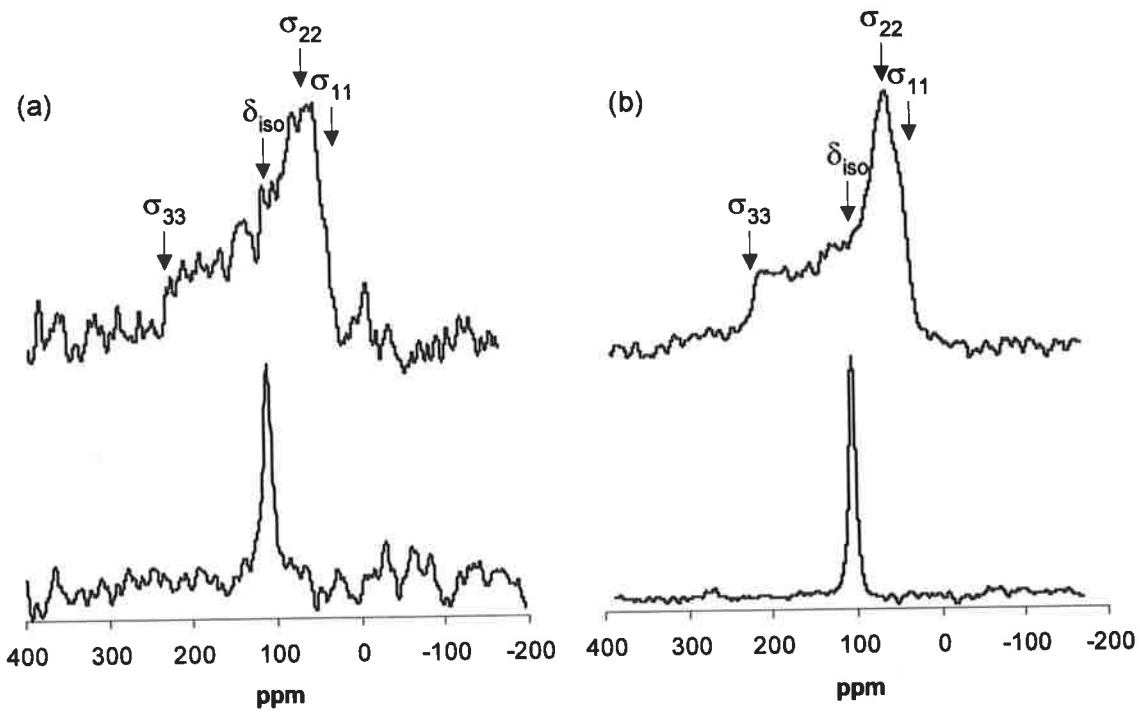

Figure 6.29 ^{15}N powder spectra for (a) citropin 1.1 and (b) aurein 1.2. The peptides were labelled with ^{15}N-L-Alanine at position 10. The upper spectra were acquired on static samples, while the lower spectra were acquired on samples spun at the magic angle. The principal elements of the chemical shift tensor are indicated (σ_{11}, σ_{22} and σ_{33}), as well as the isotropic shifts (δ_{iso}).

^{15}N spectra for these peptides, when incorporated into mechanically aligned multilayers, are shown in Figure 6.30. These spectra have low signal-to-noise ratios, despite being run for over 56000 scans and taking several days to acquire. This is due, in part, to the small amounts of labelled peptide used (~ 5 mg, compared with the 10-45 mg used in similar experiments by Bechinger *et al.* [207] and Marassi *et al.* [154]).

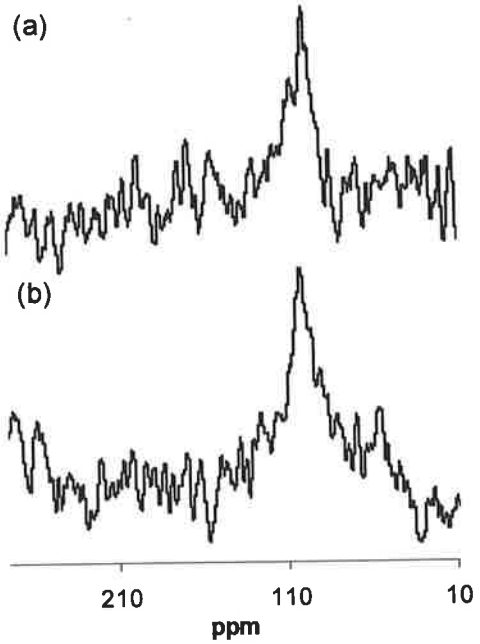

Figure 6.30 ^{15}N spectra of (a) citropin 1.1 and (b) aurein 1.2 in multilayers, at L/P ratios of 15:1 and 35°C. The peptides were labelled with ^{15}N-L-Alanine at position 10.

The ^{15}N peaks in Figure 6.30 are broad and occur at a chemical shift of around 100 ppm for each peptide. These values are close to δ_{iso} (Figure 6.29), suggesting the peptides may be reorienting isotropically in the water layer. However, if this were the case the peaks would be narrower, assuming that peptide motion between the multilayers is not restricted. Further evidence that the peptides are not reorienting in the water between the bilayers comes from similar experiments undertaken with bicelles. The ^{15}N spectrum (Figure 6.31) for aurein 1.2 in bicelles also gave a broad signal at ~100 ppm, suggesting it was not isotropically tumbling in the excess water space (unpublished data obtained in collaboration with Assoc. Prof. F. Separovic, University of Melbourne). Furthermore, the CD and ^{31}P and ^{2}H NMR results indicated that both citropin 1.1 and aurein 1.2 interact with the lipid bilayer.

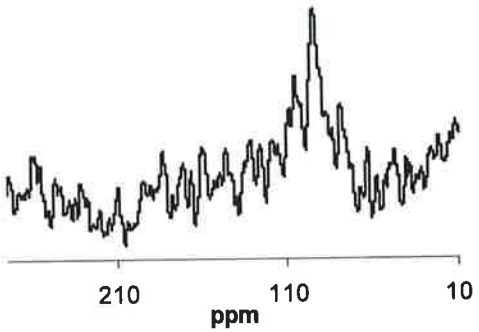

Figure 6.31 ^{15}N spectra of aurein 1.2 in DMPC/DHPC bicelles (3:1), at a L/P ratio of 15:1, 35°C. The peptide was labelled with ^{15}N-L-Alanine at position 10.

Due to the low signal-to-noise ratio, it is difficult to draw a conclusion about the peptide orientation. However, it seems unlikely that the peptide is oriented on the surface of the bilayers because the ^{15}N spectrum does not have the expected catenary line-shape (Figure 6.32). This pattern is predicted since surface-bound peptides would orient at a range of angles to B_0 (0-90°) when the membrane surface is parallel to B_0. However, a surface orientation could only be ruled out completely by obtaining a spectrum with improved signal-to-noise.

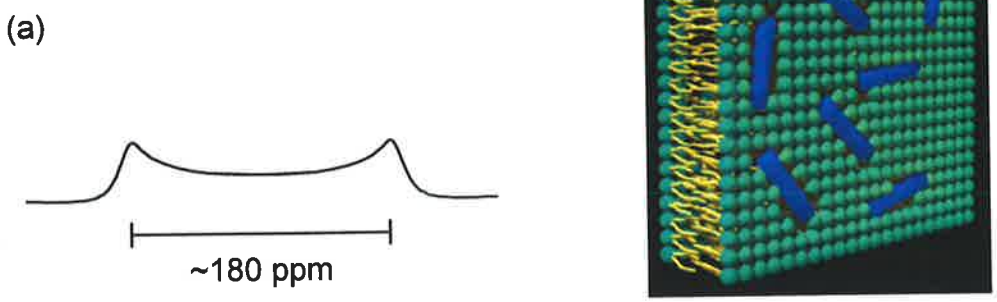

Figure 6.32 (a) Catenary spectrum expected for surface oriented peptides when the bilayers are oriented as in (b), with the membrane normal perpendicular to the external field (B_0). The peptides, indicated in (b) by cylinders, are arranged at many different angles to B_0. The hydrophilic regions of the bilayer and peptides are coloured green and blue respectively, while the hydrophobic regions are coloured yellow and red.

A transmembrane orientation would result in a ^{15}N peak at around 60 ppm, provided the ^{15}N CSA is identical to that of the peptide powder. No peaks were evident in this region of the ^{15}N spectra for either peptide.

The CSA can be reduced significantly if the peptide is subject to motional averaging [122, 153]. Alamethicin in lipid bilayers, for example, has a reduced ^{15}N CSA compared to the pure peptide, due to fast uniaxial rotation about the helix long axis [123]. With increased motion, the chemical shifts of the 0° and 90° orientations shift upfield and downfield respectively. However, a ^{15}N shift around δ_{iso} would only occur if the motion were almost isotropic or the peptide was oriented close to the magic angle, relative to B_0.

Obliquely oriented peptides have been detected recently by solid-state NMR [333, 349] and other techniques [350, 351] so it is possible that citropin 1.1 and aurein 1.2 also adopt oblique orientations. Alternatively, the peptides may be rapidly reorienting on the NMR time-scale, while bound to the lipid bilayer. Although such motion may seem unlikely, since rotation must take place about the radial axes (i.e., perpendicular to the long axis), there is evidence that motion of this kind can occur. For example, both the surface-bound peptide ovispirin and the oblique oriented M2-TMP, from the influenza A virus, have been shown to undergo rapid motion about the bilayer normal [333, 349].

6.5 Discussion

The results of the solution NMR studies presented in Sections 6.2 and 6.3 indicate citropin 1.1 and aurein 1.2 form essentially linear amphipathic α-helical structures in mixtures of TFE and H_2O. TFE acts as a membrane mimicking solvent by promoting the formation of intramolecular hydrogen bonds within the solute [34, 35] so it is anticipated that the structures determined here persist in a bilayer environment. This is supported by the results of the CD experiments, which show the peptides are unstructured in water alone but adopt α-helical structures in the presence of DMPC vesicles.

Citropin 1.1 was found to be around 20 Å in length in TFE/H_2O, while aurein 1.2 had a length of around 16 Å. Since the hydrophobic core of a membrane is typically 30 Å [129, 185], these peptides are not long enough to form barrel-stave type channels. It is conceivable, however, that the peptides could form toroidal model pores if the bilayer lipids are capable of stabilising the ends of the shorter pores.

Solid-state NMR studies were used to investigate the effect of citropin 1.1 and aurein 1.2 on DMPC bilayers. The ^{31}P NMR results on unoriented DMPC bilayers suggest the lipids remain in the bilayer phase when citropin 1.1 is present but the CSA is significantly reduced due to increased motional averaging. This implies that citropin 1.1 interacts with the bilayer in the region of the lipid headgroups.

Citropin 1.1 was also found to induce the formation of an additional isotropic phase of DMPC when stored at ~ 4°C for a long period of time. Bechinger *et al.*, [352] have previously reported that magainin also induces an isotropic phase in phosphatidylcholine bilayers under certain conditions. This is compatible with the latter stages of the carpet mechanism, where the membrane structure disintegrates and segments break off as micelles [152] (Section 3.2d). However, Hori *et al.* [353] have suggested it could also be indicative of a toroidal mechanism (Section 3.2c) since the phospholipids involved in the pore structures should also give rise to an isotropic signal.

Both citropin 1.1 and aurein 1.2 were found to decrease the order of the lipid acyl-chains in oriented samples, with the disorder greater toward the centre of the lipid bilayers.

A similar effect has been reported for surface oriented peptides [332, 333]. The peptides are thought to insert into the lipid-water interface and laterally separate the lipids. The acyl chains now have greater spatial freedom, particularly in the hydrophobic core of the membrane, and thus are more disordered [332]. The change in order for these peptides was greater, however, than that found here for citropin 1.1 and aurein 1.2.

Peptide orientation was investigated using both ^{15}N solid-state NMR and OCD. The OCD studies indicated that at a L/P ratio of 50:1, neither citropin 1.1 nor aurein 1.2 had a preferred orientation in the membrane. As the L/P ratio was ~~increased~~ decreased to 15:1, however, the peptide helices were found to orient at an average angle of 35° to the membrane normal. Thus, as peptide concentration increases, the peptides move toward a transmembrane orientation. It is not known, however, whether all the peptides orient at this angle or whether a mixture of transmembrane and surface oriented peptides is present because the angle determined by OCD is an average.

While the ^{15}N spectra obtained for citropin 1.1 and aurein 1.2 were poorly resolved, they did allow certain possibilities to be eliminated as the results were not consistent with either a surface or transmembrane peptide orientation. Instead, the peaks observed were centred around δ_{iso}, suggesting the peptides were either reorienting almost isotropically between the lipid bilayers or had orientations close to the magic angle (54.7°), relative to the external field. Since the OCD results indicated the peptides had a preferential orientation, it seems more likely that the peptides are arranged obliquely, with an average angle of 35° to the bilayer normal. The ^{15}N spectra are more consistent with this scenario than with either the transmembrane or surface orientations, particularly if the peptides undergo additional motional averaging.

A number of peptides have previously been shown to have a tilted orientation in lipid bilayers [349-351]. This is thought to occur because of asymmetry in the distribution of hydrophobic residues along the helix long axis i.e., there is a hydrophobicity gradient. These peptides insert at an angle around 30-60° to the lipid-water interface [354].

The N-terminal half of citropin 1.1 (residues 1-8) is significantly more hydrophilic than the C-terminal half (9-16) because all of the charged groups are in this portion. Ser11 is

the only hydrophilic residue in the C-terminal half. This could explain an oblique orientation for this peptide. Aurein 1.2, however, has a more even distribution of hydrophobic and hydrophilic residues along the length of the peptide. This is consistent with the OCD results that indicated aurein 1.2 had a greater average angle to the membrane normal than citropin 1.1. Nevertheless, an oblique orientation for aurein 1.2 is surprising. An alternative explanation is that both citropin 1.1 and aurein 1.2 partially insert into the membrane because of their high concentration in the bilayers. This would be consistent with the carpet model, where peptide insertion occurs once a threshold concentration is reached [343].

Taken together, the evidence suggests that the unstructured peptides bind to the membrane, inducing a conformational rearrangement to an α-helical structure. At a L/P ratio of 50:1, the peptides are randomly oriented with respect to the bilayer, with an average orientation of 45°. As the peptide concentration increases, the average orientation of the helices approaches a transmembrane orientation, compatible with the latter stages of the carpet mechanism [343].

Interpretation of the ^{15}N spectra was limited by the poor signal-to-noise ratios obtained, despite running the experiments over a number of days. To obtain a clearer indication of the peptide location, the sensitivity of the experiments must be improved. Since ^{15}N is an inherently insensitive nucleus, the experiments were conducted at the highest field-strengths accessible (50.69 MHz). Unfortunately, cross-polarisation (CP) was not available with the probe used. Attempts to acquire spectra at a lower field-strength (30.4 MHz) using CP were unsuccessful. This is probably because the peptide is too mobile in the fluid-phase bilayers, resulting in inefficient CP [207] since the same experiments were successful for the dry peptide powders.

In addition, CP parameters for ^{15}N can be difficult to optimise because of the length of time it takes to obtain a ^{15}N signal. It may be possible, however, to optimise the parameters by maximising the ^{1}H signal obtained from magnetisation transferred from ^{15}N, instead of the other way around, and using these settings to obtain ^{15}N spectra [355].

Peptide mobility could be detected by obtaining ^{15}N spectra for unoriented bilayer samples. A reduced CSA would imply motional averaging. If the peptides are indeed rotating isotropically, a single peak at δ_{iso} would be expected. A greater amount of sample would be required to get a satisfactory signal-to-noise ratio for these fluid phase experiments. Alternatively, the ^{15}N experiments on oriented samples could be repeated at low temperatures, below the gel-to-liquid crystalline transition temperature. Peptide motion would be frozen at this temperature making CP more efficient. If the peptides are oriented, the ^{15}N spectrum would be similar to that found in the fluid phase but if the peptides have random orientations, a powder pattern would be expected [333, 356]. However, it is possible that the peptide will have a different orientation at the lower temperature.

It would also be informative to attempt the ^{15}N NMR studies on samples aligned with the membrane normal parallel to the external field. If the peptides were reorientating isotropically, no chemical shift change would be expected. However, if the peptides were arranged around an average angle of 35° to the bilayer normal, the chemical shift of the peak would shift downfield from δ_{iso}. In addition, any surface oriented peptide, which may have been obscured in the samples oriented perpendicular to the field (by a combination of broad line-shape and low signal-to-noise), would be expected to give a peak around 60 ppm. Unfortunately, the probes used in the present study did not permit placement of the glass-plates at this angle.

To further investigate the mechanism of action of these peptides, it would be desirable to determine the orientation of the peptides at higher L/P ratios. The OCD experiments were not sensitive enough to explore L/P ratios higher than 50:1. ^{15}N NMR studies may be applicable, but to improve the sensitivity it would be preferable to use greater amounts of labelled peptides than were used in the present study.

It would also be informative to further investigate the induction of isotropic lipid phases by these peptides. The phase-change induced by citropin 1.1 was observed after several months of storage. The time-course of this transition should be explored more fully to see if it is a biologically relevant effect.

Aurein 1.2 has no ~~affect~~ effect on erythrocytes at 100 $\mu g \cdot mL^{-1}$ but inhibits the growth of bacteria and cancer cells at this or lower concentrations [14]. Since bacterial and cancer cell

membranes are anionic and those of erythrocytes are neutral, it would be interesting to determine the structure and orientation of aurein 1.2 and citropin 1.1 in acidic lipid bilayers. By comparing the results with those determined here for neutral bilayers, we may gain insight into the reasons behind membrane specificity.

In addition, since neither citropin 1.1 nor aurein 1.2 ~~are~~ is active against the G- *E. coli* bacterium, there may be a difference in how these peptides bind and orient when lipopolysaccharides (LPS) are present in the outer leaflet of the membrane. Relatively few studies have investigated the interactions between antibacterial peptides and LPS due to problems obtaining suitable model membrane systems [173]. However, Matsuzaki *et al.* [173] were successful in using CD spectroscopy to determine the structure of magainin in LPS-containing phosphatidylcholine vesicles. Magainin, which has activity against *E. coli*, was shown to form an α-helix in the presence of LPS. Similar studies could be attempted with citropin 1.1 and aurein 1.2 to see what structure they adopt in this medium and whether or not they actually bind to the LPS-containing vesicles.

6.6 Conclusion

The solution NMR spectroscopy and restrained molecular dynamics calculations indicate citropin 1.1 and aurein 1.2 form amphipathic α-helical structures in TFE/H_2O – a membrane-mimicking medium. CD studies show that these peptides are unstructured in water but bind to DMPC vesicles, where they rearrange to an α-helical structure. OCD results suggest these peptides are randomly oriented at low peptide concentrations (L/P 50:1), with an average orientation of 45°, but are oriented closer to the membrane normal as the peptide concentration is increased (~35°). The results of solid-state NMR experiments were compatible with an average orientation around 35°, however further experiments are required to exclude other possibilities and to further explore the membrane activity of these peptides. The current results are most consistent with the carpet model [343] of antibacterial action.

Chapter 7 The Caerin Peptides

7.1 Introduction

At present, the caerin family comprises over 30 different peptides, isolated from the dermal secretions of six Australian frog species – *L. splendida*, *L. caerulea*, *L. xanthomera*, *L. gilleni*, *L. ewingi* and *L. chloris* [23, 32, 357-360]. Approximately half of these peptides are antimicrobially active, while the remainder, presumed to be the products of enzymic degradation, are inactive [12].

The caerins can be divided into four groups - caerins 1, 2, 3 and 4, each of which contains a number of antimicrobially active compounds. The caerin 1 peptides are broad-spectrum antibiotics, while the caerins 2, 3 and 4 are only active against a few of the species tested, typically *Escherichia coli* and *Micrococcus luteus* (unpublished data). The sequences and antibacterial activity data for several members of the caerin 1 family are given in Table 7-1. The sequences and activity data for several synthetic analogues are also presented in this table.

Table 7-1 Antibiotic activities (MIC, $\mu g \cdot mL^{-1}$) of selected caerin 1.1 peptides and synthetically modified analogues. Values for the hydrophobicity[d], hydrophobic moment[e] and hydrophilic angle (ϕ) of the first helix (residues 1-14) of caerin 1.1 and caerin 1.4 are also indicated.

Caerin	Sequence
1.1	GLLSVLGSVAKHVLPHVVPVIAEHL-NH_2
1.1D	Gllsvlgsvakhvlphvvpviaehl-NH_2
1.1GP	GLLSVLGSVAKHVLGHVVPVIAEHL-NH_2
1.1PG	GLLSVLGSVAKHVLPHVVGVIAEHL-NH_2
1.1GG	GLLSVLGSVAKHVLGHVVGVIAEHL-NH_2
1.1.1	LSVLGSVAKHVLPHVVPVIAEHL-NH_2
1.1.3	VLPHVVPVIAEHL-NH_2
1.1.5	GLLSVLGSVAKHVLPH-OH
1.4	GLLSSLSSVAKHVLPHVVPVIAEHL-NH_2

Organism	MIC ($\mu g \cdot mL^{-1}$)[a] Caerin[b]					
	1.1	1.1D	1.1GP	1.1PG	1.1GG	1.4[c]
Bacillus cereus	50	50	100	100	50	50
Escherichia coli						50
Leuconostoc lactis	1.5	3	12	12	12	12
Listeria innocua	25	50	50	25	50	100
Micrococcus luteus	12	6	25	12	12	0.4
Pasteurella multocida	25	25	50	50	100	25
Staphylococcus aureus	3	6	25	25	25	100
Staphylococcus epidermis	12	12	100	100	100	25
Streptococcus uberis	12	25	50	25	12	100
Charge	+1					+1
Helix 1 (1-14)						
H[d]	0.16					0.08
μ[e]	0.26					0.27
ϕ[f]	100°					160°

[a] Where there is no figure listed the MIC value is >100 $\mu g \cdot mL^{-1}$.
[b] Data for caerin 1.1 and synthetic modifications are from Wong *et al.* [97].
[c] Unpublished data.
[d] Mean residue hydrophobicity (H) [197]
[e] Hydrophobic moment (μ) per residue [67].
[f] Hydrophilic angle (ϕ).

Interestingly, the all-D isomer of caerin 1.1 has comparable activity to that of the natural L-form. This rules out interactions with a specific chiral receptor and is therefore compatible with the idea that caerin 1.1 targets the bacterial cell membrane.

The structure of caerin 1.1 has been determined in the membrane mimicking solvent TFE/H_2O [97] (Figure 7.1). It appears to form an amphipathic α-helical structure along the length of the peptide, with a region of high flexibility in the vicinity of Pro15. Proline residues are known to disrupt helical structure because they do not have an amide proton that can form a hydrogen bond with the backbone carbonyl group four residues previous in the sequence. Pro19, in caerin 1.1, occurs near the start of the second helix so it does not interfere with helical structure [97].

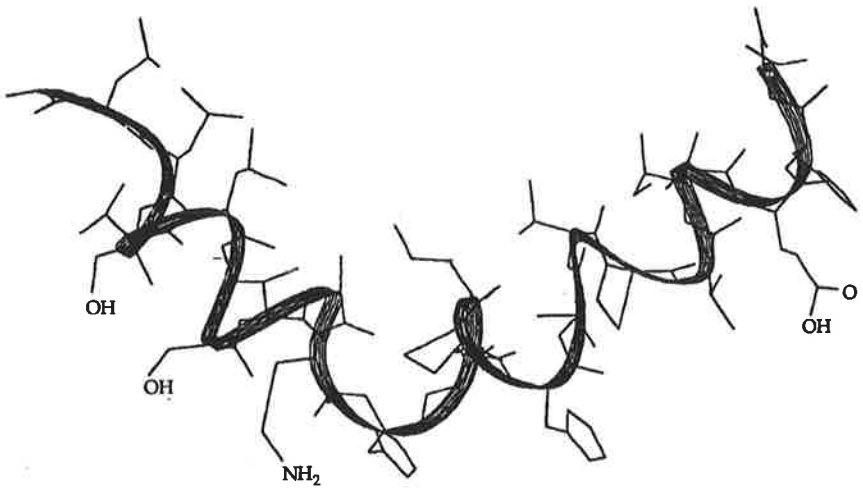

Figure 7.1 Lowest energy structure calculated for caerin 1.1 in TFE/H_2O (1:1 by volume) [97].

Replacing either or both of the proline residues with glycine decreases the activity of the peptide slightly [97]. While glycine residues have an amide proton that can form intramolecular hydrogen bonds, it is a helix-disrupting residue since it has high conformational freedom (Section 4.6g). Thus, the antibacterial activity is reduced but not wiped out completely. These results suggest the hinge region is important for activity.

A number of shortened analogues of caerin 1.1 have been found in secretions together with caerin 1.1. These peptides (e.g. caerin 1.1.1, 1.1.3 and 1.1.5 in Table 7-1) are completely inactive and are presumably the products of enzymatic degradation [23]. Interestingly, caerin 1.1.5 and 1.1.3 are made up of the residues from the first and second helices of caerin 1.1, respectively. This demonstrates that the N- and C-terminal helices of caerin 1.1 are inactive on their own. Thus, it would seem that the flexible hinge region and both helices are necessary for antibacterial activity.

While mixed organic solvents are often used to mimic a membrane environment, there is still dispute over how well they accomplish this (Section 4.7a). It is therefore of interest to know whether the structure of caerin 1.1 found in TFE/H_2O persists in a lipid bilayer. It is thought that micelles provide a more accurate model for a lipid bilayer since they mimic the lipid-water interface. Thus, one of the aims of the present study was to determine the structure of caerin 1.1 in DPC micelles and to compare this structure with that found by Wong *et al.* in TFE/H_2O [97].

The sequence and activity data for caerin 1.4 is also given in Table 7-1. This peptide is identical to caerin 1.1 except that it has serine residues at positions five and seven, replacing the hydrophobic residues valine and glycine, respectively. These substitutions have the effect of decreasing the antibacterial activity against the majority of organisms tested. Interestingly though, caerin 1.4 is active against the G- bacterium *E. coli*, an organism that is not significantly affected by caerin 1.1. In addition, caerin 1.4 has greatly increased activity against *M. luteus*.

Since the differences between the sequences of caerin 1.1 and caerin 1.4 only occur in the first helix, the difference in activity must be due to differences in the structure in this region. Some of the structural parameters for these helices are given in Table 7-1. The overall charge is the same for both peptides and there is very little difference in their hydrophobic moments. The first helix of caerin 1.4 is less hydrophobic, however, than that of caerin 1.1 and the hydrophilic angle (i.e., the angle subtended by the hydrophilic face, Section 3.4f) is much greater for this peptide (160° for caerin 1.4 versus 100° for caerin 1.1). The latter property can be seen more clearly in the Schiffer-Edmundson wheel projections for the first 14 residues of each peptide (Figure 7.2).

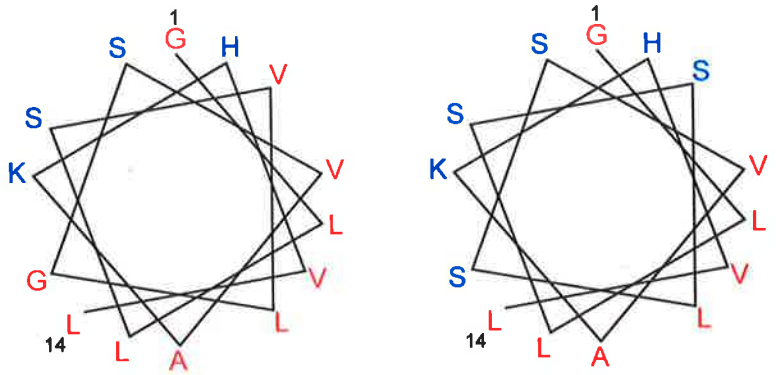

Figure 7.2 Schiffer-Edmundson wheel projections for residues 1-14 of caerin 1.1 and caerin 1.4. Hydrophilic residues are indicated in blue and hydrophobic residues in red [67].

The activity of caerin 1.4 against *E. coli* and *M. luteus* is very similar to that of members of the caerin 2, 3 and 4 peptides, which are narrow-spectrum antibiotics. The structure of caerin 4.1 has been determined in TFE/H_2O by NMR spectroscopy and consists of a helix-bend-helix structure [98] (Figure 7.3). The average angle between the two helices is approximately 35° for this peptide, which is significantly less than that found for caerin 1.1 (~80° [97]). Caerin 4.1 is also amphipathic, with a 160° hydrophilic angle for the residues of the first helix (1-15). The hydrophobicity of this peptide, and that of other members of the caerins 2, 3 and 4 peptides, is negative, indicating these peptides are more hydrophilic than hydrophobic. These results suggest there could be a correlation between hydrophobicity and/or hydrophilic angle and the specificity of these peptides for *E. coli* and *M. luteus*.

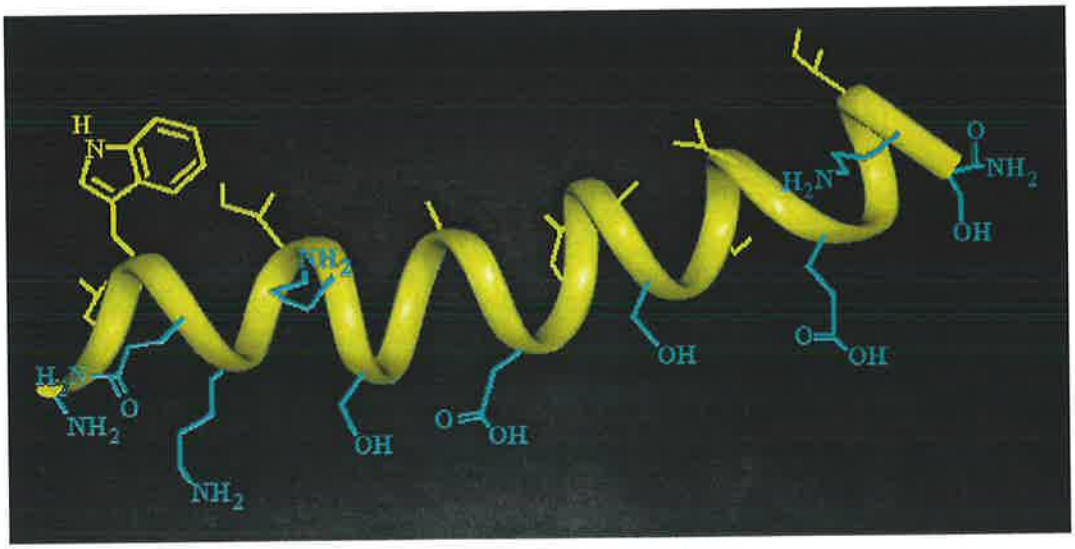

Figure 7.3 Lowest energy structure calculated for caerin 4.1 in TFE/H_2O (1:1 by volume) [98].

Calculation of the hydrophobic moment and the hydrophilic angle assume an ideal α-helical structure is adopted by the peptide. Determining the three-dimensional structure of caerin 1.4 would firstly determine whether it adopts a similar structure to caerin 1.1 and secondly, it would enable the N-terminal halves of caerin 1.4 and caerin 1.1 to be more accurately compared.

The aims of the present study were to:

1) determine the structure of caerin 1.1 in DPC micelles and compare it with the structure determined in TFE/H_2O by Wong *et al.* [97].
2) determine and compare the structure of caerin 1.4 in TFE/H_2O and DPC micelles.
3) compare the structures of caerin 1.1 and caerin 1.4.

7.2 Structure of Caerin 1.1 in DPC Micelles

7.2a NMR Studies - Assignments

NMR spectra were acquired on caerin 1.1 dissolved in DPC micelles (CA11DPC). Proton chemical shifts were assigned using standard methods, as outlined in Section 4.4a. These assignments are illustrated in the partial TOCSY and NOESY spectra shown in Figure 7.4. Note that αH resonances for His12 and His16 were not present, probably because they were saturated by the water resonance. In TFE these resonances were assigned at 4.61 and 4.59 ppm respectively, which is very close to the water resonance (4.64 ppm) [97]. Note also that the cross-peaks for CA11DPC are broader than the corresponding cross-peaks in TFE/H_2O (CA11TFE). This indicates an increase in rotational correlation time, suggesting that the peptide has been incorporated into the micelles [207, 295]. The cross-peaks are sharp enough, however, to be compatible with high-resolution NMR techniques.

α-Carbon resonances were assigned from the HSQC spectrum. The αCs of His12 and His16 could not be assigned as these peaks were obscured by water breakthrough. A summary of the assigned proton and αC resonances is given in Table 7-2.

Attempts were made to obtain HMBC spectra suitable for assigning the C′ ^{13}C resonances, however the only peaks found in the C′ region were due to the βHs of the two alanine residues. This may be a result of peak broadening, which decreases the signal-to-noise ratio. Presumably, these peaks were evident above the signal-to-noise because they were each due to three protons. The Ala10 and Ala22 C′ resonances were assigned as 177.9 and 178.9 ppm respectively.

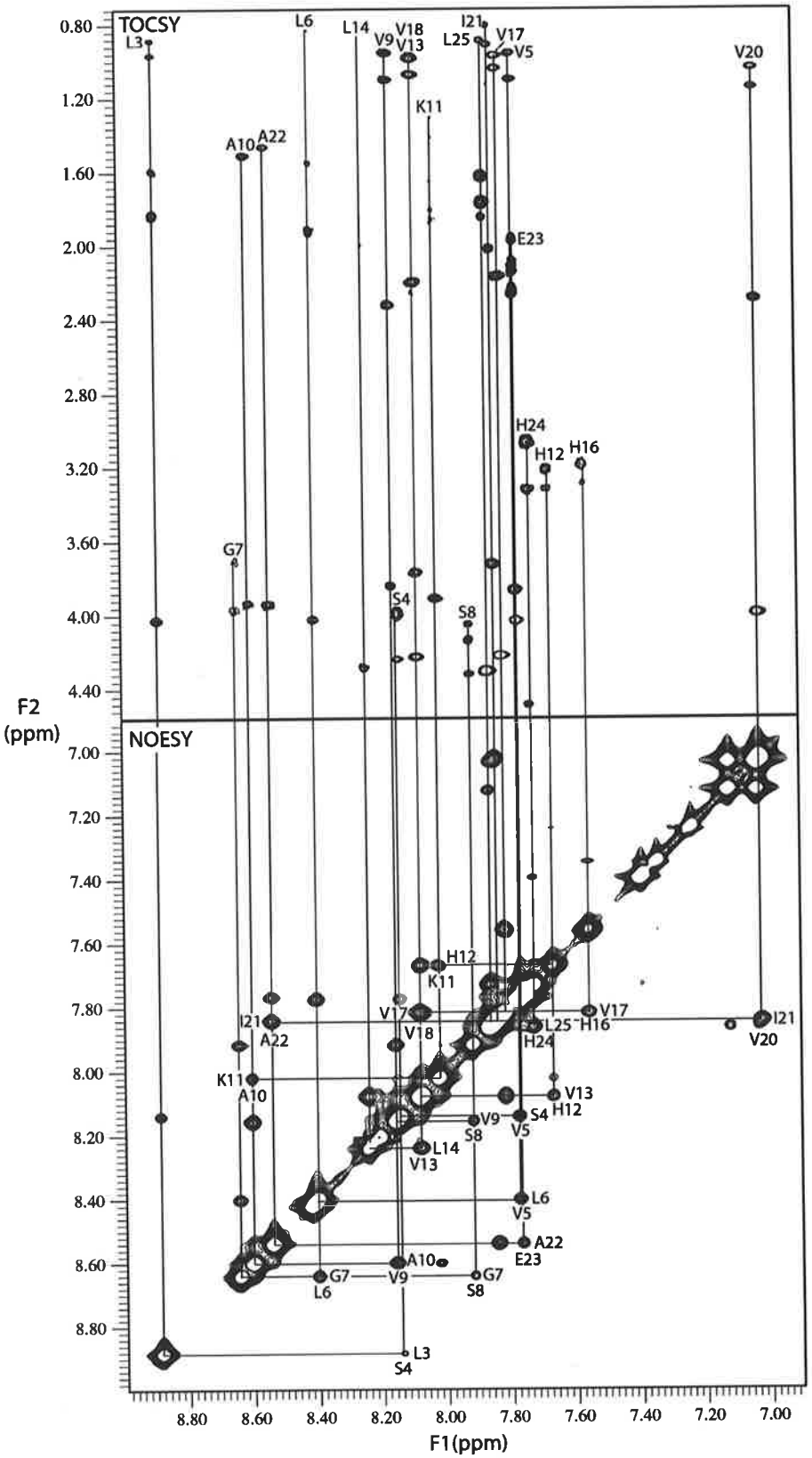

Figure 7.4 Partial NOESY (mixing time = 100 ms) and TOCSY (70 ms spin-lock time) spectra of caerin 1.1 in DPC micelles at pH 6.07, 37°C. Vertical lines connect the resonances in each spin system. These are labelled with the standard single-letter abbreviation for the residue type and a number indicating the sequential position of the residue. NOEs between sequential NH protons are indicated in the NOESY spectrum.

Table 7-2 ^{1}H and ^{13}C-NMR chemical shifts (ppm) for caerin 1.1 in dodecylphosphatidylcholine micelles, pH 6.07, 37°C. Assignments for all the ^{1}H resonances are tabulated whereas only the αC ^{13}C chemical shifts are listed; n.o., not observed.

Residue	Chemical shift of				
	NH	α-CH	β-CH	Others	α-^{13}C
	ppm				
Gly1	n.o.	4.05, 3.89			n.o.
Leu2	n.o.	4.04	1.77, 1.69	γ–CH 1.67 δ–CH_3 0.98, 93	57.9
Leu3	8.88	4.03	1.83	γ–CH 1.60 δ–CH_3 0.97, 0.89	57.8
Ser4	8.14	4.24	4.01, 3.98		61
Val5	7.77	3.87	2.27	γ–CH_3 1.10, 0.96	65.6
Leu6	8.40	4.02	1.93, 1.90	γ–CH 1.56 δ–CH_3 0.88, 0.84	57.8
Gly7	8.64	3.98, 3.70			n.o.
Ser8	7.92	4.32	4.14, 4.05		61.4
Val9	8.16	3.85	2.32	γ–CH_3 1.10, 0.96	65.6
Ala10	8.60	3.93	1.51		55.1
Lys11	8.02	3.91	1.86, 1.80	γ–CH_2 1.40, 1.32 δ–CH_2 1.65 ε–CH_2 2.89 NH_3^+ n.o.	58.8
His12	7.67	n.o.	3.32, 3.22	H2 8.22 H4 7.24	n.o.
Val13	8.08	4.23	2.20	γ–CH_3 1.08, 0.99	63.1
Leu14	8.24	4.29	2.01, 1.85	γ–CH 1.57 δ–CH_3 0.92, 0.86	58.6
Pro15	–	4.25	2.30, 1.41	γ–CH_2 2.01, 1.88 δ–CH_2 3.67, 3.36	65.2
His16	7.56	n.o.	3.29, 3.18	H2 8.21 H4 7.35	n.o.
Val17	7.82	4.22	2.17	γ–CH_3 1.04, 0.97	63.7
Val18	8.08	3.77	2.26	γ–CH 1.08, 0.97	67.8
Pro19	–	4.35	2.40, 1.88	γ–CH_2 2.15, 1.98 δ–CH_2 3.61, 3.51	65.4
Val20	7.03	3.99	2.30	γ–CH_3 1.15, 1.04	64.6
Ile21	7.84	3.72	2.02	γ–CH_2 1.75, 1.12 γ–CH_3 0.91 δ–CH_3 0.81	64.4
Ala22	8.54	3.94	1.46		54.9
Glu23	7.77	4.03	2.11, 1.97	γ–CH_2 2.23	57.9
His24	7.73	4.48	3.32, 3.07	H2 8.43 H4 7.40	57.4
Leu25	7.86	4.3	1.85, 1.77	γ–CH 1.63 δ–CH_3 0.89 $CONH_2$ 7.12, 7.04	54.8

7.2b Secondary Shifts

αH and αC secondary shifts (i.e., the chemical shift difference from random coil values, Δδs), smoothed over a window of n = ±2 residues, were plotted against the sequence for CA11DPC (Figure 7.5). The corresponding values for CA11TFE, taken from Wong *et al* [97], were also plotted for comparison.

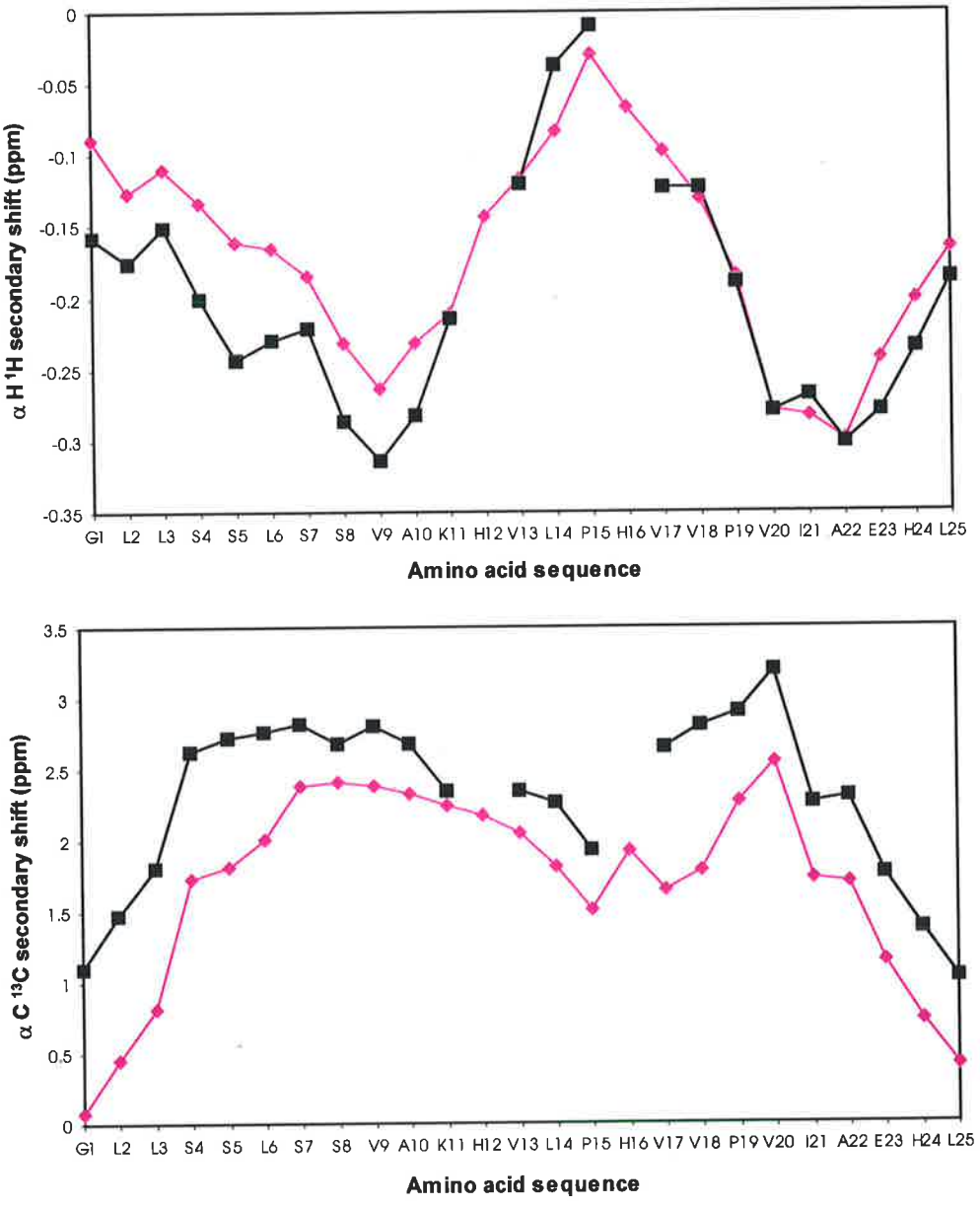

Figure 7.5 (a) αH ^{1}H and (b) αC ^{13}C secondary shifts of caerin 1.1 in (♦) TFE/H_2O (1:1 by volume) [97] and (■) DPC micelles. Negative values indicate an upfield shift from the random coil value, while positive values indicate a downfield shift. Secondary shifts were smoothed over a window of n = ±2 residues [246].

Figure 7.5 shows distinct upfield shifts for the αH resonances and downfield shifts for αC resonances over the majority of the peptide, consistent with α-helical structure. The exception to this is in the vicinity of Pro15 and the N and C-termini. In these regions, the resonances are random-coil like, suggesting the peptide is more flexible. The shape of the Δδ plots of CA11DPC were similar to those determined for CA11TFE (Figure 7.5), indicating similar structures are formed in both media.

7.2c Amide Secondary Shifts

A plot of the unsmoothed NH Δδ values is shown in Figure 7.6, revealing a 3-4 residue periodic variation. In general, the resonances from the hydrophobic residues are further downfield than those from the hydrophilic residues - a pattern that is characteristic of amphipathic α-helices [245]. The periodic variation is believed to be due to differences in the length of hydrogen bonds on either side of the helix, resulting in slight curvature along the length of the helix [245, 248]. Once again, the plot for CA11TFE is very similar to that for CA11DPC, indicating the peptide forms similar structures in each medium.

There is also a general trend for the NH Δδ values to decrease as we move along the sequence, such that the Δδs at the N-terminal are more upfield than those at the C-terminal. This is consistent with α-helical structure, since the presence of a helix dipole has been observed to affect NH chemical shifts this way [244].

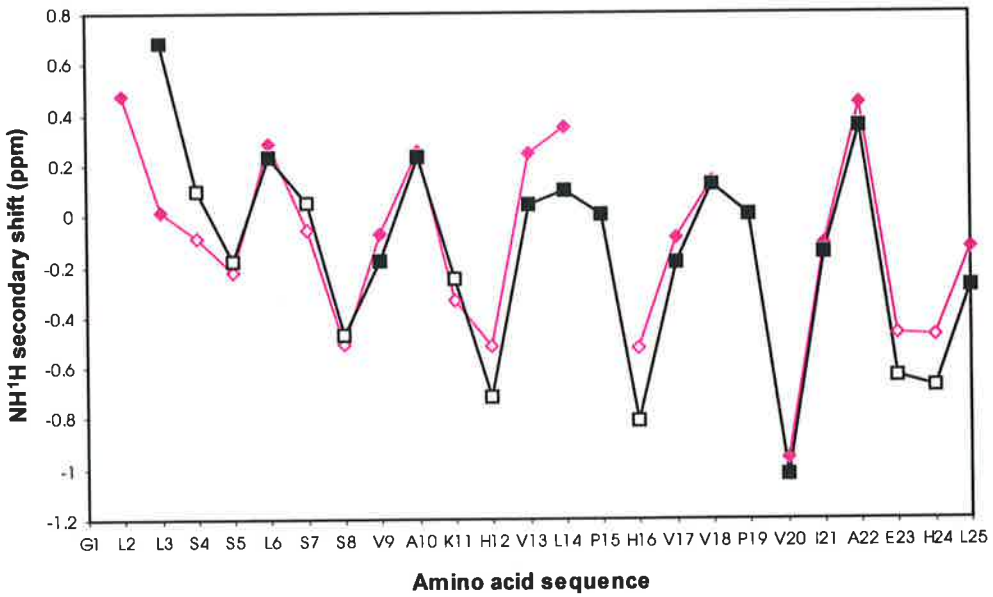

Figure 7.6 NH ^{1}H secondary shifts of caerin 1.1 in (♦) TFE/H_2O (1:1 by volume) [97] and (■) DPC micelles. Negative values indicate an upfield shift from the random coil value while positive values indicate a downfield shift. Secondary shifts were not smoothed. Hydrophilic residues [67] are indicated by open symbols.

7.2d NOE Connectivities

A summary of the diagnostic NOE connectivities found for CA11DPC is shown below in Figure 7.7. The d_{NN} NOEs seen in Figure 7.4 are shown here, together with the weaker $d_{NN(i,i+2)}$ NOEs that were found at a lower contour level. Sequential $d_{\alpha N}$ NOEs occurred throughout the sequence, as did the medium-range $d_{\alpha N(i,i+3)}$, $d_{\alpha\beta(i,i+3)}$ and $d_{\alpha N(i,i+4)}$ NOEs. There was some disruption of the NOE patterns in the central region of the peptide, primarily due to the absence of αH resonances for His12 and His16. As a whole, these NOE connectivities indicate that helical structure is present along the majority of the peptide.

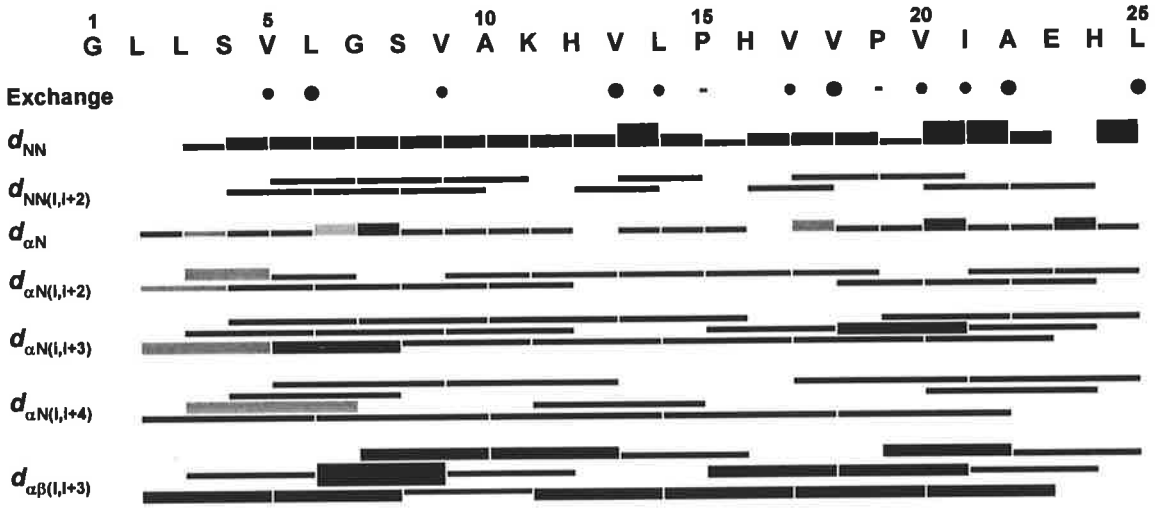

Figure 7.7 A summary of NOEs used in structure calculations for caerin 1.1 in DPC micelles. The thickness of the bars indicates the relative strength of the NOEs (strong < 3.1 Å, medium 3.1-3.7 Å or weak > 3.7 Å). Grey shaded boxes represent NOEs that could not be unambiguously assigned. Relative rates of amide exchange at pH 2.7 are indicated by small (≥ 2 h) and large circles (≥ 5 h). Exchange was complete in less than 2 h for the unmarked residues (no circle).

7.2e Amide Exchange

Relative NH exchange rates were measured for caerin 1.1 and are indicated in Figure 7.7. The pH was lowered to 2.7 for these experiments in order to slow exchange to measurable rates [242] (Section 4.5d)†. Even so, almost half of the NHs had exchanged within two hours. Eleven NHs remained after this time (Val5, Val9, Val13, Leu14, Val17, Val18, Val20, Ile21, Ala22 and Leu25) and five of these (Leu6, Val13, Val18, Ala22, Leu25) remained after a further three hours. Interestingly, all of these slowly exchanging NHs were from hydrophobic residues, indicating that these protons were in a hydrophobic environment from which water was excluded. Conversely, the hydrophilic NHs exchanged quickly suggesting they were in frequent contact with water molecules. Micelles are dynamic species so the peptide would be expected to be in equilibrium between the micelle and the surrounding water [215, 295]. However, caerin 1.1 is poorly soluble in water so the equilibrium would be expected to favour the micelle-bound form. The NH exchange results suggest that, on average, caerin 1.1 is located on the surface of the micelle, with the hydrophilic residues in contact with the lipid head-groups and the water phase, and the hydrophobic residues buried in the hydrophobic core.

† experiments conducted at pH 6 showed that exchange was too rapid to gain useful information.

7.2f Structure Calculations

The NOESY spectrum of CA11DPC (mixing time = 100 ms) was fully assigned and the volumes of the cross-peaks converted to distance restraints using the method of Xu *et al.* [266]. A total of 495 non-redundant restraints were produced. Thirty-four of these distance restraints were ambiguous. A full breakdown of the restraints is given in Table 7-3. The number of restraints found was more than double the number determined for CA11TFE.

RMD and dynamical SA procedures generated sixty structures and the ten structures† of lowest potential energy were chosen for analysis. These ten structures had only minor deviations from idealised covalent geometry (≤ 0.05Å for bonds and ≤ 5° for angles and impropers) and the maximum violation was 0.49 Å. Table 7-3 shows the X-PLOR energies for these structures.

Table 7-3 Comparison of the number of experimental restraints used for caerin 1.1 in DPC micelles (CA11DPC) and caerin 1.1 in trifluoroethanol/H_2O (CA11TFE)[a]. The final X-PLOR energies (kcal·mol^{-1}) and violation statistics for the 10 calculated structures of lowest energy are also given.

No. of experimental restraints	**CA11DPC**		**CA11TFE[a]**
Sequential NOEs	153		59
Medium-range NOEs	153		34
Long-range NOEs	0		0
Intra-residue NOEs	155		138
Ambiguous NOEs	34		0
Total	495		231
X-PLOR energies (kcal·mol^{-1})	**<SA>[b]**	**$(SA)_r$[c]**	
E_{tot}	184.02 ± 11.36	153.6	
E_{bond}	12.93 ± 1.03	11.72	
E_{angle}	57.49 ± 2.09	48.98	
$E_{improper}$	7.16 ± 0.52	4.98	
E_{vdw}	21.03 ± 2.04	17.24	
E_{NOE}	85.42 ± 8.01	70.71	
Violations			
No. of NOEs violated > 0.3 Å	10		
Maximum violation (Å)	0.49		

[a] Data obtained from Wong *et al.* [97].
[b] <SA> is the ensemble of the final 10 structures.
[c] (SA) is the mean structure obtained by best-fitting and averaging the coordinates of the well-defined backbone atoms (N, αC and C') of the 10 final structures. $(SA)_r$ is the structure obtained after restrained energy minimisation of the mean structure.

† 10 structures were chosen to be consistent with Wong et al. [97]. RMSD values were similar when 20 structures were used and the structures were comparable.

The most energetically stable of the 10 calculated structures is shown in Figure 7.8. This representation shows that caerin 1.1 forms an amphipathic α-helical structure along the length of the peptide, with a distinct bend between residues His12 and His16. Thus, the bend encompasses Pro15, which is not surprising since proline residues lack an NH proton and therefore disrupt the hydrogen bonding pattern of the helix [210]. Pro19, on the other hand, occurs at the start of the second helix so the absence of an NH proton has little effect. The helix-bend-helix motif is also present for the other 9 structures.

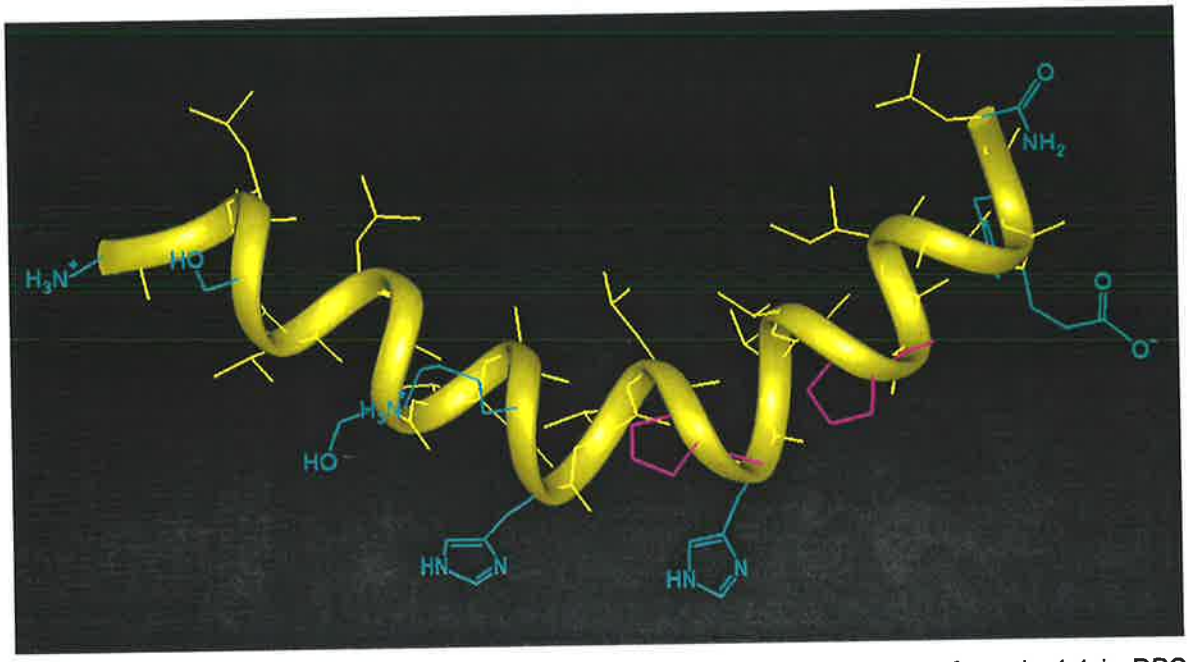

Figure 7.8 Side view of the most stable structure (lowest potential energy) of caerin 1.1 in DPC micelles. The hydrophilic groups are shown in blue and proline residues in pink.

Some conformational variability is evident for the hinge region, as was found for this peptide in TFE/H_2O. The superimposition of the 10 lowest energy structures over the backbone atoms (N, αC and C′) of the well-defined residues reveals a RMSD of 0.46 Å from the average structure. Overlaying these structures over residues 3-12, as in Figure 7.9 (a), shows that these residues form a well-defined α-helix. The RMSD from the average structure for these residues is reduced to 0.24 Å. Similarly, the superimposition of the structures over residues 17-24 (Figure 7.1 (b)) indicates these residues also form a regular α-helix with RMSD of 0.09 Å. These figures also reveal variability around the bend region. A summary of the RMSD values is given in Table 7-4.

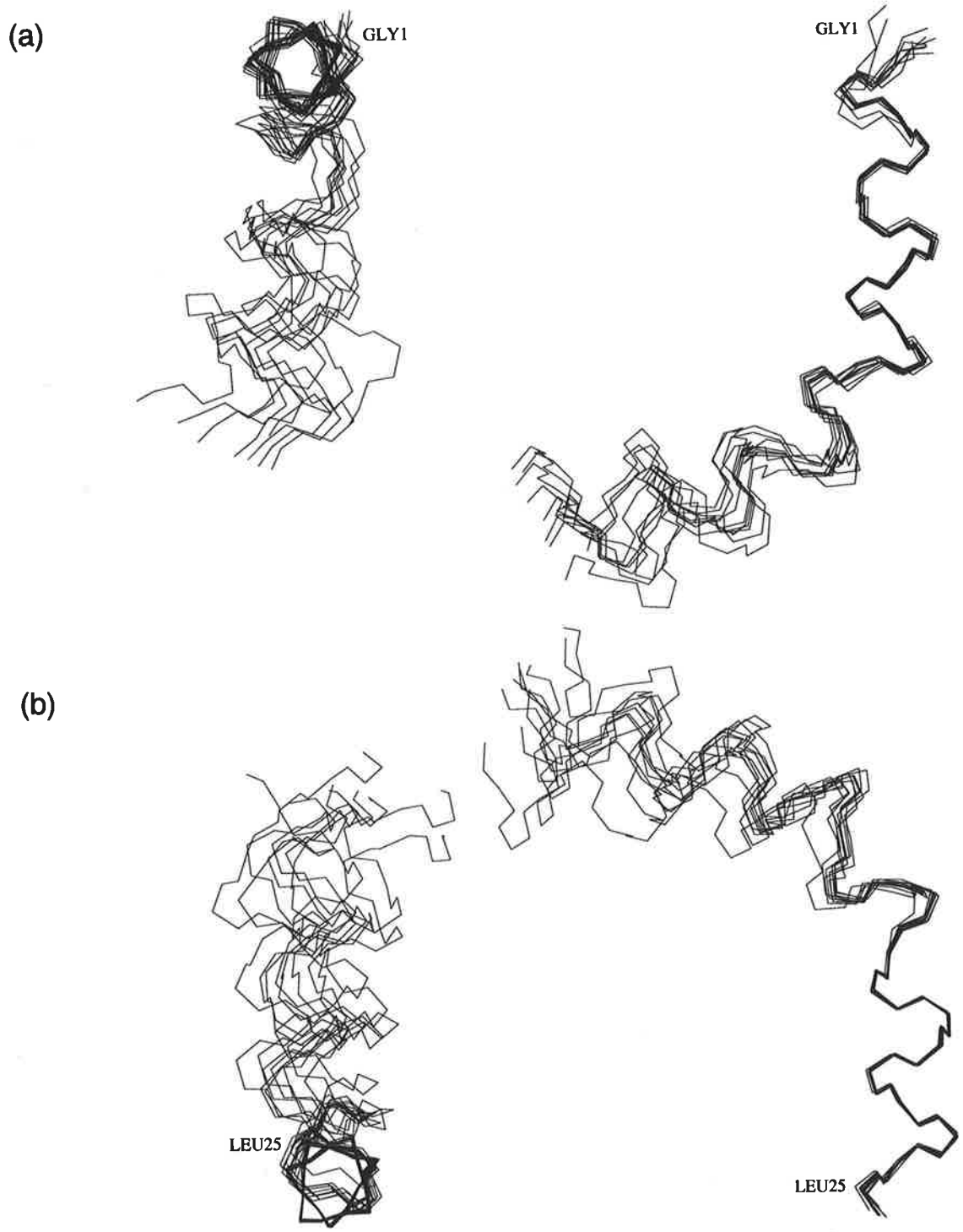

Figure 7.9 The 10 most stable calculated structures of caerin 1.1 in DPC micelles, superimposed along the backbone atoms (N, αC and C') of residues (a) 3-12 and (b) 17-24. The structures are viewed down the centre of the helices (left) or from the side (right). This picture was prepared using the program MOLMOL [346].

Table 7-4 Comparison of the root mean squared deviation (RMSD, Å) values for the 10 lowest energy structures of caerin 1.1 in DPC micelles (CA11DPC) and caerin 1.1 in trifluoroethanol/H_2O (CA11TFE)[a].

	RMSD from mean geometry (Å)	
Structures	**Backbone atoms**	**Heavy atoms**
CA11DPC (all)	0.64 ± 0.22	0.90 ± 0.20
CA11DPC (well-defined residues 3-24)	0.46 ± 0.18	0.79 ± 0.19
CA11DPC (residues 3-12)	0.24 ± 0.15	0.65 ± 0.27
CA11DPC (residues 17-24)	0.09 ± 0.03	0.45 ± 0.09
CA11TFE (residues 2-11)		0.86 ± 0.48[a]
CA11TFE (residues 17-24)		0.69 ± 0.37[a]

[a] Data obtained from Wong *et al.* [97].

The average bend angle between the two helices was calculated as 75.2° ± 7.4° with a maximum angle of 88° and a minimum of 63°. No value was given for this angle for CA11TFE, however the angle for the representative structure given by Wong *et al.* [97] was 82°.

Analysis of the angular order parameters (S, ϕ and ψ) for the 10 structures shows that all residues were well-defined (S >0.9 for both their ϕ and ψ angles) with the exception of Leu2 and the N- and C- terminal residues (Gly1 and Leu25).

A Ramachandran plot of the average ϕ and ψ angles for the well-defined residues shows that 90% of residues are distributed within the favoured region for α-helical structure, with the remaining 10% falling in the allowable region (Val13 and Val17) (Figure 7.10). The well-defined residues include those in the bend region. The Ramachandran plot shows that their ϕ and ψ dihedral angles are also consistent with helical structure.

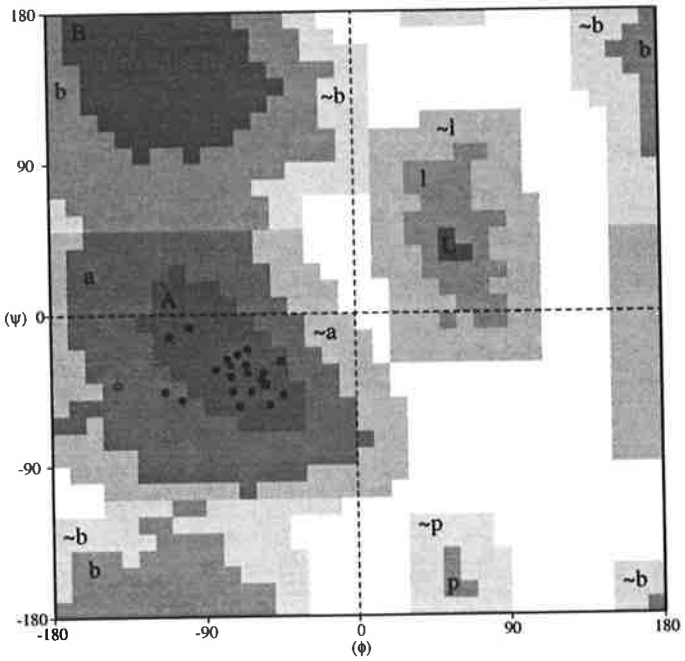

Figure 7.10 Ramachandran plot of caerin 1.1 in DPC micelles showing that 90% of the residues fall in the favourable region for α-helices (A). The remaining 10% fall in the allowable region (a). The generous region for α-helices is labelled '~a'. Glycine residues are indicated by triangles, prolines by squares and the remainder by circles. Open symbols indicate residues that are not well-defined.

7.3 Caerin 1.4

7.3a Circular Dichroism Studies

CD spectra were recorded for caerin 1.4 in mixtures of TFE and water (0-50% by volume) (Figure 7.11). A broad trough around 200 nm was observed for 0-10% TFE, indicating the peptide was unstructured. For 20-50% TFE, two minima appeared around 208 nm (π-π^*) and 222 nm, consistent with α-helical structure. These minima were at their lowest values (greatest ellipticity) at 50% TFE in water, indicating maximal helical conformation had been attained.

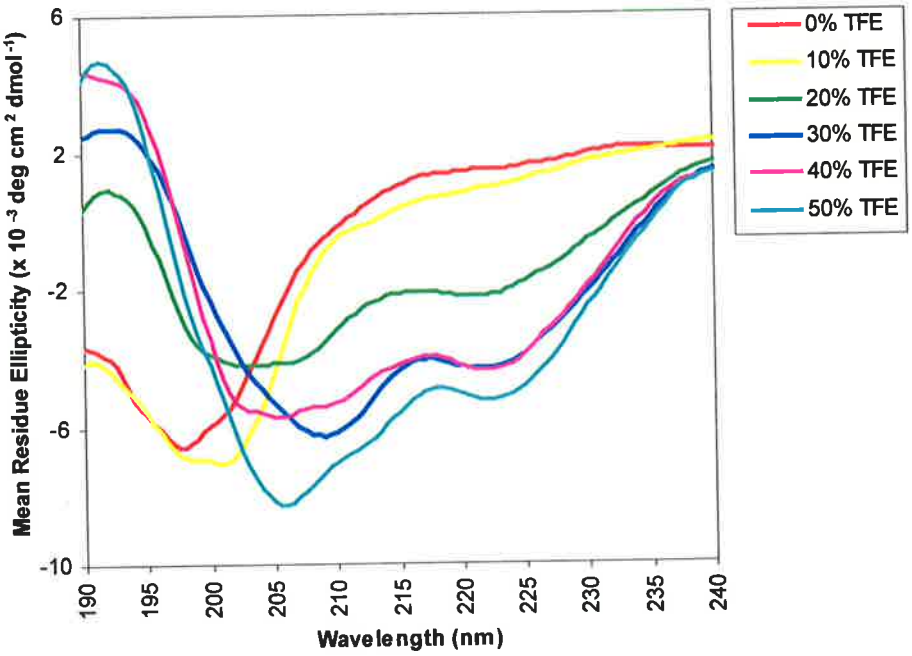

Figure 7.11 CD spectra of caerin 1.4 at the varying concentrations of TFE (by volume) indicated.

7.3b NMR Studies – Assignments

NMR spectra were acquired for samples of caerin 1.4 in 50% TFE/H_2O (CA14TFE) and in DPC micelles (CA14DPC). The ^1H chemical shifts were assigned using the standard methods described in Section 4.4a, and these assignments are indicated in the partial TOCSY and NOESY spectra shown in Figures 7.12 and 7.13. The peaks for CA14DPC are noticeably broader than those for the same peptide in TFE/H_2O. This observation can

be attributed to the slower tumbling rate (longer correlation time) of the peptide-micelle complex, compared with the peptide alone. However, the cross-peaks are still sharp enough for high-resolution NMR studies to be carried out.

αC and C′ ^{13}C resonances were assigned from HSQC and HMBC spectra respectively. However, low signal-to-noise in the HMBC spectra limited the C′ assignments that could be made. Fifteen C′ resonances were assigned for CA14TFE, while only two could be assigned for CA14DPC, probably because of increased linewidth for the peptide in micelles. In the latter sample, the cross-peaks from the βHs of Ala10 and Ala22 to their C′ carbons were present because they each originated from three protons and were therefore intense enough to be seen over the signal-to-noise. These resonances were at 178.3 and 179.1 ppm respectively. Summaries of the assigned ^{1}H and ^{13}C resonances are given in Tables 7-5 and 7-6.†

† NMR spectra for the DPC sample were acquired at pH 6, 37°C, to simulate physiological conditions more closely. There are no ionisable groups (between pH 3 and 6) for this peptide so the structures formed at pH 6 should be comparable to those formed at pH 3.

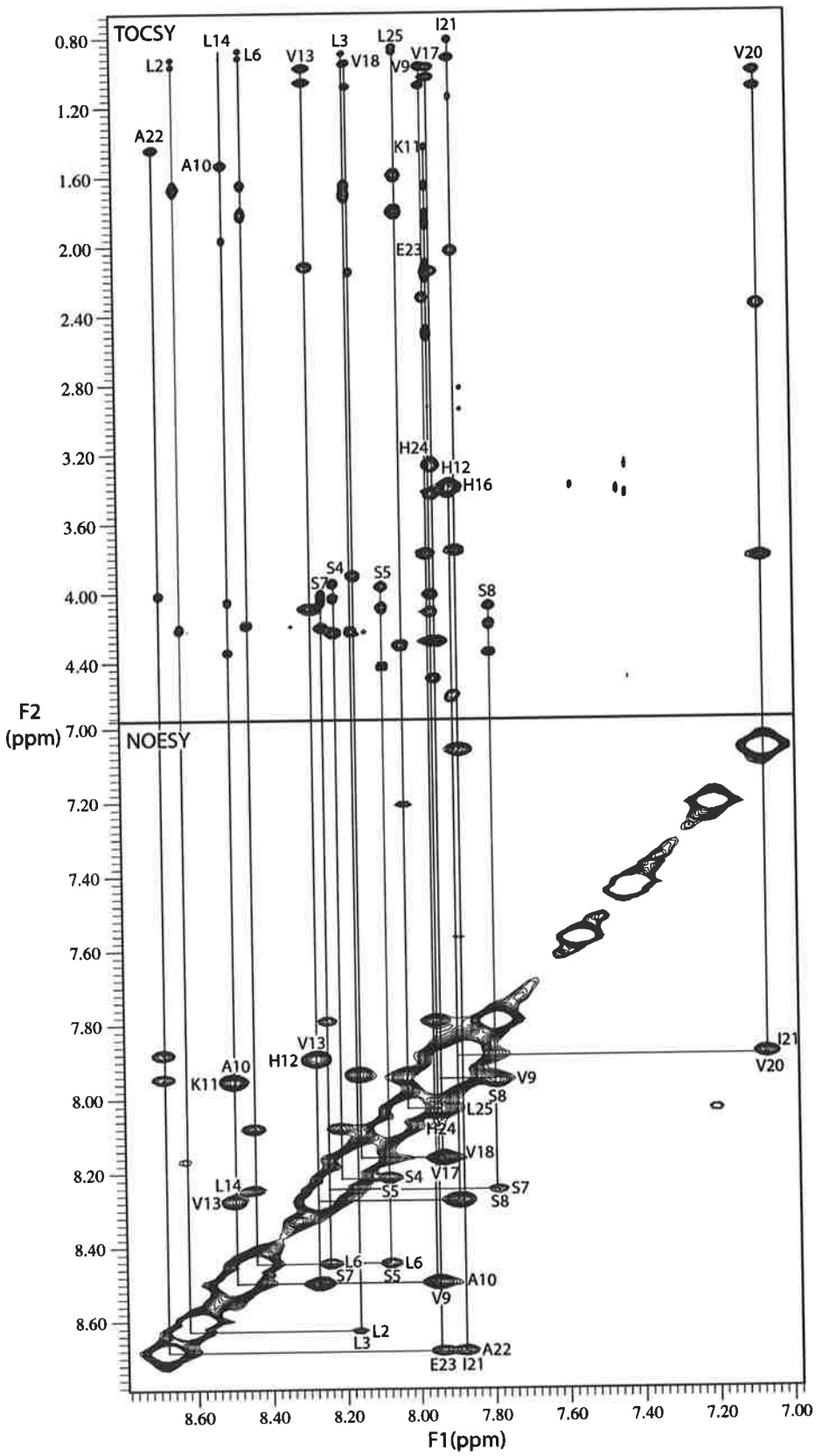

Figure 7.12 Partial NOESY (mixing time = 150 ms) and TOCSY (70 ms spin-lock time) spectra of caerin 1.4 in TFE/H_2O (1:1 by volume) at pH 3.13, 25°C. Vertical lines connect the resonances in each spin system. These are labelled with the standard single-letter abbreviation for the residue type and a number indicating the sequential position of the residue. NOEs between sequential NH protons are indicated in the NOESY spectrum.

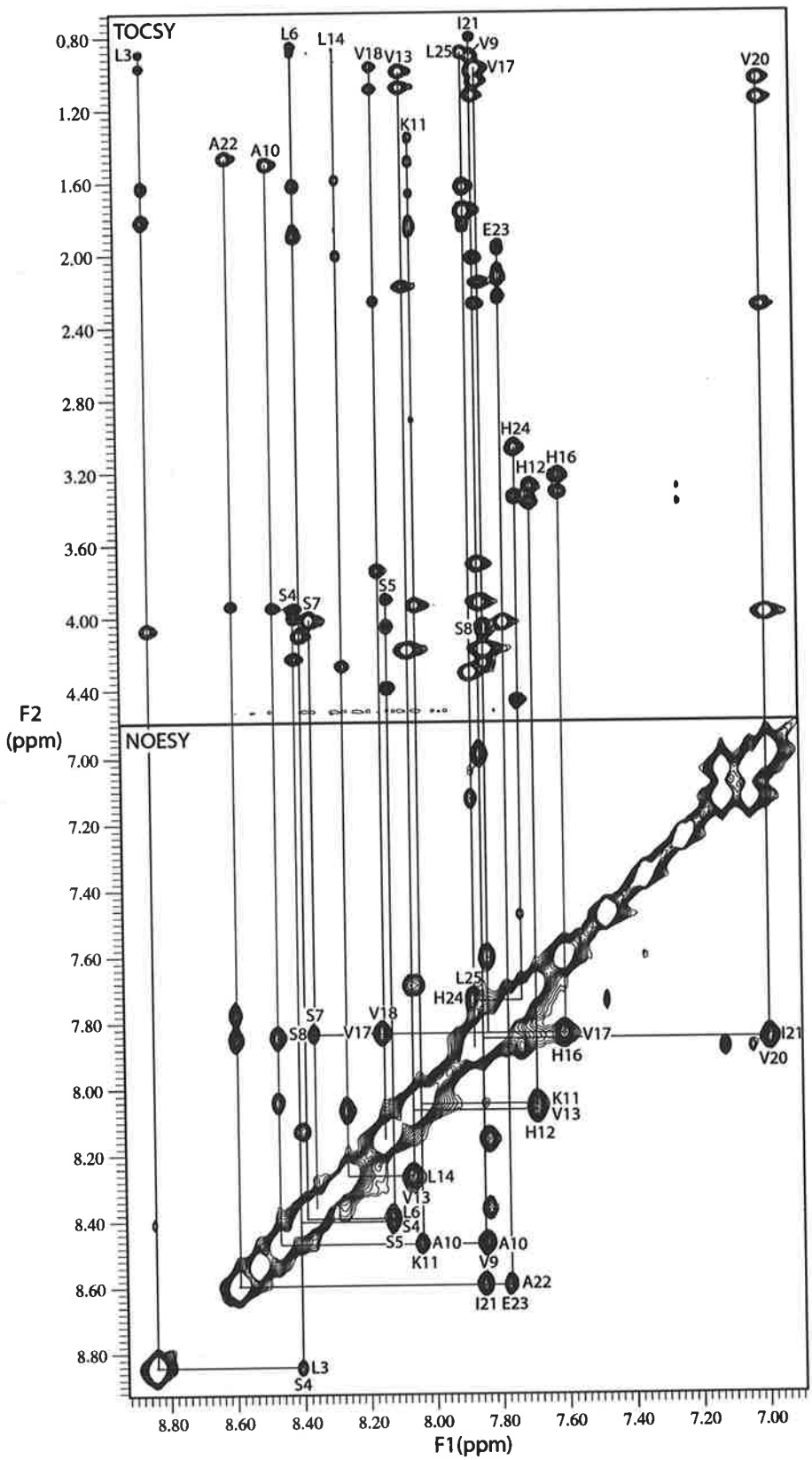

Figure 7.13 Partial NOESY (mixing time = 80 ms) and TOCSY (70 ms spin-lock time) spectra of caerin 1.4 in DPC micelles at pH 5.97, 37°C. Vertical lines connect the resonances in each spin system. These are labelled with the standard single-letter abbreviation for the residue type and a number indicating the sequential position of the residue. NOEs between sequential NH protons are indicated in the NOESY spectrum.

Table 7-5 ^{1}H and ^{13}C-NMR chemical shifts for caerin 1.4 in trifluoroethanol/H_2O (1:1, by volume) pH 3.13, 25°C. Assignments for all the ^{1}H resonances are tabulated, whereas only the αC and C' ^{13}C chemical shifts are listed; n.o., not observed.

Residue	Chemical shift (ppm)					
	NH	α-CH	β-CH	Others	α-^{13}C	$^{13}C'$
Gly1	n.o.	3.98, 3.88			42.2	165.5
Leu2	8.63	4.21	1.68	γ–CH 1.66 δ–CH_3 0.97, 0.93	56.8	176.6
Leu3	8.17	4.23	1.70	γ–CH 1.67 δ–CH_3 0.98, 0.90	56.5	178.1
Ser4	8.22	4.23	4.03, 3.95		59.9	175.5
Ser5	8.08	4.43	4.09, 3.97		60.5	174.4
Leu6	8.44	4.19	1.82	γ–CH 1.66 δ–CH_3 0.92, 0.88	56.8	
Ser7	8.25	4.20	4.05, 4.02		60.4	174.8
Ser8	7.80	4.34	4.19, 4.08		60.7	175.5
Val9	7.95	3.78	2.31	γ–CH_3 1.08, 0.98	65.7	n.o.
Ala10	8.49	4.05	1.54		54.8	178.0
Lys11	7.95	4.01	1.88, 1.81	γ–CH_2 1.44 δ–CH_2 1.67 ε–CH_2 2.94 NH_3^+ 7.56	57.8	n.o.
His12	7.90	4.62	3.42	H2 8.59 H4 7.45	56.8	174.2
Val13	8.27	4.09	2.13	γ–CH_3 1.07, 0.98	64.2	n.o.
Leu14	8.50	4.34	1.97, 1.85	γ–CH 1.53 δ–CH_3 0.92, 0.89	58.2	n.o.
Pro15	–	4.28	2.27, 1.42	γ–CH_2 2.04, 1.89 δ–CH_2 3.73, 3.33	65.0	n.o.
His16	7.89	4.59	3.39	H2 8.60 H4 7.58	55.4	173.5
Val17	7.94	4.28	2.15	γ–CH_3 1.04, 0.98	62.5	n.o.
Val18	8.16	3.90	2.15	γ–CH 1.09, 0.96	66.3	n.o.
Pro19	–	4.27	2.34, 1.80	γ–CH_2 2.15, 1.93 δ–CH_2 3.67, 3.47	65	n.o.
Val20	7.07	3.81	2.36	γ–CH_3 1.11, 1.01	64.6	177.6
Ile21	7.88	3.76	2.04	γ–CH_2 1.66, 1.15 γ–CH_3 0.93 δ–CH_3 0.82	63.9	n.o.
Ala22	8.68	4.01	1.45		54.2	178.8
Glu23	7.95	4.11	2.18, 2.12	γ–CH_2 2.51	56.6	176
His24	7.94	4.50	3.44, 3.27	H2 8.47 H4 7.43	56.6	173.6
Leu25	8.03	4.31	1.81	γ–CH 1.60 δ–CH_3 0.89, 0.87 $CONH_2$ 7.21, 6.80	54.7	179

Table 7-6 ^{1}H and ^{13}C-NMR chemical shifts for caerin 1.4 in dodecylphosphatidylcholine micelles, pH 5.97, 37°C. Assignments for all the ^{1}H resonances are tabulated, whereas only the αC ^{13}C chemical shifts are listed; n.o., not observed.

Residue	Chemical shift (ppm)				
	NH	α-CH	β-CH	Others	α-^{13}CH
Gly1	n.o.	4.03, 3.92			43.0
Leu2	n.o.	4.12	1.80	γ–CH 1.71 δ–CH_3 0.94	57.9
Leu3	8.84	4.07	1.82	γ–CH 1.64 δ–CH_3 0.97, 0.89	57.7
Ser4	8.41	4.24	4.01, 3.96		60.9
Ser5	8.13	4.42	4.01, 3.91		61.4
Leu6	8.39	4.11	1.90, 1.87	γ–CH 1.63 δ–CH_3 0.90, 0.86	57.1
Ser7	8.36	4.03	4.03, 4.01		61.6
Ser8	7.84	4.27	4.10, 4.06		61.1
Val9	7.85	3.93	2.28	γ–CH_3 1.13, 1.00	65.1
Ala10	8.47	3.95	1.51		54.9
Lys11	8.04	3.95	1.88, 1.82	γ–CH_2 1.50, 1.37 δ–CH_2 1.67 ε–CH_2 2.92 NH_3^+ 7.25	58.8
His12	7.70	n.o.	3.37, 3.29	H2 8.30 H4 7.25	n.o.
Val13	8.07	4.19	2.18	γ–CH_3 1.09, 1.00	63.7
Leu14	8.26	4.29	2.01, 1.86	γ–CH 1.59 δ–CH_3 0.94, 0.87	58.6
Pro15	–	4.29	2.32, 1.44	γ–CH_2 2.00, 1.90 δ–CH_2 3.67, 3.37	65.1
His16	7.61	n.o.	3.32, 3.23	H2 8.32 H4 7.36	n.o.
Val17	7.84	4.19	2.16	γ–CH_3 1.06, 0.98	63.1
Val18	8.15	3.75	2.26	γ–CH 1.09, 0.97	68.1
Pro19	–	4.36	2.39, 1.87	γ–CH_2 2.15, 1.99 δ–CH_2 3.61, 3.49	65.3
Val20	7.00	3.99	2.30	γ–CH_3 1.15, 1.05	64.6
Ile21	7.85	3.71	2.03	γ–CH_2 1.76, 1.12 γ–CH_3 0.92 δ–CH_3 0.81	64.4
Ala22	8.59	3.94	1.47		54.9
Glu23	7.78	4.04	2.11, 1.97	γ–CH_2 2.23, 2.15	57.8
His24	7.74	4.50	3.34, 3.08	H2 8.53 H4 7.48	57.2
Leu25	7.88	4.32	1.85, 1.77	γ–CH 1.63 δ–CH_3 0.89 $CONH_2$ 7.13, 7.05	54.8

7.3c Secondary Shifts

αH and αC secondary shifts (i.e., the chemical shift difference from random coil values, Δδ), smoothed over a window of n = ±2 residues, were plotted against sequence for CA14TFE and CA14DPC (Figure 7.14).

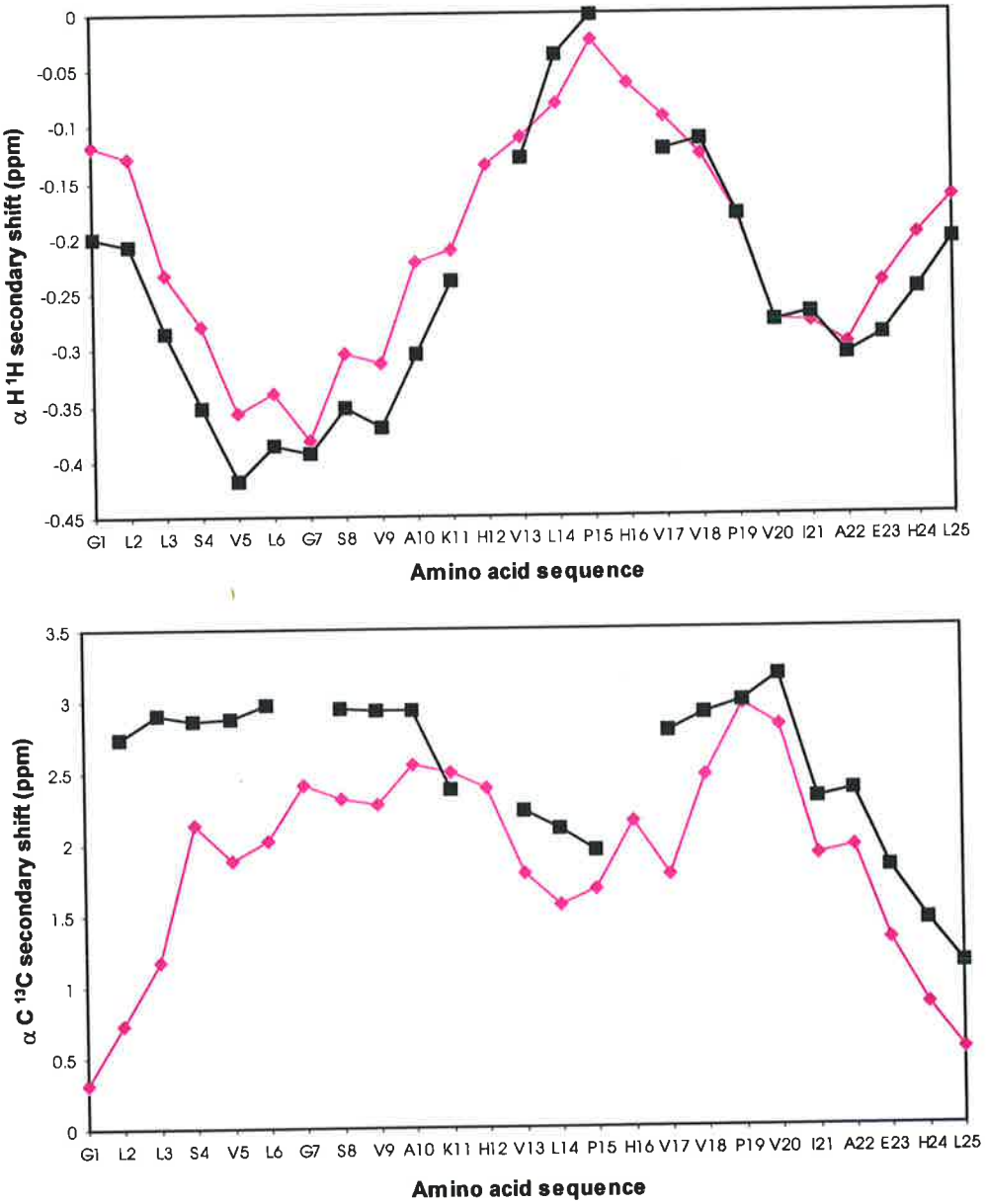

Figure 7.14 (a) αH ^{1}H and (b) αC ^{13}C secondary shifts of caerin 1.4 in (♦) TFE/H_2O (1:1 by volume) and (■) DPC micelles. Negative values indicate an upfield shift from the random coil value, while positive values indicate a downfield shift. Secondary shifts were smoothed over a window of n = ±2 residues [246].

Figure 7.14 shows distinct upfield shifts for the αH resonances and downfield shifts for the αC resonances over the majority of the peptide, in both media types, consistent with α-helical structure. The regions around Pro15 and the N- and C-termini have more random-coil like shifts however, suggesting these regions have more flexibility. The Δδ plots for CA14DPC and CA14TFE are very similar, indicating similar structures are formed in each medium. In addition, these plots have similar shapes to those determined for caerin 1.1 in both of these media (Section 7.2b), suggesting that caerin 1.4 also forms a helix-bend-helix type structure.

7.3d Amide Secondary Shifts

Figure 7.15 shows plots of the unsmoothed NH Δδ values for caerin 1.4 in TFE/H_2O and in DPC micelles. These plots reveal a 3-4 residue periodic variation in the NH Δδ values and, in general, the resonances from the hydrophobic residues are further downfield than those from the hydrophilic residues. This pattern is consistent with an amphipathic α-helical structure [245]. The plot for caerin 1.4 in TFE/H_2O is very similar to that for the peptide in micelles, indicating the peptide adopts a similar structure in each medium.

The presence of a helix dipole has been observed to influence NH chemical shifts, such that those at the N-terminal of the helix are further upfield than those at the C-terminal [244]. Such a trend can be seen for the NH Δδ values of caerin 1.4, which decrease along the sequence, consistent with α-helical structure.

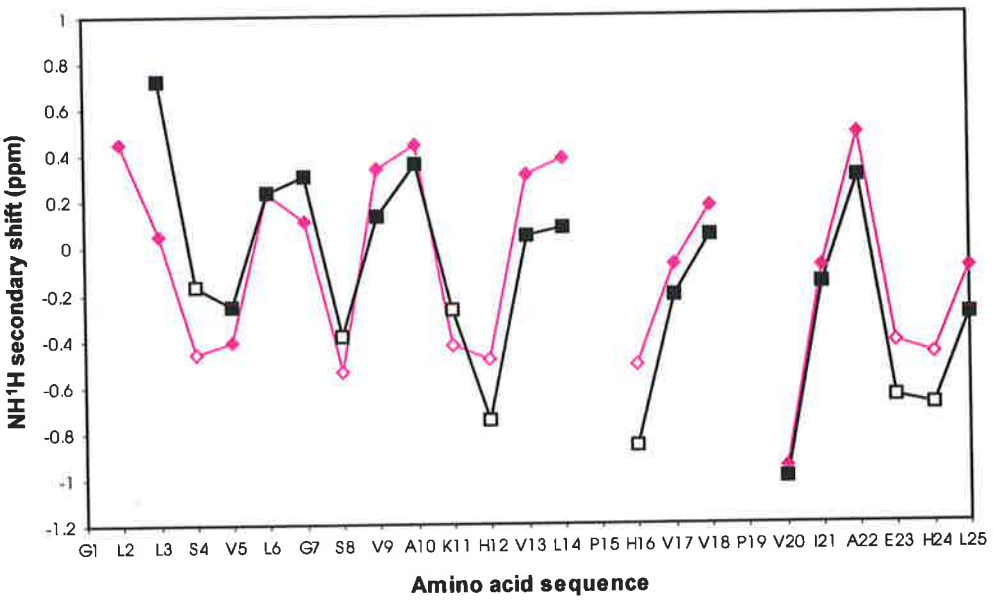

Figure 7.15 NH ^{1}H secondary shifts of caerin 1.4 in (♦) TFE/H_2O (1:1 by volume) and (■) DPC micelles. Negative values indicate an upfield shift from the random coil value while positive values indicate a downfield shift. Secondary shifts were not smoothed. Hydrophilic residues [67] are indicated by open symbols.

7.3e NOE Connectivities

The diagnostic NOE connectivities for CA14TFE and CA14DPC are shown below in Figure 7.16. The sequences of strong d_{NN} and weak $d_{NN(i,i+2)}$ NOEs, as well as the $d_{\alpha N}$, $d_{\alpha N(i,i+3)}$, $d_{\alpha N(i,i+4)}$ and $d_{\alpha\beta(i,i+3)}$ NOEs, indicate that helical structure is present for the majority of the sequence. Also evident in this figure is the high degree of assignment ambiguity due to resonance overlap, particularly for CA14TFE.

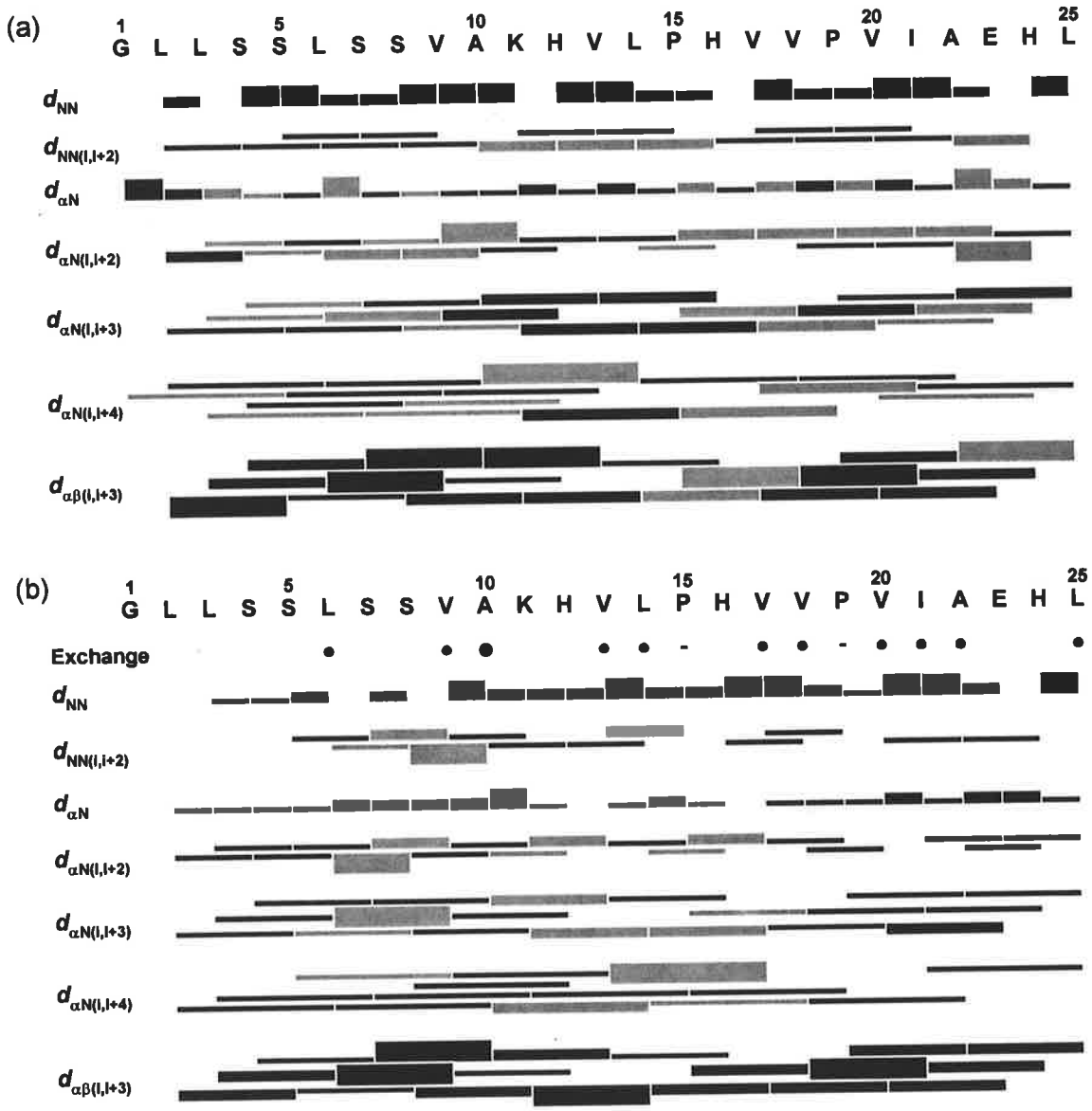

Figure 7.16 A summary of NOEs used in structure calculations for caerin 1.4 in (a) TFE/H_2O (1:1 by volume) and (b) DPC micelles. The thickness of the bars indicates the relative strength of the NOEs (strong < 3.1 Å, medium 3.1-3.7 Å or weak > 3.7 Å). Grey shaded boxes represent NOEs that could not be unambiguously assigned. Relative rates of amide exchange at pH 3.1 are indicated for the DPC micelle sample by small (≥ 2 h) and large circles (≥ 5 h). Exchange was complete in less than 2 h for the unmarked residues (no circle).

7.3f Amide Exchange

Relative NH exchange rates were measured for caerin 1.4 in DPC micelles at a pH of 3.1†. These are indicated in Figure 7.16. Eleven NHs remained after two hours (Leu6, Val9, Ala10, Val13, Leu14, Val17, Val18, Val20, Ile21 and Ala22) and just one of these (Ala10) remained after a further three hours. These slowly exchanging protons were all from hydrophobic residues. The quickly exchanging protons were either from hydrophilic

† Experiments showed exchange was too rapid at pH 6.

residues or those at the N- and C-termini, where helical structure decreases. While caerin 1.4 is expected to rapidly shift between the micelle and the surrounding water [215, 295], this peptide is poorly water soluble so it is anticipated that the equilibrium lies toward the micelle-bound form. The NH exchange results suggest that, on average, caerin 1.4 is located on the surface of the micelle, with the hydrophobic residues directed toward the hydrophobic core of the micelle and the hydrophilic residues facing the lipid head-groups and the surrounding water.

7.3g Structure Calculations

NOESY spectra of CA14TFE (mixing time = 150 ms) and CA14DPC (mixing time = 80 ms) were fully assigned and the volumes of the cross-peaks converted to distance restraints using the method of Xu *et al.* [266]. For CA14TFE, a total of 436 non-redundant restraints were produced. Over a third of these were ambiguous. Four hundred and forty-eight restraints were calculated for CA14DPC, including 65 ambiguous restraints.

RMD and dynamical SA procedures generated sixty structures and the ten structures of lowest potential energy were chosen for analysis. The final structures had only minor deviations from idealised covalent geometry ($\leq$ 0.05Å for bonds and $\leq 5°$ for angles and impropers). The maximum violation for CA14TFE was 0.42 Å and 0.34 Å for CA14DPC. Table 7-7 gives a break-down of the distance restraints and the X-PLOR energies for these structures.

Table 7-7 Comparison of the number of experimental restraints used for caerin 1.4 in trifluoroethanol/H_2O (CA14TFE) and caerin 1.4 in DPC micelles (CA14DPC). The final X-PLOR energies (kcal·mol^{-1}) and violation statistics for the 10 lowest energy calculated structures are also given.

No. of experimental restraints	**CA14TFE**		**CA14DPC**	
Sequential NOEs	98		122	
Medium-range NOEs	85		110	
Long-range NOEs	0		0	
Intra-residue NOEs	103		151	
Ambiguous NOEs	150		65	
Total	436		448	
XPLOR energies (kcal mol^{-1})	**<SA>[a]**	**$(SA)_r$[b]**	**<SA>**	**$(SA)_r$**
E_{tot}	178.06 ± 17.96	144.45	145.63 ± 8.59	124.85
E_{bond}	11.62 ± 0.87	10.25	11.62 ± 0.79	10.2
E_{angle}	54.66 ± 4.49	47.07	44.74 ± 3.27	38.01
$E_{improper}$	7.13 ± 1.87	4.86	4.55 ± 1.18	2.61
E_{vdw}	25.33 ± 3.52	22.45	16.59 ± 2.44	15
E_{NOE}	80.33 ± 11.13	59.81	68.13 ± 4.04	59.03
Violations				
No. of NOEs violated > 0.3 Å	13		2	
Maximum violation (Å)	0.42		0.34	

[a] <SA> is the ensemble of the final 10 structures.
[b] (SA) is the mean structure obtained by best-fitting and averaging the coordinates of the well-defined backbone atoms (N, αC and C') of the 10 final structures. $(SA)_r$ is the structure obtained after restrained energy minimisation of the mean structure.

The most energetically stable structures for caerin 1.4, in each medium, are shown in Figure 7.17. It is evident that in both TFE/H_2O and in DPC micelles, caerin 1.4 has an α-helical structure, which is disrupted by a bend around residues 12-16. Similar motifs are also observed for the remaining accepted structures. The amphipathic nature of the α-helices can also be seen in Figure 7.17.

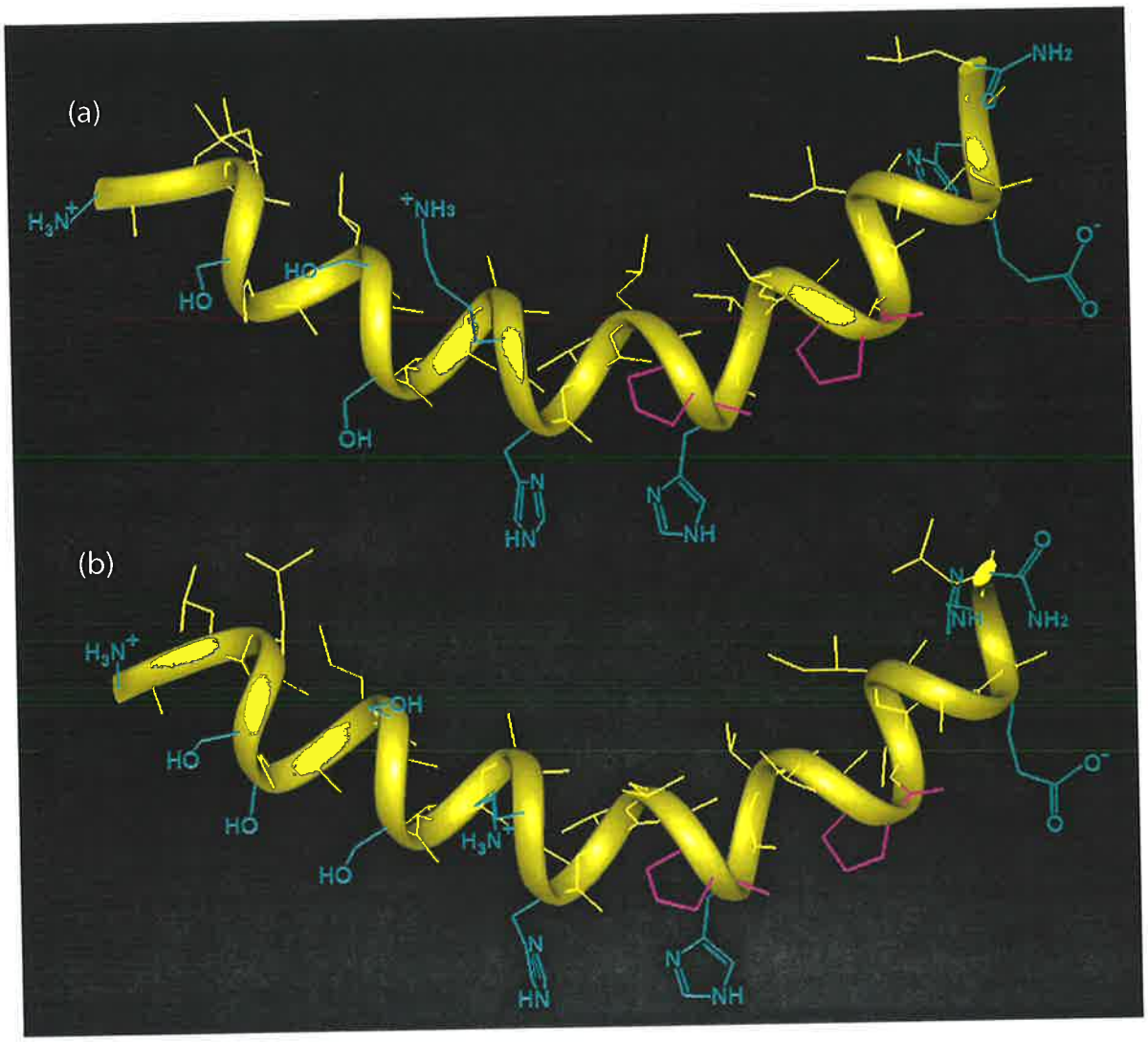

Figure 7.17 Side views of the most stable calculated structures for caerin 1.4 (a) in TFE/H_2O and (b) in DPC micelles. Hydrophilic groups are shown in blue and proline residues in pink.

Conformational variability is observed around the bend region. This can be seen in Figures 7.18 and 7.19, which show overlays of the 10 lowest energy structures, superimposed over the residues of the first and second helices. Clearly, two well-defined helices are present, separated by a more flexible hinge region. RMSD values for these helices, as well as the overall RMSD values, are summarised in Table 7-8. The average bend angles between the two helices were calculated as 65.0° ± 11.8° for CA14TFE and 65.0° ± 11.2° for CA14DPC.

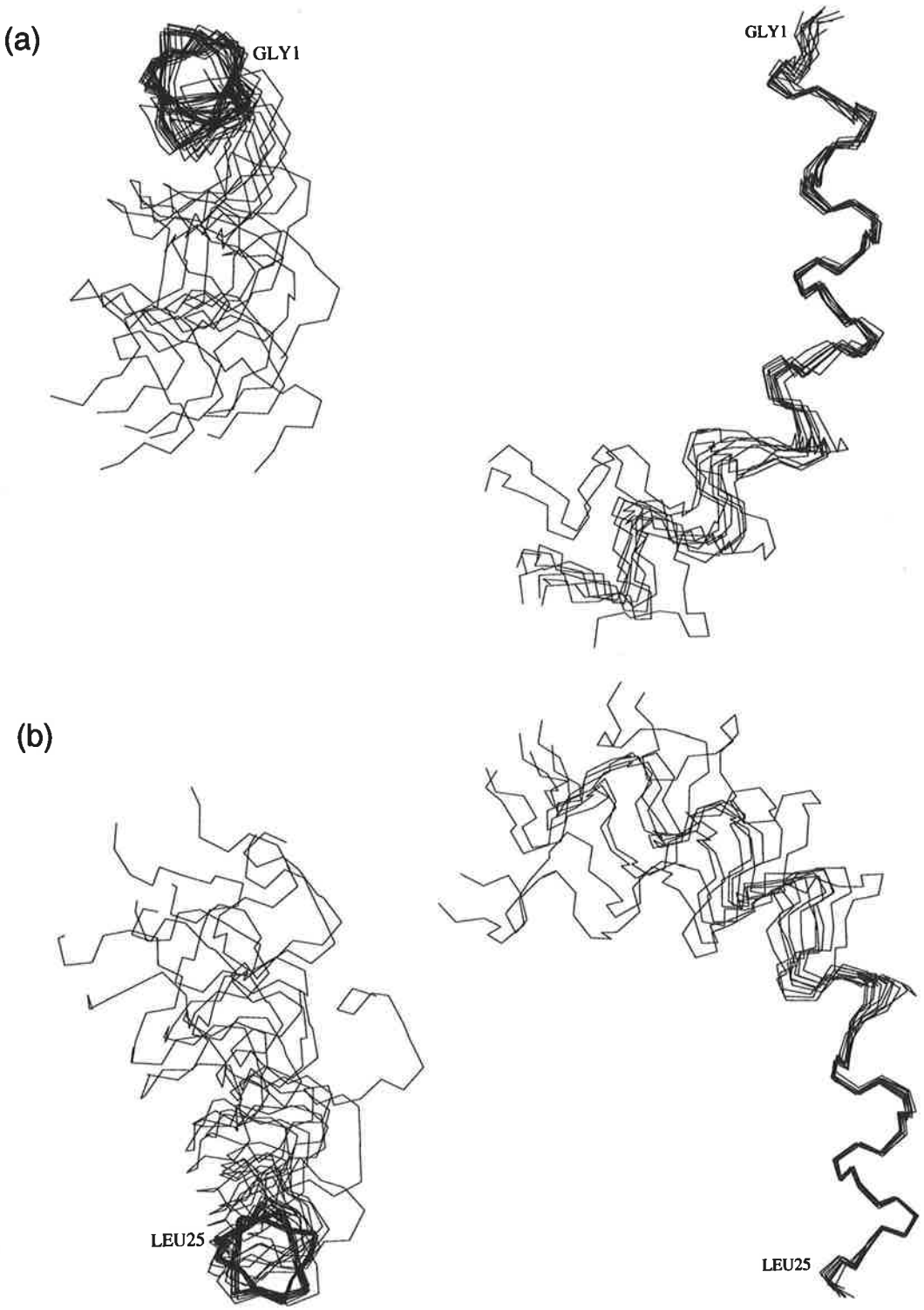

Figure 7.18 The 10 most stable calculated structures of caerin 1.4 in TFE/H_2O (1:1 by volume), superimposed along the backbone atoms (N, αC and C') of residues (a) 2-12 and (b) 17-24. The structures are viewed down the centre of the helices (left) or from the side (right). This picture was prepared using the program MOLMOL [346].

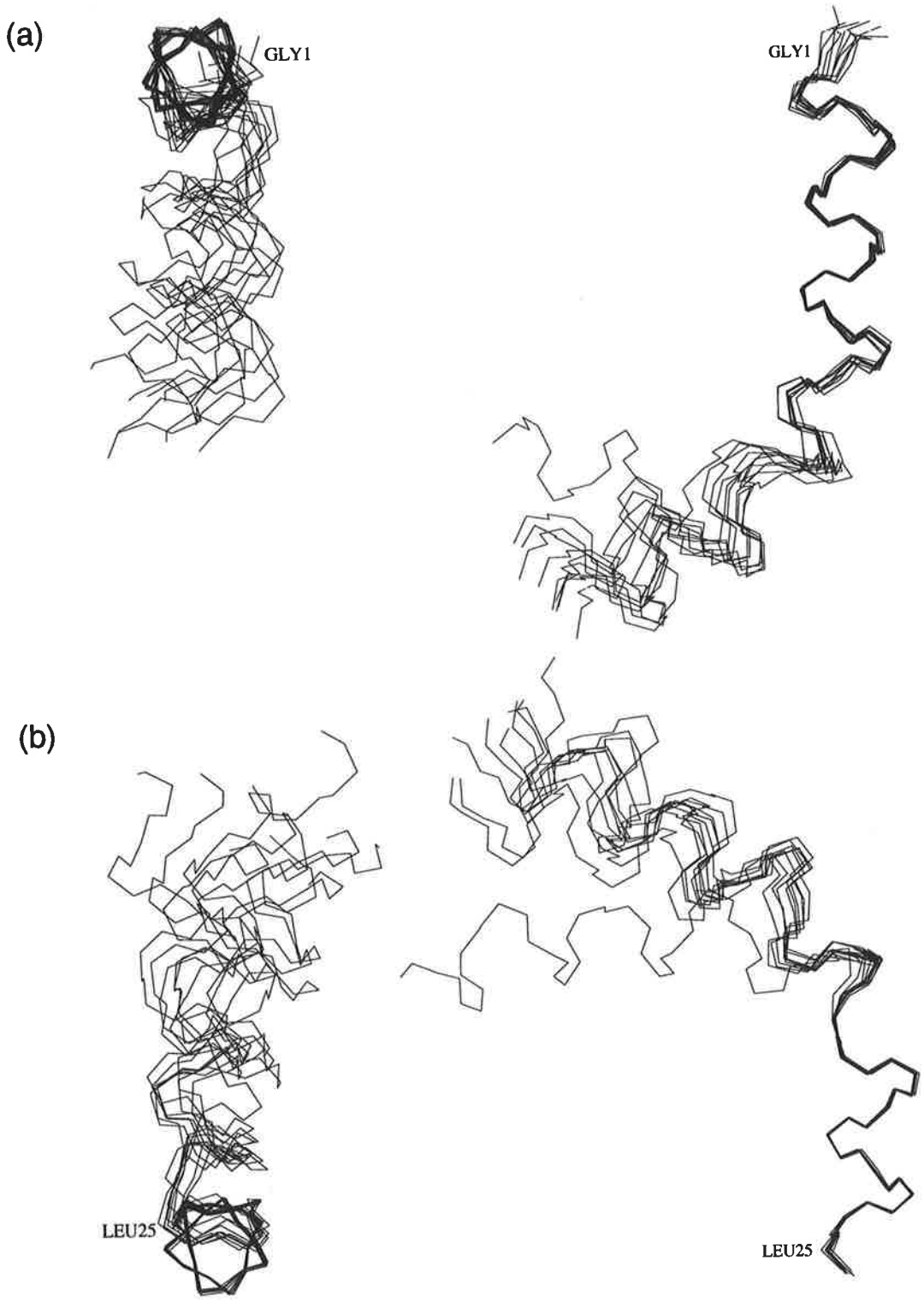

Figure 7.19 The 10 most stable calculated structures of caerin 1.4 in DPC micelles, superimposed along the backbone atoms (N, αC and C') of residues (a) 4-12 and (b) 17-24. The structures are viewed down the centre of the helices (left) or from the side (right). This picture was prepared using the program MOLMOL [346].

Table 7-8 Comparison of the root mean squared deviation (RMSD, Å) values for the 10 lowest energy structures of caerin 1.4 in trifluoroethanol/H_2O (CA14TFE) and caerin 1.4 in DPC micelles (CA14DPC).

	RMSD from mean geometry (Å)	
Structures	**Backbone atoms**	**Heavy atoms**
CA14TFE (all)	0.78 ± 0.27	1.05 ± 0.27
CA14TFE (well-defined residues 2-24)	0.62 ± 0.22	0.97 ± 0.23
CA14TFE (residues 2-12)	0.32 ± 0.08	0.80 ± 0.14
CA14TFE (residues 17-24)	0.19 ± 0.06	0.52 ± 0.05
CA14DPC (all)	0.73 ± 0.37	1.06 ± 0.34
CA14DPC (well-defined residues 4-24)	0.47 ± 0.27	0.84 ± 0.26
CA14DPC (residues 4-12)	0.17 ± 0.04	0.90 ± 0.15
CA14DPC (residues 17-24)	0.09 ± 0.03	0.39 ± 0.12

Analysis of the angular order parameters (S, ϕ and ψ) for the 10 structures of CA14TFE shows that, with the exception of the N- and C- terminal residues (Gly1 and Leu25), all residues were well-defined (S >0.9 for both ϕ and ψ angles). Twenty-one residues, or more than 80%, were well-defined for CA14DPC. Residues Leu2 and Leu3, as well as the N- and C-terminal residues, were the exceptions, indicating some additional flexibility around the N-terminal was present for caerin 1.4 in micelles.

Ramachandran plots of the average ϕ and ψ angles for the well-defined residues of CA14TFE and CA14DPC are shown in Figure 7.20. Each shows that 95% of residues are distributed within the favoured region for α-helical structure, with the remaining 5% falling in the allowable region (Val17 in each case). The residues of the hinge fall in the favoured region, indicating that these residues are also consistent with α-helical structure.

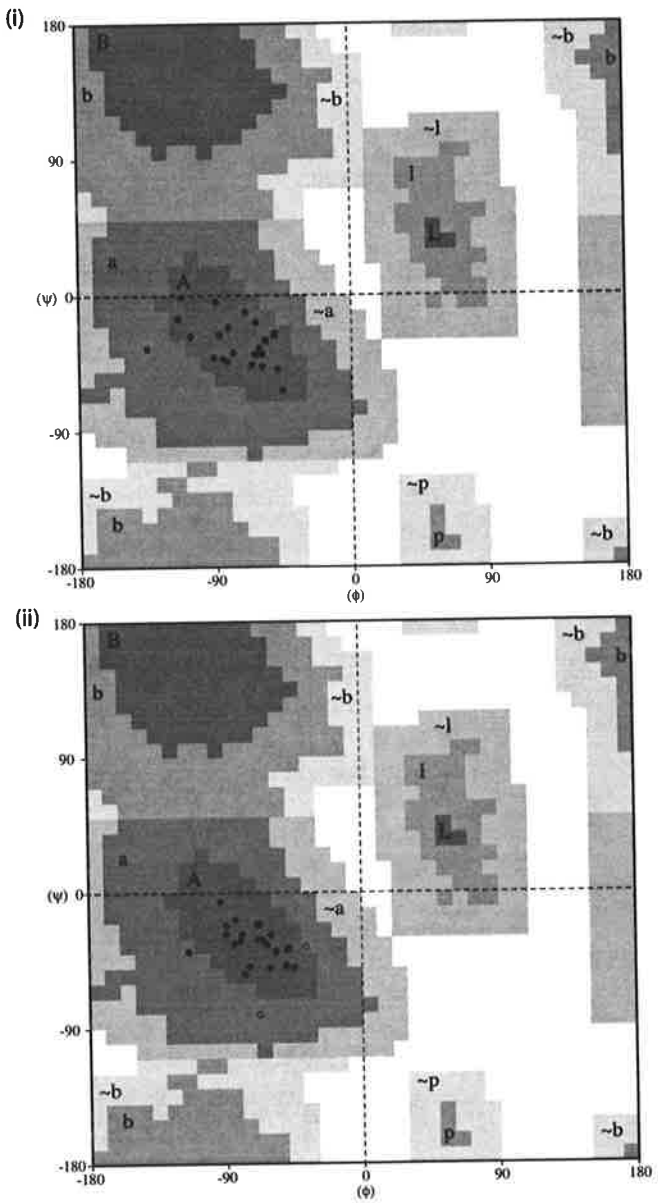

Figure 7.20 Ramachandran plots of caerin 1.4 in (i) TFE/H_2O (1:1 by volume) and (ii) DPC micelles, showing that 95% of the residues fall in the favourable region for α-helices (A). The remaining 5% fall in the allowable region (a). The generous region for α-helices is labelled '~a'. Glycine residues are indicated by triangles, prolines by squares and the remainder by circles. Open symbols indicate residues that are not well-defined.

7.4 Discussion

The NMR data and structural calculations presented here show that caerin 1.1 forms a structure in DPC micelles that is similar to that determined in TFE/H_2O. That is, caerin 1.1 forms an amphipathic α-helical structure with a central region of high flexibility around Pro15. However, there were some differences in the structure of the peptide in these two media. These will be discussed below.

Firstly, while the number of intra-residue NOEs was similar in both solvent systems, there were approximately two and a half times as many sequential NOEs and five times as many medium range NOEs for caerin 1.1 in DPC micelles than in TFE/H_2O. This could be explained if the DPC micelles stabilise the α-helical structure of caerin 1.1 to a greater extent than TFE. Alternatively, a higher contour level may have been used in the TFE/H_2O studies or the NMR data may have been of lesser quality.

There also seem to be differences in peptide flexibility in each solvent. The RMSD values given for the first and second helices in TFE/H_2O [97] are not significantly different from those found here in DPC micelles. However, greater disorder is observed around the hinge region for the structures determined in TFE/H_2O. Wong *et al.* [97] did not provide an average bend angle for caerin 1.1 in TFE/ H_2O, however examination of the lowest energy structure reveals the angle for this structure is 82°. This is within the range found for caerin 1.1 in DPC (63° to 88°). The increase in disorder for the TFE/H_2O structures may be a result of the lower number of NOE restraints used in the calculations, as well as differences in how the structures were calculated (Wong *et al.* [97] used NMRchitect (MSI) software which incorporates distance geometry calculations followed by dynamical simulated annealing or restrained molecular dynamics). In any event, the main structural features are the same in both solvent systems.

The structure of caerin 1.4 was also determined in TFE/H_2O and DPC micelles, revealing a helix-bend-helix motif in both media types. Since the same experimenter determined both structures, using the same procedures, any differences must be due to the solvent systems. As found for caerin 1.1, there were significantly more sequential, medium and intra-residue NOE restraints for caerin 1.4 in DPC micelles. However, there were many

more ambiguous restraints for the peptide in TFE. Thus, the additional sequential, medium and intra-residue restraints present in the ambiguous category could account for the discrepancy. The overall number of NOE restraints was similar in both solvents. The RMSD values were not significantly different and the average bend angles were almost identical for the two structures. Residues 2-24 were well-defined for caerin 1.4 in TFE/H_2O, while only residues 4-24 were well-defined for the structures in DPC. This suggests that the first three residues have more variable conformations in DPC than they do in TFE/H_2O.

Thus, caerin 1.4 seems to have very similar structures in TFE/H_2O and DPC micelles. This implies that the differences observed for caerin 1.1 in these solvent systems were due to experimental differences. It also suggests that, for these peptides, aqueous TFE mixtures are at least as good at representing a bilayer environment as DPC micelles.

The structures of caerin 1.1 and caerin 1.4 can be compared to see if there are any differences that could explain the different spectra of antibacterial activity they possess. Qualitatively, their structures are very similar as they both adopt helix-bend-helix motifs. The average bend angles are slightly different for caerin 1.1 (75.2° ± 7.4°) and caerin 1.4 (65.0° ± 11.2°) but not significantly so. The RMSD values of the two peptides were also similar. Residues 3-24 of caerin 1.1 and 4-24 of caerin 1.4 were well-defined, suggesting additional conformational freedom at the N-terminal ends of both peptides. Thus, the peptides have very similar backbone structures and their bacterial specificity must arise from side-chain properties.

Caerin 1.4 is less hydrophobic than caerin 1.1 and its predicted hydrophilic angle is greater. The latter parameter assumes the peptide is an ideal α-helix, which is rarely the case in practice. Figure 7.21 shows representative structures of caerin 1.4 and caerin 1.1 as calculated for the peptides in DPC micelles. In this view, looking down the N-terminal helix (residues 1-12), it can be seen that the hydrophilic angle is around 180° for caerin 1.4 and 120° for caerin 1.1. These values are slightly higher than predicted but the angle for caerin 1.4 is still markedly higher than that for caerin 1.1. It is therefore possible that this difference has a bearing on bacterial specificity.

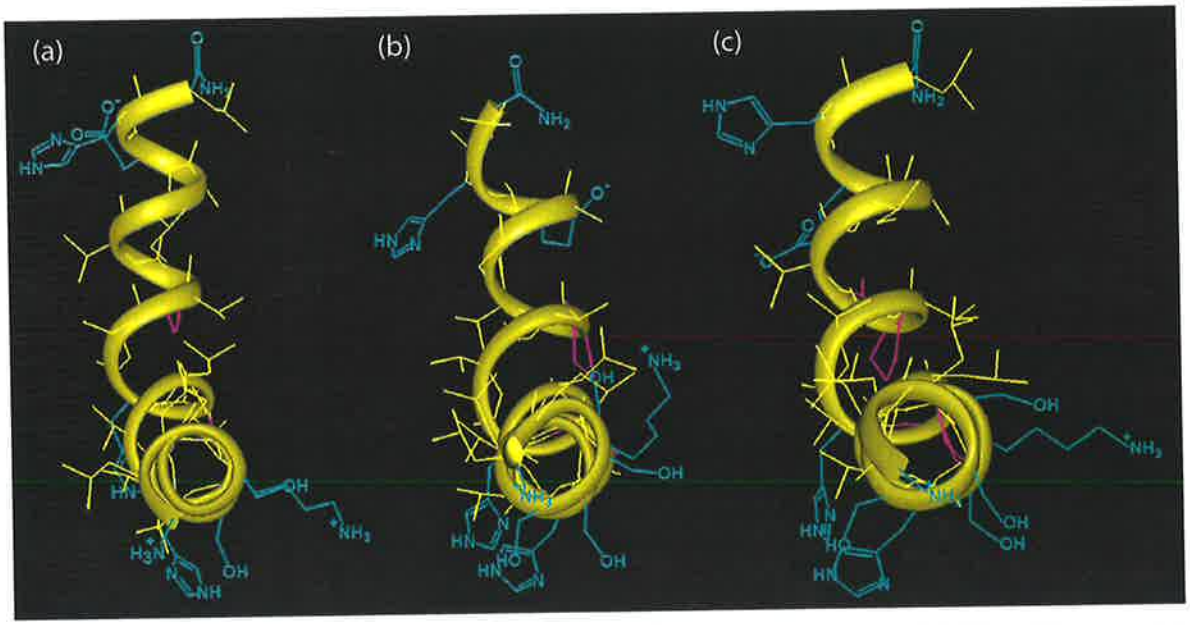

Figure 7.21 The most stable calculated structures of (a) caerin 1.1 in DPC micelles, (b) caerin 1.4 in TFE/H_2O (1:1 by volume) and (c) caerin 1.4 in DPC micelles, viewed down the centre of the N-terminal helix. Hydrophilic groups are shown in blue and proline residues in pink.

Peptides with hydrophilic angles around 180° bind to lipid bilayers with high affinity but are less able to permeabilise the membranes once bound [191]. The angle of 180° favours a surface location in the membrane and disfavours the formation of transmembrane pores because of electrostatic repulsion between the peptide monomers [117] (Figure 7.22). Many antibacterial peptides have hydrophilic angles around 100° [68], which would be more conducive to the formation of channel structures but decreases affinity for the membrane. Caerin 1.4 would therefore be expected to bind more strongly to bacterial membranes, while caerin 1.1 might have greater permeabilising activity.

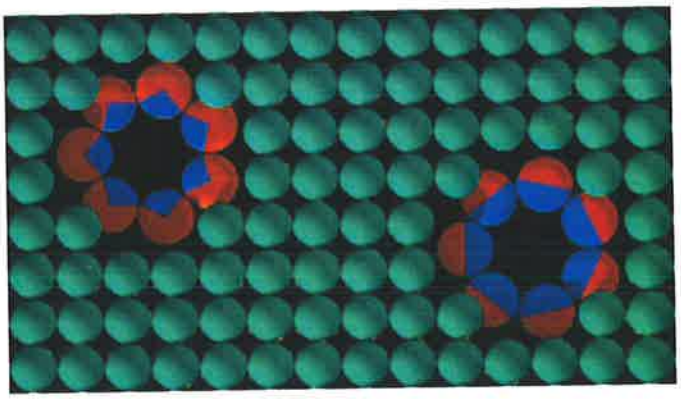

Figure 7.22 Top-view of barrel-stave pores formed by α-helical peptides with hydrophobicity angles of 100° (left) or 180° (right). Hydrophilic regions of the helices are coloured blue and the hydrophobic portions red. Green circles represent the polar lipid head-groups.

Caerin 1.4 is also less hydrophobic than caerin 1.1 since Val5 and Gly7 have been replaced with serine residues. Thus, the two main differences between caerin 1.1 and caerin 1.4 are the hydrophilic angle and the hydrophobicity and these factors may be responsible for the difference in activity toward *Micrococcus luteus* and *Escherichia coli*. The caerins 2, 3 and 4 have similar activity to caerin 1.4 towards these organisms and they also have large hydrophilic angles and lower hydrophobicity than caerin 1.1. Therefore, it seems that differences in the membrane composition of *M. luteus* and *E. coli* make them more susceptible to peptides with large hydrophilic angles and/or low hydrophobicity. However, the details of how this occurs are unknown at this stage.

The structures of caerin 1.1 and caerin 1.4 show that the hydrophobic and hydrophilic residues are located on opposite sides of the helices. Amide exchange experiments showed that the amide protons from the hydrophobic residues of caerin 1.1 and caerin 1.4, exchanged more slowly than those from the hydrophilic residues. Thus, it seems that the hydrophobic surface of the peptide is shielded from the aqueous phase to a greater extent than the hydrophilic surface. This, in turn, suggests the peptides, on average, adopt a surface orientation when incorporated into micelles, with the hydrophilic residues directed toward the water and the DPC head-groups and the hydrophobic residues located near the hydrophobic tails of the lipid molecules. Similar experiments have previously shown that melittin adopts a surface orientation in micelles [215], while a model transmembrane peptide (32) was shown to be predominantly located within the micelle core [260].

(32) Ac-KKLALALALALALALALALALALALAKK-NH_2

Bechinger [149] demonstrated that the orientation of His-containing peptides can depend on pH. He showed that the model peptide LAH_4 (30) adopts a surface orientation at low pH, where the His residues are protonated. At high pH, the His residues are uncharged and the peptide was found to have a transmembrane orientation. At the low pH used for the amide exchange experiments on the caerin peptides, the three His residues would be positively charged and therefore more likely to adopt a surface orientation. Nevertheless, the results presented here suggest caerin 1.1 and caerin 1.4 prefer a surface orientation in micelles at low pH.

(30) LAH_4 KKALLALALHHLAHLALHLALALKKA-OH

Molecular dynamics simulations conducted by La Rocca *et al.* [304] on caerin 1.1 in a lipid bilayer also suggest that caerin 1.1 prefers a surface location, with only the relative orientation of the N- and C-terminal helices changing over time due to the flexibility of the central hinge. While this is consistent with the results presented here for a micellar environment, the computer simulations must be supported by physical evidence determined in a bilayer system, since the high degree of curvature in the micelles could be affecting the orientation of the peptides. Techniques, such as solid-state NMR spectroscopy, should be conducted on the caerin 1 peptides to conclusively determine their orientation in lipid bilayers.

7.5 Conclusion

Caerin 1.1 was found to form an amphipathic α-helical structure in DPC micelles, with a region of high flexibility around Pro15. This structure was similar to that determined in TFE/H_2O by Wong *et al.* [97]. The structure of the related peptide, caerin 1.4, was determined in both TFE/H_2O and DPC micelles, showing that in both solvents it forms a helix-bend-helix structure. The hydrophilic angle of the N-terminal helix was found to be significantly greater for caerin 1.4 and the hydrophobicity of this helix is reduced, compared with that of caerin 1.1, suggesting that either or both of these properties may be responsible for the marked variation in the bacterial specificity of these peptides. Amide exchange data also indicated that at low pH both caerin 1.1 and caerin 1.4 are, on average, located on the surface of the DPC micelles, with their hydrophobic portions directed toward the micelle core and the hydrophilic residues directed toward the lipid head-groups and the water phase. This tends to support a carpet mechanism of action for these peptides but it should be noted that this orientation may be dependent on pH and peptide concentration and/or influenced by the curvature of the micelles. Orientation experiments using bilayer systems should be performed to further investigate their mechanism/s of action.

Chapter 8 Experimental

8.1 Materials

Peptides were synthesised by Mimotopes (Clayton, Victoria) using L-amino acids via the standard N-α-Fmoc method. Full details, including protecting groups and deprotection, have been reported [78]. Samples used for NMR studies were > 90% pure by HPLC and electrospray mass spectrometry. Citropin 1.1 and aurein 1.2 samples for solid-state NMR studies were specifically labelled with ^{15}N-L-alanine at position 10. Phospholipids were purchased from Avanti Polar-Lipids (Alabaster, AL, USA) and were used as received. Water used was filtered by the Milli-Q system.

8.2 CD Spectroscopy – Trifluoroethanol Titrations

CD spectra were recorded on a Jobin-Yvon CD-6 spectrophotometer at room temperature. CD spectra were acquired for citropin 1.1 (31 μM) or caerin 1.4 (27 μM) in solutions of TFE in water (0-50% by volume). Each spectrum represents the average of five scans, with the data smoothed over n = ±5 data points.

8.3 Solution NMR Spectroscopy

8.3a Sample Preparation

NMR experiments were carried out on peptides in either TFE/H_2O or dodecylphosphocholine-d_{38} (DPC) micelles. Aqueous TFE samples were prepared by dissolving the peptide in a mixture of d_3-TFE and water in the required ratio, with a total volume of 0.7 mL. For DPC samples, the peptide and 40 mol. equivalents of DPC were dissolved in 10% D_2O in H_2O, with 50 mM NaH_2PO_4 buffer. The concentration of DPC was in vast excess of the critical micelle concentration [293] (see Table 8-1) and the lipid to peptide ratio of 40:1 was chosen to give a solution with approximately one peptide molecule per micelle [281, 283, 294]. Micelle samples were adjusted to pH 6 using NaOH

or HCl as appropriate. All pH measurements were taken using a Eutech Cyberscan pH 500 Meter with an AEP 331 Glass-body pH probe (183 x 4 mm, thin stem).

A small amount of sodium 2,2-dimethyl-2-silapentane-5-sulphonate (DSS) was added to the DPC samples as a reference. The final peptide concentrations and specific sample conditions for all samples are outlined in Table 8-1.

Table 8-1 Sample conditions for citropin 1.1, aurein 1.2, caerin 1.1 and caerin 1.4.

Aqueous TFE samples				
Peptide	**Mass (mg)**	**Conc. (mM)**	**pH**	**% TFE[a]**
Citropin 1.1	8	7.1	2.25	50
Aurein 1.2	10	9.7	2.04	70
Caerin 1.4	8.5	4.7	3.13	50
DPC samples				
Peptide	**Mass (mg)**	**Conc. (mM)**	**pH**	**DPC Conc. (mM)**
Caerin 1.4	6.6	3.6	5.97	145
Caerin 1.1	11.1	5.6	6.07	222

[a] % TFE in water, by volume.

8.3b NMR Spectroscopy

NMR experiments were acquired on a Varian Inova-600 NMR spectrometer at a ^{1}H frequency of 600 MHz and ^{13}C frequency of 150 MHz. Experiments were run at 25°C for aqueous TFE samples and 37°C for DPC samples. ^{1}H-NMR spectra were referenced either to the methylene protons of residual unlabelled TFE (3.918 ppm) or to DSS (0.0 ppm). The ^{13}C (F1) dimensions of the HSQC and HMBC spectra were referenced to the $^{13}CH_2$ (60.975 ppm) and $^{13}CF_3$ (125.9 ppm) of TFE, respectively, or to DSS (0 ppm).

TOCSY [235], DQF-COSY [234] and NOESY [239] experiments were all collected in the phase-sensitive mode using time proportional phase incrementation in t_1 [233]. These experiments were typically acquired over 256 increments, with 32 time-averaged scans per increment.

The FID in t_2 consisted of either 2048 or 4096 data points over the spectral width, which varied between samples (citropin 1.1 – 5564.1 Hz, aurein 1.2 – 5345.1 Hz, caerin 1.1

(DPC) – 5739.7 Hz, caerin 1.4 (TFE) – 5445.1 Hz and caerin 1.4 (DPC) – 5654.9 Hz). Water suppression in the TOCSY and NOESY experiments was achieved by presaturation [361]. The transmitter frequency was centred on the water resonance and conventional low power presaturation from the same frequency synthesiser (proton transmitter) was applied during a 1.5s relaxation delay between scans. Gradient methods for water suppression were used in the DQF-COSY experiment [362].

The TOCSY experiments were acquired with the pulse sequence of Griesinger *et al* [236], which minimises cross-relaxation effects using a 70ms MLEV-17 spin-lock. NOESY spectra were acquired with a mixing time of 150 ms for the aqueous TFE samples and 80 and 100 ms for the caerin 1.4 and caerin 1.1 DPC samples, respectively.

A series of TOCSY spectra were also acquired, over a period of 24 hours, on freshly prepared samples of peptide and DPC in D_2O to detect slowly exchanging amide protons. The pH was lowered to 2.7 for caerin 1.1 and 3.1 for caerin 1.4 so that amide exchange rates were at a minimum [259, 363]. TOCSY experiments were acquired with 64 t_1 increments, each comprising 4 time averaged scans over 2048 data points, with each experiment taking approximately 15 minutes to run.

after initial experiments at pH 6 showed exchange was too rapid.

HSQC experiments [237] were recorded with the interpulse delay set to $1/2J_{CH}$ = 3.6 ms, corresponding to J_{CH} = 140 Hz. Typically 256 t_1 increments, each comprising 32 transients, were acquired over 2048 data points in the directly detected (^1H, F_2) dimension. For the DPC samples, the number of transients was increased to 64 for caerin 1.1 and 128 for caerin 1.4 and 4096 data points were used. In the ^{13}C (F_1) dimension, a spectral width of 24140 Hz was used. HMBC experiments [364] were collected with the interpulse delay set to $1/2J_{CH}$ = 62.5 ms for J_{CH} = 8 Hz. Typically 512 increments, each comprising 64 scans, were acquired over 4096 data points in the ^1H (F_2) dimension. The spectral width for the ^{13}C (F_1) dimension was typically 36200 Hz.

All 2D NMR spectra were processed on a Sun Microsystems Ultra Sparc 1/170 workstation using VNMR software (version 6.1A). The data matrices were multiplied by a Gaussian function in both dimensions before zero-filling to 4096 data points in F_1 (and F2 if necessary) prior to Fourier transformation. Final processed 2D NMR matrices consisted of 4096 x 4096 real points.

8.3c Structural Restraints

Cross-peaks in the TOCSY and NOESY spectra were assigned using XEASY software (version 1.3.13) [365]. The volumes of these cross-peaks were converted to distance restraints using the method of Xu *et al.* [266]. For each symmetric pair of cross-peaks, the peak of smaller volume was used.

$^3J_{NH\alpha H}$ values were measured from high-resolution 1D ^1H NMR spectra for citropin 1.1 and aurein 1.2, acquired with 0.012 and 0.082 Hz per point digital resolution respectively. The 1D spectra of the caerin peptides were too overlapped to be useful. Attempts at measuring the $^3J_{NH\alpha H}$ values from DQF-COSY spectra were made using the method of Kim and Prestegard [256], however, the line-widths were too broad to determine these accurately.

Dihedral angles were restrained as follows: $^3J_{NH\alpha H} < 5$ Hz, $\phi = -60° \pm 30°$ and $5 < {}^3J_{NH\alpha H} < 6$ Hz, $\phi = -60° \pm 40°$. For the $^3J_{NH\alpha H}$ values ≥ 6 Hz, ϕ angles were not restrained. The absence of resolved splitting for an NH resonance implies that its $^3J_{NH\alpha H}$ value is < 5 Hz, i.e., the residue is part of a helical conformation. Hence the ϕ angles for these residues were restrained to $-60° \pm 30°$.

8.3d Structure Calculations

Structures were generated on a Sun Microsystems Sparc 1/170 workstation using X-PLOR software (version 3.851) [366, 367]. The RMD and SA protocol was used [368], including the use of floating stereo-specific assignments [271]. Sum-averaging was used to take care of the ambiguous restraints. The ambiguous restraints were refined based on the structures from the initial calculations [251].

The All Hydrogen Distance Geometry (ALLHDG) force field (version 4.03) was used for all calculations [369]. Each calculation run began with a family of 60 structures generated with random ϕ and ψ dihedral angles. These were subjected to 6500 steps (19.5 ps) of high temperature dynamics at 2000 K. The K_{noe} and K_{repel} force constants were increased from 1000 to 5000 kcal·mol^{-1}nm^{-2} and 200-1000 kcal·mol^{-1}nm^{-4}, respectively. This was

followed by 2500 steps (7.5 ps) of cooling to 1000 K with K_{repel} increasing from 1000 to 40000 kcal·mol^{-1}nm^{-4} and the atomic radii decreased from 0.9 to 0.75 times those in the ALLHDG parameter set. The last step involved 1000 steps (3 ps) of cooling from 1000 K to 100 K. Final structures were subjected to 200 steps of conjugate gradient energy minimisation. The structures produced with the lowest potential energies (20 for citropin 1.1 and aurein 1.2 and 10 for the caerin peptides) were selected for analysis. Three-dimensional structures were displayed using INSIGHT II software (version 95.0, MSI) and the program MOLMOL [346].

8.4 Oriented Circular Dichroism

8.4a Sample Preparation

A stock solution of peptide (aurein 1.2 or citropin 1.1) in TFE was prepared (*ca.* 2.7 mM) and an appropriate volume added to two tubes containing dry DMPC (7 mg) to obtain L/P ratios of 15:1 and 50:1. Samples with a L/P ratio of 100:1 were prepared by adding the appropriate volume of peptide stock to dry DMPC (14 mg). A control sample of peptide alone was prepared using stock solution (100 μg peptide equivalent) as well as one of DMPC (7 mg) alone. The TFE was removed under vacuum and the samples made up to a volume of 1 mL with Milli-Q water. Samples were then sonicated and centrifuged to produce small unilamellar vesicles (SUV).

Isotropic vesicle samples were prepared by diluting a proportion of the lipid-peptide or lipid only stock solutions by a factor of ten with Milli-Q water. These samples were placed in a quartz cuvette (~300 μL volume, 1 mm path length) for the CD measurement. Oriented samples were obtained by applying the lipid-containing stock solutions (100 μL) to a quartz plate made from a CD cuvette. The solution was spread evenly over the plate with a stream of nitrogen gas, covering an area of approximately 2.5 cm^2, until the plate appeared dry. This resulted in oriented DMPC bilayers.

8.4b CD Measurement

CD spectra were recorded on an AVIV Model 62DS spectrometer with the light beam at normal incidence to the quartz cuvette or plate, at a temperature of 30°C. All spectra were acquired over the wavelengths 260-185 nm with 0.5 nm steps.

For the isotropic samples, a 1.5 nm spectral width was used with an integration time of 1s. Three scans were acquired for each of the isotropic vesicle samples. Five scans were completed for the DMPC blank sample and the aqueous peptide samples to obtain improved signal-to-noise ratios. The control vesicle CD spectra were subtracted from the peptide-vesicle spectra.

The oriented samples were acquired using a 2 nm spectral width with an integration time of 5 s and two scans per sample. The second scan was obtained on the same sample but with the quartz plate rotated by 180° about the long axis. Verification of the sample uniformity was made by comparison of the line-shape of the two scans. The scans were then averaged and the spectrum of the control oriented bilayers was subtracted.

Isotropic spectra were converted from measured ellipticity (mdeg) to mean residue ellipticity ($deg \cdot cm^2.dmol^{-1}$). The oriented CD spectra were left in units of mdeg because the thickness of the oriented bilayers, and therefore the exact amount of peptide, was unknown. However, for comparison with the isotropic samples, the oriented spectra were scaled such that the intensities of the isotropic and oriented spectra were equal for the bands around 222 nm.

8.5 Solid-state NMR Spectroscopy

8.5a Sample Preparation - Unoriented Bilayers

Citropin 1.1 (3.1 mg) and 1,2-dimyristoyl-d_{54}-sn-glycero-3-phosphocholine (d_{54}-DMPC) (20.8 mg) were co-dissolved in methanol (50 µL), lyophilised and hydrated to 50% water (vol/wt). The sample was then alternately vortexed and centrifuged between freeze-thaw cycles (-196°C) until thoroughly

mixed. The lipid to peptide (L/P) molar ratio was 15:1. A control sample of d_{54}-DMPC alone was prepared in a similar manner.

8.5b Mechanically Oriented Bilayers

Each peptide (typically 5 mg) was co-dissolved with d_{54}-DMPC (typically 35 mg) in a mixture of chloroform and TFE (~1 mL), resulting in a L/P molar ratio of 15:1 for each sample. The mixture was applied to microscope coverslips, each 20 mm long and ranging in width (4.5 – 6 mm) such that, when stacked, a circular cross-section was obtained. The solvent was removed under vacuum overnight. Samples were then hydrated with water (50% vol/wt), stacked and placed in an NMR tube (7 mm diam.) with additional water (10-15 μL), before heat-sealing to give a tube approximately 3 cm long. A control sample was made in the same way using d_{54}-DMPC alone.

8.5c NMR Spectroscopy - Unoriented Bilayers

Proton-decoupled phosphorus (^{31}P) NMR experiments on unoriented bilayer samples were carried out on an Inova 300 Varian spectrometer, using a 5 mm Doty MAS (Magic Angle Spinning) probe at an operating frequency of 121.46 MHz (^{31}P). Samples were not spun during acquisition. Spectra were recorded at room temperature with gated decoupling. Typical operating conditions were: 90° pulse duration, 6 μs; repetition delay, 4 s; sweep width, 62.5 kHz; number of scans, 100. Spectra were processed with 100 Hz of line broadening. ^{31}P spectra were referenced to H_3PO_4 (0 ppm).

8.5d Mechanically Oriented Bilayers

Phosphorus (^{31}P) and deuterium (^{2}H) NMR experiments on the mechanically aligned multilayers were recorded on an Inova 400 Unity+ Varian spectrometer using a 10 mm broad-band probe. Samples were not spun. Both ^{31}P and ^{2}H experiments were recorded at 30, 35 and 40°C. Samples were equilibrated for 10 minutes at each temperature prior to acquisition.

Proton-decoupled ^{31}P spectra were acquired at 161.8 MHz with a spectral width of 32 kHz. Other parameters used were: 90° pulse width, 12 μs; decoupler power, 60; recycle delay 2.4 s; number of data points, 2k with zero-filling to 8k data points; number of scans, 256; line broadening, 100 Hz. ^{31}P spectra were referenced to H_3PO_4 (0 ppm).

Deuterium quadrupole echo spectra were recorded at 61.4 MHz over a spectral width of 100 kHz. Typical operating conditions were: 90° pulse, 12 μs; echo spacing, 40 μs; recycle delay, 300 ms; number of data points, 16k; number of scans, 32k; line broadening, 50 Hz. Deuterium spectra were referenced to D_2O (0 ppm).

Proton-decoupled ^{15}N spectra were acquired at 50.7 MHz on a Bruker DMX-500 NMR spectrometer. A 10 mm multinuclear probe was used and the spectra were acquired at a temperature of 35°C. Typical operating conditions were: 90° pulse width, 15 μs; spectral width, 22 kHz; recycle delay, 3.6 s; number of points, 16k; number of scans, 56k; line broadening, 100 Hz. ^{15}N spectra were referenced to the ammonium signal of $^{15}NH_4NO_3$ (0 ppm).

8.5e Peptide Powders

^{15}N cross-polarisation experiments [316] were performed on peptide powder samples at 30.4 MHz on an Inova 300 Varian spectrometer. A 5 mm Doty MAS (Magic Angle Spinning) probe was used and spectra were recorded on both spinning (5 kHz MAS) and static samples at ambient temperature. Typical parameter settings were: 90° pulse, 8 μs (static), 6.8 μs (spinning); recycle delay, 2s; contact time, 2 ms; acquisition time, 60 ms; spectral width, 20 kHz; number of scans, 50 k (static), 1k (spinning); line broadening, 150 Hz. ^{15}N spectra were referenced to the ammonium signal of $^{15}NH_4NO_3$ (0 ppm).

Summary and Future Directions

Eleven novel peptides were discovered in the skin secretion of *Litoria dahlii*, as well as the potent neuropeptide caerulein. The eleven dahlein peptides are similar to the aureins 1, 4 and 5 from *L. aurea* and *L. raniformis*, suggesting that these frogs share a common ancestor. However, the absence of potent broad-spectrum antibiotics in the *L. dahlii* secretions, similar to the aureins 2 and 3, indicate evolutionary divergence. This probably occurred because of the different climates and predators to which these species are exposed, since *L. dahlii* is found in the tropical north of Australia, while *L. aurea* and *L. raniformis* inhabit Australia's temperate southeast.

The dahleins 1 were shown to have moderate broad-spectrum antibacterial activity similar to the aureins 1, while dahleins 5.3 and 5.6 were found to be effective against a variety of different cancer cell-lines. The dahleins 5 were also shown to inhibit the enzyme nNOS at micromolar concentrations. Similarities between the dahleins 5 and the amphibian pheromone splendipherin suggest that these peptides could have an additional role in chemical communication. Behavioural studies may be carried out in the future to determine whether or not this is the case.

The short antimicrobial peptides citropin 1.1 (16 residues) and aurein 1.2 (13 residues) were investigated in an attempt to shed light on their mechanisms of action. CD studies indicated these peptides were unstructured in water but bound to neutral DMPC vesicles, where they adopted α-helical structures. Their three-dimensional structures were studied in more detail in the membrane mimicking solvent mixture TFE/H_2O, using NMR spectroscopy and restrained molecular dynamics calculations. This showed that citropin 1.1 and aurein 1.2 form linear amphipathic α-helices in this medium.

OCD experiments showed that citropin 1.1 and aurein 1.2 had no preferred orientation in DMPC bilayers at a L/P ratio of 50:1 but oriented closer to the membrane normal (~35°) at higher peptide concentrations (L/P 15:1). Solid-state NMR experiments were consistent with the peptides having oblique orientations in the lipid bilayers. Taken together, these results are compatible with a carpet mechanism of action. However, additional

experiments are required to confirm these findings, as well as to investigate the effect of anionic lipids, peptide mobility and peptide concentration on the peptide-lipid interactions.

The structures of caerin 1.1 and caerin 1.4 were determined in DPC micelles and TFE/H_2O (caerin 1.4 only) using NMR spectroscopy and restrained molecular dynamics calculations. In each case, the peptides formed amphipathic α-helical structures, with a flexible hinge region around Pro15. There was little difference in the structure of caerin 1.4 in the two media and the structure of caerin 1.1 in DPC micelles was comparable to that determined by Wong *et al.* [97] in TFE/H_2O. Thus, for these peptides at least, mixed organic solvents are as effective as DPC micelles at mimicking the membrane environment. It would be helpful to also determine the structure of these peptides in bicelles, as these disc-shaped lipid structures resemble flat lipid bilayers more closely and, at suitable ratios of long- to short-chain lipids, reorient rapidly enough to be suitable for solution NMR spectroscopy. This would determine whether the high degree of curvature present in the micelles affects the overall peptide structure.

Caerin 1.1 and caerin 1.4 differ at only two points in their sequences. In caerin 1.4, serine residues at positions 5 and 7 replace valine and glycine residues, respectively. This results in decreased hydrophobicity for caerin 1.4 as well as an increased hydrophilic angle for the N-terminal helix. The calculated structures reveal the hydrophilic angles to be around 120° for caerin 1.1 and 180° for caerin 1.4. These structural differences result in the different patterns of antimicrobial activity observed for caerin 1.1 and caerin 1.4.

Amide exchange experiments suggested that, on average, both of the caerin 1 peptides were located on the surface of the micelles. Additional experiments are necessary to discover if this is also the case in lipid bilayers. These orientation studies must be designed to determine the orientation of both the N- and C-terminal helices of the helix-bend-helix motif. The effect of lipid composition and peptide concentration should also be examined to probe membrane specificity and the mechanism of action of these peptides.

It is hoped that by investigating the mechanism of action of antibacterial and anticancer peptides, more potent and cell-specific compounds will be developed and used in the treatment of disease. Peptide antibiotics may provide an answer to the increasing problem

of bacterial resistance, since their action at the cell membrane may make it more difficult for the bacteria to adapt. No measurable rates of resistance have been found so far, for antibiotic peptides [87, 94].

The major impediment to the clinical use of peptides is their susceptibility to proteases. Orally administered peptides are broken down to their constituent amino acids before they even enter the circulation, while peptides injected directly into the blood-stream are deactivated in minutes to hours by plasma proteases [36]. It may be possible to get around this problem by using the all-D enantiomers, which could still interact with the bacterial cell membranes but would be unaffected by proteases.

An alternative use for antibacterial peptides is as a food preservative. In this case, susceptibility to host proteases is an aid, not an obstacle, since the antibacterial activity is only required prior to consumption. The peptide is then degraded in the gut so that selectivity for pathogenic cells is not as important. Nisin, a 34-residue antibiotic peptide from the G+ bacterium *Lactococcus lactis*, has already found wide-spread use as a preservative in the food industry [370, 371].

The research presented in this thesis demonstrates that amphibian skin secretions are a valuable resource of novel compounds. Isolating and identifying peptides from different species and investigating their biological activities may lead to potentially useful products for the future.

References

1. Tyler, M.J. (1987) Frog and Cane Toad Skin Secretions. In *Toxic Plants and Animals. A Guide for Australia.* (Covacevich, J., ed) pp. 329-339, Queensland Museum, Brisbane.
2. Lazarus, L.H. & Attila, M. (1993) Evolutionary significance of amphibian skin peptides, *Prog. Neurobiol. 41*, 473-507.
3. Erspamer, V., Erspamer, G.F., Severini, C., Potenza, R.L., Barra, D., Mignogna, G. & Bianchi, A. (1993) Pharmacological studies of 'sapo' from the frog *Phyllomedusa-bicolor* skin: a drug used by the Peruvian Matses Indians in shamanic hunting practices, *Toxicon. 31*, 1099-1111.
4. Grenard, S. (1994) Frogs and Toads. In *Medical Herpetology* pp. 2-127, Reptiles and Amphibian Magazine, Pottsville, PA, USA.
5. Zasloff, M. (1987) Magainins, a class of antimicrobial peptides from *Xenopus* skin: isolation, characterization of two active forms, and partial cDNA sequence of a precursor, *Proc. Natl. Acad. Sci. USA. 84*, 5449-5453.
6. Erspamer, V. & Melchiorri, P. (1980) Active polypeptides: from amphibian skin to gastrointestinal tract and brain of mammals, *Trends Pharmacol. Sci. 1*, 391-395.
7. Cei, J.M., Erspamer, V. & Rosechini, M. (1967) Taxonomic and evolutionary significance of biogenic amines and polypeptides occurring in amphibian skin. I. Neotropical leptodactylid frogs, *Syst. Zool. 16*, 328-342.
8. Daly, J.W. (1998) Thirty years of discovering arthropod alkaloids in amphibian skin, *J. Nat. Prod. 61*, 162-172.
9. Barra, D. & Simmaco, M. (1995) Amphibian skin - a promising resource for antimicrobial peptides, *Trends Biotechnol. 13*, 205-209.
10. Negri, L., Lattanzi, R. & Melchiorri, P. (1995) Production of antinociception by peripheral administration of [Lys^7]dermorphin, a naturally occurring peptide with high affinity for μ-opioid receptors, *Brit. J. Pharmacol. 114*, 57-66.
11. Simmaco, M., Mignogna, G. & Barra, D. (1998) Antimicrobial peptides from amphibian skin: what do they tell us?, *Biopolymers. 47*, 435-450.
12. Bowie, J.H., Wegener, K.L., Chia, B.C.S., Wabnitz, P.A., Carver, J.A., Tyler, M.J. & Wallace, J.C. (1999) Host defence antibacterial peptides from skin secretions of

Australian amphibians. The relationship between structure and activity, *Protein Pept. Lett. 6*, 259-269.

13. Baker, M.A., Maloy, W.L., Zasloff, M. & Jacob, L.S. (1993) Anticancer efficacy of magainin2 and analogue peptides, *Cancer Res. 53*, 3052-3057.
14. Rozek, T., Wegener, K.L., Bowie, J.H., Olver, I.N., Carver, J.A., Wallace, J.C. & Tyler, M.J. (2000) The antibiotic and anticancer active aurein peptides from the Australian Bell Frogs *Litoria aurea* and *Litoria raniformis*. The solution structure of aurein 1.2, *Eur. J. Biochem. 267*, 5330-5341.
15. Pouny, Y., Rapaport, D., Mor, A., Nicolas, P. & Shai, Y. (1992) Interaction of antimicrobial dermaseptin and its fluorescently labeled analogues with phospholipid membranes, *Biochemistry. 31*, 12416-12423.
16. Wegener, K.L., Wabnitz, P.A., Carver, J.A., Bowie, J.H., Chia, B.C.S., Wallace, J.C. & Tyler, M.J. (1999) Host defence peptides from the skin glands of the Australian Blue Mountains tree-frog *Litoria citropa*. Solution structure of the antibacterial peptide citropin 1.1, *Eur. J. Biochem. 265*, 627-637.
17. Wabnitz, P.A., Bowie, J.H., Tyler, M.J., Wallace, J.C. & Smith, B.P. (2000) Differences in the skin peptides of the male and female Australian tree frog *Litoria splendida* - the discovery of the aquatic male sex pheromone splendipherin, together with Phe8 caerulein and a new antibiotic peptide caerin 1.10, *Eur. J. Biochem. 267*, 269-275.
18. Oren, Z. & Shai, Y. (1996) A class of highly potent antibacterial peptides derived from pardaxin, a pore-forming peptide isolated from Moses sole fish *Pardachirus marmoratus*, *Eur. J. Biochem. 237*, 303-310.
19. Hiramatsu, K., Aritaka, N., Hanaki, H., Kawasaki, S., Hosoda, Y., Hori, S., Fukuchi, Y. & Kobayashi, I. (1997) Dissemination in Japanese hospitals of strains of *Staphylococcus aureus* heterogeneously resistant to vancomycin, *Lancet. 350*, 1670-1673.
20. Anastasi, A., Erspamer, V. & Endean, R. (1968) Isolation and amino acid sequence of caerulein, the active decapeptide of the skin of *Hyla caerulea*, *Arch. Biochem. Biophys. 125*, 57-68.
21. Bevins, C.L. & Zasloff, M. (1990) Peptides from frog skin, *Annu. Rev. Biochem. 59*, 395-414.
22. Cei, J.M. (1985) Taxonomic and evolutionary significance of peptides in amphibian skin, *Peptides. 6*, 13-16.

23. Waugh, R.J., Stone, D.J.M., Bowie, J.H., Wallace, J.C. & Tyler, M.J. (1993) Peptides from Australian frogs. The structures of the caerins and caeridins from *Litoria gilleni*, *J. Chem. Res. (S)*, 139.

24. Bowie, J.H., Chia, B.C.S. & Tyler, M.J. (1998) Host defence peptides from the skin glands of Australian amphibians: a powerful chemical arsenal, *Pharmacol. News. 5*, 16-21.

25. Wabnitz, P.A., Bowie, J.H., Wallace, J.C. & Tyler, M.J. (1999) Peptides from the skin glands of the Australian buzzing tree frog *Litoria electrica*. Comparison with the skin peptides of the red tree frog *Litoria rubella*, *Aust. J.Chem. 52*, 639-645.

26. Wabnitz, P.A., Bowie, J.H. & Tyler, M.J. (1999) Caerulein-like peptides from the skin glands of the Australian Blue Mountains tree frog *Litoria citropa*. Part 1. Sequence determination using electrospray mass spectrometry, *Rapid Commun. Mass Spectrom. 13*, 2498-2502.

27. Erspamer, V. (1993) Bioactive secretions of the amphibian integument. In *Amphibian Biology* (Heatwole, H., ed) pp. 178-350, Surrey, Beatty and Sons, Chipping Norton, NSW, Australia.

28. Bradford, A.M., Raftery, M.J., Bowie, J.H., Tyler, M.J., Wallace, J.C., Adams, G.W. & Severini, C. (1996) Novel uperin peptides from the dorsal glands of the Australian floodplain toadlet *Uperoleia inundata*, *Aust. J.Chem. 49*, 475-484.

29. Doyle, J., Llewellyn, L.E., Brinkworth, C.S., Bowie, J.H., Wegener, K.L., Rozek, T., Wabnitz, P.A., Wallace, J.C. & Tyler, M.J. (2001) Amphibian peptides that inhibit neuronal nitric oxide synthase: the isolation of lesueurin from the skin secretion of the Australian Stony Creek Frog *Litoria lesueuri*, *Eur. J. Biochem. in press.*

30. Nicolas, P. & Mor, A. (1995) Peptides as weapons against microorganisms in the chemical defense system of vertebrates, *Annu. Rev. Microbiol. 49*, 277-304.

31. Epand, R.M. & Vogel, H.J. (1999) Diversity of antimicrobial peptides and their mechanisms of action, *Biochim. Biophys. Acta Biomembranes. 1462*, 11-28.

32. Waugh, R.J., Stone, D.J.M., Bowie, J.H., Wallace, J.C. & Tyler, M.J. (1993) Peptides from Australian frogs. Structures of the caeridins from *Litoria caerulea*, *J. Chem. Soc. Perkin Trans. I*, 573-576.

33. Bradford, A.M., Raftery, M.J., Bowie, J.H., Wallace, J.C. & Tyler, M.J. (1993) Peptides from Australian frogs - the structures of the dynastins from *Limnodynastes salmini* and fletcherin from *Limnodynastes fletcheri*, *Aust. J.Chem. 46*, 1235-1244.

34. Steinborner, S.T., Gao, C.W., Raftery, M.J., Waugh, R.J., Blumenthal, T., Bowie, J.H., Wallace, J.C. & Tyler, M.J. (1994) The structures of four tryptophyllin and three rubellidin peptides from the Australian red tree frog *Litoria rubella*, *Aust. J.Chem. 47*, 2099-2108.

35. Barra, D., Simmaco, M. & Boman, H.G. (1998) Gene-encoded peptide antibiotics and innate immunity. Do 'animalcules' have defence budgets?, *FEBS Letters. 430*, 130-134.

36. Sherwood, L. (1993) *Human Physiology From Cells to Systems* 2nd edn, West Publishing Co., Minneapolis/St Paul.

37. Zubay, G. (1986) *Biochemistry*, Addison-Wesley Pub. Co., Massachusetts.

38. Ganz, T. (1994) Biosynthesis of defensins and other antimicrobial peptides. In *Antimicrobial Peptides. Ciba Foundation Symposium 186* (Marsh, J. & Goode, J.A., eds), John Wiley and Sons, London.

39. Boman, H.G. (2000) Innate immunity and the normal microflora, *Immunol. Rev. 173*, 5-16.

40. Sjoberg, E. & Flock, A. (1976) Innervation of Skin Glands in the Frog, *Cell Tissue Res. 172*, 81-91.

41. Erspamer, W., Erspamer, G.F. & Cei, J.M. (1986) Active peptides in the skins of two hundred and thirty American amphibian species, *Comp. Biochem. Physiol. 85C*, 125-137.

42. Erspamer, V., Erspamer, G.F., Mazzanti, G. & Endean, R. (1984) Active peptides in the skins of one hundred amphibian species from Australia and Papua New Guinea, *Comp. Biochem. Physiol. 77C.*

43. Campbell, A. (1999) *Declines and Disappearances of Australian Frogs*, Biodiversity Group, Environment Australia, Canberra.

44. Tyler, M.J. & Davies, M. (1985) In *Biology of Australasian Frogs and Reptiles* (Grigg, G., Shine, R. & Ehmann, H., eds) pp. 469-470, Surrey Beatty and Sons Pty. Ltd., NSW.

45. Tyler, M.J., Stone, D.J.M. & Bowie, J.H. (1992) A novel method for the release and collection of dermal, glandular secretions from the skin of frogs, *J. Pharm. Toxicol. Methods. 28*, 199-200.

46. Blondelle, S.E., Lohner, K. & Aguilar, M.I. (1999) Lipid-induced conformation and lipid-binding properties of cytolytic and antimicrobial peptides: determination and biological specificity, *Biochim. Biophys. Acta Biomembranes. 1462*, 89-108.

47. Hill, H.C. (1966) *Introduction to Mass Spectrometry*, Heyden and Son Limited, London.

48. Williams, D.H. & Fleming, I. (1995) *Spectroscopic Methods in Organic Chemistry*, McGraw-Hill Book Co., London.

49. Dole, M., Mack, L.L. & Hines, R.L. (1968) Molecular beams of macro-ions, *J. Chem. Physics. 49*, 2240-2249.

50. Fenn, J.B., Mann, M., Meng, C.K., Wong, S.F. & Whitehouse, C.M. (1990) Electrospray ionization - principles and practice, *Mass Spectrom. Rev. 9*, 37-70.

51. Smith, R.D., Loo, J.A., Ogorzalek Loo, R.R., Busman, M. & Udseth, H.R. (1991) Principles and practice of electrospray ionization - mass spectrometry for large polypeptides and proteins, *Mass Spectrom. Rev. 10*, 359-451.

52. Cotter, R.J. (1994) Time-of-flight mass spectrometry. In *Time-of-Flight Mass Spectrometry* (Cotter, R.J., ed) pp. 16-48, American Chemical Society, Washington, D.C.

53. Biemann, K. & Martin, S.A. (1987) Mass spectrometric determination of the amino acid sequence of peptides and proteins, *Mass Spectrom. Rev. 6*, 1-76.

54. Roepstorff, P., Hojrup, P. & Moller, J. (1985) Evaluation of fast atom bombardment mass spectrometry for sequence determination of peptides, *Biomed. Mass Spectrometry. 12*, 181-189.

55. Mueller, D.R., Eckersley, M. & Richter, W.J. (1988) Hydrogen transfer reactions in the formation of 'Y+2' sequence ions from protonated peptides, *Org. Mass Spectrom. 23*, 217-222.

56. Hunkapiller, M.W., Hewick, R.M., Dreyer, W.J. & Hood, L.E. (1983) High-sensitivity sequencing with a gas-phase sequenator, *Methods Enzymol. 91*, 399-413.

57. Bodanszky, M. (1988) *Peptide Chemistry. A Practical Textbook*, Springer-Verlag, Berlin.

58. Jorgensen, J.H., Cleeland, W.A., Craig, G., Doern, M., Ferraro, J., Finegold, C.M., Hansen, S.L., Jenkins, S.G., Novick, W.J., Pfaller, M.S., Preston, D.A., Reller, L.B. & Swanson, J.M. (1993) Methods for dilution antimicrobial susceptibility tests for bacteria that grow aerobically, 3rd approved standard. Document M7-A3, *National committee for clinical laboratory standards. 33*, 1-12.

59. Monks, A., Scudiero, D., Skehan, P., Shoemaker, R., Paull, K., Vistica, D., Hose, C., Langley, J., Cronise, P. & Vaigro-Wolff, A. (1991) Feasibility of high-flux

anticancer drug screen using a diverse panel of cultured human tumor cell lines, *J. Nat. Cancer Inst. 83*, 757-766.

60. Tyler, M.J., Smith, L.A. & Johnstone, R.E. (1994) *Frogs of Western Australia*, Western Australian Museum, WA.
61. Barker, J., Grigg, G.C. & Tyler, M.J. (1995) *A Field Guide to Australian Frogs*, Surrey Beatty and Sons, NSW.
62. Tyler, M.J. & Davies, M. (1986) *Frogs of the Northern Territory*, Conservation Commission of the Northern Territory, NT.
63. Tyler, M.J. (1992) *Encyclopedia of Australian Animals. Frogs*, Angus & Robertson, Pymble, NSW.
64. Madsen, T. & Shine, R. (1994) Toxicity of a tropical Australian frog, *Litoria dahlii*, to sympatric snakes, *Wildlife Res. 21*, 21-25.
65. Steinborner, S.T., Wabnitz, P.A., Bowie, J.H. & Tyler, M.J. (1996) The application of mass spectrometry to the study of evolutionary trends in amphibians, *Rapid Commun. Mass Spectrom. 10*, 92-95.
66. Developmental Therapeutics Program, http://dtp.nci.nih.gov, National Cancer Institute, Washington, D.C., USA.
67. Eisenberg, D., Wesson, M. & Wilcox, W. (1989) Hydrophobic moments as tools for analyzing protein sequences and structures. In *Prediction of Protein Structure and Principles of Protein Conformation* (Fasman, G., ed) pp. 635-646, Plenum Press, New York.
68. Segrest, J.P., De Loof, H., Dohlman, J.G., Brouillette, C.G. & Anantharamaiah, G.M. (1990) Amphipathic helix motif: classes and properties, *Proteins Struct. Funct. Genet. 8*, 103-117.
69. Marletta, M.A. (1994) Nitric oxide synthase: aspects concerning structure and catalysis, *Cell. 78*, 729-730.
70. Gorren, A.C.F. & Mayer, B. (1998) The versatile and complex enzymology of nitric oxide synthase, *Biochemistry - Moscow. 63*, 734-743.
71. Marletta, M.A. (1994) Approaches toward selective inhibition of nitric oxide synthase, *J. Med. Chem. 37*, 1903-1907.
72. O'Neil, K.T. & DeGrado, W.F. (1990) How calmodulin binds its targets: sequence independent recognition of amphiphilic α-helices, *Trends Biochem. Sci. 15*, 59-64.

73. Afshar, M., Caves, L.S.D., Guimard, L., Hubbard, R.E., Calas, B., Grassy, G. & Haiech, J. (1994) Investigating the high affinity and low sequence specificity of calmodulin binding to its targets, *J. Mol. Biol. 244*, 554-571.

74. Ikura, M., Clore, G.M., Gronenborn, A.M., Zhu, G., Klee, C.B. & Bax, A. (1992) Solution structure of a calmodulin-target peptide complex by multidimensional NMR, *Science. 256*, 632-638.

75. Comte, M., Maulet, Y. & Cox, J.A. (1983) Ca^{2+}-dependent high-affinity complex formation between calmodulin and melittin, *Biochemical J. 209*, 269-273.

76. Malencik, D.A. & Anderson, S.B. (1983) High affinity binding of the mastoparans by calmodulin, *Biochem. Biophys. Res. Commun. 114*, 50-56.

77. Zhang, M. & Vogel, H.J. (1994) Characterization of the calmodulin-binding domain of rat cerebellar nitric oxide synthase, *J. Biol. Chem. 269*, 981-985.

78. Maeji, N.J., Bray, A.M., Valerio, R.M. & Wang, W. (1995) Larger scale multipin peptide synthesis, *Pept. Res. 8*, 33-38.

79. Clark, D.P., Durell, S., Maloy, W.L. & Zasloff, M. (1994) Ranalexin - a novel antimicrobial peptide from bullfrog (*Rana catesbeiana*) skin, structurally related to the bacterial antibiotic, polymyxin, *J. Biol. Chem. 269*, 10849-10855.

80. Goldman, M.J., Anderson, G.M., Stolzenberg, E.D., Karl, U.P., Zasloff, M. & Wilson, J.M. (1997) Human β-defensin-1 is a salt-sensitive antibiotic in lung that is inactivated in cystic fibrosis, *Cell. 88*, 553-560.

81. Rosebury, T. (1962) *Microorganisms Indigenous to Man*, McGraw-Hill, New York.

82. Moore, K.S., Bevins, C.L., Brasseur, M.M., Tomassini, N., Turner, K., Eck, H. & Zasloff, M. (1991) Antimicrobial peptides in the stomach of *Xenopus laevis*, *J. Biol. Chem. 266*, 19851-19857.

83. Bulet, P., Hetru, C., Dimarcq, J. & Hoffmann, D. (1999) Antimicrobial peptides in insects; structure and function, *Dev. Comp. Immunol. 23*, 329-344.

84. Boman, H.G. (1991) Antibacterial Peptides: Key Components Needed in Immunity, *Cell. 65*, 205-207.

85. Vaz Gomes, A., de Waal, A., Berden, J.A. & Westerhoff, H.V. (1993) Electric potentiation, cooperativity, and synergism of magainin peptides in protein-free liposomes, *Biochemistry. 32*, 5365-5372.

86. Mor, A., Hani, K. & Nicolas, P. (1994) The vertebrate peptide antibiotics dermaseptins have overlapping structural features but target specific microorganisms, *J. Biol. Chem. 269*, 31635-31641.

87. Hancock, R.E.W., Falla, T. & Brown, F. (1995) Cationic Bactericidal Peptides. In *Adv. Microbial Physiol.* (Poole, R.K., ed) pp. 135-175, Academic Press, London.

88. Matsuzaki, K. (1999) Why and how are peptide-lipid interactions utilized for self-defense? Magainins and tachyplesins as archetypes, *Biochim. Biophys. Acta Biomembranes. 1462*, 1-10.

89. Habermann, E. (1972) Bee and wasp venoms, *Science. 177*, 314-322.

90. Dathe, M., Kaduk, C., Tachikawa, E., Melzig, M.F., Wenschuh, H. & Bienert, M. (1998) Proline at position 14 of alamethicin is essential for hemolytic activity, catecholamine secretion from chromaffin cells and enhanced metabolic activity in endothelial cells, *Biochim. Biophys. Acta. 1370*, 175-183.

91. Crease, R. (1989) Righting the Antibiotic Record, *Science. 246*, 883-884.

92. Arseniev, A.S., Barsukov, I.F., Bystrov, V.F., A.L., L. & Ovchinnikov, Y.A. (1985) ^{1}H-NMR study of gramicidin A transmembrane ion channel, *FEBS Letters. 186*, 168-174.

93. Tortora, G.J. (1982) Antimicrobial Drugs. In *Microbiology; an Introduction* (Tortora, G.J., Funke, B.R. & Case, C.L., eds), Benjamin/Cummings Publishing Co. Inc., Menlo Park, California.

94. Hancock, R.E.W. (1997) Peptide antibiotics, *Lancet. 349*, 418-422.

95. Gazit, E., Boman, A., Boman, H.G. & Shai, Y. (1995) Interaction of the mammalian antibacterial peptide cecropin P1 with phospholipid vesicles, *Biochemistry. 34*, 11479-11488.

96. Wu, M., Maier, E., Benz, R. & Hancock, R.E.W. (1999) Mechanism of interaction of different classes of cationic antimicrobial peptides with planar bilayers and with the cytoplasmic membrane of *Escherichia coli*, *Biochemistry. 38*, 7235-7242.

97. Wong, H., Bowie, J.H. & Carver, J.A. (1997) The solution structure and activity of caerin 1.1, an antimicrobial peptide from the Australian green tree frog, *Litoria splendida*, *Eur. J. Biochem. 247*, 545-557.

98. Chia, B.C.S., Carver, J.A., Lindner, R.A., Bowie, J.H., Wong, H. & Lie, W. (2000) Caerin 4.1, an antibiotic peptide from the Australian tree frog, *Litoria caerulea*. The NMR-derived solution structure, *Aust. J.Chem. 53*, 257-265.

99. Chia, B.C.S., Carver, J.A., Mulhern, T.D. & Bowie, J.H. (2000) Maculatin 1.1, an anti-microbial peptide from the Australian tree frog, *Litoria genimaculata* - Solution structure and biological activity, *Eur. J. Biochem. 267*, 1894-1908.

100. Chia, B.C.S., Carver, J.A., Mulhern, T.D. & Bowie, J.H. (1999) The solution structure of uperin 3.6, an antibiotic peptide from the granular dorsal glands of the Australian toadlet, *Uperoleia mjobergii*, *J. Peptide Res. 54*, 137-145.

101. Silvestro, L., Gupta, K., Weiser, J.N. & Axelsen, P.H. (1997) The concentration-dependent membrane activity of cecropin A, *Biochemistry. 36*, 11452-11460.

102. de Waal, A., Vaz Gomes, A., Mensink, A., Grootegoed, J.A. & Westerhoff, H.V. (1991) Magainins affect respiratory control, membrane potential and motility of hamster spermatozoa, *FEBS Letters. 293*, 219-223.

103. Juretic, D., Hendler, R.W., Kamp, F., Caughey, W.S., Zasloff, M. & Westerhoff, H.V. (1994) Magainin oligomers reversibly dissipate $\Delta\mu_{H+}$ in cytochrome oxidase liposomes, *Biochemistry. 33*, 4562-4570.

104. Westerhoff, H.V., Juretic, D., Hendler, R.W. & Zasloff, M. (1989) Magainins and the disruption of membrane-linked free-energy transduction, *Proc. Natl. Acad. Sci. USA. 86*, 6597-6601.

105. Alvarez-Bravo, J., Kurata, S. & Natori, S. (1995) Mode of action of an antibacterial peptide, KLKLLLLLKLK-NH_2, *J. Biochem. 117*, 1312-1316.

106. Tytler, E.M., Anantharamaiah, G.M., Walker, D.E., Mishra, V.K., Palgunachari, M.N. & Segrest, J.P. (1995) Molecular basis for prokaryotic specificity of magainin-induced lysis, *Biochemistry. 34*, 4393-4401.

107. Wade, D., Boman, A., Wahlin, B., Drain, C.M., Andreu, D., Boman, H.G. & Merrifield, R.B. (1990) All-D amino acid-containing channel-forming antibiotic peptides, *Proc. Natl. Acad. Sci. USA. 87*, 4761-4765.

108. Park, C.B., Kim, H.S. & Kim, S.C. (1998) Mechanism of action of the antimicrobial peptide buforin II: buforin II kills microorganisms by penetrating the cell membrane and inhibiting cellular functions, *Biochem. Biophys. Res. Commun. 244*, 253-257.

109. Breukink, E., Wiedemann, I., van Kraaij, C., Kuipers, O.P., Sahl, H. & de Kruijff, B. (1999) Use of the cell wall precursor lipid II by a pore-forming peptide antibiotic, *Science. 286*, 2361-2364.

110. Subbalakshmi, C. & Sitaram, N. (1998) Mechanism of antimicrobial action of indolicidin, *FEMS Microbiol. Lett. 160*, 91-96.

111. Shai, Y. (1999) Mechanism of the binding, insertion and destabilization of phospholipid bilayer membranes by α-helical antimicrobial and cell non-selective membrane-lytic peptides, *Biochim. Biophys. Acta. 1462*, 55-70.

112. Ehrenstein, G. & Lecar, H. (1977) Electrically gated ionic channels in lipid bilayers, *Quart. Rev. Biophys. 10*, 1-34.

113. Sansom, M.S.P. (1991) The biophysics of peptide models of ion channels, *Prog. Biophys. Mol. Biol. 55*, 139-235.

114. Matsuzaki, K., Sugishita, K., Harada, M., Fujii, N. & Miyajima, K. (1997) Interactions of an antimicrobial peptide, magainin 2, with outer and inner membranes of Gram-negative bacteria, *Biochim. Biophys. Acta. 1327*, 119-130.

115. Marion, D., Zasloff, M. & Bax, A. (1988) A two-dimensional NMR study of the antimicrobial peptide magainin 2, *FEBS Letters. 227*, 21-26.

116. Holak, T.A., Engstrom, A., Kraulis, P.J., Lindeberg, G., Bennich, H., Jones, T.A., Gronenborn, A.M. & Clore, G.M. (1988) The solution conformation of the antibacterial peptide cecropin A: a nuclear magnetic resonance and dynamical simulated annealing study, *Biochemistry. 27*, 7620-7629.

117. Epand, R.M., Shai, Y.C., Segrest, J.P. & Anantharamaiah, G.M. (1995) Mechanisms for the modulation of membrane bilayer properties by amphipathic helical peptides, *Biopolymers. 37*, 319-338.

118. Schwarz, G. & Robert, C.H. (1990) Pore formation kinetics in membranes, determined from the release of marker molecules out of liposomes or cells, *Biophys. J. 58*, 577-583.

119. Baumann, G. & Mueller, P. (1974) A molecular model of membrane excitability, *J. Supramol. Struct. 2*, 538-557.

120. Molle, G., Duclohier, H., Julien, S. & Spach, G. (1991) Synthetic analogues of alamethicin: effect of C-terminal residue substitutions and chain length on the ion channel lifetimes, *Biochim. Biophys. Acta. 1064*, 365-369.

121. Mak, D.D. & Webb, W.W. (1995) Two classes of alamethicin transmembrane channels: molecular models form single-channel properties, *Biophys. J. 69*, 2323-2336.

122. Yang, L., Harroun, T.A., Weiss, T.M., Dong, L. & Huang, H.W. (2001) Barrel-stave model or toroidal model? A case study on melittin pores, *Biophys. J. 81*, 1475-1485.

123. North, C.L., Barranger-Mathys, M. & Cafiso, D.S. (1995) Membrane orientation of the N-terminal segment of alamethicin determined by solid-state ^{15}N NMR, *Biophys. J. 69*, 2392-2397.

124. Vogel, H. (1987) Comparison of the conformation and orientation of alamethicin and melittin in lipid membranes, *Biochemistry. 26*, 4562-4571.

125. Huang, H.W. & Wu, Y. (1991) Lipid-alamethicin interactions influence alamethicin orientation, *Biophys. J. 60*, 1079-1087.

126. Huang, H.W. (2000) Action of antimicrobial peptides: two-state model, *Biochemistry. 39*, 8347-8352.

127. He, K., Ludtke, S.J., Huang, H.W. & Worcester, D.L. (1995) Antimicrobial peptide pores in membranes detected by neutron in-plane scattering, *Biochemistry. 34*, 15614-15618.

128. He, K., Ludtke, S.J., Worcester, D.L. & Huang, C.M. (1996) Neutron scattering in the plane of membranes: structure of alamethicin pores, *Biophys. J. 70*, 2659-2666.

129. Vogt, B., Ducarme, P., Schinzel, S., Brasseur, R. & Bechinger, B. (2000) The topology of lysine-containing amphipathic peptides in bilayers by circular dichroism, solid-state NMR and molecular modelling, *Biophys. J. 79*, 2644-2656.

130. Bikshapathy, E., Sitaram, N. & Nagaraj, R. (1999) Addition and omission analogs of the 13-residue antibacterial and hemolytic peptide PKLLKTFLSKWIG: structural preferences, model membrane binding and biological activities, *J. Peptide Res. 53*, 47-55.

131. Mangoni, M.L., Rinaldi, A.C., Giulio, A.D., Mignogna, G., Bozzi, A., Barra, D. & Simmaco, M. (2000) Structure-function relationship of temporins, small antimicrobial peptides from amphibian skin, *Eur. J. Biochem. 267*, 1447-1454.

132. Andreu, D., Ubach, J., Boman, A., Wahlin, B., Wade, D., Merrifield, R.B. & Boman, H.G. (1992) Shortened cecropin A-melittin hybrids - Significant size reduction retains potent antibiotic activity, *FEBS Letters. 296*, 190-194.

133. Anzai, K., Hamasuna, M., Kadono, H., Lee, S., Aoyagi, H. & Kirino, Y. (1991) Formation of ion channels in planar lipid bilayer membranes by synthetic basic peptides, *Biochim. Biophys. Acta. 1064*, 256.

134. Cross, T.A. (1997) Solid-state nuclear magnetic resonance characterization of gramicidin channel structure, *Methods Enzymol. 289*, 672-696.

135. Cruciani, R.A., Barker, J.L., Durell, S.R., Raghunathan, G., Guy, H.R., Zasloff, M. & Stanley, E.F. (1992) Magainin 2, a natural antibiotic from frog skin, forms ion channels in lipid bilayer membranes, *Eur. J. Biochem. 226*, 287-296.

136. Ludtke, S.J., He, K., Heller, W.T., Harroun, T.A., Yang, L. & Huang, H.W. (1996) Membrane pores induced by magainin, *Biochemistry. 35*, 13723-13728.

137. Matsuzaki, K. (1998) Magainins as paradigm for the mode of action of pore forming polypeptides, *Biochim. Biophys. Acta Rev Biomembranes. 10*, 391-400.

138. Matsuzaki, K., Murase, O., Tokuda, H., Funakoshi, S., Fujii, N. & Miyajima, K. (1994) Orientational and aggregational states of magainin 2 in phospholipid bilayers, *Biochemistry. 33*, 3342-3349.

139. Bechinger, B., Zasloff, M. & Opella, S.J. (1993) Structure and orientation of the antibiotic peptide magainin in membranes by solid-state nuclear magnetic resonance spectroscopy, *Protein Sci. 2*, 2077-2084.

140. Ludtke, S.J., He, K., Wu, Y. & Huang, H.W. (1994) Cooperative membrane insertion of magainin correlated with its cytolytic activity, *Biochim. Biophys. Acta. 1190*, 181-184.

141. Matsuzaki, K., Murase, O., Fujii, N. & Miyajima, K. (1995) Translocation of a channel-forming antimicrobial peptide, magainin 2, across lipid bilayers by forming a pore, *Biochemistry. 34*, 6521-6526.

142. Matsuzaki, K., Murase, O., Fujii, N. & Miyajima, K. (1996) An antimicrobial peptide, magainin 2, induced rapid flip-flop of phospholipids coupled with pore formation and peptide translocation, *Biochemistry. 35*, 11361-11368.

143. Smith, R., Separovic, F., Milne, T.J., Whittaker, A., Bennett, F.M., Cornell, B.A. & Makriyannis, A. (1994) Structure and orientation of the pore-forming peptide, melittin, in lipid bilayers, *J. Mol. Biol. 241*, 456-466.

144. Mellor, I.R. & Sansom, M.S.P. (1990) Ion-channel properties of mastoparan, 14-residue peptide from wasp venom, and of MP3, a 12-residue analogue, *Proc. R. Soc. Lond. B. 239*, 383-400.

145. Lear, J.D., Wasserman, Z.R. & DeGrado, W.F. (1988) Synthetic amphiphilic peptide models for protein ion channels, *Science. 240*, 1177-1181.

146. Blondelle, S.E. & Houghten, R.A. (1992) Design of model amphipathic peptides having potent antimicrobial activities, *Biochemistry. 31*, 12688-12694.

147. Castano, S., Cornut, I., Buttner, K., Dasseux, J.L. & Dufourcq, J. (1999) The amphipathic helix concept: length effects on ideally amphipathic $L_iK_j(i=2j)$ peptides to acquire optimal hemolytic activity, *Biochim. Biophys. Acta. 1416*, 161-175.

148. Castano, S., Desbat, B., Laguerre, M. & Dufourcq, J. (1999) Structure, orientation and affinity for interfaces and lipids of ideally amphipathic lytic $L_iK_j(i=2j)$ peptides, *Biochim. Biophys. Acta. 1416*, 176-194.

149. Bechinger, B. (1996) Towards membrane protein design - pH-sensitive topology of histidine-containing polypeptides, *J. Mol. Biol. 263*, 768-775.

150. Vogt, T.C.B. & Bechinger, B. (1999) The interactions of histidine-containing amphipathic helical peptide antibiotics with lipid bilayers, *J. Biol. Chem. 274*, 29115-29121.

151. Shai, Y. & Oren, Z. (2001) From "carpet" mechanism to de-novo designed diastereomeric cell-selective antimicrobial peptides, *Peptides. 22*, 1629-1641.

152. Bechinger, B. (1999) The structure, dynamics and orientation of antimicrobial peptides in membranes by multidimensional solid-state NMR spectroscopy, *Biochim. Biophys. Acta. 1462*, 157-183.

153. Gazit, E., Lee, W.J., Brey, P.T. & Shai, Y.C. (1994) Mode of action of the antibacterial cecropin B2 - a spectrofluorometric study, *Biochemistry. 33*, 10681-10692.

154. Marassi, F.M., Opella, S.J., Juvvadi, P. & Merrifield, R.B. (1999) Orientation of cecropin A helices in phospholipid bilayers determined by solid-state NMR spectroscopy, *Biophys. J. 77*, 3152-3155.

155. Gazit, E., Miller, I.R., Biggin, P.C., Sansom, M.S.P. & Shai, Y. (1996) Structure and orientation of the mammalian antibacterial peptide cecropin P1 within phospholipid membranes, *J. Mol. Biol. 258*, 860-870.

156. Steiner, H., Andreu, D. & Merrifield, R.B. (1988) Binding and action of cecropin and cecropin analogues: antibacterial peptides from insects, *Biochim. Biophys. Acta. 939*, 260-266.

157. Oren, Z., Hong, J. & Shai, Y. (1997) A repertoire of novel antibacterial diastereomeric peptides with selective cytolytic activity, *J. Biol. Chem. 272*, 14643-14649.

158. Unger, T., Oren, Z. & Shai, Y. (2001) The effect of cyclization of magainin 2 and melittin analogues on structure, function and model membrane interactions: implication to their mode of action, *Biochemistry. 40*, 6388-6397.

159. Chen, H., Brown, J.H., Morell, J.L. & Huang, C.M. (1988) Synthetic magainin analogues with improved antimicrobial activity, *FEBS Letters. 236*, 462-466.

160. Dempsey, C.E. (1990) The actions of melittin on membranes, *Biochim. Biophys. Acta. 1031*, 143-161.

161. Hammond, S.M., Lambert, P.A. & Rycroft, A.N. (1984) *The Bacterial Cell Surface*, Kapiton Szabo Publishers, London.

162. Lugtenberg, B. & Van Alphen, L. (1983) Molecular architecture and functioning of the outer membrane of *Escherichia coli* and other Gram-negative bacteria, *Biochim. Biophys. Acta. 737*, 51-115.

163. Gennis, R.B. (1989) The structure and properties of membrane lipids. In *Biomembranes: Molecular Structure and Function* pp. 154-158, Springer-Verlag, New York.

164. Ghosh, A.K., Rukmini, R. & Chattopadhyay, A. (1997) Modulation of tryptophan environment in membrane-bound melittin by negatively charged phospholipids: implications in membrane organization and function, *Biochemistry. 36*, 14291-14305.

165. Nakajima, Y., Qu, X. & Natori, S. (1987) Interaction between liposomes and sarcotoxin IA, a potent antibacterial protein of *Sarcophaga peregrina* (Flesh Fly), *J. Biol. Chem. 262*, 1665-1669.

166. Skerlavaj, B., Romeo, D. & Gennaro, R. (1990) Rapid membrane permeabilization and inhibition of vital functions of Gram-negative bacteria by bactenecins, *Infection and Immunity. 58*, 3724-3730.

167. Matsuzaki, K., Harada, M., Funakoshi, S., Fujii, N. & Miyajima, K. (1991) Physiochemical determinants for the interactions of magainins 1 and 2 with acidic lipid bilayers, *Biochim. Biophys. Acta. 1063*, 162-170.

168. Matsuzaki, K., Harada, M., Handa, T., Funakoshi, S., Fujii, N., Yajima, H. & Miyajima, K. (1989) Magainin 1-induced leakage of entrapped calcein out of negatively-charged lipid vesicles, *Biochim. Biophys. Acta. 981*, 130-134.

169. Peschel, A., Otto, M., Jack, R.W., Kalbacher, H., Jung, G. & Gotz, F. (1999) Inactivation of the *dlt* operon in *Staphylococcus aureus* confers sensitivity to defensins, protegrins and other antimicrobial peptides, *J. Biol. Chem. 274*, 8405-8410.

170. Nikaido, H. & Hancock, R.E.W. (1986) Outer membrane permeability of *Pseudomonas aeruginosa*. In *The Bacteria: A Treatise on Structure and Function*

(Gunsalus, I.C., Sokatch, J.R. & Ornstan, L.N., eds) pp. 145-183, Academic Press, New York.

171. Hancock, R.E.W., Piers, K., Brown, M., Falla, T., Gough, M., Wu, M. & Fidai, S. (1996) Cationic peptides: a class of antibiotics able to access the self-promoted uptake pathway across the *Pseudomonas aeruginosa* outer membrane. In *Molecular Biology of Pseudomonads* (Nakazawa, N., ed) pp. 441-450, ASM Press, Washington, DC.
172. Piers, K.L. & Hancock, R.E.W. (1994) The interaction of a recombinant cecropin/melittin hybrid peptide with the outer membrane of *Pseudomonas aeruginosa*, *Mol. Microbiol. 12*, 951-958.
173. Matsuzaki, K., Sugishita, K. & Miyajima, K. (1999) Interactions of an antimicrobial peptide, magainin 2, with lipopolysaccharide-containing liposomes as a model for outer membranes of Gram-negative bacteria, *FEBS Letters. 449*, 221-224.
174. Sawyer, J.G., Martin, N.L. & Hancock, R.E.W. (1988) Interaction of macrophage cationic proteins with the outer membrane of *Pseudomonas aeruginosa*, *Infect. Immun. 56*, 693-698.
175. Rana, F.R. & Blazyk, J. (1991) Interactions between the antimicrobial peptide, magainin 2, and *Salmonella typhimurium* lipopolysaccharides, *FEBS Letters. 293*, 11-15.
176. Tossi, A., Tarantino, C. & Romeo, D. (1997) Design of synthetic antimicrobial peptides based on sequence analogy and amphipathicity, *Eur. J. Biochem. 250*, 549-558.
177. Matsuzaki, K., Sugishita, K., Fujii, N. & Miyajima, K. (1995) Molecular basis for membrane selectivity of an antimicrobial peptide, magainin 2, *Biochemistry. 34*, 3423-3429.
178. Christensen, B., Fink, J., Merrifield, R.B. & Mauzerall, D. (1988) Channel-forming properties of cecropins and related model compounds incorporated into planar lipid membranes, *Proc. Natl. Acad. Sci. USA. 85*, 5072-5076.
179. Szabo, G. (1974) Dual mechanism for the action of cholesterol on membrane permeability, *Nature. 252*, 47-49.
180. Urbina, J.A., Pekerar, S., Le, H., Patterson, J., Montez, B. & Oldfield, E. (1995) Molecular order and dynamics of phosphatidylcholine bilayer membranes in the presence of cholesterol, ergosterol and lanosterol: a comparative study using ^{2}H-, ^{13}C- and ^{31}P-NMR spectroscopy, *Biochim. Biophys. Acta. 1238*, 163-176.

181. Kagan, B.L., Selsted, M.E., Ganz, T. & Lehrer, R.I. (1990) Antimicrobial defensin peptides form voltage-dependent ion-permeable channels in planar lipid bilayer membranes, *Proc. Natl. Acad. Sci. USA. 87*, 210-214.

182. Cruciani, R.A., Barker, J.L., Zasloff, M., Chen, H. & Colamonici, O. (1991) Antibiotic magainins exert cytolytic activity against transformed cell lines through channel formation, *Proc. Natl. Acad. Sci. USA. 88*, 3792-3796.

183. Utsugi, T., Schroit, A.J., Connor, J., Bucana, C.D. & Fidler, I.J. (1991) Elevated expression of phosphatidylserine in the outer membrane leaflet of human tumor cells and recognition by activated human blood monocytes, *Cancer Res. 51*, 3062-3066.

184. Li, Z., Merrifield, R.B., Boman, I.A. & Boman, H.G. (1988) Effects on electrophoretic mobility and antibacterial spectrum of removal of two residues from synthetic sarcotoxin IA and addition of the same residues to cecropin B, *FEBS Letters. 231*, 299-302.

185. Maloy, W.L. & Kari, U.P. (1995) Structure-activity studies on magainins and other host defense peptides, *Biopolymers. 37*, 105-122.

186. Shoemaker, K.R., Kim, P.S., York, E.J., Stewart, J.M. & Baldwin, R.L. (1987) Tests of the helix dipole model for stabilization of α-helices, *Nature. 326*, 563-567.

187. Fairman, R., Shoemaker, K.R., York, E.J., Stewart, J.M. & Baldwin, R.L. (1989) Further studies of the helix dipole model: effects of a free α-NH_3^+ or α-COO^- group on helix stability, *Proteins Struct. Funct. Genet. 5*, 1-7.

188. Venkatachalapathi, Y.V., Philips, M.C., Epand, R.M., Epand, R.F., Tytler, E.M., Segrest, J.P. & Anantharamaiah, G.M. (1993) Effect of end group blockage on the properties of a class A amphipathic helical peptide, *Proteins Struct. Funct. Genet. 15*, 349-359.

189. Chou, P.Y. & Fasman, G.D. (1978) Empirical predictions of protein conformation, *Annu. Rev. Biochem. 47*, 251-276.

190. Andreu, D. & Merrifield, R.B. (1985) N-terminal analogues of cecropin A: synthesis, antibacterial activity, and conformational properties, *Biochemistry. 24*, 1683-1688.

191. Dathe, M. & Wieprecht, T. (1999) Structural features of helical antimicrobial peptides: their potential to modulate activity on model membranes and biological cells, *Biochim. Biophys. Acta Biomembranes. 1462*, 71-87.

192. Wieprecht, T., Dathe, M., Schumann, M., Krause, E., Beyermann, M. & Bienert, M. (1996) Conformational and functional study of magainin 2 in model membrane environments using the new approach of systematic double-D-amino acid replacement, *Biochemistry. 35*, 10844-10853.

193. Dathe, M., Schumann, M., Wieprecht, T., Winkler, A., Beyermann, M., Krause, E., Matsuzaki, K., Murase, O. & Bienert, M. (1996) Peptide helicity and membrane surface charge modulate the balance of electrostatic and hydrophobic interactions with lipid bilayers and biological membranes, *Biochemistry. 35*, 12612-12622.

194. Shai, Y. & Oren, Z. (1996) Diastereomers of cytolysins, a novel class of potent antibacterial peptides, *J. Biol. Chem. 271*, 7305-7308.

195. Sitaram, N. & Nagaraj, R. (1999) Interaction of antimicrobial peptides with biological and model membranes: structural and charge requirements for activity, *Biochim. Biophys. Acta Biomembranes. 1462*, 29-54.

196. Thennarasu, S. & Nagaraj, R. (1995) Design of 16-residue peptides possessing antimicrobial and hemolytic activities or only antimicrobial activity from an inactive peptide, *Int. J. Peptide Protein Res. 46*, 480-486.

197. Eisenberg, D. (1984) Three-dimensional structure of membrane and surface proteins, *Annu. Rev. Biochem. 53*, 595-623.

198. Wieprecht, T., Dathe, M., Beyermann, M., Krause, E., Maloy, W.L., MacDonald, D.L. & Bienert, M. (1997) Peptide hydrophobicity controls the activity and selectivity of magainin 2 amide in interaction with membranes, *Biochemistry. 36*, 6133-6140.

199. Dathe, M., Wieprecht, T., Nikolenko, H., Handel, L., Maloy, W.L., MacDonald, D.L., Beyermann, M. & Bienert, M. (1997) Hydrophobicity, hydrophobic moment and angle subtended by charged residues modulate antibacterial and haemolytic activity of amphipathic helical peptides, *FEBS Letters. 403*, 208-212.

200. Eisenberg, D., Weiss, R.M. & Terwilliger, T.C. (1982) The helical hydrophobic moment: a measure of the amphiphilicity of a helix, *Nature. 299*, 371-374.

201. Subbalakshmi, C., Nagaraj, R. & Sitaram, N. (1999) Biological activities of C-terminal 15-residue synthetic fragment of melittin: design of an analog with improved antibacterial activity, *FEBS Letters. 448*, 62-66.

202. Pérez-Payá, E., Houghten, R.A. & Blondelle, S.E. (1995) The role of amphipathicity in the folding, self-association and biological activity of multiple subunit small proteins, *J. Biol. Chem. 270*, 1048-1056.

203. Wieprecht, T., Dathe, M., Krause, E., Beyermann, M., Maloy, W.L., MacDonald, D.L. & Bienert, M. (1997) Modulation of membrane activity of amphipathic, antibacterial peptides by slight modifications of the hydrophobic moment, *FEBS Letters. 417*, 135-140.

204. Pathak, N., Salasauvert, R., Ruche, G., Janna, M.H., McCarthy, D. & Harrison, R.G. (1995) Comparison of the effects of hydrophobicity, amphiphilicity, and alpha-helicity on the activities of antimicrobial peptides, *Proteins Struct. Funct. Genet. 22*, 182-186.

205. Wieprecht, T., Dathe, M., Epand, R.M., Beyermann, M., Krause, E., Maloy, W.L., MacDonald, D.L. & Bienert, M. (1997) Influence of the angle subtended by the positively charged helix face on the membrane activity of amphipathic, antibacterial peptides, *Biochemistry. 36*, 12869-12880.

206. Gesell, J., Zasloff, M. & Opella, S.J. (1997) Two-dimensional ^{1}H NMR experiments show that the 23-residue magainin antibiotic peptide is an alpha-helix in dodecylphosphocholine micelles, sodium dodecylsulfate micelles, and trifluoroethanol/water solution, *J. Biomol. NMR. 9*, 127-135.

207. Bechinger, B., Zasloff, M. & Opella, S.J. (1998) Structure and dynamics of the antibiotic peptide PGLa in membranes by solution and solid-state nuclear magnetic resonance spectroscopy, *Biophys. J. 74*, 981-987.

208. Shin, S.Y., Kang, J.H., Jang, S.Y., Kim, Y., Kim, K.L. & Hahm, K. (2000) Effects of the hinge region of cecropin A(1-8)-magainin 2(1-12), a synthetic antimicrobial peptide, on liposomes, bacterial and tumor cells, *Biochim. Biophys. Acta. 1463*, 209-218.

209. Pastore, A., Harvey, T.S., Dempsey, C.E. & Campbell, I.D. (1989) The dynamic properties of melittin in solution, *Eur. J. Biochem. 16*, 363-367.

210. Woolfson, D.N. & Williams, D.H. (1990) The influence of proline residues on α-helical structure, *FEBS Letters. 277*, 185-188.

211. Ikura, T., Go, N. & Inagaki, F. (1991) Refined structure of melittin bound to perdeuterated dodecylphosphocholine micelles as studied by 2D-NMR and distance geometry calculation, *Proteins Struct. Funct. Genet. 9*, 81-91.

212. Esposito, G., Carver, J.A., Boyd, J. & Campbell, I.D. (1986) High-resolution ^{1}H NMR study of the solution structure of alamethicin, *Biochemistry. 26*, 1043-1050.

213. Oh, D., Shin, S.Y., Lee, S., Kang, J.H., Kim, S.D., Ryu, P.D., Hahm, K. & Kim, Y. (2000) Role of the hinge region and the tryptophan residue in the synthetic antimicrobial peptides, cecropin A(1-8)-magainin 1(1-12) and its analogues, on their antibiotic activities and structures, *Biochemistry. 39*, 11855-11864.

214. Fink, J., Boman, A., Boman, H.G. & Merrifield, R.B. (1989) Design, synthesis and antibacterial activity of cecropin-like model peptides, *Int. J. Peptide Protein Res. 33*, 412-421.

215. Inagaki, F., Shimada, I., Kawaguchi, K., Hirano, M., Terasawa, I., Ikura, T. & Go, N. (1989) Structure of melittin bound to perdeuterated dodecylphosphocholine micelles as studied by two-dimensional NMR and distance geometry calculations, *Biochemistry. 28*, 5985-5991.

216. Park, C.B., Yi, K., Matsuzaki, K., Kim, M.S. & Kim, S.C. (2000) Structure-activity analysis of buforin II, a histone H2A-derived antimicrobial peptide: the proline hinge is responsible for the cell-penetrating ability of buforin II, *Proc. Natl. Acad. Sci. 97*, 8245-8250.

217. Oh, D., Shin, S.Y., Kang, J.H., Hahm, K., Kim, K.L. & Kim, Y. (1999) NMR structural characterization of cecropin A(1-8) - magainin 2(1-12) and cecropin A(1-8) - melittin(1-12) hybrid peptides, *J. Peptide Res. 53*, 578-589.

218. Nilges, M. & O'Donoghue, S.I. (1998) Ambiguous NOEs and automated NOE assignment, *Prog. Nucl. Magn. Reson. Spectrosc. 32*, 107-139.

219. Kaptein, R., Boelens, R., Scheek, R.M. & van Gunsteren, W.F. (1988) Protein structures from NMR, *Biochemistry. 27*, 5389-5395.

220. Wider, G. (2000) Structure determination of biological macromolecules in solution using nuclear magnetic resonance spectroscopy, *Biotechniques. 29*, 1278-1294.

221. Johnson (Jr), G.S. (1990) Protein secondary structure and circular dichroism: a practical guide, *Proteins Struct. Funct. Genet. 7*, 205-214.

222. Creighton, T.E. (1993) *Proteins, Structures and Molecular Properties* 2nd edn, W.H. Freeman and Co., New York.

223. Crabbe, P. (1965) *Optical Rotatory Dispersion and Circular Dichroism in Organic Chemistry*, Holden-Day, San Francisco.

224. Creighton, T.E. (1989) *Protein Structure: A Practical Approach*, Oxford University Press, Oxford.

225. Blout, E.R. (1973) Polypeptides and Proteins. In *Fundamental Aspects and Recent Developments in Optical Rotatory Dispersion and Circular Dichroism* (Ciardell, F. & Salvadori, P., eds) pp. 352-372, Heyden and Son Ltd., London.

226. Olah, G.A. & Huang, H.W. (1988) Circular dichroism of oriented α helices. I. Proof of exciton theory, *J. Chem. Phys. 89*, 2531-2538.

227. Mason, S.F. (1982) *Molecular Optical Activity and the Chiral Discriminations*, Cambridge University Press, Cambridge.

228. Chen, Y., Yang, J.T. & Martinez, H.M. (1972) Determination of the secondary structures of proteins by circular dichroism and optical rotatory dispersion, *Biochemistry. 11*, 4120-4131.

229. Sonnichsen, F.D., Van Eyk, J.A., Hodges, R.S. & Sykes, B.D. (1992) Effect of trifluoroethanol on protein secondary structure: an NMR and CD study using a synthetic actin peptide, *Biochemistry. 31*, 8790-8798.

230. Evans, J.N.S. (1995) *Biomolecular NMR Spectroscopy*, Oxford University Press, Oxford.

231. Derome, A.E. (1987) *Modern NMR Techniques for Chemistry Research*, Permagon Press Ltd., Oxford.

232. Redfield, C. (1993) Resonance assignment strategies for small proteins. In *NMR of Macromolecules: A Practical Approach* (Roberts, G.C.K., ed), Oxford University Press, New York.

233. Marion, D. & Wüthrich, K. (1983) Application of phase sensitive two-dimensional correlated spectroscopy (COSY) for measurements of ^{1}H-^{1}H spin-spin coupling constants in proteins, *Biochem. Biophys. Res. Commun. 113*, 967-974.

234. Rance, M., Sorensen, O.W., Bodenhausen, G., Wagner, G., Ernst, R.R. & Wüthrich, K. (1983) Improved spectral resolution in COSY ^{1}H NMR spectra of proteins via double quantum filtering, *Biochem. Biophys. Res. Commun. 117*, 479-485.

235. Davis, D.G. & Bax, A. (1985) Assignment of complex ^{1}H NMR spectra via two-dimensional homonuclear Hartmann-Hahn spectroscopy, *J. Am. Chem. Soc. 107*, 2820-2821.

236. Griesinger, C., Otting, G., Wüthrich, K. & Ernst, R.R. (1988) Clean TOCSY for ^{1}H spin system identification in macromolecules, *J. Am. Chem. Soc. 110*, 7870-7872.

237. Kay, L.E., Keifer, P. & Saarinen, T. (1992) Pure absorption gradient enhanced heteronuclear single quantum correlation spectroscopy with improved sensitivity, *J. Am. Chem. Soc. 114*, 10663-10665.

238. Braun, W., Bosch, C., Brown, L.R., Go, N. & Wüthrich, K. (1981) Combined use of proton-proton Overhauser enhancements and a distance geometry algorithm for determination of polypeptide conformations - application to micelle-bound glucagon, *Biochim. Biophys. Acta. 667*, 377-396.

239. Jeener, J. (1979) Investigation of exchange processes by two-dimensional NMR spectroscopy, *J. Chem. Phys. 71*, 4546-4553.

240. Wagner, R. & Berger, S. (1996) Gradient-selected NOESY - a fourfold reduction of the measurement time for the NOESY experiment, *J. Magn. Res. A. 123*, 119-121.

241. Kalk, A. & Berendsen, H.J.C. (1976) Proton magnetic relaxation and spin diffusion in proteins, *J. Magn. Res. 24*, 343-366.

242. Wüthrich, K. (1986) *NMR of Proteins and Nucleic Acids*, John Wiley & Sons, New York.

243. Wishart, D.S., Bigam, C.G., Holm, A., Hodges, R.S. & Sykes, B.D. (1995) H-1, C-13 and N-15 random coil NMR chemical shifts of the common amino acids.1. Investigations of nearest-neighbor effects, *J. Biomol. NMR. 5*, 67-81.

244. Wishart, D.S., Sykes, B.D. & Richards, F.M. (1991) Relationship between nuclear magnetic resonance chemical shift and protein secondary structure, *J. Mol. Biol. 222*, 311-333.

245. Zhou, N.E., Zhu, B., Sykes, B.D. & Hodges, R.S. (1992) Relationship between amide proton chemical shifts and hydrogen bonding in amphipathic α-helical peptides, *J. Am. Chem. Soc. 114*, 4320-4326.

246. Pastore, A. & Saudek, V. (1990) The relationship between chemical shift and secondary structure in proteins, *J. Magn. Res. 90*, 165-176.

247. Merutka, G., Dyson, H.J. & Wright, P.E. (1995) Random coil H-1 chemical shifts obtained as a function of temperature and trifluoroethanol concentration for the peptide series GGXGG, *J. Biomol. NMR. 5*, 14-24.

248. Kuntz, I.D., Kosen, P.A. & Craig, E.C. (1991) Amide chemical shifts in many helices in peptides and proteins are periodic, *J. Am. Chem. Soc. 113*, 1406-1408.

249. Blundell, T., Barlow, D., Borkakoti, N. & Thornton, J. (1983) Solvent-induced distortions and the curvature of α-helices, *Nature. 306*, 281-283.

250. Chakrabarti, P., Bernard, M. & Rees, D.C. (1986) Peptide-bond distortions and the curvature of α-helices, *Biopolymers. 25*, 1087-1093.

251. Barsukov, I.L. & Lian, L. (1993) Structure determination from NMR data. I. Analysis of NMR data. In *NMR of Macromolecules: A Practical Approach* (Roberts, G.C.K., ed) pp. 315-357, Oxford University Press, New York.

252. Karplus, M. (1959) *J. Chem. Phys. 30*, 11. Contact electron-spin coupling of nuclear magnetic moments.

253. Pardi, A., Billeter, M. & Wüthrich, K. (1984) Calibration of the angular dependence of the amide proton-Cα coupling constants, $^3J_{HN\alpha}$, in a globular protein, *J. Mol. Biol. 180*, 741-751.

254. Richardson, J.S. (1981) The anatomy and taxonomy of protein structure, *Adv. Protein Chem. 34*, 167-339.

255. Sutcliffe, M.J. (1993) Structure determination from NMR data II. Computational approaches. In *NMR of Macromolecules: A Practical Approach* (Roberts, G.C.K., ed) pp. 359-390, Oxford University Press, New York.

256. Kim, Y. & Prestegard, J.H. (1989) Measurement of vicinal couplings from cross peaks in COSY spectra, *J. Magn. Res. 84*, 9-13.

257. Andrec, M. & Prestegard, J.H. (1998) Metropolis Monte Carlo implementation of bayesian time-domain parameter estimation - application to coupling constant estimation from antiphase multiplets, *J. Magn. Res. 130*, 217-232.

258. Lian, L.Y. & Barsukov, I.L. (1995) NMR and dynamics of biopolymers. In *Dynamics of Solutions and Fluid Mixtures by NMR* (Delpuech, J., ed) pp. 439-477, Wiley, Chichester.

259. Dempsey, C.E. (1995) Hydrogen bond stabilities in the isolated alamethicin helix: pH-dependent amide exchange measurements in methanol, *J. Am. Chem. Soc. 117*, 7526-7534.

260. Zhang, Y., Lewis, R.N.A.H., Henry, G.D., Sykes, B.D., Hodges, R.S. & McElhaney, R.N. (1995) Peptide models of helical hydrophobic transmembrane segments of membrane proteins. I. Studies of the conformation, intrabilayer orientation, and amide hydrogen exchangeability of Ac-K_2-$(LA)_{12}$-K_2-amide, *Biochemistry. 34*, 2348-2361.

261. Doak, D.G., Mulvey, D., Kawaguchi, K., Villalain, J. & Campbell, I.D. (1996) Structural studies of synthetic peptides dissected from the voltage-gated sodium channel, *J. Mol. Biol. 258*, 672-687.

262. Fregeau Gallagher, N.L., Sailer, M., Niemezura, W.P., Nakashima, T.T., Stiles, M.E. & Vederas, J.C. (1997) Three-dimensional structure of leucocin A in trifluoroethanol and dodecylphosphocholine micelles: Spatial location of residues critical for biological activity in type IIa bacteriocins from lactic acid bacteria, *Biochemistry. 36*, 15062-15072.

263. Fernandez, I., Ubach, J., Fuxreiter, M., Andreu, J.M., Andreu, D. & Pons, M. (1996) Conformation and self-association of a hybrid peptide of cecropin A and melittin with improved antibiotic activity, *Chem. Eur. J. 2*, 838-846.

264. Iwai, H., Nakajima, Y., Natori, S., Arata, Y. & Shimada, I. (1993) Solution conformation of an antibacterial peptide, sarcotoxin-IA, as determined by H-1-NMR, *Eur. J. Biochem. 217*, 639-644.

265. Mulhern, T.D., Howlett, G.J., Reid, G.E., Simpson, R.J., McColl, D.J., Anders, R.F. & Norton, R.S. (1995) Solution structure of a polypeptide containing four heptad repeat units from a merozoite surface antigen of *Plasmodium falciparum*, *Biochemistry. 34*, 3479-3491.

266. Xu, R.X., Word, J.M., Davis, D.G., Rink, M.J., Willard, D.H. & Gampe, R.T. (1995) Solution structure of the human $pp60^{c\text{-}src}$ SH2 domain complexed with a phosphorylated tyrosine pentapeptide, *Biochemistry. 34*, 2107-2121.

267. Clore, G.M. & Gronenborn, A.M. (1989) Determination of three-dimensional structures of proteins and nucleic acids in solution by nuclear magnetic resonance spectroscopy, *Crit. Rev. Biochem. Mol. Biol. 24*, 479-564.

268. Weaver, J.L. & Prestegard, J.H. (1998) Nuclear magnetic resonance structural and ligand binding studies of BLBC, a two-domain fragment of barley lectin, *Biochemistry. 37*, 116-128.

269. Weber, P.L., Morrison, R. & Hare, D. (1988) Determining stereo-specific ^{1}H nuclear magnetic resonance assignments from distance geometry calculations, *J. Mol. Biol. 204*, 483-487.

270. Zuiderweg, E.R.P., Boelens, R. & Kaptein, R. (1985) Stereospecific assignments of ^{1}H-NMR methyl lines and conformation of valyl residues in the *lac* repressor headpiece, *Biopolymers. 24*, 601-611.

271. Folmer, R.H.A., Hilbers, C.W., Konings, R.N.H. & Nilges, M. (1997) Floating stereospecific assignment revisited - application to an 18 kda protein and comparison with J-coupling data, *J. Biomol. NMR. 9*, 245-258.

272. Wüthrich, K., Billeter, M. & Braun, W. (1983) Pseudo-structures for the 20 common amino acids for use in studies of protein conformations by measurements of intramolecular proton-proton distance constraints with nuclear magnetic resonance, *J. Mol. Biol. 169*, 949-961.

273. Nilges, M., Clore, G.M. & Gronenborn, A.M. (1988) Determination of three-dimensional structures of proteins from interproton distance data by dynamical simulated annealing from a random array of atoms - circumventing problems associated with folding, *FEBS Letters. 239*, 129-136.

274. Nilges, M. (1995) Calculation of protein structures with ambiguous distance restraints. Automated assignment of ambiguous NOE crosspeaks and disulphide connectivities, *J. Mol. Biol. 245*, 645-660.

275. Karplus, M. & Petsko, G.A. (1990) Molecular dynamics simulations in biology, *Nature. 347*, 631-639.

276. Haile, J.M. (1992) *Molecular Dynamics Simulation - Elementary Methods*, John Wiley & Sons, Inc., New York.

277. Pallaghy, P.K., Duggan, B.M., Pennington, M.W. & Norton, R.S. (1993) Three-dimensional structure in solution of the calcium channel blocker ω-conotoxin, *J. Mol. Biol. 234*, 405-420.

278. Hyberts, S.G., Goldberg, M.S., Havel, T.F. & Wagner, G. (1992) The solution structure of eglin C based on measurements of many NOEs and coupling constants and its comparison with X-ray structures, *Protein Sci. 1*, 736-751.

279. Ramachandran, G.N., Ramakrishnan, C. & Sasisekharan, V. (1963) Stereochemistry of polypeptide chain configurations, *J. Mol. Biol. 7*, 95-99.

280. Morris, A.L., MacArthur, M.W., Hutchinson, E.G. & Thornton, J.M. (1992) Stereochemical quality of protein structure coordinates, *Proteins Struct. Funct. Genet. 12*, 345-364.

281. Lauterwein, J., Bosch, C., Brown, L.R. & Wüthrich, K. (1979) Physicochemical studies of the protein-lipid interactions in melittin-containing micelles, *Biochim. Biophys. Acta. 556*, 244-264.

282. Mendz, G.L., Moore, W.J., Brown, L.R. & Martenson, R.E. (1984) Interaction of myelin basic protein with micelles of dodecylphosphocholine, *Biochemistry. 23*, 6041-6046.

283. Brown, L.R. (1979) Use of fully deuterated micelles for conformational studies of membrane proteins by high resolution ^{1}H nuclear magnetic resonance, *Biochim. Biophys. Acta. 557*, 135-148.

284. Opella, S.J., Chirlian, L.E. & Bechinger, B. (1997) A solid-state NMR approach to structure determination of membrane-associated peptides and proteins. In *Biological NMR Spectroscopy* pp. 161-179, Oxford University Press, New York.

285. Cross, T.A. & Opella, S.J. (1994) Solid-state NMR structural studies of peptides and proteins in membranes, *Curr. Opin. Struct. Biol. 4*, 574-581.

286. Rajan, R. & Balaram, P. (1996) A model for the interaction of trifluoroethanol with peptides and proteins, *Int. J. Peptide Protein Res. 48*, 328-336.

287. Hong, D.P., Hoshino, M., Kuboi, R. & Goto, Y. (1999) Clustering of fluorine-substituted alcohols as a factor responsible for their marked effects on proteins and peptides, *J. Am. Chem. Soc. 121*, 8427-8433.

288. Nelson, J.W. & Kallenbach, N.R. (1986) Stabilization of the ribonuclease S-peptide α-helix by trifluoroethanol, *Proteins Struct. Funct. Genet. 1*, 211-217.

289. Hirota, N., Mizuno, K. & Goto, Y. (1998) Group additive contributions to the alcohol-induced alpha-helix formation of melittin - implication for the mechanism of the alcohol effects on proteins, *J. Mol. Biol. 275*, 365-378.

290. Schonbrunner, N., Wey, J., Engels, J., Georg, H. & Kiefhaber, T. (1996) Native-like β-structure in a trifluoroethanol-induced partially folded state of the all-β-sheet protein tendamistat, *J. Mol. Biol. 260*, 432-445.

291. Dong, A., Matsuura, J., Manning, M.C. & Carpenter, J.F. (1998) Intermolecular β-sheet results from trifluoroethanol-induced nonnative α-helical structure in β-sheet predominant proteins - infrared and circular dichroism spectroscopic study, *Arch. Biochem. Biophys. 355*, 275-281.

292. Bazzo, R., Tappin, M.J., Pastore, A., Harvey, T.S., Carver, J.A. & Campbell, I.D. (1988) The structure of melittin: a ^{1}H-NMR study in methanol, *Eur. J. Biochem. 173*, 139-146.

293. McDonnell, P.A. & Opella, S.J. (1993) Effect of detergent concentration on multidimensional solution NMR spectra of membrane proteins in micelles, *J. Magn. Res. B. 102*, 120-125.

294. Bosch, C., Brown, L.R. & Wüthrich, K. (1980) Physiochemical characterization of glucagon-containing lipid micelles, *Biochim. Biophys. Acta. 603*, 298-312.

295. Roumestand, C., Louis, V., Aumelas, A., Grassy, G., Calas, B. & Chavanieu, A. (1998) Oligomerization of protegrin-1 in the presence of DPC micelles. A proton high-resolution NMR study, *FEBS Letters. 421*, 263-267.

296. Vold, R.R., Prosser, R.S. & Deese, A.J. (1997) Isotropic solutions of phospholipid bicelles - a new membrane mimetic for high-resolution NMR studies of polypeptides, *J. Biomol. NMR. 9*, 329-335.

297. Braun, W., Wider, G., Lee, K.H. & Wüthrich, K. (1983) Conformation of glucagon in a lipid-water interphase by ^{1}H nuclear magnetic resonance, *J. Mol. Biol. 169*, 921-948.

298. Breukink, E., van Kraaij, C., van Dalen, A., Demel, R.A., Siezen, R.J., de Kruijff, B. & Kuipers, O.P. (1998) The orientation of nisin in membranes, *Biochemistry. 37*, 8153-8162.

299. Maiorano, J.N. & Davidson, W.S. (2000) The orientation of helix 4 in apolipoprotein A-I-containing reconstituted high density lipoproteins, *J. Biol. Chem. 275*, 17374-17380.

300. Clayton, A.H.A. & Sawyer, W.H. (1999) The structure and orientation of class-A amphipathic peptides on a phospholipid bilayer surface, *Eur. Biophys. J. 28*, 133-141.

301. Picard, F., Buffeteau, T., Desbat, B., Auger, M. & Pezolet, M. (1999) Quantitative orientation measurements in thin lipid films by attenuated total reflection infrared spectroscopy, *Biophys. J. 76*, 539-551.

302. Frey, S. & Tamm, L.K. (1991) Orientation of melittin in phospholipid bilayers - a polarized attenuated total reflection infrared study, *Biophys. J. 60*, 922-930.

303. Bechinger, B., Ruysschaert, M. & Goormaghtigh, E. (1999) Membrane helix orientation from linear dichroism of infrared attenuated total reflection spectra, *Biophys. J. 76*, 552-563.

304. La Rocca, P., Biggin, P.C., Tieleman, D.P. & Sansom, M.S.P. (1999) Simulation studies of the interaction of antimicrobial peptides and lipid bilayers, *Biochim. Biophys. Acta Biomembranes. 1462*, 185-200.

305. de Jongh, H.H.J., Goormaghtigh, E. & Killian, J.A. (1994) Analysis of circular dichroism spectra of oriented protein-lipid complexes: toward a general application, *Biochemistry. 33*, 14521-14528.

306. Bazzi, M.D. & Woody, R.W. (1985) Oriented secondary structure in integral membrane proteins, *Biophys. J. 48*, 957-966.

307. Clayton, A.H.A. & Sawyer, W.H. (2000) Oriented circular dichroism of a class A amphipathic helix in aligned phospholipid multilayers, *Biochim. Biophys. Acta. 1467*, 124-130.

308. Mehring, M. (1983) *Principles of High Resolution NMR in Solids*, Springer-Verlag, Berlin.

309. Seelig, J. (1978) ^{31}P Nuclear magnetic resonance and the head group structure of phospholipids in membranes, *Biochim. Biophys. Acta. 515*, 105-140.

310. Sanders, C.R., Hare, B.J., Howard, K.P. & Prestegard, J.H. (1994) Magnetically-oriented phospholipid micelles as a tool for the study of membrane-associated molecules, *Prog. Nucl. Magn. Reson. Spectrosc. 26*, 421-444.

311. Sanders, C.R. & Prosser, R.S. (1998) Bicelles: a model membrane system for all seasons?, *Structure. 6*, 1227-1234.

312. Wu, C.H., Ramamoorthy, A., Gierasch, L.M. & Opella, S.J. (1995) Simultaneous characterization of the amide ^{1}H chemical shift, ^{1}H-^{15}N dipolar, and ^{15}N chemical shift interaction tensors in a peptide bond by three-dimensional solid-state NMR spectroscopy, *J. Am. Chem. Soc. 117*, 6148-6149.

313. Brender, J.R., Taylor, D.M. & Ramamoorthy, A. (2001) Orientation of amide-nitrogen-15 chemical shift tensors in peptides: a quantum chemical study, *J. Am. Chem. Soc. 123*, 914-922.

314. Opella, S.J., Marassi, F.M., Gesell, J.J., Valente, A.P., Kim, Y., Oblatt-Montal, M. & Montal, M. (1999) Structures of the M2 channel-lining segments from nicotinic acetylcholine and NMDA receptors by NMR spectroscopy, *Nat. Struct. Biol. 6*, 374-379.

315. Martin, G.J., Martin, M.L. & Gouesnard, J. (1981) *^{15}N-NMR Spectroscopy*, Springer-Verlag, Berlin.

316. Pines, A., Gibby, M.C. & Waugh, J.S. (1973) Proton enhanced nuclear magnetic resonance of dilute spins in solids, *J. Chem. Phys. 59*, 569-590.

317. Levitt, M.H., Suter, D. & Ernst, R.R. (1986) Spin dynamics and thermodynamics in solid-state NMR cross polarization, *J. Chem. Phys. 84*, 4243-.

318. Yeagle, P.L. (1987) ^{31}P NMR and the phospholipid headgroups of membranes. In *Phosphorus NMR in Biology* (Burt, C.T., ed), CRC Press, Inc., Florida.

319. Smith, I.C.P. & Ekiel, I.H. (1984) Phosphorus-31 NMR of phospholipids in membranes. In *Phosphorus-31 NMR. Principles and Applications* (Garenstein, D.G., ed) pp. 447-475, Academic Press Inc., London.

320. Banerjee, U., Zidovetzki, R., Birge, R.R. & Chan, S.I. (1985) Interaction of alamethicin with lecithin bilayers: a ^{31}P and ^{2}H NMR study, *Biochemistry. 24*, 7621-7627.

321. Seelig, J. (1984) Lipid polymorphism, reverse micelles, and phosphorus-31 nuclear magnetic resonance. In *Reverse Micelles* (Luisi, P.L. & Straub, B.E., eds) pp. 209-220, Plenum Publishing Corporation.

322. Thayer, A.M. & Kohler, S.J. (1981) Phosphorus-31 nuclear magnetic resonance spectra characteristic of hexagonal and isotropic phospholipid phases generated from phosphatidylethanolamine in the bilayer phase, *Biochemistry. 20*, 6831-6834.

323. Niederberger, W. & Seelig, J. (1976) Phosphorus-31 chemical shift anisotropy in unsonicated phospholipid bilayers, *J. Am. Chem. Soc. 98*, 3704-3706.

324. Lafleur, M., Fine, B., Sternin, E., Cullis, P.R. & Bloom, M. (1989) Smoothed orientational order profile of lipid bilayers by ^{2}H-nuclear magnetic resonance, *Biophys. J. 56*, 1037-1041.

325. Howard, K.P. & Opella, S.J. (1996) High-resolution solid-state NMR spectra of integral membrane proteins reconstituted into magnetically oriented phospholipid bilayers, *J. Magn. Res. 112*, 91-94.

326. Lafleur, M., Cullis, P.R., Fine, B. & Bloom, M. (1990) Comparison of the orientational order of lipid chains in the L_α and H_{II} Phases, *Biochemistry. 29*, 8325-8333.

327. Davis, J.H. (1983) The description of membrane lipid conformation, order and dynamics by ^{2}H-NMR, *Biochim. Biophys. Acta. 737*, 117-171.

328. Seelig, J. & Niederberger, W. (1974) Deuterium-labelled lipids as structural probes in liquid crystalline bilayers. A deuterium magnetic resonance study, *J. Am. Chem. Soc. 96*, 2069-2072.

329. Trouard, T.P., Nevzorov, A.A., Alam, T.M., Job, C., Zajicek, J. & Brown, M.F. (1999) Influence of cholesterol on dynamics of dimyristoylphosphatidylcholine bilayers as studied by deuterium NMR relaxation, *J. Chem. Phys. 110*, 8802-8818.

330. Seelig, A. & Seelig, J. (1974) The dynamic structure of fatty acyl chains in a phospholipid bilayer measured by deuterium magnetic resonance, *Biochemistry. 13*, 4839-4845.

331. de Planque, M.R.R., Greathouse, D.V., Koeppe, R.E., Schafer, H., Marsh, D. & Killian, J.A. (1998) Influence of lipid/peptide hydrophobic mismatch on the

thickness of diacylphosphatidylcholine bilayers. A ^{2}H NMR and ESR study using designed transmembrane α-helical peptides and gramicidin A, *Biochemistry. 37*, 9333-9345.

332. Koenig, B.W., Ferretti, J.A. & Gawrisch, K. (1999) Site-specific deuterium order parameters and membrane-bound behaviour of a peptide fragment from the intracellular domain of HIV-1 gp41, *Biochemistry. 38*, 6327-6334.
333. Yamaguchi, S., Huster, D., Waring, A., Lehrer, R.I., Kearney, W., Tack, B.F. & Hong, M. (2001) Orientation and dynamics of an antimicrobial peptide in the lipid bilayer, *Biophys. J. 81*, 2203-2214.
334. Bechinger, B., Zasloff, M. & Opella, S.J. (1992) Structure and interactions of magainin antibiotic peptides in lipid bilayers: a solid-state nuclear magnetic resonance investigation, *Biophys. J. 62*, 12-14.
335. Pope, J.M., Walker, L., Cornell, B.A. & Separovic, F. (1982) A study of the angular dependence of NMR relaxation times in macroscopically oriented lyotropic liquid lamellar phases, *Mol. Cryst. Liq. Cryst. 89*, 137-150.
336. Crowell, K.J. & Macdonald, P.M. (1999) Surface charge response of the phosphatidylcholine head group in bilayered micelles from phosphorus and deuterium nuclear magnetic resonance, *Biochim. Biophys. Acta. 1416*, 21-30.
337. Struppe, J., Komives, E.A., Taylor, S.S. & Vold, R.R. (1998) ^{2}H NMR studies of myristoylated peptide in neutral and acidic phospholipid bicelles, *Biochemistry. 37*, 15523-15527.
338. Sanders, C.R. & Schwonek, J.P. (1992) Characterization of magnetically orientable bilayers in mixtures of dihexanoylphosphatidylcholine and dimyristoylphosphatidylcholine by solid-state NMR, *Biochemistry. 31*, 8898-8905.
339. Fringeli, U.P. & Gunthard, H.H. (1981) Infrared membrane spectroscopy. In *Molecular Biology, Biochemistry and Biophysics* (Grell, E., ed) pp. 270-327, Springer-Verlag, Berlin.
340. Muccio, D.D. & Cassim, J.Y. (1979) Interpretation of the absorption and circular dichroic spectra of oriented purple membrane films, *Biophys. J. 26*, 427-440.
341. Wu, Y., Huang, H.W. & Olah, G.A. (1990) Method of oriented circular dichroism, *Biophys. J. 57*, 797-806.
342. Wabnitz, P.A., Bowie, J.H., Wallace, J.C. & Tyler, M.J. (1999) The citropin peptides from the skin glands of the Australian Blue Mountains tree frog *Litoria citropa*. Part

2: Sequence determination using electrospray mass spectrometry, *Rapid Commun. Mass Spectrom. 13*, 1724-1732.

343. Shai, Y. (1995) Molecular recognition between membrane-spanning polypeptides, *Trends Biochem. Sci. 20*, 460-464.
344. Cantor, C.R. & Timasheff, S.N. (1982) Optical spectroscopy of proteins. In *The Proteins* (Neurath, H. & Hill, R.L., eds) pp. 145-230, Academic Press, New York.
345. Wüthrich, K. & Wider, G. (1982) Sequential resonance assignments as a basis for determination of spatial protein structures by high resolution proton nuclear magnetic resonance, *J. Mol. Biol. 155*, 311-319.
346. Koradi, R., Billeter, M. & Wüthrich, K. (1996) MOLMOL - a program for display and analysis of macromolecular structures, *J. Mol. Graphics. 14*, 51-55.
347. Wishart, D.S. & Sykes, B.D. (1994) The C-13 chemical-shift index - a simple method for the identification of protein secondary structure using C-13 chemical-shift data, *J. Biomol. NMR. 4*, 171-180.
348. Smith, R., Separovic, F., Bennett, F.C. & Cornell, B.A. (1992) Melittin-induced changes in lipid multilayers, *Biophys. J. 63*, 469-474.
349. Song, Z., Kovacs, F.A., Wang, J., Denny, J.K., Shekar, S.C., Quine, J.R. & Cross, T.A. (2000) Transmembrane domain of M2 protein from influenza A virus studied by solid-state ^{15}N polarization inversion spin exchange at magic angle NMR, *Biophys. J. 79*, 767-775.
350. Bradshaw, J.P., Darkes, M.J.M., Harroun, T.A., Katsaras, J. & Epand, R.M. (2000) Oblique membrane insertion of viral fusion peptide probed by neutron diffraction, *Biochemistry. 39*, 6581-6585.
351. Ishiguro, R., Matsumoto, M. & Takahashi, S. (1996) Interaction of fusogenic synthetic peptide with phospholipid bilayers - orientation of the peptide alpha-helix and binding isotherm, *Biochemistry. 35*, 4976-4983.
352. Bechinger, B., Kinder, R., Helmle, M., Vogt, T.B., Harzer, U. & Schinzel, S. (1999) Peptide structural analysis by solid-state NMR spectroscopy [review], *Biopolymers. 51*, 174-190.
353. Hori, Y., Demura, M., Niidome, T., Aoyagi, H. & Asakura, T. (1999) Orientational behaviour of phospholipid membranes with mastoparan studied by ^{31}P solid state NMR, *FEBS Letters. 455*, 228-232.

354. Brasseur, R., Pillot, T., Lins, L., Vandekerckhove, J. & Rosseneu, M. (1997) Peptides in membranes: tipping the balance of membrane stability, *Trends Biochem. Sci. 22*, 167-171.

355. Hong, M. & Yamaguchi, S. (2001) Sensitivity-enhanced static ^{15}N NMR of solids by ^{1}H indirect detection, *J. Magn. Res. 150*, 43-48.

356. Cornell, B.A., Separovic, F., Baldassi, A.J. & Smith, R. (1988) Conformation and orientation of gramicidin A in oriented phospholipid bilayers measured by solid state carbon-13 NMR, *Biophys. J. 53*, 67-76.

357. Stone, D.J.M., Waugh, R.J., Bowie, J.H., Wallace, J.C. & Tyler, M.J. (1992) Peptides from Australian Frogs. Structures of the Caerins and Caeridin 1 from *Litoria splendida*, *J. Chem. Soc. Perkin Trans. I*, 3173-3178.

358. Steinborner, S.T., Waugh, R.J., Bowie, J.H. & Tyler, M.J. (1997) New caerin antibacterial peptides from the skin glands of the Australian tree frog *Litoria xanthomera*. 2. Sequence determination using mass spectrometry and associated techniques, *Rapid Commun. Mass Spectrom. 11*, 997-1000.

359. Steinborner, S.T., Bowie, J.H., Tyler, M.J. & Wallace, J.C. (1997) An unusual combination of peptides from the skin glands of Ewings tree frog, *Litoria ewingi* - sequence determination and antimicrobial activity, *Aust. J.Chem. 50*, 889-894.

360. Steinborner, S.T., Currie, G.J., Bowie, J.H., Wallace, J.C. & Tyler, M.J. (1998) New antibiotic caerin 1 peptides from the skin secretion of the Australian tree frog *Litoria chloris* - comparison of the activities of the caerin 1 peptides from the genus *Litoria*, *Int. J. Peptide Protein Res. 51*, 121-126.

361. Gueron, M., Plateau, P. & Decorps, M. (1991) Solvent signal suppression in NMR, *Prog. Nucl. Magn. Reson. Spectrosc. 23*, 135-209.

362. John, B.K., Plant, D., Webb, P. & Hurd, R.E. (1992) Effective combination of gradients and crafted RF pulses for water suppression in biological samples, *J. Magn. Res. 98*, 200-206.

363. O'Neil, J.D.J. & Sykes, B.D. (1989) NMR studies of the influence of dodecyl sulfate on the amide hydrogen exchange kinetics of a micelle-solubilized hydrophobic tripeptide, *Biochemistry. 28*, 699-707.

364. Summers, M.F., Marzilli, L.G. & Bax, A. (1986) Complete ^{1}H and ^{13}C assignments of coenzyme B_{12} through the use of the new two-dimensional NMR experiments, *J. Am. Chem. Soc. 108*, 4285-4294.

365. Bartels, C., Xia, T.H., Billeter, M., Guntert, P. & Wüthrich, K. (1995) The program XEASY for computer-supported NMR spectral analysis of biological macromolecules, *J. Biomol. NMR. 6*, 1-10.

366. Brunger, A.T. (1992) A system for X-ray crystallography and NMR. In *X-PLOR (version 3.851)*, Yale University, New Haven, CT.

367. Brunger, A.T. & Nilges, M. (1993) Computational challenges for macromolecular structure determination by X-ray crystallography and solution NMR-spectroscopy, *Quart. Rev. Biophys. 26*, 49-125.

368. Nilges, M., Kuszewski, J. & Brunger, A.T. (1992) Sampling properties of simulated annealing. In *Proceedings of the NATO Advanced Research Workshop on Computational Aspects of the Study of Biological Macromolecules by NMR*,, Il Ciocco, Italy.

369. Engh, R.A. & Huber, R. (1991) Accurate Bond and Angle Parameters for X-ray Protein Structure Refinement, *Acta Cryst. A47*, 392-400.

370. Hansen, J.N. (1994) Nisin as a model food preservative (Review), *Crit. Rev. Food Sci. Nutrition. 34*, 69-93.

371. Beuchat, L.R., Clavero, M.R.S. & Jaquette, C.B. (1997) Effects of nisin and temperature on survival, growth and enterotoxin production characteristics of psychrotrophic *Bacillus cereus* in beef gravy, *Appl. Environ. Microbiol. 63*, 1953-1958.

Appendix – HSQC and HMBC Spectra

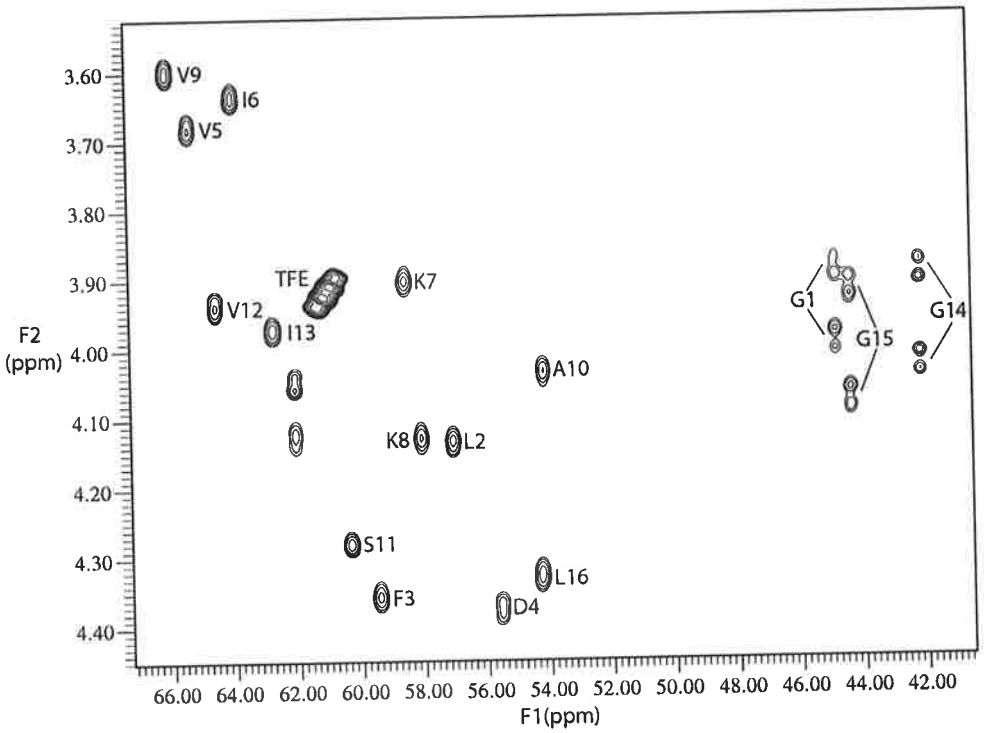

Figure 1 αH-αC region of the HSQC spectrum of citropin 1.1 in TFE/H_2O (1:1 by volume) at pH 2.25, 25°C. αH-αC cross-peaks are labelled with the standard single-letter abbreviation for the residue type and a number indicating the sequential position of the residue.

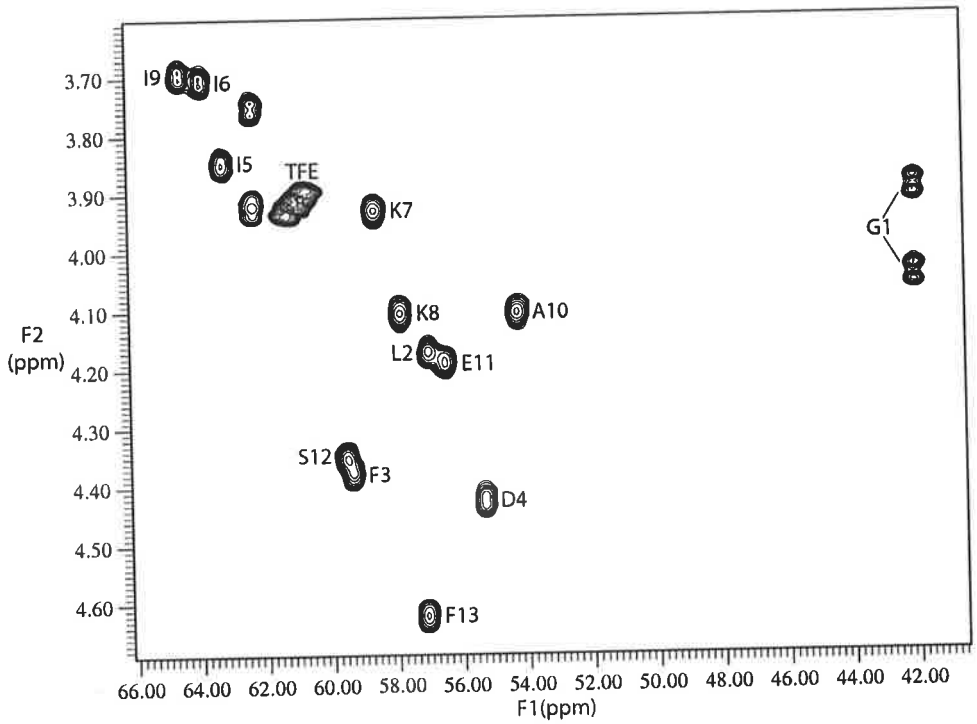

Figure 2 αH-αC region of the HSQC spectrum of aurein 1.2 in 70% TFE in H_2O (by volume) at pH 2.04, 25°C. αH-αC cross-peaks are labelled with the standard single-letter abbreviation for the residue type and a number indicating the sequential position of the residue.

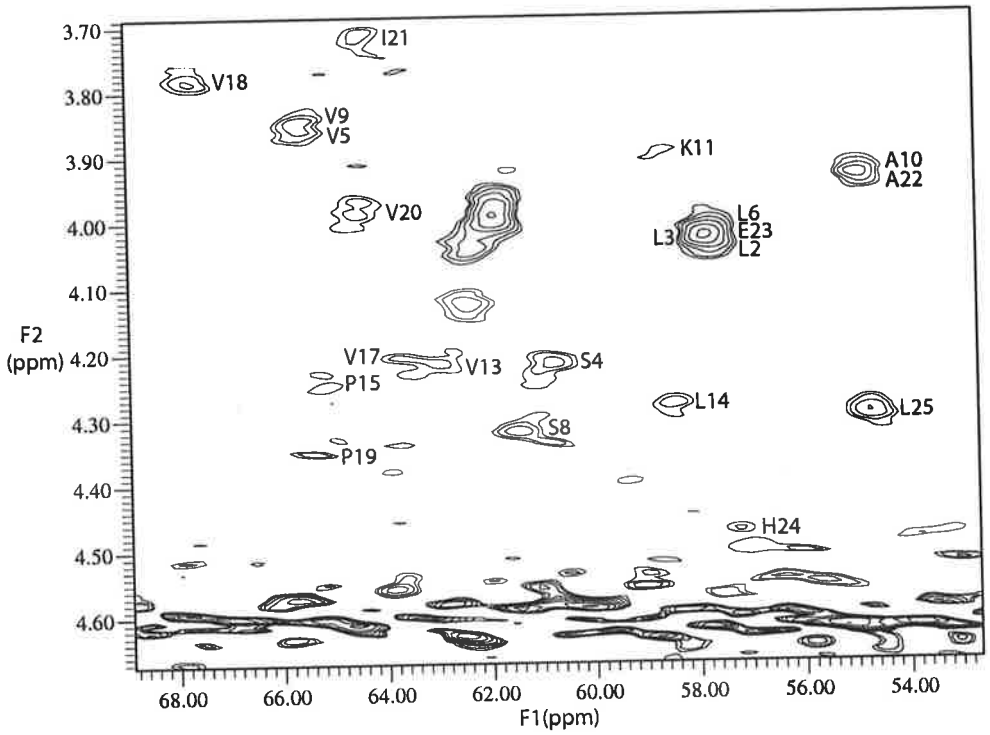

Figure 3 αH-αC region of the HSQC spectrum of caerin 1.1 in DPC micelles at pH 6.07, 37°C. αH-αC cross-peaks are labelled with the standard single-letter abbreviation for the residue type and a number indicating the sequential position of the residue.

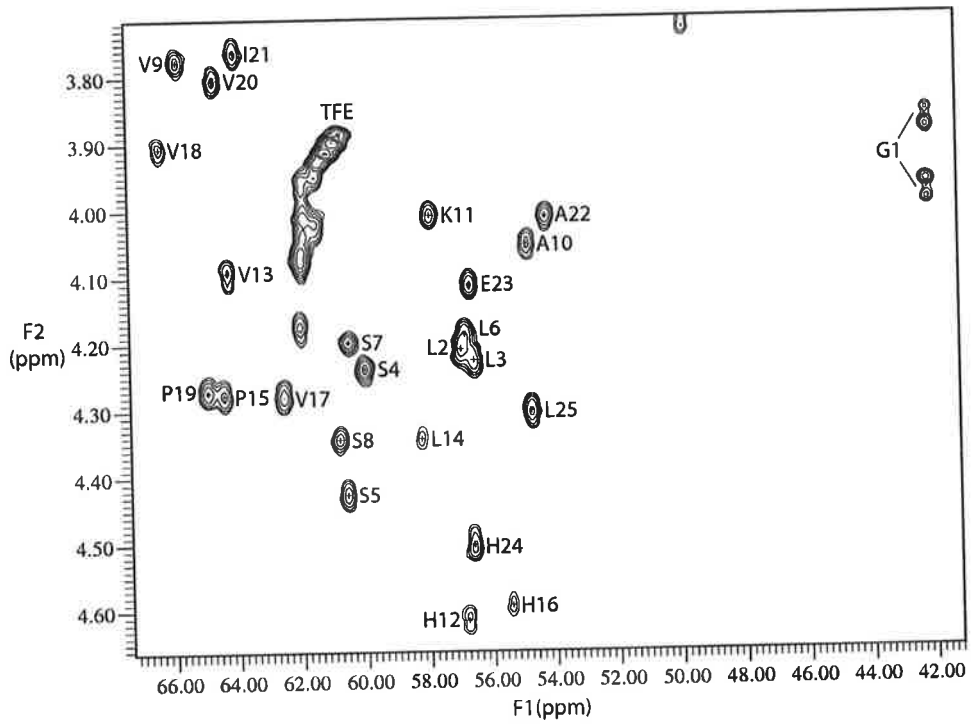

Figure 4 αH-αC region of the HSQC spectrum of caerin 1.4 in TFE/H_2O (1:1 by volume) at pH 3.13, 25°C. αH-αC cross-peaks are labelled with the standard single-letter abbreviation for the residue type and a number indicating the sequential position of the residue.

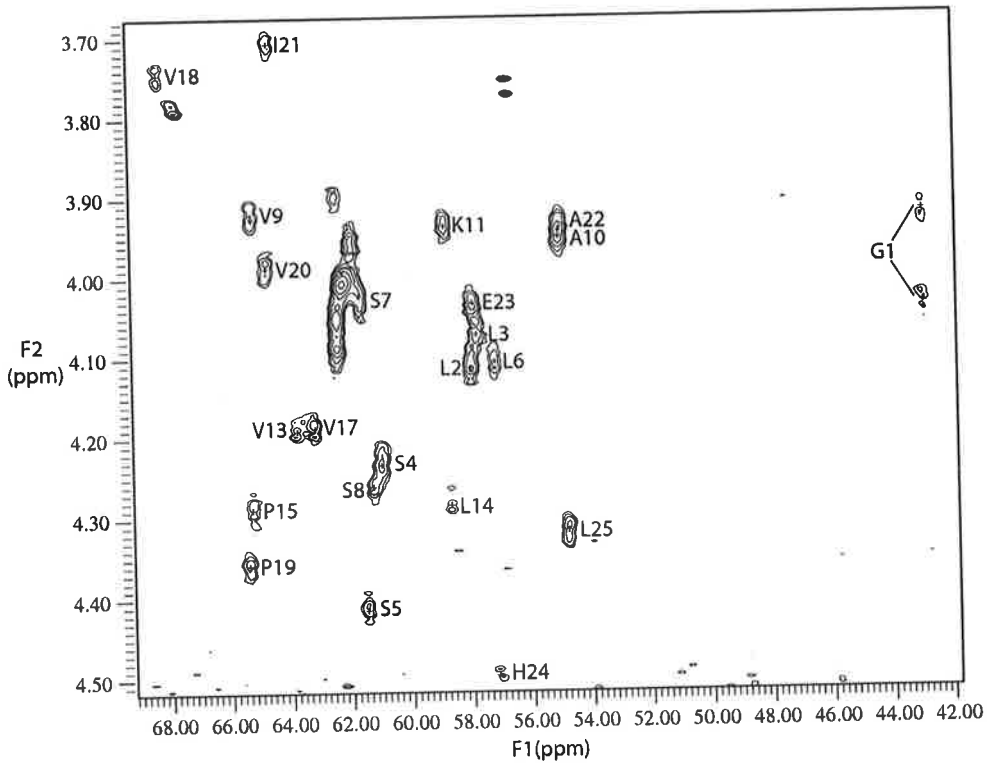

Figure 5 αH-αC region of the HSQC spectrum of caerin 1.4 in DPC micelles at pH 5.97, 37°C. αH-αC cross-peaks are labelled with the standard single-letter abbreviation for the residue type and a number indicating the sequential position of the residue.

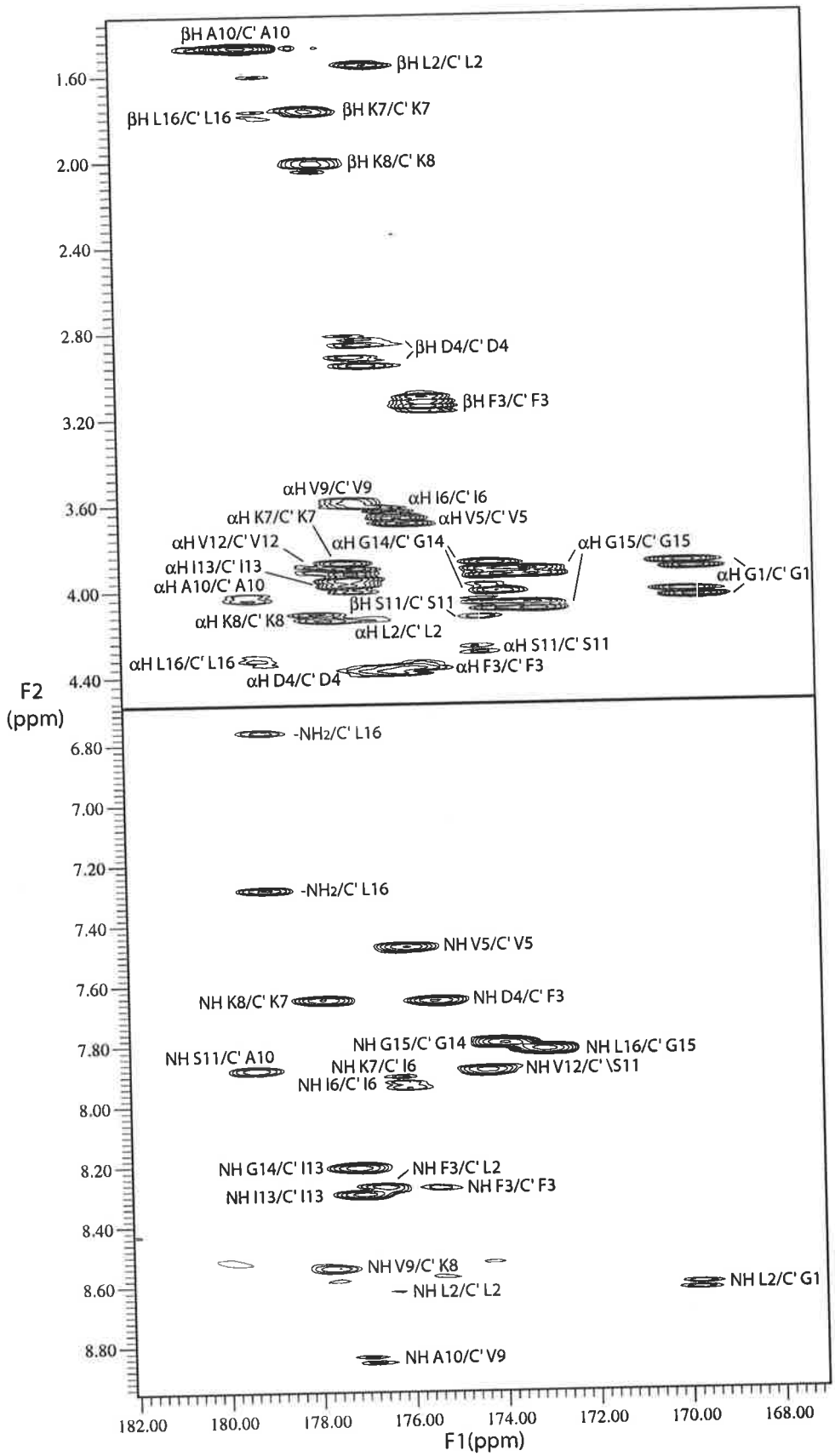

Figure 6 αH/βH-C′ and NH-C′ regions of the HMBC spectrum of citropin 1.1 in TFE/H_2O (1:1 by volume) at pH 2.25, 25°C.

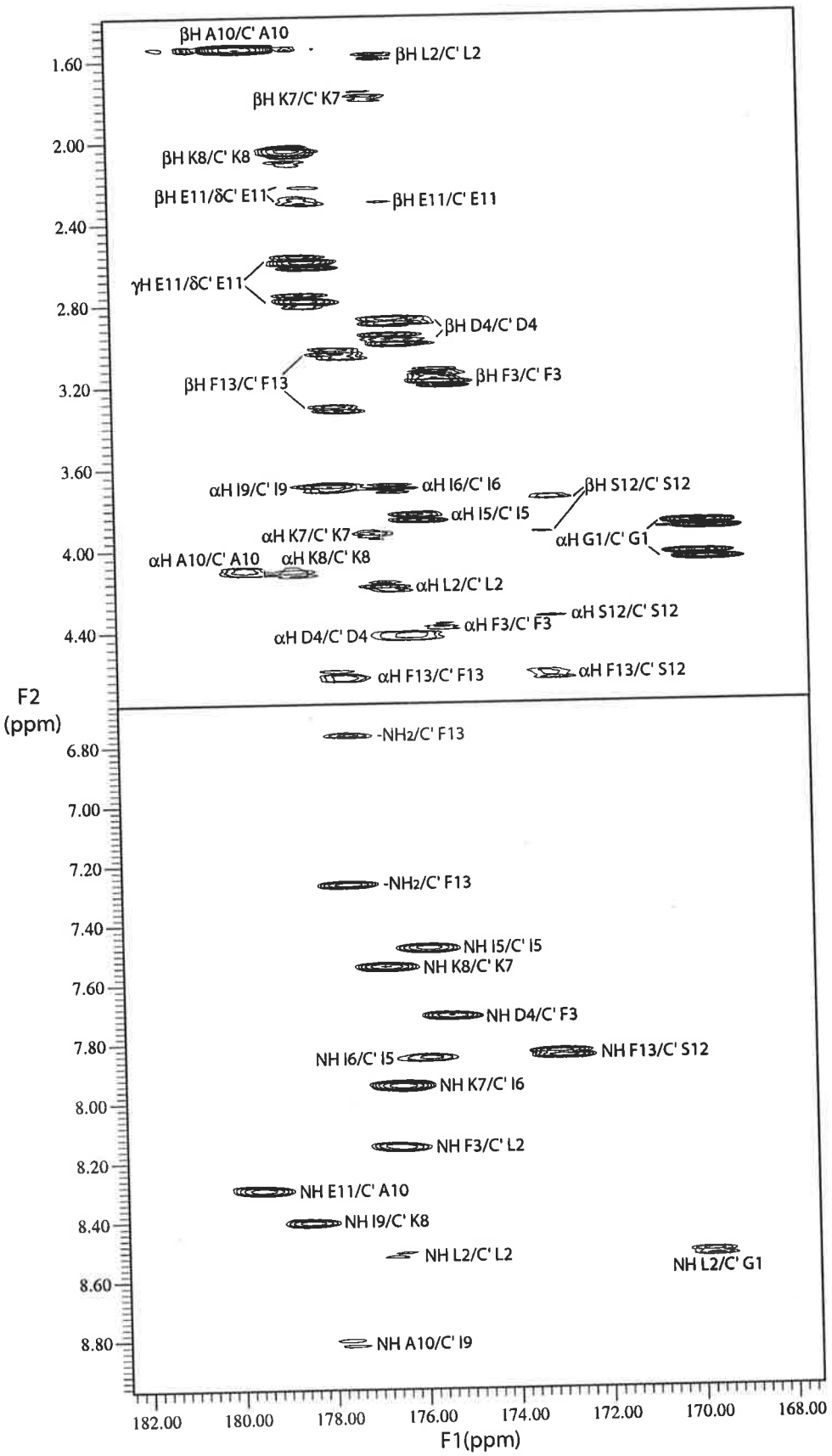

Figure 7 αH/βH-C' and NH-C' regions of the HMBC spectrum of aurein 1.2 in 70% TFE in H_2O (by volume) at pH 2.04, 25°C.

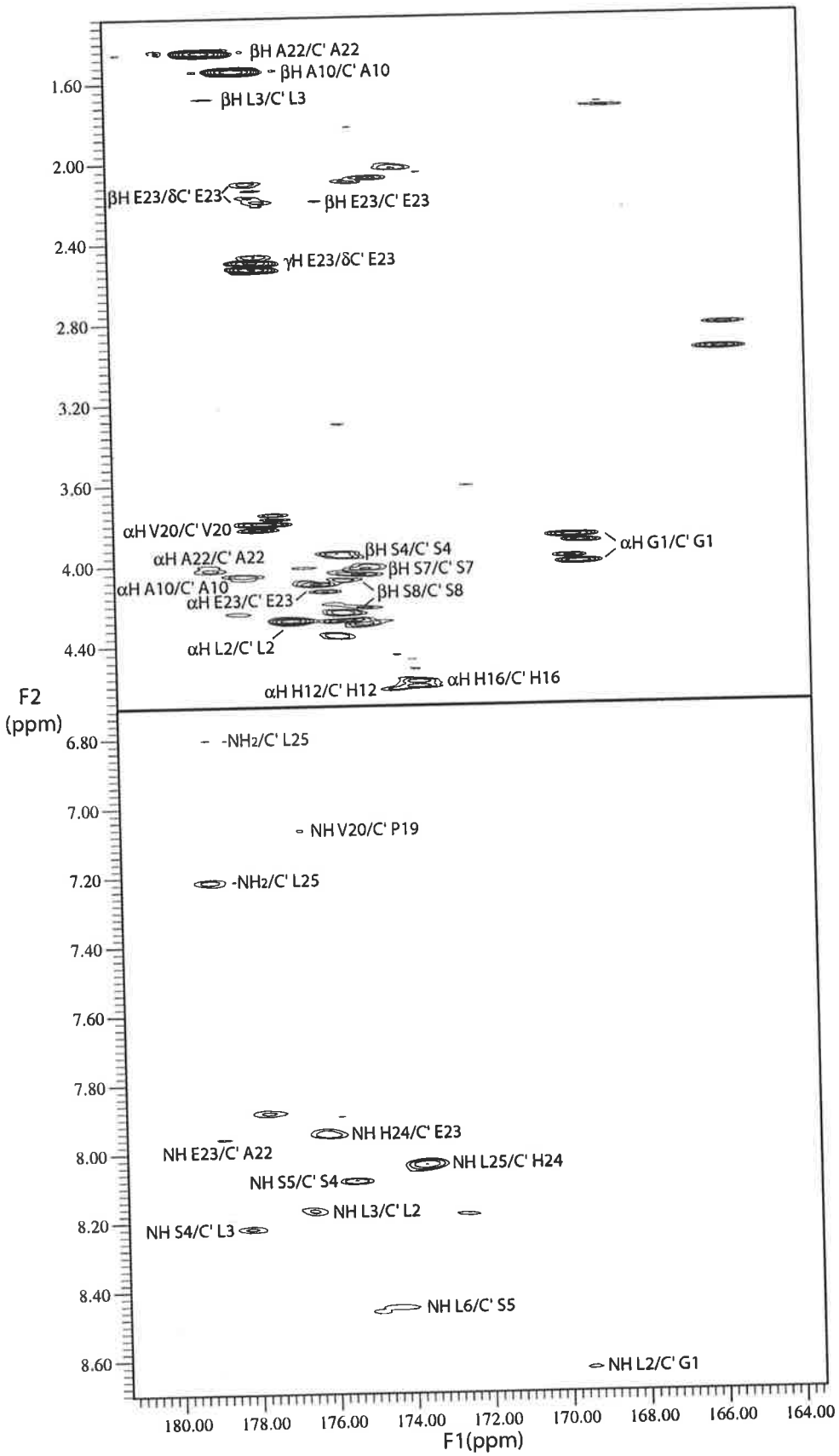

Figure 8 αH/βH-C′ and NH-C′ regions of the HMBC spectrum of caerin 1.4 in TFE/H_2O (1:1 by volume) at pH 3.13, 25°C.

Publications

Journals Related to Thesis

Wegener, K.L., Brinkworth, C.S., Bowie, J.H., Wallace, J.C. & Tyler, M.J. (2001) Bioactive dahlein peptides from the skin secretions of the Australian aquatic frog *Litoria dahlii*: sequence determination by electrospray mass spectrometry, *R. Commun. Mass Spectrom. 15*, 1726-1734.

Wegener, K.L., Wabnitz, P.A., Carver, J.A., Bowie, J.H., Chia, B.C.S., Wallace, J.C. & Tyler, M.J. (1999) Host defence peptides from the skin glands of the Australian Blue Mountains tree-frog *Litoria citropa*. Solution structure of the antibacterial peptide citropin 1.1, *Eur. J. Biochem. 265*, 627-637.

Rozek, T., Wegener, K.L., Bowie, J.H., Olver, I.N., Carver, J.A., Wallace, J.C. & Tyler, M.J. (2000) The antibiotic and anticancer active aurein peptides from the Australian Bell Frogs *Litoria aurea* and *Litoria raniformis*. The solution structure of aurein 1.2, *Eur. J. Biochem. 267*, 5330-5341.

Bowie, J.H., Wegener, K.L., Chia, B.C.S., Wabnitz, P.A., Carver, J.A., Tyler, M.J. & Wallace, J.C. (1999) Host defence antibacterial peptides from skin secretions of Australian amphibians. The relationship between structure and activity, *Protein Pept. Lett. 6*, 259-269.

Doyle, J., Llewellyn, L.E., Brinkworth, C.S., Bowie, J.H., Wegener, K.L., Rozek, T., Wabnitz, P.A., Wallace, J.C. & Tyler, M.J. (2001) Amphibian peptides that inhibit neuronal nitric oxide synthase: the isolation of lesueurin from the skin secretion of the Australian Stony Creek Frog *Litoria lesueuri*, *Eur. J. Biochem. in press.*

Wegener, K.L., Brinkworth, C.S., Bowie, J.H., Wallace, J.C., and Tyler, M.J., (2001) Bioactive dahlein peptides from the skin secretions of the Australian aquatic frog *Litoria dahlii*: sequence determination by electrospray mass spectrometry. *Rapid Communications in Mass Spectrometry, v. 15 (18), pp. 1726-1734.*

NOTE:
This publication is included in the print copy
of the thesis held in the University of Adelaide Library.

It is also available online to authorised users at:

http://dx.doi.org/10.1002/rcm.429

Wegener, K.L., Wabnitz, P.A., Carver, J.A., Bowie, J.H., Chia, B.C.S., Wallace, J.C., and Tyler, M.J., (1999) Host defence peptides from the skin glands of the Australian Blue Mountains tree-frog *Litoria citropa:* solution structure of the antibacterial peptide citropin 1.1.
European Journal of Biochemistry, *v. 265 (2), pp. 627-637.*

NOTE:
This publication is included in the print copy
of the thesis held in the University of Adelaide Library.

It is also available online to authorised users at:

http://dx.doi.org/10.1046/j.1432-1327.1999.00750.x

Rozek, J., Wegener, K.L., Bowie, J.H., Olver, I.N., Carver, J.A., Wallace, J.C., and Tyler, M.J., (2000) The antibiotic and anticancer active aurein peptides from the Australian Bell Frogs *Litoria aurea* and *Litoria raniformis:* the solution structure of aurein 1.2,
European Journal of Biochemistry, *v. 267 (17), pp. 5330-5341*.

NOTE:
This publication is included in the print copy
of the thesis held in the University of Adelaide Library.

It is also available online to authorised users at:

http://dx.doi.org/10.1046/j.1432-1327.2000.01536.x

Bowie, J.H., Wegener, K.L., Chia, B.C.S., Wabnitz, P.A., Carver, J.A., Tyler, M.J., Wallace, J.C., (1999) Host defence antibacterial peptides from skin secretions of Australian amphibians: the relationship between structure and activity.
Protein and Peptide Letters, v. 6 (5), pp. 259-269.

NOTE:
This publication is included in the print copy
of the thesis held in the University of Adelaide Library.